UNIVERSITY
OF OSLO

Master's thesis

Recent changes in groundwater levels for different regimes in Norway

Torkel Andreassen Bjørbæk

Hydrology and Glaciology
60 ECTS study points

Department of Geosciences
Faculty of Mathematics and Natural Sciences

Spring 2024

Torkel Andreassen Bjørbæk

Recent changes in groundwater levels for different regimes in Norway

Supervisors:
Lena M. Tallaksen
Sigrid J. Bakke
Anne K. Fleig
Raoul A. Collenteur

Abstract

High latitudes regions are experiencing a rapid warming, with pronounced impacts on frost and snow cover. How this affects the seasonal variation in groundwater dynamics is not well understood. The main aim of this study was to analyse recent trends in observed groundwater levels (GWL) for different regimes in Norway. We used a reference dataset of 25 near-natural GWL time series from unconfined aquifers. The series are of varying temporal resolutions and cover different time periods. All except one cover the period 1991-2022. Gaps of different lengths (a few days to years) are present in all series. To analyse trends, the time series first needed to be gap filled. For this, the Pastas software was used to simulate GWL using a lumped-parameter model and impulse response functions. Gridded, daily precipitation, potential evaporation, and temperature data from E-OBS and SeNorge were used as input. Different models were tested and the best R2 performing model, ranging from 0.47 to 0.94, was chosen for each well. Finally, the simulated values were used to gap-fill the series using a weighted linear scaling method. The daily gap-filled time series were then used to calculate trends in GWL. Nine wells depicted significant trends in mean annual GWL between 1982-2022, of which seven were positive and two negative. Five stations showed consistent significant positive or negative trends in all months, whereas most stations with significant monthly trends had positive trends in spring, autumn and winter, and negative trends in summer. Stations within the same groundwater regime depicted similar monthly trends. In summary, there is a general positive GWL trend in autumn, spring, and winter (towards wetter conditions), and a negative trend in the summer (towards drier conditions). Furthermore, we see a tendency to a shift in the peak groundwater levels towards earlier in the year for snow dominated sites.

Sammendrag

De nordlige regionene har undergått en økning i temperatur med en påvirkning på frost og snødekke. Hvordan dette påvirker sesongvariasjonen i grunnvanns dynamikken er ikke så godt kjent. Hoved målet for denne studien var å analysere nylige trender i observerte grunnvanns nivå (GVN) for ulike regimer i Norge. Vi brukte et referansedatasett av 25 nær naturlige GVN tidsserier fra ubegrensede akviferer. Data seriene har varierende tids oppløsning og dekker forskjellige perioder. Alle bortsett fra en, dekker perioden 1991-2022. Hull av forskjellig lengde (noen dager til år) er til stede i alle tidsseriene. For å analysere trendene, trengte vi først å fylle igjen hullene i tidsseriene. Vi brukte programmet «Pastas» for å simulere GVN ved bruk av en klumpet-parameter-modell og en impuls respons funksjon. Modellerte daglig nedbør, potensiell evapotranspirasjon og temperatur data fra E-OBS og SeNorge var brukt som input. Forskjellige modeller ble testet og modellen med best R^2-score, fra 0.47 til 0.94, ble valgt for hver grunnvanns brønn. Til slutt, ble de simulerte verdiene fylt inn i hullene ved å bruke en liner skalerings metode. De resulterende gjenfylte tidsseriene med daglig oppløsning ble brukt i å undersøke for trender i GVN. Ni brønner viste signifikante trender i gjennomsnittlig årlig GVN mellom 1982-2022, hvor syv var positive og to negative. Fem stasjoner viste gjennomgående signifikante positiv eller negative trender alle måneder. Majoriteten av stasjonene med signifikante månedlige trender hadde positive trender i vår, høst og vinter månedene, og negative trender i sommer månedene. I tillegg viste stasjonene i samme grunnvannsregime lignende månedlige trender. Som oppsummering var det en generell positive trend i GVN om våren, høsten og vinteren (mot våtere forhold), og negativ trend om sommeren (mot tørrere forhold). Videre ser vi en tendens til en tidligere topp i GVN for stasjoner som er dominert av snø om vinteren.

Contents

List of Figures

List of Tables

Preface

Foremost, I want to thank all my supervisors Lena M. Tallaksen, Sigrid J. Bakke, Anne K. Fleig and Raoul A. Collenteur. Thank you for taking the time to all the good and productive meetings. You went beyond any expectations I had in answering my many questions about literature, calculations, modeling, and any other questions I might have had. I also want to thank you for all the detailed feedback on my writing, thesis structure and overall content. Without your help, I wouldn't have been able to write this thesis. I want to thank my father for all the discussions and advice. It helped me make good decisions that were crucial for the thesis, and through our discussions, I got a better understanding of the thesis. I would also like to thank for the extensive proofreading, which without, would have made the thesis very flawed. I also want to thank my girlfriend, for supporting me and always being prepared to help me in any way she could. Thanks for being patient and making my long working days easier. Lastly, I want to thank my parents and family, who with interest in my work, helped me stay motivated while working with the thesis, and my friends for all the good discussions and making all the weekends working at ZEB a pleasant experience.

Chapter 1

Introduction

1.1 Background and motivation

Water is an absolute necessity to sustain all life on earth. With increasing population, water is becoming an increasingly more valuable resource all over the world. In addition, increasing water usage in industry, energy production and agriculture, is all competing with the human consumption. Groundwater amount to approximately 99 % of the liquid freshwater on earth [UNESCO World Water Assessment Programme, 2022], and amount to about 35 % of the total global water use [Döll et al., 2012]. As opposed to surface water, groundwater is often slow responding to precipitation and or snowmelt, and recharge could take several months or years. Because of this, groundwater deficits, caused by drought and/or overconsumption could have devastating long-term consequences. Therefore, it is important to manage good water surveillance in order to avoid overconsumption, and to implement mitigation measures in event of a drought.

In Hydrology, the term "drought" is used to describe "a sustained and regional extensive occurrence of below normal natural water availability"[Tallaksen and van Lanen, 2023]. Here, the "natural water availability" is referring to the known natural conditions. Like any other part of the hydrological system, these natural conditions are connected to complicated phenomenons involving many drivers that include global oceanic, atmospheric currents and meteorological conditions [Bakke et al., 2020a]. This way, the natural conditions is subjugated to changes and seasonal patterns in the drivers.

In Norway, stable and easily accessible surface water is abundant almost all over the country. This water is usually of good quality and enough quantity. Thus, most people are not relying on groundwater for consumption. Groundwater usage is more common in agriculture and as a drinking water source at cabins located in rural areas. However, in 2018, warm weather combined with low precipitation put a strain on the surface water reservoirs and led to water shortage. This drought forced many farmers to buy and import sufficient water for their crops and animals, putting an additional strain on the water resources. In the end, the consequence of this drought was a bad harvest, rationing of water, wildfires and other ecological damages [NVE, 2019].

Changes in the climate have been projected to change the climate zones in the high latitudes, from cold climate to warmer, temperate climate during this century [Nygren, 2022]. In addition, [Dyrrdal et al., 2012] have analysed precipitation in Norway the past century and found that there has been a general increase in annual and seasonal precipitation. Warmer climate and increasing precipitation, are examples of change in conditions and drivers that propagates through the

hydrological cycle. Therefore, the "normal" hydrological conditions we see today might be different from the ones we had in the past, or the ones we will have in the future. However, there has been less studies on how this might impact the groundwater variations and its seasonality patterns.

Groundwater recharge

We know that groundwater is connected to the meteorological conditions through recharge. Water from the surface infiltrates through the soil and eventually percolates down as recharge to the groundwater. According to the dominant features affecting this percolation, we divide the subsurface into different zones as shown in figure 1.1.

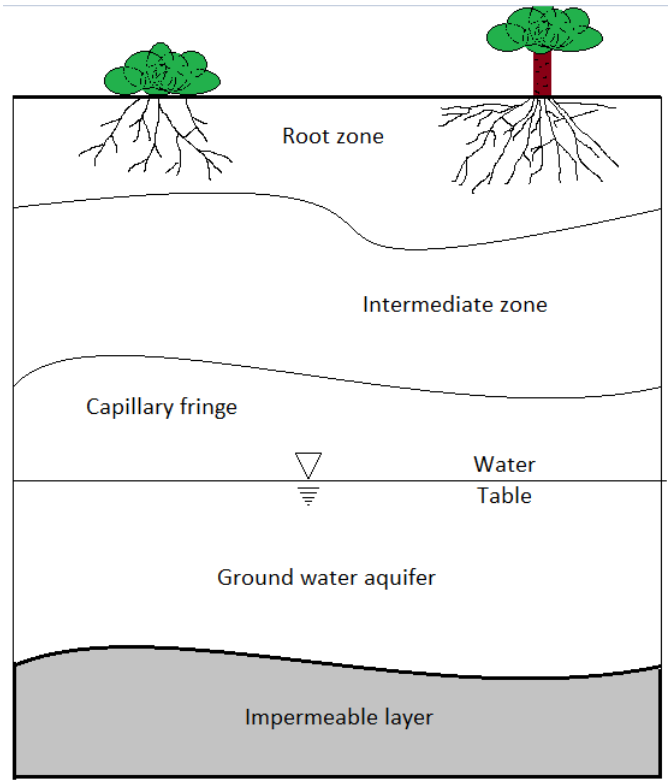

Figure 1.1: Figure is modified from [Dingman, 2015], and shows a conceptual drawing of the different subsurface layers.

At the bottom, above an impermeable layer, we find the groundwater aquifer. An aquifer is a "formation that can store enough water and transmit it at a rate fast enough to be hydrologically significant" [Dingman, 2015]. Here, water exists between cracks and open pore spaces between the grains in the soils. If the cracks and pore space is fully filled with water, we say that the soil is saturated. Groundwater table is defined as the level of which the water within the saturated soil is of positive pressure (i.e., greater than atmospheric pressure) [Dingman, 2015]. Consequently, we refer to the groundwater table or level as the upper boundary of the groundwater aquifer.

Above the groundwater level, we find the capillary fringe. Here the soil is nearly saturated. Water enter this zone as recharge form above, or with capillary rise from the groundwater table. This level moves down as a response to the water withdrawal from roots or evaporation, or up as a response to groundwater recharge [Dingman, 2015]. The third zone is the intermediate zone. Here, water enter as percolation from above and leaves as drainage to the capillary

fringe [Dingman, 2015]. The upper part is the root zone. This is the layer where vegetation can extract water during transpiration. Depending on the vegetation type, this zone can be from a few cm deep to over a meter deep. The soil moisture will in precipitation or snowmelt events approach saturation, but between the events it will be under the field capacity. When we look at a groundwater storage as a resource, we usually refer to it as a aquifer. We distinguish between unconfined and confined aquifers. Unconfined aquifers are aquifers where the upper boundary of the ground water flow is at atmospheric pressure (ground water level). In this case the total head is equal to the elevation over the selected datum z. In confined aquifers, the soil is fully saturated within the aquifer, with a boundary both above and below that has a significantly lower hydraulic conductivity. Here, the pressure is higher than the atmospheric pressure, and its major recharge is occurring from infiltration in the areas upstream where the aquifer is not confined [Dingman, 2015]. Here, the groundwater head might be higher than the elevation over the datum z.

When speaking of groundwater at a regional scale we refer to it as a "groundwater system". A groundwater system includes one or several connected aquifers and its surrounding environment. Depending on scale, this can take into account everything from soil moisture, water propagation, vegetation and long term climate conditions [Nygren, 2022]. Because of the spatial and temporal variability of the conditions affecting the groundwater recharge, predictions of how the climate change effects the groundwater is highly uncertain.

Seasonality and regions

In cold regions, the hydrometeorological variations are highly seasonal. Typically, each season is hydrological different as shown in Figure 1.2. In the wintertime, the soil is continuously frozen, and precipitation comes as snowfall covering the ground. In springtime, the ground thaws and the snow melts. With low evapotranspiration and low vegetation grow rates, the groundwater recharge is therefore highly related to the snow melt. In the summer season, lower effective precipitation due to the high evapotranspiration and vegetation interception. In addition, high vegetation grow rates leads to water being extracted from the soil and reducing groundwater recharge from precipitation. In autumn, the temperature and evapotranspiration from vegetation lowers and the groundwater recharge is mainly from precipitation. With a general shift from cold to more temperate climate, evapotranspiration rates and reduced snowfall might change the governing seasonal patterns.

Data coverage

Since Norway has mainly relied on the surface water, there has been little focus on groundwater. Because of this, there is a low coverage of high-quality monitoring wells, making a regional study difficult. In addition, the existing data is filled with gaps and irregular observation frequencies. Common ways to resolve this problem of frequent gaps and irregular timesteps in the data, is to cut the time series to maximum length and minimum gaps, replace the observation data altogether with simulated values, or fill the gaps with estimated values.

Cutting the time series to achieve maximum length, while achieving a minimal number of gaps, is a viable method when dealing with time series that has large gaps. However, this could lose important data, and is therefore not a good option when dealing with short time series.

In order to replace the observation series with simulated values, one need to have a model

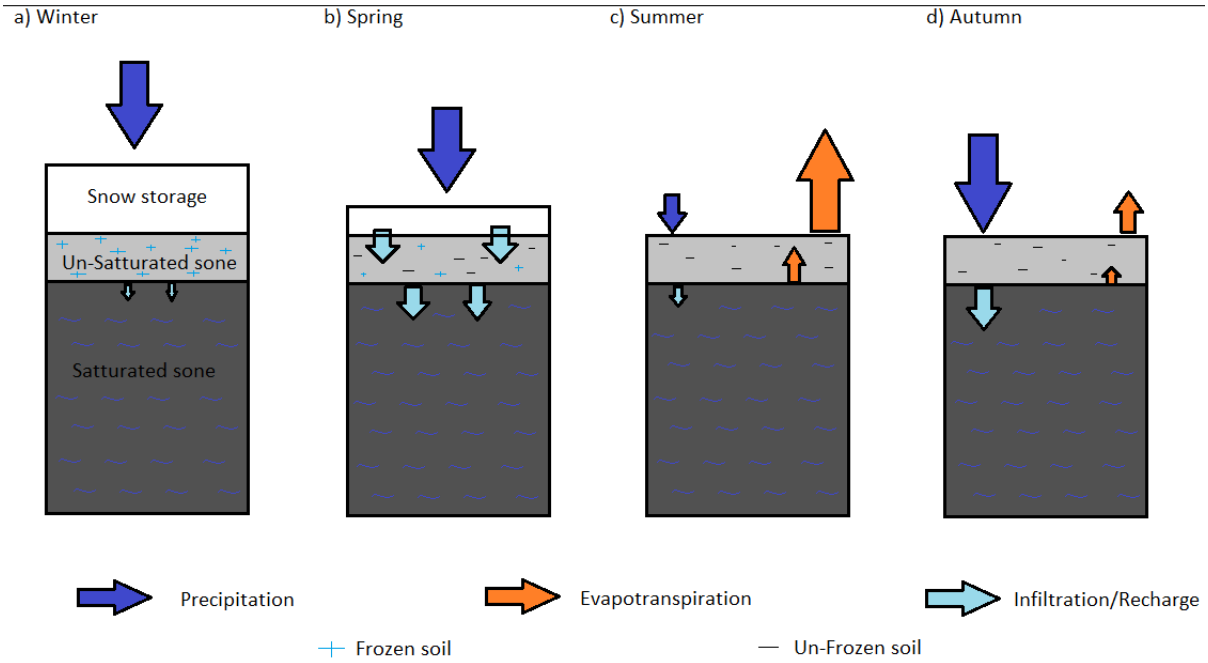

Figure 1.2: Figure is modified from [Nygren, 2022]. Conceptual illustration of the recharge in each season into the groundwater aquifer. a) Winter recharge of groundwater is limited as precipitation is stored in the snow layer and the ground is frozen. b) Spring melt occurs, and recharge to the groundwater is occurring unrelated to precipitation, evapotranspiration is limited. c) Summer, Evapotranspiration is high due to growing season and high temperatures, precipitation and recharge is limited. c) Autumn, evapotranspiration is limited and precipitation related recharge is high.

that is able to sufficiently recreate the hydrological variations, based on the available input. To do this, physically based hydrological models of different complexity are often used. These models are based on the physical laws depending on hydrological processes and use physically based equations to solve for water movement and storage in the catchment [Yoosefdoost et al., 2022]. General equations used are water balance equations, energy-saving and motion and kinematics, Darcy equations, St. Venant equations, Richards equation and Boussinesq equation [Yoosefdoost et al., 2022]. If the model is accurate enough, we can use the simulated values instead of the observation values. The drawback of using such a physical based model, is that it can become very complex and require a lot of input data of the study area to achieve good accuracy.

The last method to resolve the problem is to fill the gaps in the observation data with estimated values. This way, we keep the observation data and values into the periods with missing data. The data we fill in could be estimated using a statistical model, interpolation or hydrological model of different complexities. Using this method, we can maximize the use of the time series by using all the data in the observation series. Depending on the length of the gaps, we can use simpler hydrological models, which requires less input data, without having the inaccuracy of the model affecting the analysis significantly. In this study we decided to fill the gaps of the observation data. Using first lumped-parameter hydrological based model with impulse response functions to simulate groundwater levels, we then use a linear gap-filling method to fill the gaps. With the gap-filled complete datasets of daily resolution, we create our drought indices, which we then calculate the trends for different periods.

Seasonality and regions

Changes in the climate in Norway between 1957 and 2010 has been analyzed by [Dyrrdal et al., 2012]. They used regions based on similarities in precipitation, temperature and altitude. They found that the average regional change (%) of precipitation intensity and frequency has increased significantly in most parts of the country. Increasing precipitation and temperature has led to more snow in cold areas and less snow in warm areas. In addition, number of days with temperatures close to zero has also become more frequent in non-coastal areas. The seasonal variation of groundwater has both been estimated by [Bakke et al., 2020a] and [Nygren, 2022]. [Bakke et al., 2020a] categorized different groundwater regimes which we use in this study to differentiate between the stations [Kirkhusmo, 1988]. The categories are based on the stream flow categories defined in [Gottschalk et al., 1979], but transformed to fit groundwater variations instead.

1.2 Aim of study

The Aim of this study is to examine the groundwater variations in Norway. In particular, we want to see if it is possible to identify trends in the groundwater levels. Further, if there is a trend, how does this relate to possible changes in drivers, and could this change the groundwater seasonality. Basing on the assumptions that the seasonality of groundwater levels in Norway are driven by seasonality of groundwater recharge, as a result of effective precipitation and snowmelt. We use the results of long-term climate trends, that where presented by [Dyrrdal et al., 2012], along with trends in the potential evapotranspiration and rain and snowmelt data from E-OBS and SeNorge database, to formulate three hypotheses.

Hypothesis 1
Stations where the seasonal variation is heavily influenced by snow accumulation and snowmelt: Will experience increasing trends of groundwater levels in the winter months, and no significant increase or a decrease in the summer months.

Hypothesis 2
Stations with a snowmelt related groundwater peak in the spring: Will have a change towards earlier GWL peak timing.

Hypothesis 3
Stations where the seasonal variations are mainly driven by rain events:
Will experience a decreasing trend in groundwater levels in the summer months, and an increasing trend in the early winter months.

However, there is a general problem in the field of groundwater hydrology with varying time resolutions and gaps in the observation data. It is common that observation data may vary between monthly, weekly and daily observation resolution, along with gaps spanning from days to years. Especially in Norway, where the tradition of groundwater studies has not been strong, the observation series are neither long nor complete at any station.

Therefore, to be able to answer the hypotheses, we need complete time series of the groundwater levels with regular spacing between each point. To obtain this, we first use a model to simulate the groundwater levels, and then linearly shift the simulated values to fill the gaps. From the complete time series, we estimate the following drought indices:

- Mean monthly groundwater level
- Yearly average groundwater level
- Lowest summer month value
- Highest summer month value

Here, Monthly trends is derived to help understand the overall trend in annual trend, focusing on changes in the seasonal patterns. In addition, the lowest and highest groundwater level around the typical minimum and maximum months are used to check for trends in the magnitude of the driest and wettest month. Following this introduction, the thesis is organised as follows:

- Section 2 presents the description of the study area and data that is used in the thesis.
- Section 3 presents the time series quality check, model description, outline of gap-filling method, groundwater regimes, groundwater indices and trend analysis.
- Section 4 present the results of the model testing, gap-filing, groundwater regimes and groundwater trend tests.
- Section 5 is the discussion of the results presented in section 4.
- Section 6 is the conclusion of the discussion.

Chapter 2

Data and study area

The study area is the country of Norway. We use data from observations wells that are located mostly in the southern half of Norway, in addition to two stations in the northern part. The stations are located across 9 different climate regions and different altitudes. There are 9 stations in located close to the ocean and the rest is located inland. All stations are influenced by the snowmelt in spring season, but some more than others. We use the seasonality of the typical variation to categorize the stations into four regimes based on [Kirkhusmo, 1988]. The geology is mostly moraine or river deposits, and each station has different degrees of vegetation cover and vegetation types. The data used is gathered from three sources. The first source is the groundwater observations gathered by Norwegian water and energy department (NVE). The second source is the rain and snowmelt data from "SeNorge". The third source is the temperature and evaporation data gathered from "EOBS" initiative. The evaporation values are based on EOBS data, but is calculated for the grid cells covering Norway using a script made by Sigrid J. Bakke.

2.1 Data

The Norwegian Water and Energy directorate (NVE) are collecting observation data from different stations all over Norway. All stations with daily observation data have been considered (63 stations) in this study. Only stations with best quality observations and daily observation length longer than 10 years, are used [Fleig et al., 2013]. This amounted to 25 stations with the longest data series being from 1950-2022. The data is quality checked by NVE and stored in the HYDRA II database. and the following 5 points is taken from [Fleig et al., 2013], describing the selection criteria:

1. Stable land-use conditions
   Stable land-use conditions including absence of significant regulations, diversions or water use, including both natural and agricultural sites. Areas which are characterized as land unit 112-artificial surfaces or 412-wetlands, following the Coordination of information on the environment (CORINE) program categorizations, are excluded since they are not considered to reflect natural climate variability. Stations with limited human influence are included.

2. Record length
   Minimum 20 years in total and more than 10 years of daily groundwater measurements.

3. Active data collection
   Currently active and is expected to continue operation.

4. Good data quality
   Data quality was checked by an explorative graphical analysis where the series where check for:
   - Inhomogeneity
   - Peaks which looked unnatural
   - Jumps in periods of changes in measurement frequency and method
5. Adequate metadata
   NVEs database (Hydra II) contains metadata about the station operations such as instrumentation, measurement location and control measurements.

The observation data were assessed using Hydrological API (HydAPI). This is connected to NVEs database for all hydrological data and is continuously updated with new data. The database has different versions for different periods of the observation time series. The different versions are then usually merged into one continuous time series. However, this had not been done at Øverbygd station (23) at the time of this thesis, and therefore we only had access to the daily observations, even though there are observations going back to 1979 (as seen in Table 2.6, and Figure 2.1).

The final list of stations in Table 2.6, in addition to information about each station. Here, the date of when daily measurement was implemented is from [Fleig et al., 2013]. The altitude of the station, average precipitation and average annual temperature, and the precipitation and temperature is calculated over the normal period between 1961-1990 (Anne K. Fleig, personal correspondence, January 18. 2023). The average annual potential evapotranspiration and days with potential snow days is calculated using the E-OBS data in this study, where potential snow days is days with average temperature under 0 ^oC.

All stations had missing values in the observation series. The Gaps had a length ranging from days to years. Most of the gaps were between 0 and 3 months. 33 gaps were longer than 3 months. This is mostly due to the varying observation frequency. At the start of almost all stations the observation frequency was one observation per month. This changed from once a month to twice a month, once a week or daily observations. In addition, the day of the observations in a given month is changing over time. For example, one period could have observations taken at the 1st and 15th day each month, but then change to the 30th and 14th for another period.

Figure 2.1 shows the time series retrieved by using HydAPI. Here the different resolutions are given a different color, with blue being daily, and green being less than daily resolution. The red color depicts gaps in the data that exceed the resolution of that given period.

The different temporal resolutions make it difficult to have consistency in the data. When counting the number of gaps in the data, we define a gap as a consecutive period of missing value of more than daily resolution. This means that between the observation points in the monthly resolution period, we count one gap, even though there is no "gap" if we consider the monthly resolution. A summary of the number of gaps with a given length across all the stations is shown in table 2.2.

2.2 Meteorological data

The temperature and potential evaporation (PET) is extracted from the E-OBS dataset (version 28.0e)[van der Schrier, 2023]. E-OBS is a land-only daily gridded regional reanalysis ensemble dataset for precipitation, temperature, sea level pressure, global radiation, wind speed and relative humidity in Europe. The spatial resolution on the data we use from E-OBS is on a 0.1 deg

Table 2.1: Here, we see the station number, ID and name, the start dates of the time series, start date of daily observation frequency, altitude, average yearly precipitation, average yearly temperature and days with potential snowfall.

Station nr.	Hydra-Id	Station Name	Start from	Daily values from	Alt. [m]	Prec. [mm/a]	Evap. [mm/a]	Temp. [^oC]	Potential snow days
0	2.725.1	Abrahamsvoll	1969	1999	717	824	459	1.0	160
1	20.34.4	Birkenes rør 4	1979	2002	74	1387	558	7.1	55
2	2.718.2	Dombås rør 2	1981	2002	524	734	433	0.8	162
3	2.727.0	Kise	1991	2000	128	695	569	5.0	100.4
4	12.343.12	Modum rør 12	1979	2001	123	771.1	616	5.5	94
5	173.28.1	Skjomen	1983	2001	10	1201	309	0.0	176
6	19.144.6	Stigvassåi rør 6	1971	2002	146	1077	590	5.5	85.9
7	16.231.9	Eikamoen rør 9	1979	2012	150	996	611	4.9	106
8	21.80.1	Evje rør 1	1982	2011	176	1388	570	6.2	71
9	56.3.2	Fana rør 2	1978	2003	51	2740	470	6.8	41.6
10	2.722.1	Finnbølseter rør 1	1977	2010	887	573	463	0.8	167
11	84.25.3	Førde/Moskog rør 3	1979	2007	53	2891	468	4.8	82
12	16.232.1	Groset grunnvannsrør 1A	1949	2004	952	728	432	1.1	159
13	2.724.9	Haslemoen rør 9	1981	2005	174	736	596	4.2	112
14	2.713.3	Hauerseter	1967	2011	216	797	583	4.8	108
15	28.14.2	Jæren rør 2	1979	2011	8	1498	463	7.9	28
16	111.14.2	Kårvatn rør 2	1981	2011	211	2002	401	1.9	141
17	23.17.4	Lindesnes rør 4	1980	2010	3	1371	457	7.7	37
18	2.721.1	Lykjestøylane rør 1	1977	2010	1050	1064	388	-0.8	188.8
19	313.12.7	Magnor rør 7	1977	2008	137	785	618	5.5	92
20	89.3.1	Nordfjordeid rør 1	1979	2008	69	2716	426	4.6	85
21	2.723.4	Settalbekken rør 4	1975	2010	957	622	383	-0.7	184
22	2.716.6	Stenerseter rør	1969	2010	604	752	486	0.7	164
23	196.47.2	Øverbygd rør 2	1979	2004	86	790	413	1.6	149
24	2.719.2	Øyangen rør 2	1977	2010	1071	641	417	-0.1	180

Table 2.2: Number of gaps with a certain length.

Length of gap	Number of gaps
Gap < 1 month	27628
1 < Gap < 4 months	176
4 < Gap < 12 months	40
Gap > 12 months	8

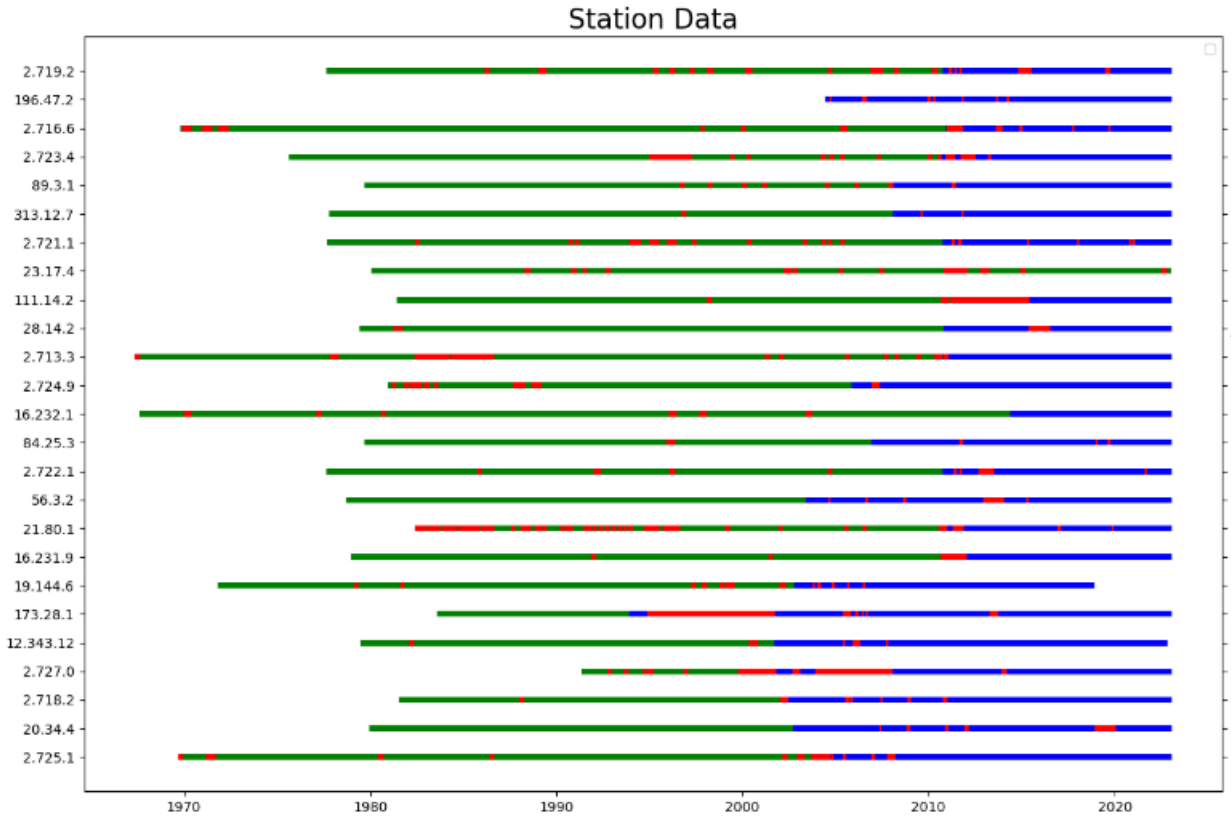

Figure 2.1: Periods with and without observation data for each groundwater station used in the study. Here the green colour marks periods with observations with a time resolution coarser than one day, and blue colour marks period with daily resolution. Red colour marks the periods with gaps in the data

grid. This is equivalent to a spatial distance of approx. 11 km. The data is simulated from 1950 until 2023. We extracted the data from the grid cell "closest" to our observation station in the time frame from the beginning of the observations until 2023.

Through all the calculations, we use the E-OBS estimated PET data as described in [Bakke et al., 2020a]. The E-OBS dataset provides Pennmann-Montheith based estimates of PET for the period 19981-2023. As we needed data of PET dating back to 1967, we used data estimated by Hargreaves method. The Hargreaves equation (2.1), described in [Allen et al., 1994], was applied to estimate the daily PET [$mm\ day^{-1}$] based on the E-OBS daily mean (T_{mean}), minimum (T_{min}) and maximum (T_{max}) air temperature [deg C] [Bakke et al., 2020a].

$$PET = 0.0023 * 0.408 R_a * (T_{mean} + 17.8) * \sqrt{T_{max} - T_{min}} \tag{2.1}$$

Where, R_a is extra-terrestrial radiation [$MJm^{-2}d^{-1}$], 0.408 is the constant for converting [MJ^{-2}] into [mm] ([Moeletsi et al., 2013]), and 0.0023 is an empirical coefficient. R_a, ($T_{max} - T_{min}$) and PET values are set to zero if they were negative. R_a is estimated using equation (2.2), as described in [Allen et al., 1994].

$$R_a = 37.6 * d_r * (\omega_S * sin(lat_r) * sin(\delta) + cos(lat_r) * cos(\delta) * sin(\omega_S)) \tag{2.2}$$

Where, d_r is the relative distance between Earth and Sun [-], ω_S is sunset hour angle [rad], lat_r is latitude in radians [rad], and δ is the solar declination in radians [rad]. The d_r, ω_S, lat_r and δ are estimated using the day of year (J) and the decimal degree latitude (lat), using Equation 2.3 - 2.6.

$$d_r = 1 + 0.033 * cos(0.0172 * J) \tag{2.3}$$

$$\omega_S = arccos(-tan(lat_r) * tan(\delta)) \tag{2.4}$$

$$lat_r = lat/57.2957795 \tag{2.5}$$

$$\delta = 0.409 * sin(0.0172 * J - 1.39) \tag{2.6}$$

In addition, hydro-meteorological data is extracted from the Norwegian database SeNorge (version 1.1). This data spans from 1957 to 2022 and covers Norway in a 1x1km grid. As with the E-OBS dataset, the data used where extracted from the grid cell closes to each station. SeNorge database, collected modelled data of total runoff from rainfall and snowmelt. The data is calculated using first temperature to differentiate between snow and rain. If it is under 0°C the precipitation is defined as snow and added to the snowpack. If the temperature is over 0°C, the precipitation is defined as rain, and added to the snowpack or considered runoff if there is no snowpack. In addition, if there is a snowpack and the temperature is over 0 degrees, the estimated snowmelt is added to the runoff [Engeset, 2016]. In addition, the model uses the energy balance with wind, cloud cover, incoming radiation and relative humidity as input to estimate the snowmelt [Engeset, 2016]. This model is sensitive to temperature errors around 0°C, since small inaccuracies could make the precipitation count as rain or snow.

2.3 Study area

2.3.1 Extent and topology

Norway is a topological and climatically varied country. It stretches from 57^o58 - 71^o08 North and 4^o56 - 31^o03 East, with a coastline stretching all along the western side. A prominent feature is a mountain chain, covering Norway from North to South. It divides the southern part of the country into; a western part with high topological gradients, and a undulating landscape on the eastern side. As shown in Figure 2.2, most of the stations are located in the southern half of Norway.

2.3.2 Climate

Because Norway is topological varied, meteorological conditions is also highly varied. In general, moist air from the prevailing westerly winds is forced up by the mountains. Here the air cools off and orographic precipitation occurs. Because of this, it can be a large difference in yearly precipitation between areas. This difference is highlighted in figure 2.3, where we see the mean annual precipitation in the period 1991-2020. Maximum yearly precipitation ranges from 6130 mm around Ålfotbreen on the west coast, to 212 mm in a small area in Saltdal in Nordland [Tveito, 2021].

In addition to mean annual precipitation, mean seasonal temperature differences have been compared between the two normal periods of 1961-1990 and 1991-2020. In Figure 2.4, we see the seasonal difference from the two periods. We see that the winter season show the larges difference. In addition, the largest change has been in the south eastern part of Norway.

Using the climate regions proposed by [Dyrrdal et al., 2012] for Norway, we divide the stations into 13 regions, with sub regions (Figure 2.5). The classifications are based on the [Hanssen-Bauer and Førland, 1998] division of monthly precipitation, where regions 2, 5, 6, 7 and 8 is subdivided into high- and lowland based on the general elevation under 1000 m.a.s. In addition, region 10 is divided based on the temperature regions proposed in [Hanssen-Bauer and Nordli, 1998].

The climate regions covering the stations is shown in table 4.4.

[Hanssen-Bauer and Førland, 1998] calculated trends in annual and seasonal precipitation, between 1897 to 1997. The results of the significant decadal trends of each region found in the study is shown in Table 2.4. The values are the % of the normal value per decade. Here the "s" and "ss" is denoting the significant level of the trend, with "s" being 95% and "ss"being at 99% confidence level.

In addition, [Dyrrdal et al., 2012] calculated the percentage change in each region for different metrics of precipitation (Am and Pot), maximum snow depth, snow fall frequency and days with near-0 temperatures (-1.5 to 1 ^{o}C mean temperatures). Table 2.5 shows the significant trends in the period 1958-2010, according to the regions of which the groundwater stations are located in. The values depicts the percentage change in the period and the parameters that are selected is:

- Pot10 : Frequency of events with total precipitation over 60 mm over 10 days.
- Max SD: The Maximum snow depth
- Near-0: Number of days with average daily temperature between -1.5 to +1.0 ^{o}C.

All in all we see that the general tendencies is a increasing temperature, with seasonal differences in magnitude (Figure 2.4, and more seasonal and annual precipitation, with regional differences (tables 2.5 and 2.4).

Figure 2.2: The locations of the 24 observation stations used in this study. For numbering of stations, see Table 2.6.

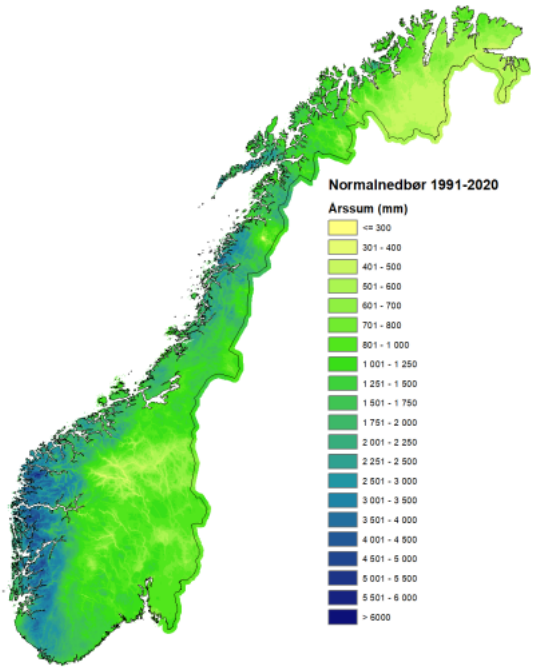

Figure 2.3: The mean annual precipitation over Norway calculated for the period 1991-2020 [Tveito, 2021].

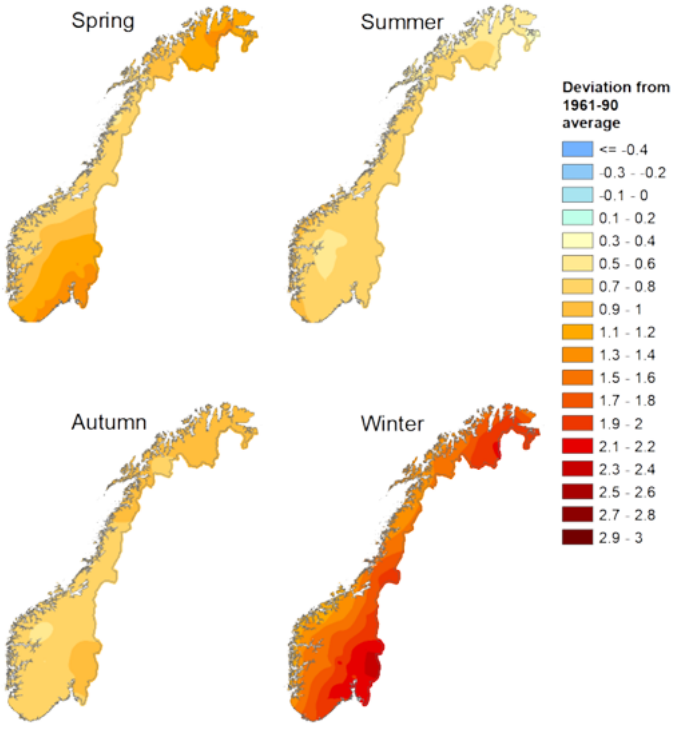

Figure 2.4: Figure from [Tveito, 2021], show the seasonal mean temperature difference between the 1991-2020 average and the 1961-1990 average.

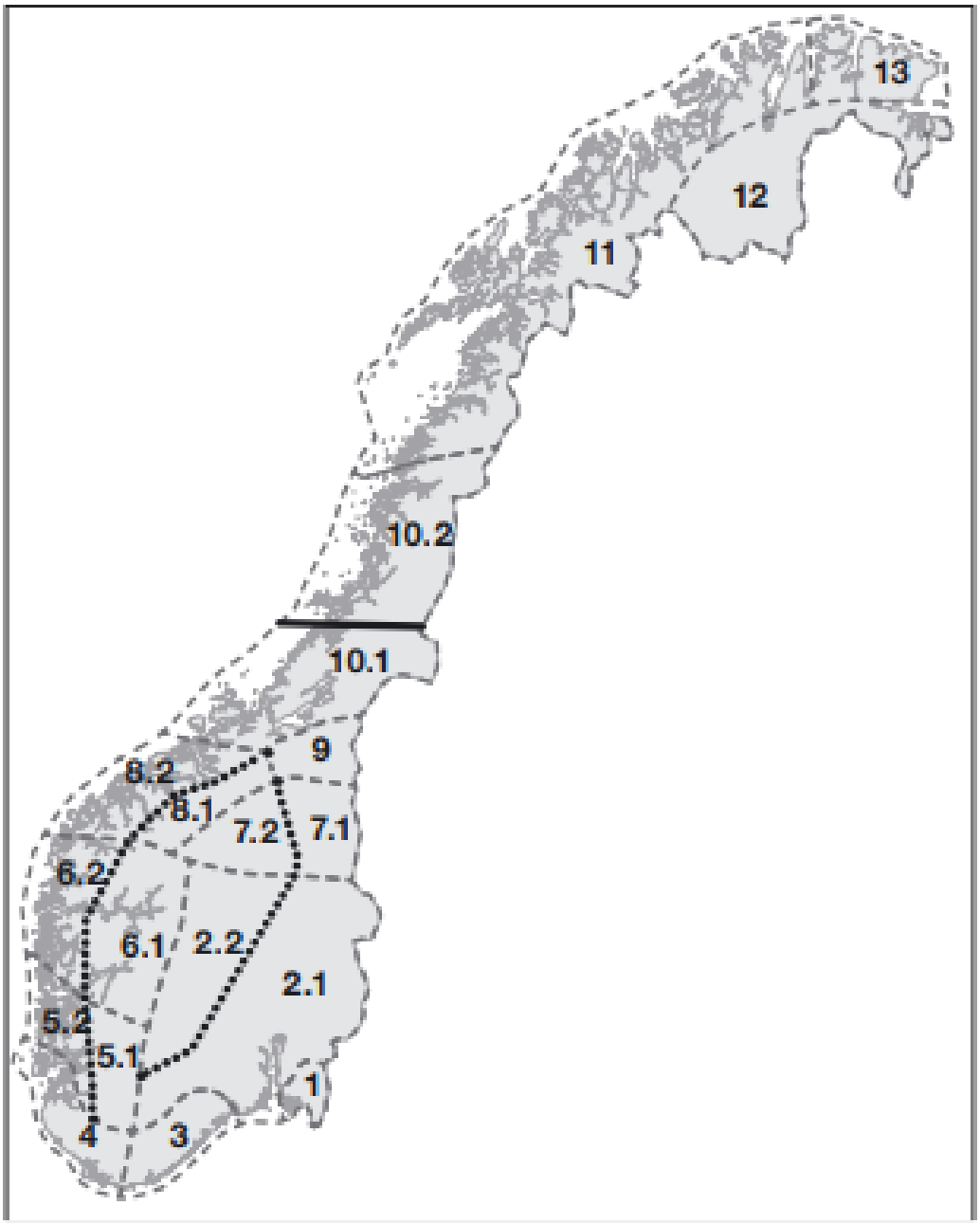

Figure 2.5: The climate regions of Norway as proposed by [Dyrrdal et al., 2012]. Here the precipitation regions are from [Hanssen-Bauer and Førland, 1998] and is marked with (- - -), the temperature regions as defined in [Hanssen-Bauer and Nordli, 1998] is marked with (___) and the sub-regions of high and low regions marked with (...). The Figure is from [Dyrrdal et al., 2012].

Table 2.3: Station number, ID and Name, with the corresponding climate region.

Station nr.	Hydra-Id	Station Name	Climate Region
0	2.725.1	Abrahamsvoll	7.1
1	20.34.4	Birkenes rør 4	3
2	2.718.2	Dombås rør 2	7.2
3	2.727.0	Kise	2.1
4	12.343.12	Modum rør 12	2.1
5	173.28.1	Skjomen	11
6	19.144.6	Stigvassåi rør 6	3
7	16.231.9	Eikamoen rør 9	2/3
8	21.80.1	Evje rør 1	3
9	56.3.2	Fana rør 2	5.2
10	2.722.1	Finnbølseter rør 1	2.2
11	84.25.3	Førde/Moskog rør 3	6.2
12	16.232.1	Groset grunnvannsrør 1A	2.2
13	2.724.9	Haslemoen rør 9	2.1
14	2.713.3	Hauerseter	2.1
15	28.14.2	Jæren rør 2	4
16	111.14.2	Kårvatn rør 2	8.2
17	23.17.4	Lindesnes rør 4	4
18	2.721.1	Lykjestøylane rør 1	2.2
19	313.12.7	Magnor rør 7	2.1
20	89.3.1	Nordfjordeid rør 1	6.2/8.2
21	2.723.4	Settalbekken rør 4	7.2
22	2.716.6	Stenerseter rør	2.1
23	196.47.2	Øverbygd rør 2	11
24	2.719.2	Øyangen rør 2	2.1

Table 2.4: Table is taken from [Hanssen-Bauer and Førland, 1998]. Here we see the decal annual and seasonal trends in the precipitation for the different regions from [Hanssen-Bauer and Førland, 1998]. Here the trends is given in % of the normal value per decade. Here, "s" is trends with 95%, and "ss" is trends with 99% confidence intervals.

Region	Annual	Winter	Spring	Summer	Autumn
1					+2.3% s
2					+2.3% s
3			-2.1% s		
4					+2.4% ss
5	+1.2% s				+2.2% ss
6					+1.8% s
7	+1.4% ss		+2.6% s		+1.8% s
8					
9	+1.3% s		+2.3% s		
10	+1.8% ss		+3.0% ss	+1.8% s	
11	+1.7% ss	+2.4% s	+2.5% ss	+2.0% ss	

Table 2.5: Table is a part from [Dyrrdal et al., 2012]. Here we see the significant average regional changes in percent for precipitation, maximum snow depth and days with near-0 temperatures in the period from 1958 to 2010. The precipitation is calculated for peak over threshold for 10 days with a threshold of 60mm. Days with near-0 temperature is defined as having an average day temperature between -1.5 to +1.0 ^{o}C. The "–" notation is given when there is no significant change.

Region	Precipitation (Pot10)	Max SD	Near-0
2.1	+12.6%	-21.6%	+27.9 %
2.2	+27.4%	–	+40.3%
3	–	-47.4%	–
4	+18.7%	–	–
5.2	–	–	–
6.2	+11.5%	–	–
7.1	–	–	+46.1%
7.2	+41.9%	+15.9%	+36.9%
8.2	+23.7%	–	–
11	+24.1%	–	+19.4%

2.4 Groundwater variation

In this study we use observations from stations in unconfined aquifers. Because it is in unconfined aquifers, we assume the observed groundwater level variation is connected to the variation in the hydrometeorology of the region. In addition, our measurements are point-specific, meaning that they are only representing a single geographical point of an aquifer in a groundwater system. This groundwater system could have a big extent and the different aquifers within the system could be varying differently within the same time frame. The recharge, as described in section 1, can occur both vertically and horizontally from surface water bodies. Under natural circumstances, groundwater is eventually drained into river, lakes or oceans, but it can also move upward toward the unsaturated zone where it is subjected to evapotranspiration ([Dingman, 2015]). In general, we can write the regional groundwater balance as Equation 2.7:

$$P + G_{in} = Q + ET + G_{out} \tag{2.7}$$

where P is precipitation, Q is stream outflow. ET is evapotranspiration, G_{in} is the water entering as groundwater and G_{out} is water leaving as groundwater. Here all the values for each parameter are a long-term time average, and have the dimensions $[L^3T^{-1}]$. Relating this water balance to an unconfined aquifer, looking only at the change in storage, which is only affected by natural processes, we can write Equation 2.7 as 2.8:

$$\Delta S = P - ET - Q_{net} \tag{2.8}$$

where we lump together the Q, G_{out} and G_{in} as the net groundwater discharge Q_{net} and ΔS is the change in storage. Since we want to look at the temporal variability and trends in the groundwater levels, we assume that the ground water horizontal fluxes remains constant in order to simplify the analysis. In addition, since all data is located in cold climate, we need to separate the precipitation input into snowmelt and rain. Hence, the groundwater balance becomes:

$$\Delta S = R + SM - ET \tag{2.9}$$

where R is rain and SM is snowmelt. This equation shows that the factors that drives the change in storage are the water input of rain (R) and snowmelt (SM), and the output of evapotranspiration (ET). In reality, there could also be input from nearby lakes and rivers, but no stations are close enough to be influenced by the water level.

Water movement through the soil is an important aspect when investigating trends and responsiveness of the groundwater. The ability of fluids to move through a porous media is determined by the hydraulic conductivity K_h $[\frac{L}{T}]$. In relation to groundwater, this is determined primarily by the characteristics of the soil. This can be used with the Darcy formula to describe vertical water movement (eq. 2.10).

$$q_{z'} = K_h(\Theta) - K_h(\Theta) * \frac{d\Psi(\Theta)}{dz'} \tag{2.10}$$

where z' is the vertical downward direction, the $q_{z'}$ is the downward flow rate, K_h is the hydraulic conductivity, Θ is the water content of the soil and $\Psi(\Theta)$ is the pressure head. Here we see that the vertical flow rate depends on the soil property (hydraulic conductivity), water content of the soil and the pressure gradient. Since both the hydraulic conductivity and the pressure gradients changes with the water content of the soil, the speed in which the water percolates down to the groundwater table is also changing [Dingman, 2015]. The minimum infiltration rate through the surface soil is approximately the saturated hydraulic conductivity of the soil [Dingman, 2015].

However, the speed at which the water percolate down to the groundwater table does not exceed the saturated hydraulic conductivity of the soil. In such a case where the water input (from rain or snowmelt) exceeds the infiltration rate, and the percolation rate, pooling occurs, and water accumulates on the surface. This excess of water on the surface will then create ponds, or drain to other areas if it is a surface gradient. This pooling and excess of water typically occurs in intensive precipitation events or with snowmelt in the spring season. In such a case, the total amount of water recharge to the groundwater is both determined by the water input, but also the time span of the input. If the input is intensive and short, a big amount of the water could drain off the surface. However, if the input is less intensive but long, the water has time to percolate down to the groundwater and a bigger portion of the water input ends up as groundwater recharge.

2.5 Groundwater regimes

The groundwater regime categorisation is a way to distinguish between different typical seasonal hydrological patterns [Kirkhusmo, 1988]. This is done by looking at the typical GWL maxima and minima. The two main regimes in Norway are the Atlantic and Mountain regimes. The Mountain regime has a clear GWL maxima in the spring/summer in relation to the snowmelt and soil thaw, while the GWL minima is in the months before the GWL maxima. The Atlantic regime has a minima in the late summer in relation to the high evapotranspiration and low precipitation. In addition, the winter is late, and the spring peak is early. In this regime, there is a relatively high amount of precipitation in winter. Combined with low soil frost cover, the recharge to the groundwater is also high as compared with the mountain regime. The third regime category is the transitional regime. This is a middle ground between the Mountain and the Atlantic regimes. Here, the yearly variations have two maxima and two minima. The maxima is related to precipitation and snowmelt. The minima is related to low winter recharge and high evaptranspiration combined with low precipitation in the summer, and soil frost and snow in the winter.

2.6 Hydrogeology

Vegetation acts as an "extractor" of water from the aquifer up to the surface and air. This is most important in the upper layer since the maximum root depth of the vegetation rarely goes deeper than a few meters. Therefore, this is an important factor for shallow aquifers. The geological setting is important factor when considering the responsiveness of the groundwater. Dense soils have low water capacity and hydraulic conductivity, and hence, the water percolation is slowed down. In general, vegetation can increase the potential transpiration, but some types can also preserve soil moisture and isolate the subsurface from the surface incoming radiation. Vegetation types like trees has deep roots compared to grass and peat and can connect the root zone with the groundwater level at deeper depths. From personal correspondence with Anne K. Fleig, January 18. 2023, the deposits, estimated soil type and dominant vegetation type within an estimated fraction of a 1x1 km^2 cell on the station, is given. This is then shown in Table 2.6.

Table 2.6: Station number, ID and name, with deposit type, soil type and dominant vegetation with fraction coverage of cell.

Station nr.	Hydra-Id	Station Name	Deposit	Soil type	Vegetation (fraction)
0	2.725.1	Abrahamsvoll	Thick moraine	Loamy sand	Forest (0.53)
1	20.34.4	Birkenes rør 4	Glacial-fluvial deposit	Sand (mSa)	Forest (0.72)
2	2.718.2	Dombås rør 2	River (moraine)	Sand (gSa)	Forest (0.54)
3	2.727.0	Kise	Thick Moraine/River	Loamy sand	Forest , Lake(0.8)
4	12.343.12	Modum rør 12	River	Sand	Forest (0.7)
5	173.28.1	Skjomen	River	Sand	Forest (1.0)
6	19.144.6	Stigvassåi rør 6	River	Sand	Forest (0.79)
7	16.231.9	Eikamoen rør 9	Glacial-fluvial deposits	Sand (mSa)	Forest (0.34)
8	21.80.1	Evje rør 1	Glacial-fluvial	Sand (mSa)	Forest (0.84
9	56.3.2	Fana rør 2	Thin moraine	Loamy sand	Forest (0.74)
10	2.722.1	Finnbølseter rør 1	Thick moraine	Loamy sand	Forest (0.5)
11	84.25.3	Førde/Moskog rør 3	Glacier river	Sand (mSa)	Forest (0.43)
12	16.232.1	Groset grunnvannsrør 1A	Thick moraine	Loamy sand	Forest (0.64)
13	2.724.9	Haslemoen rør 9	Glacier river	Sand (mSa)	Forest (0.8)
14	2.713.3	Hauerseter	Glacier river	Sand	Forest (0.71)
15	28.14.2	Jæren rør 2	Marine sand	Sand	Forest (0.19)
16	111.14.2	Kårvatn rør 2	River	Sand	Forest (0.88)
17	23.17.4	Lindesnes rør 4	Glacial-fluvial	Sand	Forest (0.81)
18	2.721.1	Lykjestøylane rør 1	Glacial-fluvial	Sand	Peat (0.8)
19	313.12.7	Magnor rør 7	River	Sand	Forest (0.79)
20	89.3.1	Nordfjordeid rør 1	Glacial-fluvial	Sand	Forest (0.38)
21	2.723.4	Settalbekken rør 4	Thick moraine	Loamy sand	peat (0.19), mountain (0.77)
22	2.716.6	Stenerseter rør	Thick moraine	Loamy sand	Forest (0.9
23	196.47.2	Øverbygd rør 2	Glacier River	Sand	Forest (0.99)
24	2.719.2	Øyangen rør 2	Thick moraine	Loamy sand	Peat (0.2), Mountain (0.8)

Chapter 3

Methods

The method used in this thesis is following analysing steps:

1. Gap-fill time series using Pastas model.
2. Derive groundwater indices.
3. Trend analysis.

In this chapter, the Pastas model section describes how we make the groundwater simulation model (step 1). The "Gap-filling method" chapter describes the method used to fill the gaps in the time series with the simulated data (step 2). The last several chapters describe the definitions and description of the groundwater indices used, and the method for trend estimation. The workflow is shown in the flowchart in figure 3.1,
sowing the input and output (black boxes), the tests and choices (blue boxes), with the models and methods (yellow boxes), for each step of the workflow.

3.1 Observation data check and processing

In quality checking the data, some unrealistic observation values at some stations were discovered at Kise (3), Lindesnes (17) and Øverbygd (23) stations. The unrealistic values for each station were:

- Kise (3) station: A unrealistic high value on the 5th of May 2001. The value showed a GWL of -0.045m, while the next day it was -1.59m. With significant autocorrleation of 276 days, this value was considered unrealistic.
- Lindesnes (17) station: A unrealistic low value on the 9th of September 2022. The value showed a GWL of -386 m which is two magnitudes lower than the rest of the GWL, and was therefore considered unrealistic.
- Øverbygd (23) station: A series of 28 consecutive values between the 9th of July to 5th of August. The first of the values were -8.8 m, then it jumped to -3.69 m the next day. For the following 5 days, the values were -3.69 m. For the rest of the values, they steadily increased from -3.69 m to -2.17m, before jumping to -1.6 m on the 29th observation point. This abnormal behaviour, in addition to that the lowest observation within the rest of the time series was -2.24 m, led to the conclusion that the 28 first values was unrealistic. Figure 3.2 show Øverbygd time serie were we see the unrealistic value (red points) as compared with the rest of the time series.

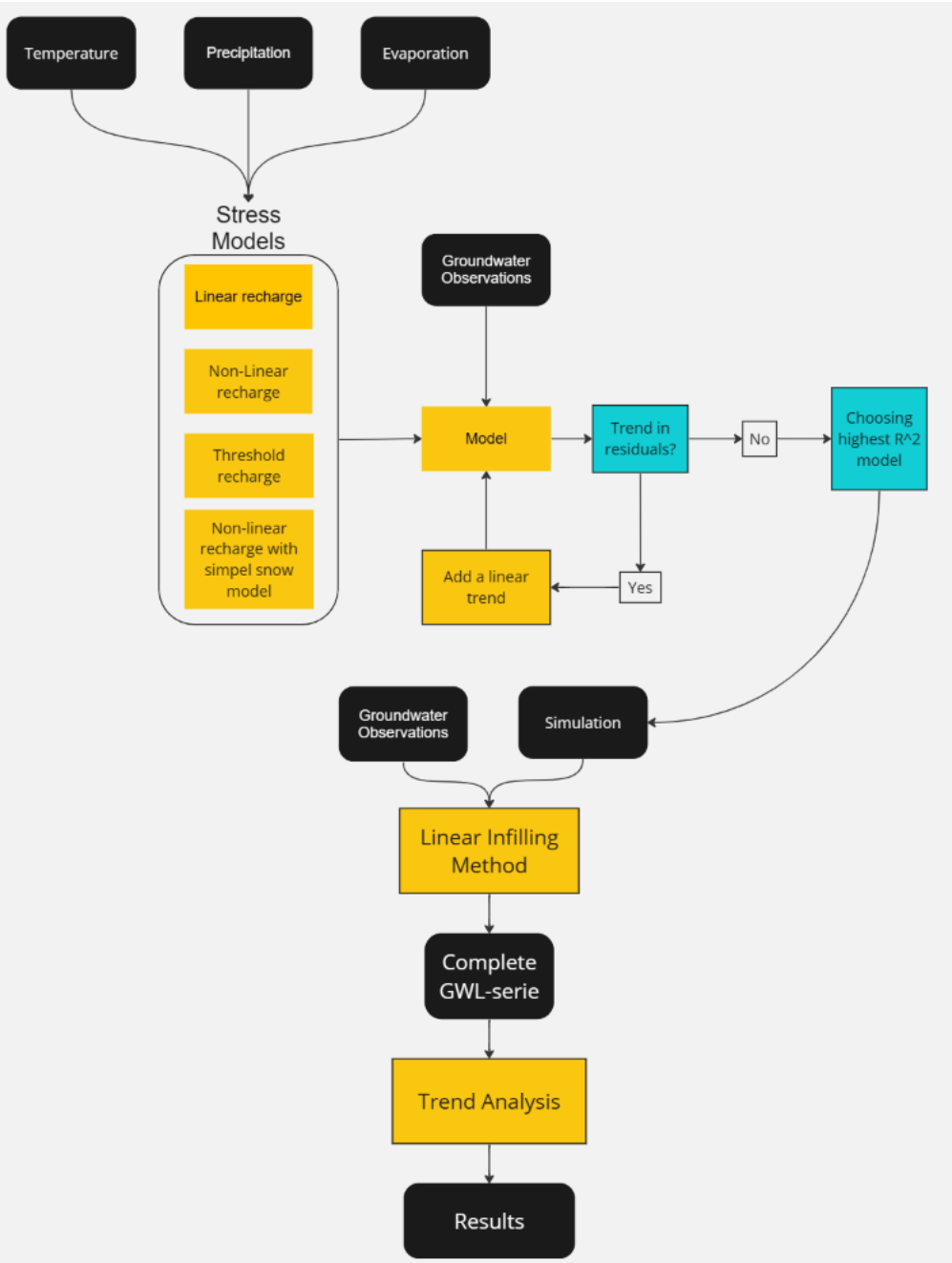

Figure 3.1: Flowchart of the working method. Here the black boxes represent the input and output. The yellow boxes are the operations that where conducted. Lastly the blue boxes are the tests and choices that were conducted.

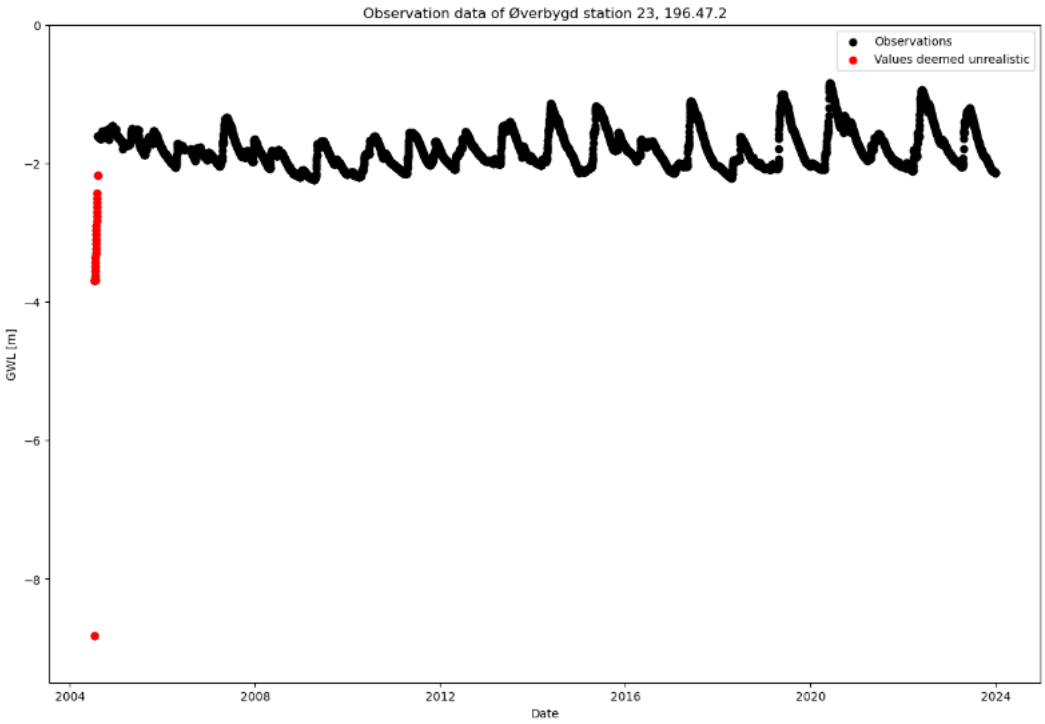

Figure 3.2: The unrealistic values is shown in red color, while the values deemed realistic is shown in black.

All the unrealistic values where deleted from the observation series. The rain and snowmelt data gathered from the SeNorge dataset covers the period between 1957 to 2022. Because we needed a warmup period of 10 year for the pastas model, only groundwater observations after 1967 were used. This only affected Groset (12) station, which has observation beginning in 1950.

3.2 Groundwater modelling using Pastas

To fill the gaps in the time series we want to simulate the groundwater level at each station. As shown in figure 3.1, we do this by making a groundwater model that takes in precipitation, evaporation, and temperature data as inputs, and fit a model to the observations. To do this we use the open-source modelling tool called Pastas [Collenteur et al., 2019]. Pastas is a python package, and is a tool specifically used to analyse the variations in the groundwater level measurements in observation wells. It is assumed that the main driving factors of the groundwater variations are the changes in the driving factors, referred to as stresses in the model, shown mathematically in equation 3.1

$$h(t) = \sum_{m=1}^{M} h_m(t) + d + r(t) \tag{3.1}$$

where $h(t)$ is the observed heads, $h_m(t)$ is the contribution of stress m to the head, d is the base elevation of the model, and $r(t)$ is the residuals. Each model can have an arbitrary number of stresses (M) that contribute to the head [Collenteur et al., 2019]. The contribution of each stress h_m is calculated through equation 3.2:

$$h_m(t) = \int_{-\infty}^{t} S_m(\tau)\theta_m(t-\tau)d\tau \tag{3.2}$$

where S_m is a time series of stress m, and ϕ_m is the impulse response function for stress m [Collenteur et al., 2019]. Here, the impulse response function translates the response from a instantaneous impulse from the input series [von Asmuth et al., 2002]. Different stresses have different impulse functions based on how they relate to the groundwater recharge.

The single stress input in the model can also be a combination of multiple stresses. A simple example of this can be the recharge $R(t)$ from precipitation ($P(t)$) and reference evaporation $E_r(t)$ as shown in equation 3.3

$$R(t) = P(t) - f * E_r(t) \tag{3.3}$$

where f is a parameter scaling the reference evaporation [Collenteur et al., 2019].

This works well for simple shallow groundwater levels in temperate climates, but for deep groundwater levels in arid climates one has to use a more complex recharge model. Therefore, we need to test different models at each station to find out what model type is preforming the best.

3.2.1 General workflow

In Python, we follow the Pastas seven-step workflow procedure from [Collenteur et al., 2019], to make a model for each station:

1. Import Pastas package.
2. Read the time series from files and store them as Pandas **Series** or **DataFrame** objects.
3. Create a **Model** object and supply the observed head series.
4. Create **StressModel** objects by supplying the observed stress and specifying a response function and add each **StressModel** object to the **Model** object.
5. Estimate the parameters of the **Model** and compute fit statistics.
6. Visualize output.
7. Analyse residuals and noise.

3.2.2 Input data

We start by importing temperature, precipitation and evaporation data over Norway, and use the nearest grid cell to each station to extract the data spanning from 10 years prior to the start of the observation until end of our analysis period (31.12.2022). Then we create a model using four different recharge models (as shown in Figure 3.1, and discussed in section 3.2.4), using the 10 years of input data as the warmup period. After this, we test the residuals for a possible trend using Mann-Kendall slope test. If there is a trend, we remove it by adding a linear trend in the model corresponding to the trend in the residuals. After removing all trends in the residuals of each model, we choose the model with the best R^2 score. This model simulated values are then used to fill the gaps in the observations with the fitting method (section 3.3).

In the preliminary study we tested two type of datasets to use as inputs in the models. The first sets where the 0.1x0.1 deg E-OBS grided dataset for precipitation, potential evaporation and temperature. The second dataset was to use the 0.1x0.1 deg E-OBS PET and temperature dataset in combination with the 1x1km gridded rain and snowmelt dataset from SeNorge. The third dataset that was tested was the 0.1x0.1 deg E-OPS PET dataset in combination with the rain and

snowmelt and temperature data from SeNorge database.

To decide the optimum dataset combination that we would use in the study, we compared performance of the best models R^2. From this we chose the 0.1x0.1 deg E-OBS PET and temperature data in combination with the 1x1km SeNorge rain and snowmelt data since it gave the overall best model performance.

3.2.3 Pastas response function

The groundwater level in an observation well is the sum of the individual effects on that groundwater level from the different stresses that act on the aquifer [Bakker and Schaars, 2019]. To estimate the response of the groundwater level to the changes in the stresses, the model fits a response function. The selection of which response function to use is based on the performance of the function to accurately simulate the groundwater variations in relation to the changes in stresses. One of the response functions is the exponential function, as shown in equation 3.4.

$$\phi_t(t) = A^a \tag{3.4}$$

This function has one scaling factor A and a shape parameter a. The most common response function for groundwater recharge is the scaled Gamma function shown in equation 3.5 ([Besbes and De Marsily, 1984, von Asmuth et al., 2002]).

$$\phi_p(t) = A\frac{t^{n-1}}{\alpha^n \Gamma(n)} e^{\frac{-t}{\alpha}} \qquad for \quad t \geq 0 \tag{3.5}$$

where A is the scaling factor, a and n are the shape parameters, and Γ is the gamma function.

Block Response The block response is the response of the stress acting in one day. As an example, we can see how the head changes with a one-day rainfall. The head will first increase, and then go back to its initial level. The total time from the start of the rainfall and when the head is back at its initial level, is called memory, t_{mem} [Bakker and Schaars, 2019]. This can be interpreted as an estimation of the autocorrelation or accumulation period of the aquifer.

Step Response The step response is the response due to continuous rainfall. If it is raining at a constant rate for a long period, we assume that the head eventually reaches a plateau. This plateau is called the gain of the response function [Bakker and Schaars, 2019]. This plateau can be interpreted as the maximum percolation rate into the aquifer. In addition, it estimates the time it takes to reach this maximum percolation rate given a constant rate of precipitation.

3.2.4 Pastas recharge model

In Pastas, stresses can be combined with a specific recharge model. This model can vary, but it relates sum of the stresses to the variation of the groundwater [Collenteur et al., 2019]. In this thesis we test four different recharge models at each station and compare them to determine what is the best model to use. The four recharge models we test are:

- **Linear recharge model**

  The "linear recharge model" uses a linear relationship between the stress parameter and response to estimate the groundwater level. This is best suited in situations where there is a shallow groundwater table, homogeneous sediments and the response time is relatively short. This recharge model is shown in equation 3.3. It simplifies the soil and unsaturated

zone processes to achieve a simple model with two assumptions; (1) The head is linearly responding to the precipitation and evaporation, independent of the state of the system. (2) The evaporation is not water limited and occur at the rate of f times the evaporation [Collenteur et al., 2023]. This way, the recharge can be both positive and negative. This is done by using the **ps.rch.linear()** function in the recharge model.

- **Non-linear recharge models**

  The Non-linear recharge model is using a Non-linear relationship between the stress parameters and the response of the groundwater. It uses a soil-water balance approach, where precipitated water, exceeding the interception capacity, continues to the root zone storage. Here the infiltrated water is temporarily stored and released as soil evaporation and transpiration, or groundwater recharge [Collenteur et al., 2023]. The water balance of the root zone over time is:

$$\frac{\Delta S_r}{\Delta t} = P_e - E_{t,s} - R \tag{3.6}$$

  Where $S_r[L]$ is the amount of water within the root zone and R is the recharge to the groundwater , and the $E_{t,s}[LT^{-1}]$ parameter is the combined evaporation from the soil and transpiration from the vegetation [Collenteur et al., 2021].The saturation at the beginning is set to half of the maximum storage capacity, and the evaptranspiration is limited by the water available in the root zone:

$$E_{t,s} = (E_{max} - Ei)min(1, \frac{S_r}{l_p * S_{r,max}} \tag{3.7}$$

  Here, l_p determine what fraction of $S_{r,max}$ the evaporation flux is limited by the availability of the soil water [Collenteur et al., 2021]. E_{max} is the maximum potential evaporation and is calculated as follows:

$$E_{max} = k_v E_p \tag{3.8}$$

  Where E_p is the potential evaporation and k_v is a parameter that needs to be calibrated. With this the, the recharge to the groundwater can be calculated as:

$$R = k_s(\frac{S_r}{S_{r,max}})^{\gamma} \tag{3.9}$$

  where $k_s[\mathrm{LT}^{-1}]$ is the saturated hydraulic conductivity, S_r is the storage capacity of the root zone, $S_{r,max}$ is the maximum storage capacity of the root zone, and γ is a parameter determining the non-linearity of the recharge flux with respect to the saturation of root zone [Collenteur et al., 2023].

  This is a more hydrological accurate model as compared with the linear model, and is better suited in situations with deep groundwater tables, homogeneous to semi homogeneous sediments and a long response time. However, it comes at a cost of six more parameters where the maximum interception capacity is fixed at 2mm, and the saturation of the root zone where actual evaporation is equal to the potential evaporation is fixed at $L_p = 0.25$. The rest of the new parameters, k_s, γ, $S_{r,max}$ and k_v is calibrated by the model [Collenteur et al., 2023]. This is done by using the **ps.rch.FlexModel()** in the pastas toolbox.

- **Non-linear recharge model with snow**

  The Non-linear recharge model with snow is adding another step to the Non-linear recharge model structure. It uses a temperature threshold to divide the precipitation into snow or rain. If the temperature is under the threshold, precipitation is defined as snowfall and added to a snow storage. If the temperature is over the threshold, the precipitation is defined as rainfall, and (if a snowpack is present) snowmelt is calculated using the degree-day method and added to the rainfall[Collenteur et al., 2023].

  The model requires temperature data and two extra parameters that has to be calibrated. The first parameter is the temperature threshold T_t, this is set to 0^oC. The second parameter is k in the degree-day factor shown in equation 3.10.

$$Melt = \begin{cases} 0 & if \quad T \leq T_t, \\ k(T - T_t) & if \quad T > T_t \end{cases} \tag{3.10}$$

  Where the $Melt$ is the total snowmelt resulting from the snowpack. Because of the added snow scheme, this model is more suited for locations with many snow days throughout the year. This is done by using **ps.rch.FlexModel(snow=True)** in the Pastas modelling toolbox.

- **Threshold recharge models**

  The threshold recharge model is made by using the "threshold autoregressive self-exciting open-loop (TARSO)" method [Knotters and De Gooijer, 1999]. It fits two exponential response functions to simulate the recharge. The model uses the exponential function depending on the simulated value is over or under the threshold. This gives a non-linearity to the model [Knotters and De Gooijer, 1999]. The TARSO model needs to estimate seven parameters in total; A0, a0, d0, A1, a1, d1 and f. Here the notation 0 and 1 refers to the corresponding exponential functions and A, a and d are the parameters as shown in equation 3.4. The parameter f is the multiplication factor of the potential evaporation as shown in equation 3.3. A physical interpretation of the TARSO model structure is that the saturation of the subsurface changes the response. Such a model is well suited for situations where there is an apparent threshold of the groundwater level. This is done by using the **ps. TarsoModel()** in the pastas modelling toolbox.

3.2.5 Parameter estimation

Estimating the parameter of the response and recharge functions is crucial in getting a good fit. Depending on the model, we need to calibrate 6 - 11 parameters. All parameters are shown according to model type, boundaries and fixed value in Table 3.1.

Table 3.1: Taken from [Collenteur et al., 2023], shows the parameters that are used in the different models, with their corresponding fixed value or boundary. Her is μ_r the mean of the residuals [Collenteur et al., 2023].

Model	Parameter	Units	Bounds	Fixed value
Base	d	m	-	μ_r
Recharge response	A	-	[1e-9, ∞]	
	α	d	[1e-2, 2e3]	
	n	-	[1e-2,1e2]	
Linear Model	f	-	[-1.5, -0.5]	
Non-Linear Model/ Non-Linear snow Model	kv	-	[0.5, 1.5]	
	$S_{i,max}$	mm	-	2
	$S_{r,max}$	mm	[1e-5, 1e3]	
	k_s	mm/d	[0, 1e4]	
	l_p	-	-	0.25
	γ	-	[1e-5, 20]	
Non-Linear snow Model	T_t	^{o}C	-	0
	k	mm/^{o}C/d	[1, 20]	
Threshold Model	$A0/A1$	-	[1e9, ⊛]	
	$a0/a1$	d	[1e2, 2e3]	
	$d0/d1$	m	-	μ_r
	f	-	[-1.5, -0.5]	
Noise	α	d	[1e9, 5e3]	

It is important to have good initial condition if possible to arrive at the best parameter values. For some of the parameters, good initial values can be specified. For example, the parameter d in equation 3.1 is commonly estimated as the mean of the observed heads $h(t)$, and the scaling parameters of the response functions (A in equations 3.4 and 3.5), are computed as $\frac{1}{\sigma_S}$, where σ_S is the standard deviation from the stress time series [Collenteur et al., 2019].

Parameter boundaries are also limited to a range with physical meaning. For example, the scaling parameter A of the Gamma function (3.5) has a lower boundary of 0, so the head will increase in response to a positive recharge. The evaporation factor f is bound to the range 0 to -2, so that the actual evaporation can vary from 0 to at most 2 times the reference evaporation [Collenteur et al., 2019]. For the calibration, Pastas use a nonlinear least squares algorithm to minimize the sum of weighted square of noise following [von Asmuth and Bierkens, 2005]. We calibrate the parameters for each model using all observation data.

3.2.6 Metrics of goodness of fit

There are different methods to evaluate how well a model simulate the observed values. The different methods to quantify the error have different approaches, but we can divide them into two general categories; The relative change metrics and absolute change error metric. Whereas the relative change metrics are dimensionless, the absolute change metrics have the same dimensions as the data [Jackson et al., 2019].

We want to use the model to fill in the gaps in the observation data. Since we use linear scaling to interpolate values between the gaps (section 3.3), the simulation does not need to simulate accurately the groundwater level. However, it is important to simulate the variation of the groundwater well. For this reason, we chose the R^2 metric to determine which model to use for

each station.

Coefficient of variation (R^2)

The Coefficient of variation R^2 is a relative error metric of the variance percentage error. It is $0 \leq R^2 \leq 1$, has no unit and does not indicate bias. We calculate it by taking the ratio of the explained variance to the observed variance. Therefore, it is a estimate of how much variance the simulation captures as compared with the variance of the observations. The R^2 is calculated according to equation 3.11:

$$R^2 = 1 - \frac{\sum_{i=1}^{N}(y_i - \hat{y}_i)^2}{\sum_{i=1}^{N}(y_i - \overline{y})^2} \tag{3.11}$$

Where y_i is the observation point i, $\hat{y}_i$ is the model estimated value at point i and $\overline{y}$ is the average of all the observation values. Pastas has built in weighted R^2 metric to account for the bias created by the often-occurring temporal change in observation point density. The R^2 equation is therefore weighted according to the data density as shown in equation 3.12:

$$R^2_w = 1 - \frac{\sum_{i=1}^{N} w_i'(y_i - \hat{y}_i)^2}{\sum_{i=1}^{N} w_i'(y_i - \overline{y})^2} \tag{3.12}$$

where w_i' is the weight assigned to point i to account for the observation density bias. All other symbols are as equation 3.11. We use this weighted R^2 value to evaluate the models and determine what is the best preforming model.

3.2.7 Sources of uncertainties

As explained in [Bakker and Schaars, 2019], challenges in using Pastas are how to assess the goodness of fit of the model and how to improve the model performance. There are statistical metrics we use to assess how good the model is. The main metrics used in the Pastas package are root mean squared error (RMSE) and the percentage of variance explained (coefficient of determination (R^2) or Nash-Sutcliffe coefficient). As stated in 3.2.6, we only use the inbuilt weighted R^2 metric (Equation 3.12) to determine the performance of the model.

The second challenge is to improve the model if is a poor fit. After checking for any elementary errors in the inputs or model implementation, the main challenges are [Bakker and Schaars, 2019]:

1. Inaccurate head measurements, for example poorly installed or leaky observation wells, or problems with automatic pressure transducers.

2. Missing or incomplete stresses, for example undocumented and/or illegal pumping, unknown surface water level variations, a regional decline in heads caused by an overall increase in pumping, or stresses that are not measured before the change that is to be evaluated.

3. Inaccurate stresses, for example poor potential evapotranspiration, temperature and rainfall estimates from weather stations that is too far away or modelled data.

4. Overparametrization, for example not enough data and/or too complex a model to estimate the parameters.

5. Convergence to a local optimum, for example the parameter estimation algorithm finds a local optimum but misses the global optimum.

6. Missing processes, for example recharge is simulated as a linear function of measured rainfall and reference evaporation while the relationship is nonlinear, or drainage systems prevent the head from rising above the level of the drains.

7. A change in the system behaviour, for example land-use change has changed the relationship between rainfall, reference evaporation, and recharge. Or a stream is dredged or deepened, as such removing or reducing the leaky stream bed, resulting in a different response function.

The challenges related to points 1,2 and 7 are generally accounted for by using the quality checked data (Section 2.1) by NVE. The other points are not directly handled for and need to be taken into account.

Time frequency model bias

The changes in observation frequency are generally accounted for in the pastas modelling package when using a noise model. However, the amount of data points used as a basis for generating the model could give the model a bias. The difference between a 30-day and a 1-day observation frequency makes the model to tend more to fit the parameters to the observation heavy part of the time series. This could lead to a bias in the response and stress estimation. This could then make it difficult to make a good model, and it could be difficult to identify a change in the response of the groundwater.

3.3 Gap filling method

As discussed in section 1.2, we want to complete our observation series before conducting the trend analysis. We want to achieve a daily temporal resolution through all our data. This means that we need to fill the gaps exceeding one day in the observation data. We do this by using the simulated data from the hydrological models created using Pastas. The advantage of this is that the variations seen in the simulation is explained by changes in the meteorological drivers. Thus, the infilled values would be consistent to the hydrological principles of groundwater recharge at the complexity of the model we use.

Such models are rarely simulating the groundwater level perfect at all time steps. Therefore, simulated values might be differing from the observation values, even though they have a high R^2-score. Because of this, we develop a method to shift the simulated values to fit with the observation data, while preserving the hydrological accurate variations from the model. The method uses linear scaling of the simulated values. First, we calculate the difference between the observation and simulation in the points just before and after the gap (dy_0, dy_n). Then we create a line that goes through dy_0 at t_0 and dy_n at t_n, where n is the number of days in the gap. Lastly, we use this line to shift the simulated values. Mathematically this can be defined as equation 3.14.

$$f(i) = (y_0 - \widehat{y_0}) + \frac{(y_n - \widehat{y_n}) - (y_0 - \widehat{y_0})}{N+1} * i \tag{3.13}$$

$$y_{adj}(i) = \widehat{y_i} + f(i) \qquad where \quad i \in \mathbb{N}[0, N+1] \tag{3.14}$$

where y and $\hat{y}$ is observation and simulation values respectively, the notation 0 and n refer to the points before and after the gap, n is the number of days in the gap, and i is the numbered days in the gap.

This method is conceptually shown in figure 3.3. The figure shows how we use the last point before the gap and last point after the gap (upper-right corner graph), to fit a "difference line". We use this line to interpolate for each daily point in the gap (Green points Figure 3.3).

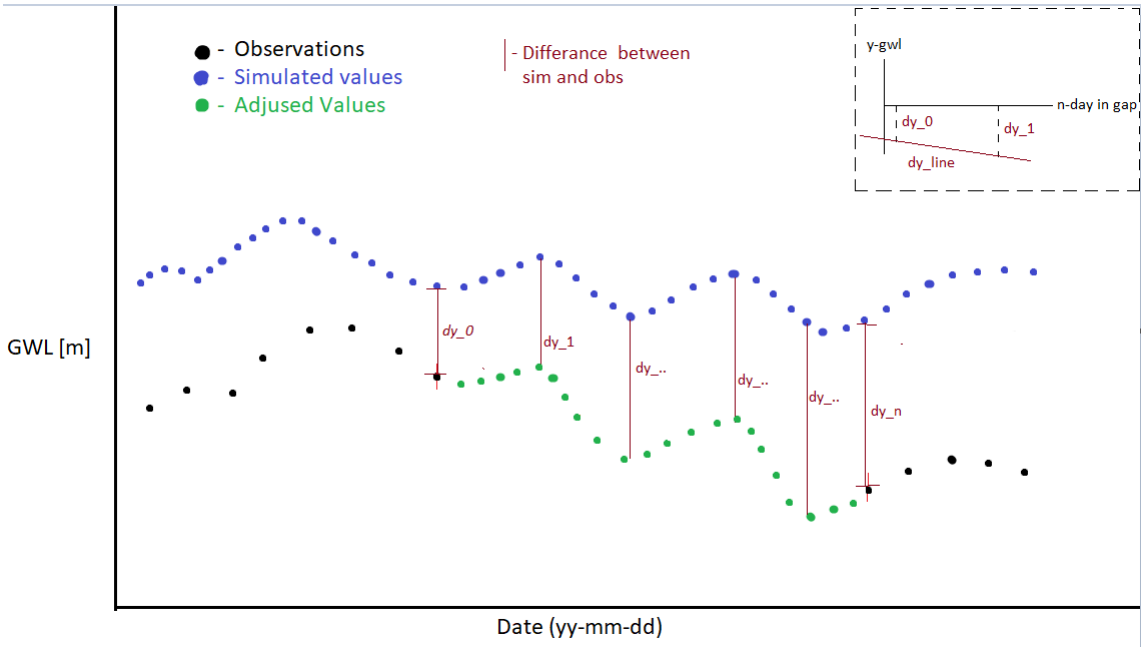

Figure 3.3: A conceptual sketch of the infilling method. Here the blue values are the simulated groundwater level (GWL) values from the model, the black dots are the observations and the green dots are the infilled. The red lines with notation $dy_0 ... dy_n$ is the value at each point from 0 to n is shifted with.

Using this method, we could be in danger of shifting the simulated values over, or under, what is a realistic value. This could be in the case where our model is simulating an increase (or decrease) in GWL due to an extreme event, and because of our shifting, the resulting values become too high (or low). To avoid this problem, we assume that the maximum and minimum observed values are not exceeded in the gaps between the observations. In this chase, we set the shifted value equal the maximum or minimum observed value.

3.4 Groundwater regimes

The groundwater regime categorisation is based on Kirkhusmo (1988), using the operational definitions by [Bakke et al., 2020b]. It uses the groundwater fluctuation patterns to divide them into idealised regions, with the possibility of a time shifted version [Bakke et al., 2020b]. These categories are similar to the stream flow regimes presented in [Gottschalk et al., 1979], but with a delay added due to the groundwater lag. The three main regimes are based on the groundwater maxima and minima. The first region is the Atlantic regime, with maximum groundwater levels in late winter or early spring, and the minimum in late summer. The second regime is the Transition regime, and consist of two annual maxima and minima that typically occur in the months between April to June. The third regime is the Mountain regime, with a minimum just before the snow

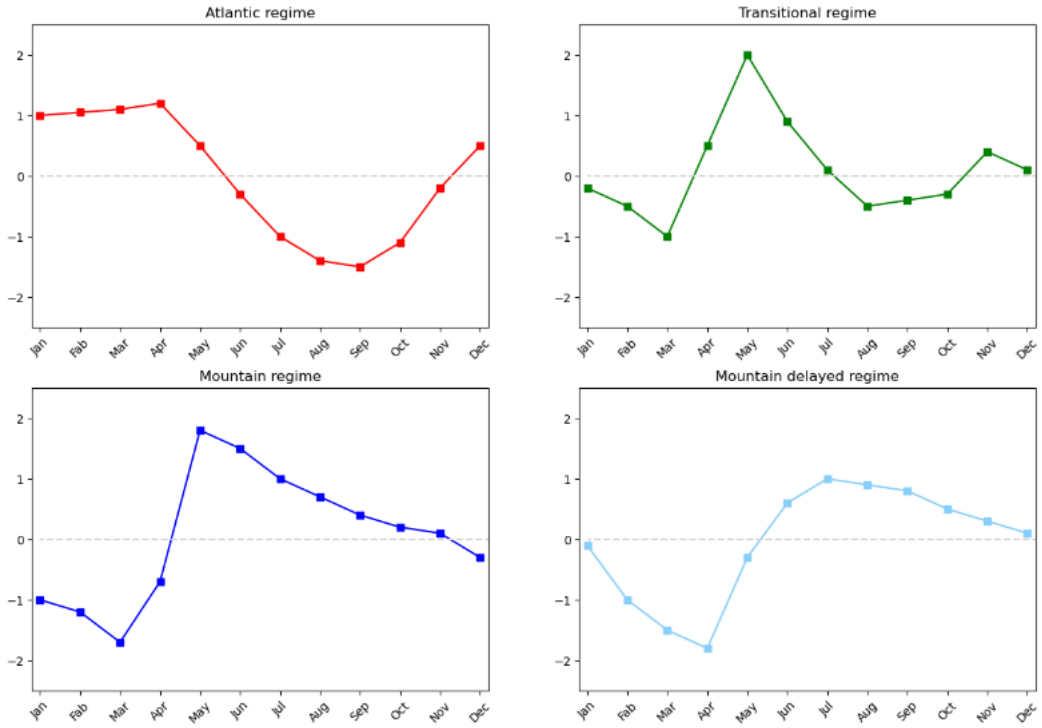

Figure 3.4: The figure is modified from [Bakke et al., 2020a], and is based on the groundwater regimes form [Kirkhusmo, 1988]. Here we see the idealized groundwater regimes witch we categorise our stations from.

melt and maximum just after the snow melt [Bakke et al., 2020b]. The idealized schematic of the different regimes is shown in Figure 3.4.

We use the whole time series at each station to calculate the typical regime. By calculating the average GWL for each month, we record the first, second and third wettest and driest month. Based on this we assign a regime to the distinct groups. The Atlantic regime is characterized by the groundwater level maxima caused by precipitation and minima caused by the high evapotranspiration and low precipitation. Therefore, if the three months with highest groundwater level occur in October-April or in January-May, and the three lowest levels are in the summer months (June-December), we classify the station as Atlantic regime.

Mountain regime is characterized by the dominant snowmelt related high groundwater level, and snow accumulation related low groundwater level. If the months with the highest groundwater levels is in April-July, and all three months with lowest levels are in December-May, the station where classified as Mountain regime.

If instead of during April-July, the three months with highest groundwater level occur in May-November and the three months with lowest groundwater level still occur in December-May, we assume a time-lag effect and the station was classified as Mountain regime delayed [Bakke et al., 2020b].

The Transitional regime is characterized by transition to secondary or dominant rain event related high groundwater level. Here if neither of the above and the groundwater level has two minima and maxima, the groundwater is categorised as Transitional regime.

The Atlantic regime delayed is classified when the three months with the highest groundwater level occurred in April-July and the three months with the lowest groundwater level occurred in October-January.

3.5 Autocorrelation

Correlation is a measure of how similar or dependent two series are. This is used to determine if the two series is somehow related to each other. Autocorrelation is the series dependencies to a shifted version of itself. This is then often used to give an estimate on how much a given value x_k is related to the previous values $x_{k-1}, x_{k-2}...x_0$.

In relation to groundwater, this is used to determine the temporal lag of the aquifer in response to an impulse recharge event. In a physical sense, this lag says something about how long a signal is an explaining factor of the groundwater level. In a statistical sense, the autocorrelation reflects the temporal dependency of the data and consequently, the minimum time span we can assume independence.

In this study, we calculate the autocorrelation at 95 % significance at each station. We use this to determine the serial independence of the time series at each station. If the time series has an autocorrelation over 1 year, we use the maximum significant autocorrelation to create subsets of the data with a temporal spacing exceeding the significant autocorrelation. This way, each point in the subset is serial independent from each other.

3.6 Groundwater indices

In order to analyse changes in different aspect of the groundwater variation, we computed the following groundwater indices based on the complete (gap-filled) series:

- Monthly average GWL
- Yearly average GWL
- Period Maxima and Minima GWL
- Occurrence of period Maxima and Minima for Mountain regime stations

The average GWL for each year is calculated at each station. This is then used for calculating the yearly GWL trends. For the stations with autocorrelations over 12 months, the yearly average for each year of the time series were calculated. Then, a sample of values were taken with a temporal step of the significant autocorrelation plus one year. For example, if a station had 18 months significant autocorrelation, then the sample would be the values of every two year.

The average groundwater level of each month is calculated and stored in separate series for each station. This way, it is 1 year between each point in each series and we avoid any autocorrelations for stations with a lag under 1 year. This is done so that we can examine each month separately, and check for trends in each month. For the stations with autocorrelations over 12 months, the same procedure as with the yearly average would be performed with the monthly values.

The high and low head series are based on the daily GWL within a time period. This is to check if we can identify any changes in the magnitude of the driest or wettest months. The periods are decided by the typical wettest and driest month at each groundwater regime. The period for each regime is shown in table 3.2.

Table 3.2: Periods used to extract the high and low GWL for each regime.

Groundwater Regime	High period	Low period
Atlantic regime	September-April	April-November
Transitional regime	October-July	July-May
Mountain regime	March-August	September-July
Mountain delayed regime	March-October	November-July

If a station had significant autocorrelation over 1 year, then a sample would be taken according to the procedure described with the yearly average series.

In addition, we want to examine the timing of the snow melt recharge peak in GWL in stations within the Mountain regime. To do this, we determine a period for each station based on the typical groundwater variations through the year at the station. We then make a period from 3 months before, to 3 months after the typical GWL peak. We then save the groundwater level in each day that is within the relevant months for each year. Then, each saved data point is given a number (timing number) according to how many days it is between the data point and the start of the period. After that, We select the data point with the highest (or lowest) groundwater level in each period. We then conduct the trend test on the timing number for all the selected data points. The outcome should then show if there is a trend in timing within the period. In Table 3.3 we see the period for each station in which we select the dates from.

Table 3.3: Periods used to extract the high and low GWL at each region.

Station nr	Station ID	Maxima period	Minima period
16	111.14.2	Feb-Jul	Nov-Apr
12	16.232.1	Mar-Aug	Dec-May
0	2.725.1	Mar-Aug	Dec-May
10	2.722.1	Mar-Aug	Dec-May
23	196.47.2	Mar-Aug	Nov-Apr
5	173.28.1	Mar-Aug	Nov-Apr
2	2.718.2	Mar-Aug	Dec-May

3.7 Trend analysis

To estimate any changes in groundwater variation over time we use the ranked-based Mann-Kendall (MK) trend test [Mann, 1945, Kendall, 1975]. This is a non-parametric method for trend detection, and therefore, it can be applied regardless of the probability distribution of the data [Önöz and Bayazit, 2012]. One important assumption of the Mann-Kenndall test is that the data is serially independent (i.e. not autocorrelated). Therefore, we need to pre-process the data such that we have only independent data. We do this by first checking the auto correlation of station, and then choosing data points that are spaced longer than the auto correlation.

The direction and magnitude of the trend is then calculated with the Sen's slope [Sen, 1968]. We use the python package "**pymannkendall**" to calculate the Sen's slope and Mann-Kendall test of our data. Sen's slope and Mann-Kendall are based on the linear slope (m_k) between each possible pair of values in a series, as shown in equation 3.15.

$$m_k = \frac{y_j - y_i}{t_j - t_i}, \quad \text{where} \quad \begin{matrix} k = 1, 2, ..., \frac{n(n-1)}{2} \\ i = 1, 2, ..., n-1 \\ j = 1, 2, ..., n \end{matrix} \tag{3.15}$$

Here, n is the length of the time series, y_i and y_j is the variable values of the time step t_i and t_j respectively [Bakke et al., 2020a].

3.7.1 Mann-Kendall trend test

The significance of the slope is calculated by using a test statistic (Z_S) approximated from a normal distribution, as given by equation 3.16 [Bakke et al., 2020a].

$$Z_S = \begin{cases} \frac{S-1}{\sigma_S} & S > 0 \\ \frac{S+1}{\sigma_S} & S < 0 \\ 0 & S = 0 \end{cases}, \quad where \quad S = \sum_{k=1}^{n(n-1)/2} \begin{cases} -1 & m_k < 0 \\ 1 & m_k > 0 \\ 0 & m_k = 0 \end{cases} \tag{3.16}$$

$$and \quad \sigma_S = \frac{n(n-1)(2n+5)}{18}$$

Positive values of Z_S indicate increasing trends, while negative Z_S values indicate negative trends. Testing the trends is done for specific significance levels α. If the $|Z_S| > Z_{1-\alpha/2}$, the null hypothesis of no trend is rejected, and a significant trend exist. The $Z_{1-\alpha/2}$ value is found in the normal distribution table.

3.7.2 Sen slope

Sen's slope is defined as the median of all slopes from equation 3.15. The N values of m_k are first ranked from smallest to largest, and the median of the Sen's slope estimator is computed as equation 3.17.

$$m_{k_{med}} = \begin{cases} m_{k_{[(N+1)/2]}} & , \quad if\ N\ is\ odd \\ \frac{m_{k_{[N/2]}} + m_{k_{[(N+2)/2]}}}{2} & , \quad if\ N\ is\ even \end{cases} \tag{3.17}$$

were the sign of $m_{k_{med}}$ reflects the direction of the data trend, and its value reflects its steepness [Sen, 1968].

3.7.3 Choice of periods

In order to compare the trends between stations, trends were calculated for the periods 1982-2022 and 1992-2022. The two overlapping periods were decided on by having as many stations as possible while having the longest period as possible. In addition, for stations that had time series data close to the start of the set periods, the trends were calculated and implemented in the tables with a notation. This was done to get as much information as possible. With the trends from the two periods, we can compare how the trends change by including the years between 1982 and 1992.

To investigate how the trends are changing over time, we apply "**Multi temporal trend plots**" with a base level of 20 years. This is a method for visualisation of the shifting trends depending on different periods inspired by [Hannaford et al., 2013]. We start to calculate the trend of a 20-year period from the beginning t_0 of the time series, and adds one year at a time, updating the trend slope. This first calculation is the first column in the nXm matrix. The second column starts at $t1 = t_0 + 1$ year and the 20-year trend is then calculated with subsequent $20 + n$ year period trends afterwards. This continue until we reach the $t_n = 01/01/2003$, which is the minimum start date, since the time series is ending at 01/01/2023.

In the trend plots, we show the p-values from the Mann-Kendall trend test (Equation 3.15). This gives an estimate on the significance on the trend in different periods. The trend directions of the Sen-Theil slope estimates are provided for the significant trends.

Chapter 4

Results

4.1 Groundwater model performances

At each station, a Linear model, Threshold model, Non-linear model without snow scheme and a Non-linear model with a snow scheme (section 3.2.4) was tested, and the best model was chosen. Figure 4.1 shows a map over Norway and the resulting best preforming model type at each station, along with its R^2 score in color. The stations where the "Linear- and "Non-linear models" are preforming the best, is located in the south east part of Norway. They are all in the Transition or in the Mountain delayed regime, and they have all relatively deep groundwater table with high auto correlation.

In Figure 4.2 we see an example of Fana station (9). Figures 4.2 **a)**-**e)** shows the summary plot of the best preforming model (Threshold model). **a)** shows the model simulated values (blue) as compared with the observations levels (black). The R^2-score of this model is 0.85, and is therefore one of the best preforming models. However, we see that the minima and maxima of the observation data tend to be missed by the model. **b)** shows the residuals between the simulated values and the observation data. Here, we see that the magnitude of the residuals seems to be higher in the period before the daily observation frequency start (ca. 2003). In **c)** we see the optimized parameter values used in this model (section 3.2.5). In **d)** we see the response function that is based on the stresses rain and snowmelt as precipitation (precipitation) and potential evapotranspiration (PET) (section 3.2.3. Here we see a periodic changes according to the seasonal variability at the station. **e)** shows the step response of the model (section 3.2.3. Here the model seems to start flatting out at $t = 100$ days, and becoming more or less constant in $t = 200$ days. **f)** shows the significant trend within of the residuals calculated with Mann-Kendall trend test and Sen's slope. In addition, in **g)** we see how the four different model types (section 3.2.4) are simulating the groundwater between 2010-2011, compared with the observation values. The Black dots are the groundwater observations, and each of the colored lines is the simulation of a model type. Same type of comparison figure as in figure 4.2 for all stations is shown in appendix A.

The summary in Table 4.1 shows the performance (R^2), of each type of model at each station. In addition, we see the best recharge model and its R^2 value in the **Best Model** and **Best Model Type** respectively. Here we see that between the four different recharge models tested for each station, the highest and lowest R^2 score is varying between 0.04 and 0.29. The best preforming models R^2-score is between 0.479 and 0.935. In addition, it is noteworthy that between the Non-linear model and the Non-linear model with a snow scheme, there is 13 stations where they have more or less the same R^2-score ($\pm$ 0.01), and 12 stations where the R^2-score differ more than

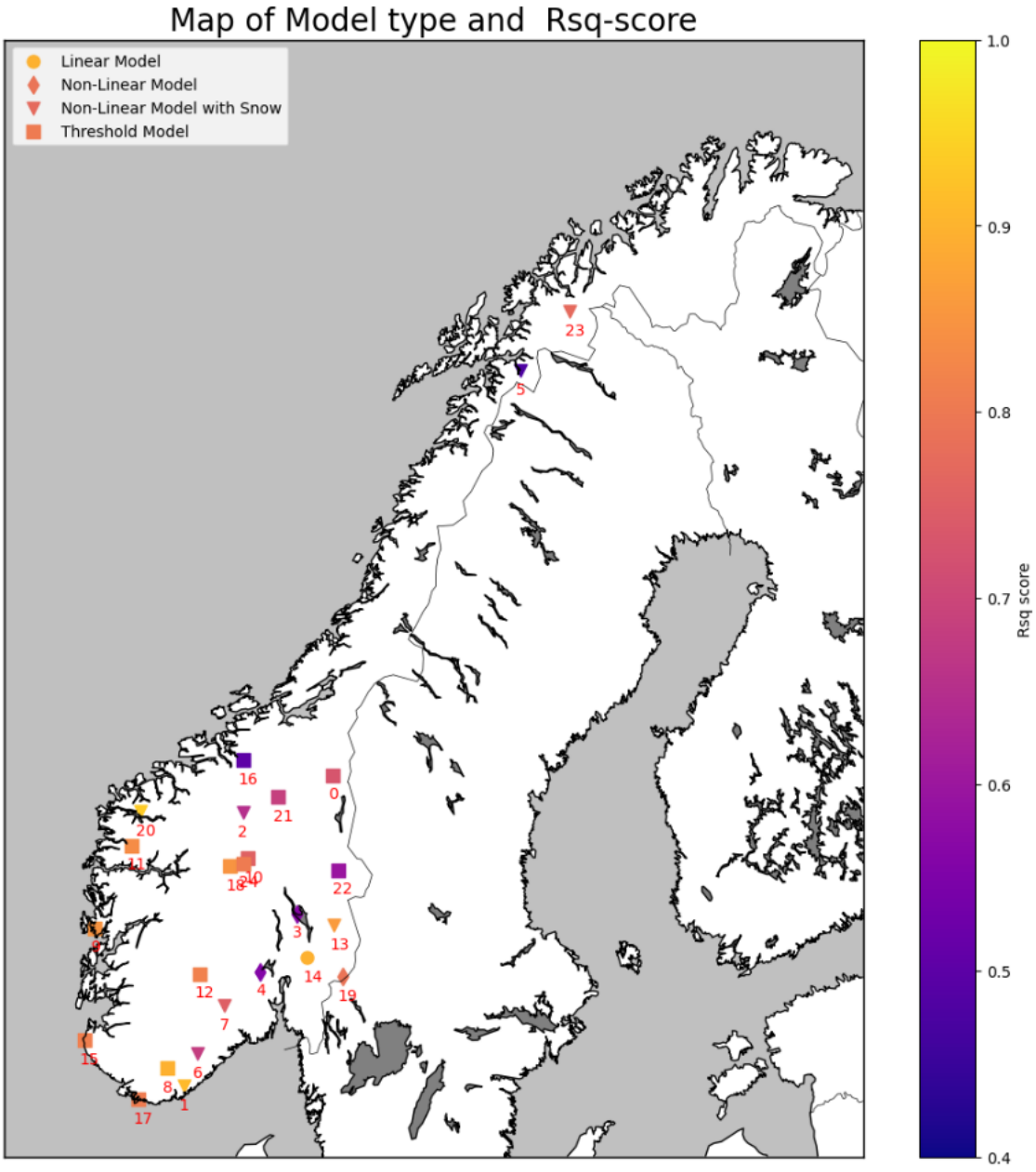

Figure 4.1: The map shows the best preforming recharge model at each station along with its R^2 score. Here a circle means a Linear model was used, the diamond is Non-linear model, the triangle is Non-linear with a snow scheme and the square is the Threshold model.

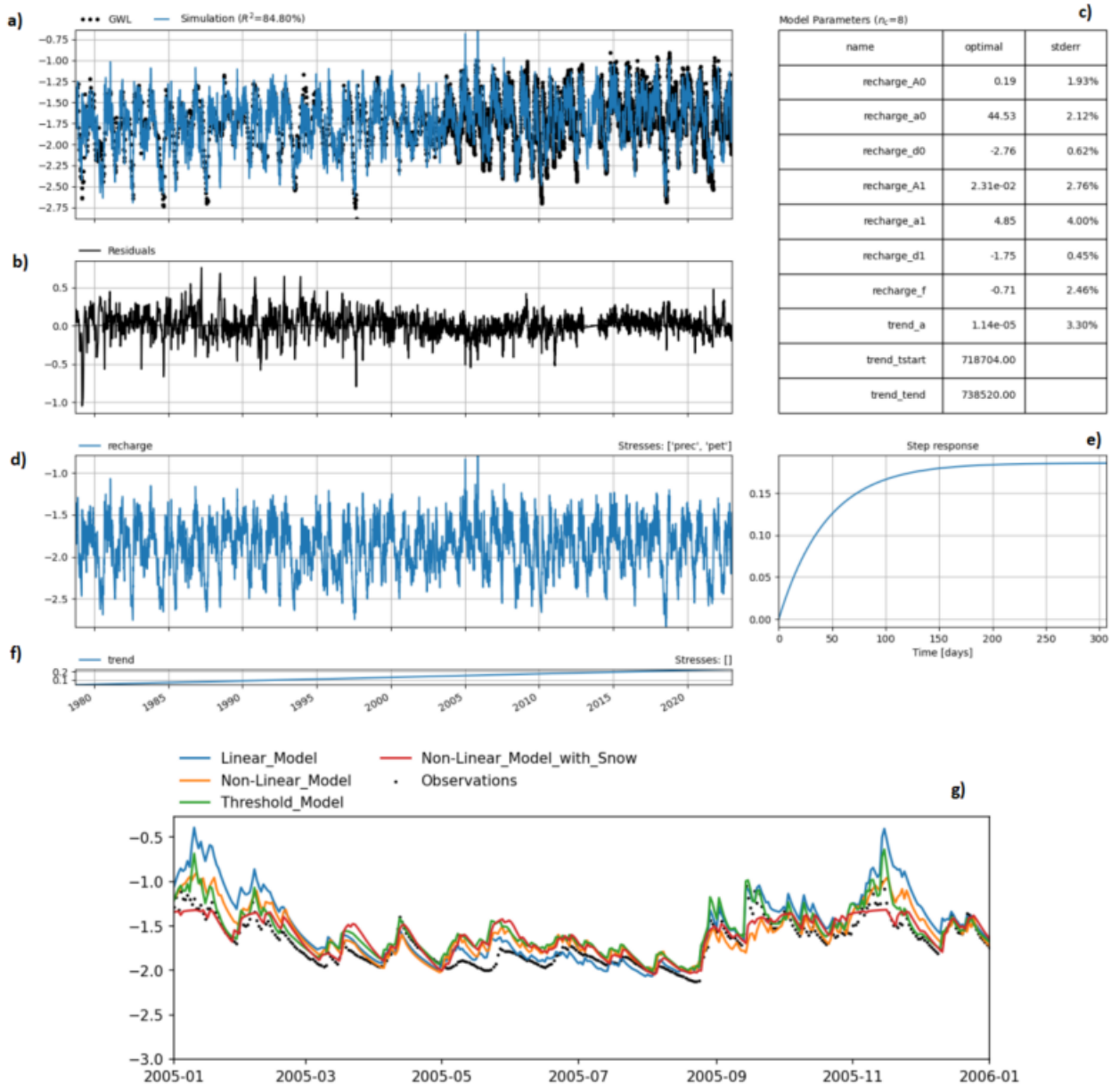

Figure 4.2: The Results of the pastas model fitted to the observations of Fana station (9). he following results are shown: a) the model simulations compared with the observations, b) the residuals between the simulation and observations, c) the parameter values of the model, d) the total recharge resulting from the stresses calculated with the response function, e) the graph over the step response of the model, f) the trend of the residuals that were added, g) the comparison of the different types of models. Each model is based on a different type of recharge function, and their simulations are plotted to the observations.

Table 4.1: Recharge model performance (R^2) at each station. In addition, we see the best model R^2 and the best preforming model type (bold type).

stationId	Linear Model R^2	Threshold Model R^2	Non-Linear Model R^2	Snow Model R^2	Best Model R^2
Abrahamsvoll (0)	0.61	**0.74**	0.59	0.59	0.74
Birkenes (1)	0.86	0.86	0.89	**0.90**	0.90
Dombås (2)	0.48	0.48	0.44	**0.65**	0.65
Kise (3)	0.50	0.50	**0.57**	0.53	0.57
Modum (4)	0.40	0.32	**0.53**	0.40	0.53
Skjomen (5)	0.32	0.47	0.30	**0.48**	0.48
Stigvassåi (6)	0.57	0.55	0.60	**0.64**	0.64
Eikamoen (7)	0.69	0.70	0.75	**0.75**	0.75
Evje (8)	0.84	**0.90**	0.86	0.86	0.90
Fana (9)	0.73	**0.85**	0.71	0.82	0.85
Finnbølseter (10)	0.67	**0.75**	0.66	0.66	0.75
Førde/Moskog (11)	0.75	**0.83**	0.81	0.82	0.83
Groset (12)	0.68	**0.82**	0.73	0.66	0.82
Haslemoen (13)	0.75	0.60	0.86	**0.86**	0.86
Hauerseter (14)	**0.90**	0.78	0.71	0.83	0.90
Jæren (15)	0.79	**0.81**	0.78	0.78	0.81
Kårvatn (16)	0.49	**0.50**	0.42	0.46	0.50
Lindesnes (17)	0.76	**0.81**	0.78	0.78	0.81
Lykjestøylane (18)	0.74	**0.85**	0.74	0.74	0.85
Magnor (19)	0.71	0.60	0.67	**0.77**	0.77
Nordfjordeid (20)	0.90	0.90	0.93	**0.94**	0.94
Settalbekken (21)	0.60	**0.68**	0.62	0.58	0.68
Stenerseter (22)	0.54	**0.60**	0.55	0.56	0.60
Øverbygd (23)	0.66	0.59	0.66	**0.77**	0.77
Øyangen (24)	0.68	**0.81**	0.68	0.68	0.81

0.04.

In Table 4.2 shows how many stations each type of recharge model is preforming the best. Here we see that the model type that is preforming the best at most stations is the Threshold model. The second best is the Non-linear model with a snow scheme. Keep in mind, the precipitation input used in each model already has the combined effect of rain and snowmelt, so each model has indirectly a snowmelt scheme.

4.2 Gap-filled groundwater time-series

Figure 4.3 shows an example of the infilling on Nordfjordeid station (20). The simulated values from the model in blue and the observation values in black. Using the gap-filling method (section 3.3 and Figure 3.3) on the simulated values, the gap is filled with daily values and we get the green values. In this example we see that even though the simulated values (blue points) do not exactly fit with the observation values (black), the gap-filled method fits the simulated values to the observation values quite well.

Table 4.2: Table over the number times each model type is the best preforming model at a station.

Model Type	Nr of best performances
Linear Model	1
Non-Linear Model	2
Non-linear Model with snow	9
Threshold Model	13

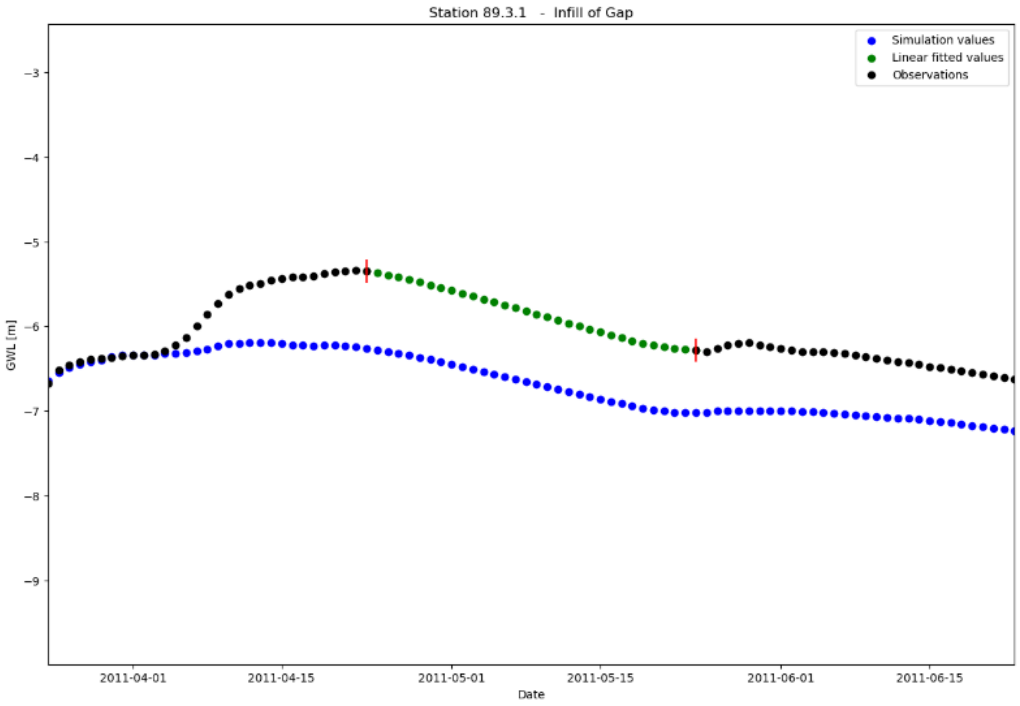

Figure 4.3: Figure showing a highlighted part of the infill process from Nordfjoreid station (20). Here we see a gap in the observations (black) and the original simulation values (blue). After the infill method, we see the resulting values that is filling the gap of the observation points (green).

We proceed to do this for all the gaps at each station, to end up with a complete time series with uniform time step of one groundwater value per day. An example of such a complete time series, with the infilled values and observation values highlighted, is shown in Figure 4.4. Here, most infilled values is between the observations within the period of monthly observation resolution. The infilled time series for all stations are shown in Appendix B. Noteworthy, the period between 1989 and 1995 has seemingly a "lower boundary" of the groundwater level that is different from the rest of the time series. We see here, the infilled values in this period are shifted lower than the apparent "lower boundary" of the groundwater level. However, the infilled values are not as low as the lowest values in the rest of the time series.

Table 4.3 shows the summary table of the infilling. The columns show the longest gap per station in number of days, the total number of gaps, and what percentage of the complete time series consists of gap-filled values. In this table we see that most stations have about $\pm 50\%$ of the time series infilled with simulated values. Exceptions to this is Øverbygd station (23), where

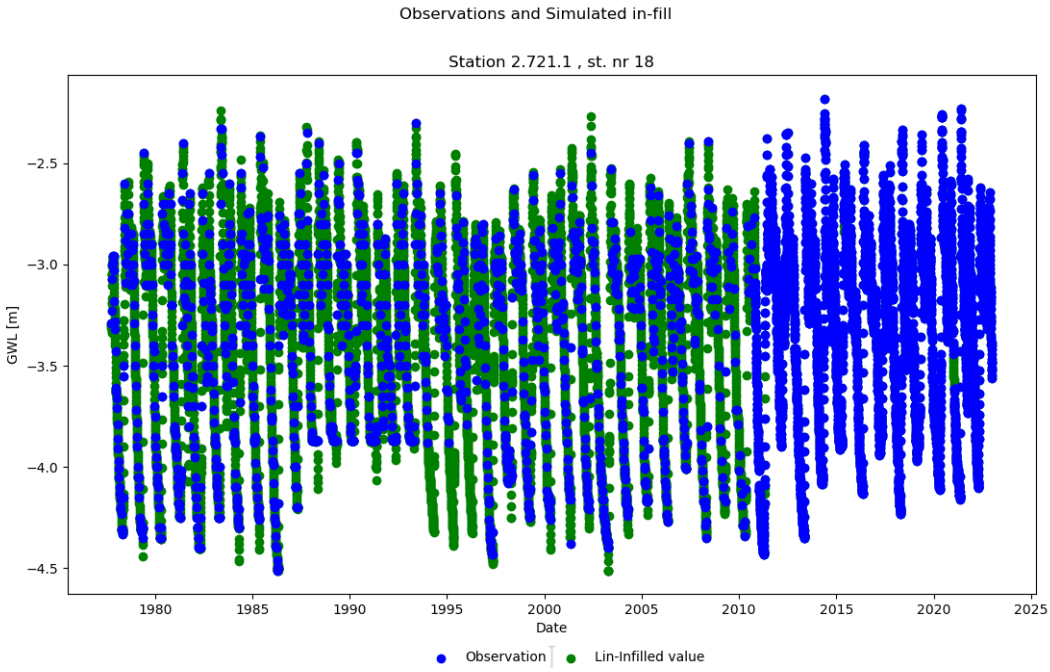

Figure 4.4: Figure over the observed values in blue, and simulated infilled values in green, from Lykjestøylane station (18).

the observation series is short (starting in 2004), and has daily observations from the start. In addition, Lindesnes station (17) has a high percentage infill (92.5%) because it only has monthly observation values throughout the time series. It's also worth noting that 9 stations have at least one gap lasting over 1 year, with the longest being 1441 days (almost 4 years) at Kårvatn station (16).

4.3 Groundwater Regimes

In order to categorize each station, we use the mean value of each month. Based on this, we calculate the difference of the monthly mean to the mean of the year. This is then divided by the standard deviation of the months at that station. From this we see how the groundwater level is typically varying through the year. From these values we select the three wettest and three driest months to categorize the different stations as described in chapter 3.4. Through the thesis, the winter months is December, January and February, the spring months is March, April and May, the summer is June, July and August, and the autumn is September, October and November.

According to figures 4.5 - 4.8, there are 7 stations in the Atlantic regime, 8 in the Transition regime, 7 in the mountain regime and 3 in the mountain delayed regime. All stations are shown with its corresponding GWL regime in the map in figure 4.9. When we compare with the auto correlations shown in table 4.5, we see that the Mountain delay region only has stations with a high auto correlation (over 1 year). Magnor station (19) also has a high auto correlation, but it is following a transitional GWL regime.

Table 4.3: Table over the longest gap present at each station, the total number of gaps at the stations, and how many percent the in-filled values are of the complete daily resolution time series.

	Station ID	Station name	Longest gap [days]	Number of gaps	Percentage infilled
0	2.725.1	Abrahamsvoll	114	1638	58.0 %
1	20.34.4	Birkenes	365	1194	48.4 %
2	2.718.2	Dombås	113	495	47.7 %
3	2.727.0	Kise	1252	342	43.8 %
4	12.343.12	Modum	42	845	46.3 %
5	173.28.1	Skjomen	251	401	42.3 %
6	19.144.6	Stigvassåi	84	802	56.6 %
7	16.231.9	Eikamoen	471	1025	68.6 %
8	21.80.1	Evje	227	514	68.1 %
9	56.3.2	Fana	365	1287	50.5 %
10	2.722.1	Finnbølseter	255	1608	65.1 %
11	84.25.3	Førde/Moskog	125	1420	54.2 %
12	16.232.1	Groset	108	2470	51.4 %
13	2.724.9	Haslemoen	192	566	56.4 %
14	2.713.3	Hauerseter	508	930	73.8 %
15	28.14.2	Jæren	381	1623	64.4 %
16	111.14.2	Kårvatn	1441	720	76.9 %
17	23.17.4	Lindesnes	410	1168	92.5 %
18	2.721.1	Lykjestøylane	167	1533	64.0 %
19	313.12.7	Magnor	47	1116	60.3 %
20	89.3.1	Nordfjordeid	46	1008	59.3 %
21	2.723.4	Settalbekken	671	1537	67.6 %
22	2.716.6	Stenerseter	163	2087	68.5 %
23	196.47.2	Øverbygd	46	8	1.2 %
24	2.719.2	Øyangen	222	1517	65.6 %

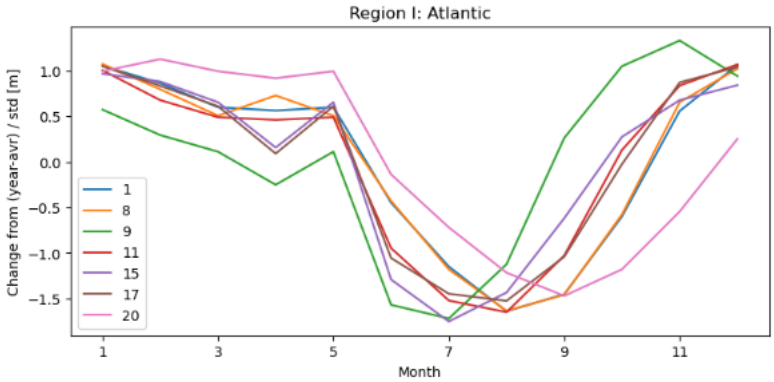

Figure 4.5: The stations within the Atlantic regime plotted with the typical GWL variation (described in section 3.4). The numbering follows Table 4.4, and the stations locations are shown in Figure 4.9.

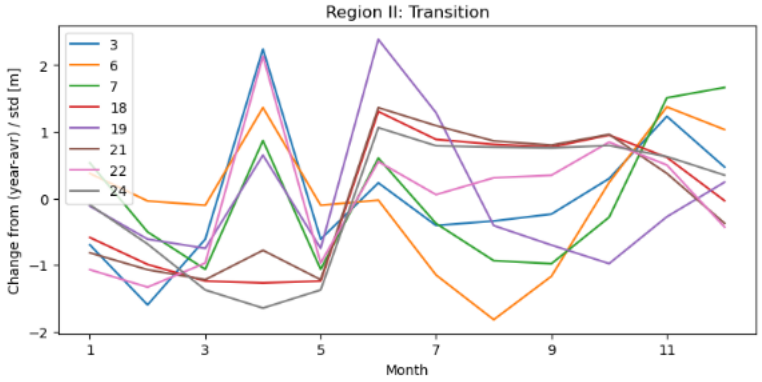

Figure 4.6: The stations within the Transitional regime plotted with the typical GWL variation (described in section 3.4). The numbering follows Table 4.4, and the stations locations are shown in Figure 4.9.

4.3.1 Region I : Atlantic

Figure 4.5 shows the stations that fit the Atlantic regime of groundwater variation. We see that the typical GWL is high in the winter months, presumably because of warm winters with a high degree of precipitation recharge combined with low PET and grow rates. The typical GWL minima is around July to September due to high PET, low precipitation and high grow rates.

4.3.2 Region II : Transition

Figure 4.6 shows the stations falling in the Transitional regime of groundwater variation. Here we see that the stations have 2-3 GWL peaks and lows. The pattern is highly varied between the stations, but the timing of the GWL peaks is in spring or summer, and autumn. The timing of the GWL lows is also in the late winter or spring, and late summer or autumn. Presumably, the spring GWL peak is related to snow melt, and the late winter peak is related to precipitation. While the GWL spring low, is related to low winter recharge and the GWL summer low is related to low precipitation and high PET.

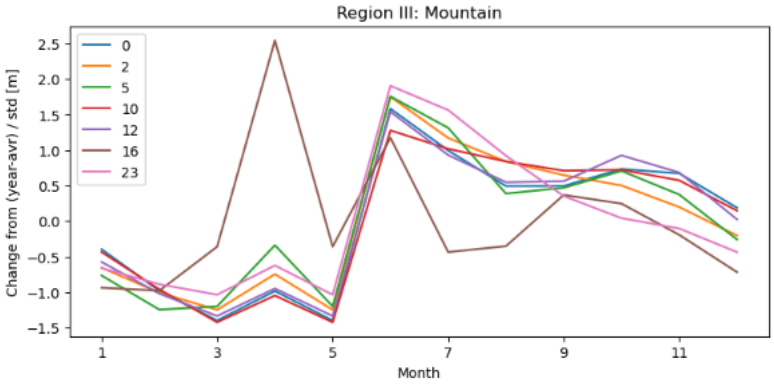

Figure 4.7: The stations within the Mountain regime plotted with the typical GWL variation (described in section 3.4). The numbering follows Table 4.4, and the stations locations are shown in Figure 4.9.

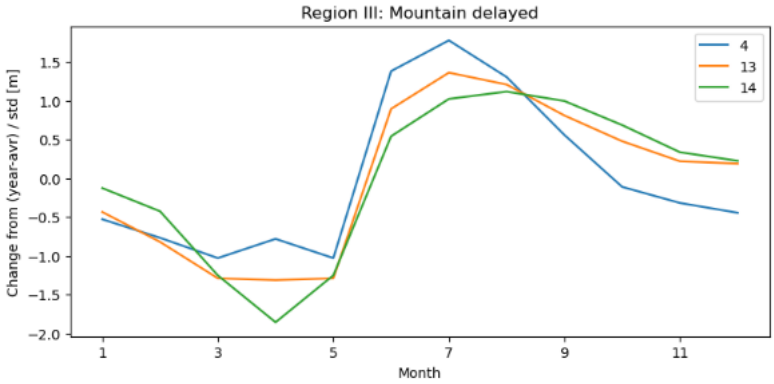

Figure 4.8: The stations within the Mountain delayed regime plotted with the typical GWL variation (described in section 3.4). The numbering follows Table 4.4, and the stations locations are shown in Figure 4.9.

4.3.3 Region III : Mountain

Figure 4.7 shows the stations falling in the Mountain regime of groundwater variation. This shows a typical GWL peak in the spring, presumably related to the snow melt. We also see that the GWL is relatively steady decreasing through the summer and winter and reaches a minima just before the spring melt. Here, Kårvatn station (16) has a particularly early spring peak (April), while also having a peak in June and a small increase in September. These peaks are however relatively small compared with the spring peak, and the station is therefore not considered within the transitional regime.

4.3.4 Region III : Mountain delayed

Figure 4.8 shows the stations falling in the delayed Mountain regime of groundwater variation. Here, all stations have a typical GWL peak in July, and a steady decrease in GWL until the minima in April or May. All three stations within this regime has a significant auto correlation exceeding 1 year.

Table 4.4: Table of station number, ID and name, with corresponding climate region and groundwater regime.

Station nr.	Hydra-Id	Station Name	Climate Region	Groundwater region
1	20.34.4	Birkenes rør 4	3	I, Atlantic
8	21.80.1	Evje rør 1	3	I, Atlantic
9	56.3.2	Fana rør 2	5.2	I, Atlantic
11	84.25.3	Førde/Moskog rør 3	6.2	I, Atlantic
15	28.14.2	Jæren rør 2	4	I, Atlantic
17	23.17.4	Lindesnes rør 4	4	I, Atlantic
20	89.3.1	Nordfjordeid rør 1	6.2/8.2	I, Atlantic
3	2.727.0	Kise	2.1	II, Transition
6	19.144.6	Stigvassåi rør 6	3	II, Transition
7	16.231.9	Eikamoen rør 9	2.1/3	II, Transition
18	2.721.1	Lykjestøylane rør 1	2.2	II, Transition
19	313.12.7	Magnor rør 7	2.1	II, Transition
21	2.723.4	Settalbekken rør 4	7.2	II, Transition
22	2.716.6	Stenerseter rør	2.1	II, Transition
24	2.719.2	Øyangen rør 2	2.2	II, Transition
0	2.725.1	Abrahamsvoll	7.1	III, Mountain
2	2.718.2	Dombås rør 2	7.2	III, Mountain
5	173.28.1	Skjomen	11	III, Mountain
10	2.722.1	Finnbølseter rør 1	2.2	III, Mountain
12	16.232.1	Groset grunnvannsrør 1A	2.2	III, Mountain
16	111.14.2	Kårvatn rør 2	8.2	III, Mountain
23	196.47.2	Øverbygd rør 2	11	III, Mountain
4	12.343.12	Modum rør 12	2.1	III, Mountain delayed
13	2.724.9	Haslemoen rør 9	2.1	III, Mountain deleayed
14	2.713.3	Hauerseter	2.2	III, Mountain delayed

4.3.5 Groundwater regime summary

From Table 4.4 and the map in figure 4.9, we see that the station within the Atlantic regime is distributed along the southern and western coast. The stations are primarily in the 3 and 4 climate region (CR), with the exception of Fana (9), Førde/Moskog (11) and Nordfjordeid (20) stations being in the 5.2 and 6.2 CR.

In the Transitional regime, the stations are distributed in the south-eastern part and eastern part of Norway. The stations are primarily in the 2.1, 2.2 and 7.1 CR, with the exception of Stigvassåi (6) and Eikamoen (7) stations being in in the CR 3.

In the Mountain regime, stations are distributed in the north-western, middle and Northern part of Norway. The stations are within CR 2.2, 7.1, 7.2, 8.2 and 11. Her, all stations have a cold climate (average temperature $< 2^oC$). They are located in high altitudes, except Skjomen (5) and Øverbygd (23) stations, which is close by a fjord in the far northern part of Norway.

In the Mountain delayed regime, the stations are clustered in the south eastern part of Norway. They are all within the 2.1 CR and have relatively high average yearly temperature $> 4^oC$. In addition, all stations have autocorrelation over 365 days.

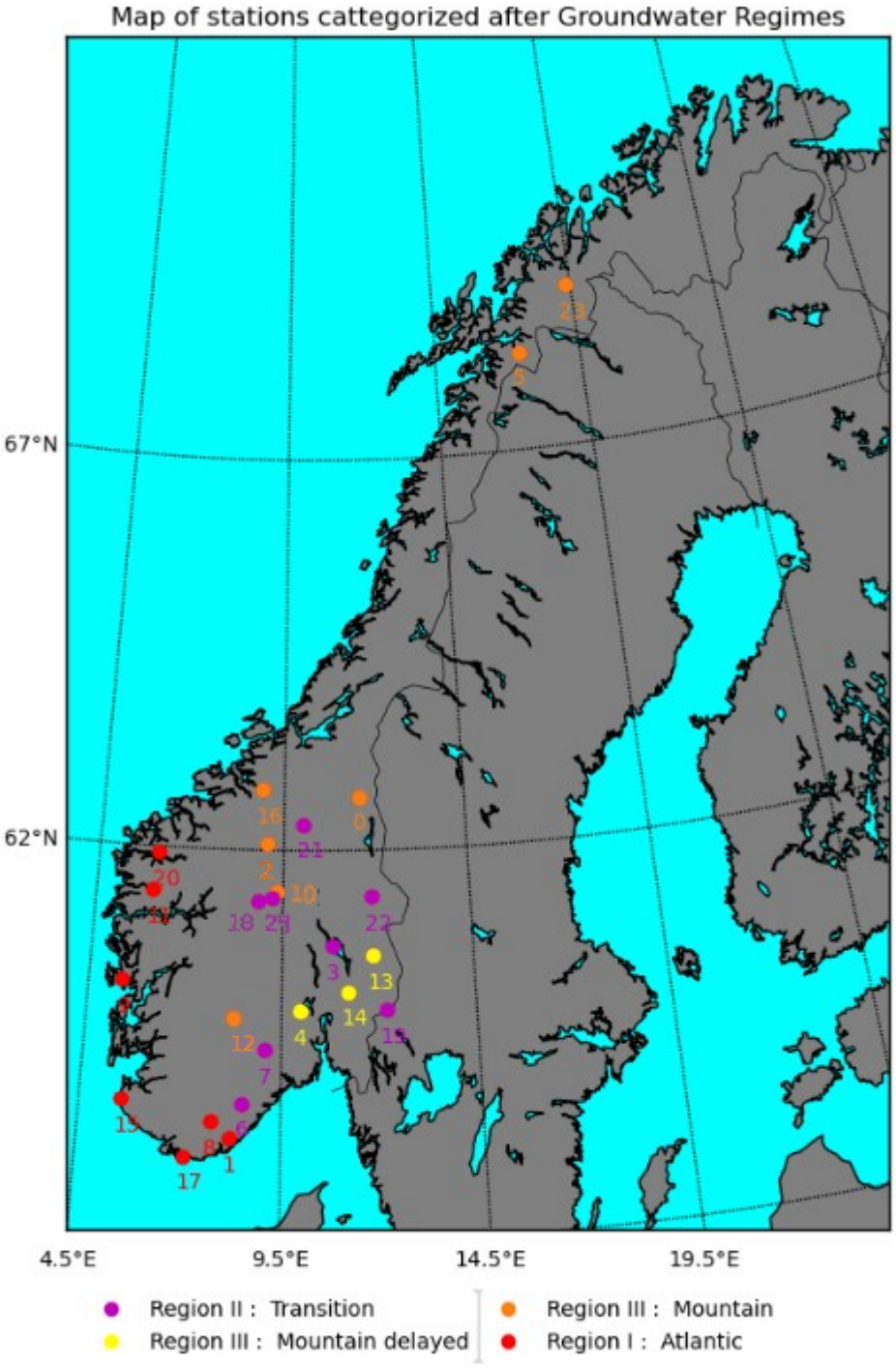

Figure 4.9: Map over the different regimes at each station used in this analysis.

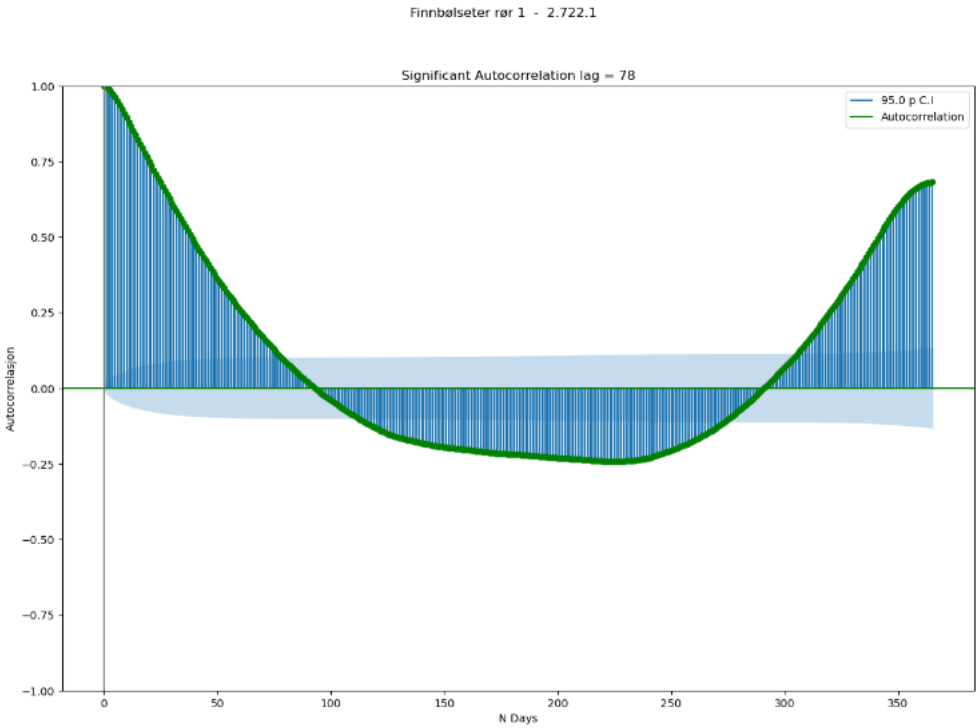

Figure 4.10: Figure of the auto correlation of Finnbølseter station (10). Here the light blue color is the significance level at 95% confidence. The station autocorelation is marked to be significant at 73 days.

4.4 Autocorrelation in the groundwater time series

The autocorrelation of the complete time series of Finnbølseter station (10), is shown in figure4.10. Here the significant autocorrelation at 95% is marked by the light blue background color. When the autocorelation crosses the confidence interval we mark the value as the stations autocorelation. Here it is marked at 78 days. Since there are seasonal variations of the time series, the autocorrelation goes up and over the confidence interval when approaching the 365 mark. In addition, we see that between 120 and 270 days, the autocorrelation is significantly negative. This does not indicate however, that these values are dependent on the preceding values, but that the seasonal variations are present in the data.

The latest significant autocorrelation for each station is then recorded in table 4.5. It shows the significant autocorrelations in number of days, at 95% confident interval for each station. Here we see that for most stations, the significant autocorrelation is between 52 to 103 days, where Kise (3), Modum (4), Eikamoen (7), Haslemoen (13), Hauerseter (14) and Magnor (19) stations has significant autocorelation between 193-1026 days.

4.5 Trends in annual and monthly groundwater levels

4.5.1 Month average groundwater level indices

In this section we use the average groundwater level of each month, calculated form the complete time series. The multi temporal p-value (MKP) plot shows the significance of the trends over

Table 4.5: Table over each station's autocorrelation in number of days over a 95% confidence interval.

Station Id	Station Name	AC lag (D)
2.725.1	Abrahamsvoll	69
20.34.4	Birkenes rør 4	99
2.718.2	Dombås rør 2	103
2.727.0	Kise	276
12.343.12	Modum rør 12	439
173.28.1	Skjomen rør 1	85
19.144.6	Stigvassåi rør 6	66
16.231.9	Eikamoen rør 9	193
21.80.1	Evje rør 1	100
56.3.2	Fana rør 2	78
2.722.1	Finnbølseter rør 1	78
84.25.3	Førde/Moskog rør 3	93
16.232.1	Groset grunnvannsrør 1A	64
2.724.9	Haslemoen rør 9	787
2.713.3	Hauerseter	1026
28.14.2	Jæren rør 2	97
111.14.2	Kårvatn rør 2	59
23.17.4	Lindesnes rør 4	84
2.721.1	Lykjestøylane rør 1	73
313.12.7	Magnor rør 7	503
89.3.1	Nordfjordeid rør 1	100
2.723.4	Settalbekken rør 4	80
2.716.6	Stenerseter rør	52
196.47.2	Øverbygd rør 2	83
2.719.2	Øyangen rør 2	74

different periods for each month at a given station. MKP plots for all stations are shown in Appendix C.

In figures 4.11-4.16 we see the MKP trend plots for two stations within the Atlantic, Transitional and Mountain groundwater regime, highlighting different patterns. Here, the p-value of the trends in each period are plotted. The colors show the trend direction of strong significant trends, reflecting a 5% significance level ($p<0.05$), and weak significant trends, reflecting a 30% significance level ($0.05<p<0.3$). The different significance with the trend direction is given a distinct shading. A positive trend means higher GWL, indicating wetter conditions, and a negative trend means lower GWL, indicating drier conditions. The labeling is only shown at the bottom of figures 4.16 and 4.13, but it follows through all MKP plots and trend tables.

Both figure 4.11 and 4.12 is within the Atlantic groundwater regime. Figure 4.11 show Førde/Moskog station (11). Here we see that there are prominent negative trends in February, April, June, July, October and November. We also see that March and August months has a notably larger cluster of negative trends for the periods with a start between 1988-1992. In addition, we see that the positive trends in September are also seen in October, November and December.

In figure 4.12 we see the MKP plot of Birkenes station (1). Here, we see that for the longest periods (1981-2022), all months except May, June and July are positive. In addition, all months (lesser extent in March, April, May and June) seem to have prominent positive trends for the periods calculated with a start date between 1988-1996.

Figure 4.11 and 4.12 show two stations within the Transitional groundwater regime. In figure 4.13 we see the monthly MKP plot of Øyangen station (24). We see that there is a continuously significant positive trend in all months. However, only April month has a strong significant positive trend for the early periods that begins before 1988 and ends in 2012. The GWL in other months have either insignificant, weak significant- or strong significant-negative trends within this period.

In figure 4.14 we see the MKP plot of Eikamoen station (7). Here May, June and July have strong negative trends when calculating for the whole period (1980-2022). We also see that August has negative trends for most of the periods that starts before 1984, and April has mostly negative trends in periods starting after 1984. In the months between September-December we see a shifting trend, from negative in the periods that start between 1980-1988 and ends before 2012, to positive for the periods that start after 1990.

Figure 4.15 and 4.16 show two stations within the Mountain groundwater regime. Figure 4.15 shows Groset station (2). Here we see that the April and May months has a prominent positive trend, followed by June month with prominent negative trend. In addition, August, September, December, January, February and March contain mostly periods with positive trends. July month seems to have periods changing from positive trends for periods starting between 1972-1992, and negative trends for the periods starting after 1992.

Figure 4.16 shows the MKP plot of Dombås station (2). Here all months have a strong significant negative trend when we calculate for the whole time series (1984-2022). However, we also see that for the periods that start later (1997-), only the June, July, October and November months have negative trends. This indicate that the negative trends are more prominent in these months as compared with the other months.

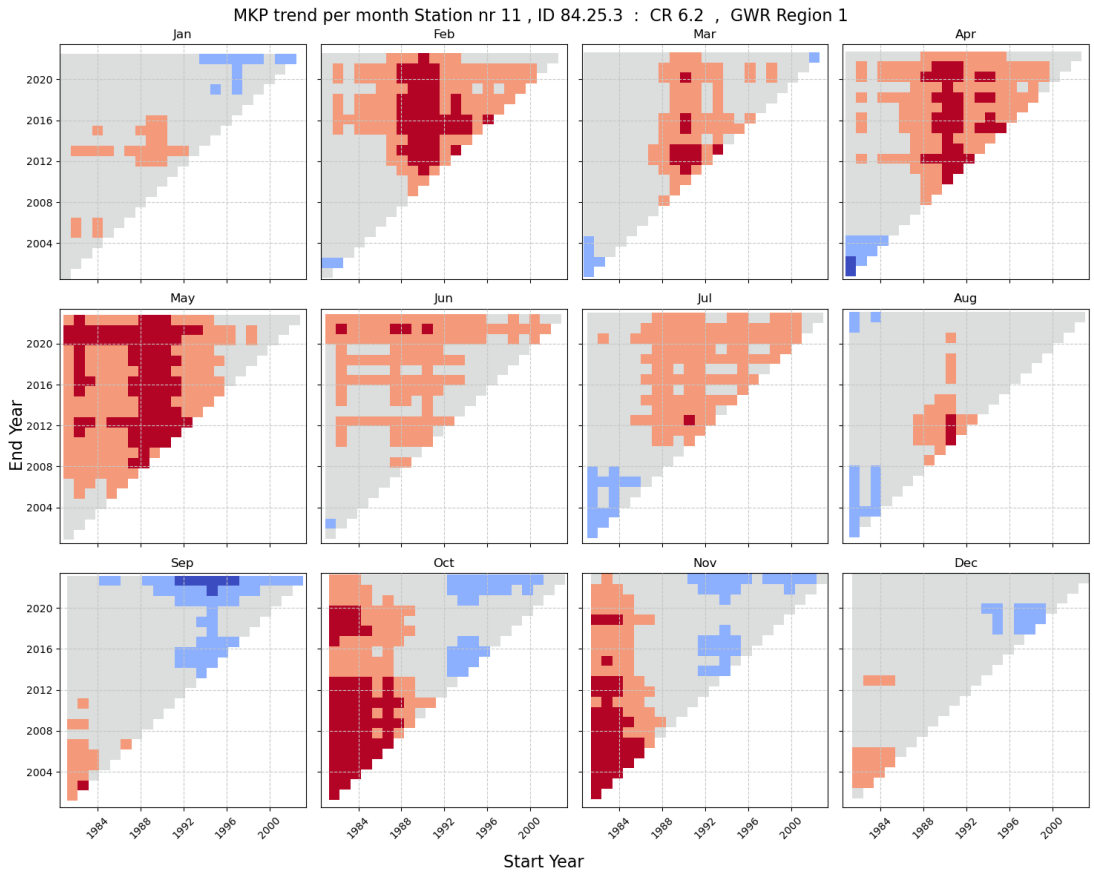

Figure 4.11: Mann-Kendall P-value plot of Førde/Moskog station (11). Here each color represent a significance level. Strong blue is positive trend with $p < 0.05$, light blue is positive trend with $0.05 < p < 0.3$, grey is $p > 0.3$ indicating no significant trend, light red is negative trends with $0.05 < p < 0.3$ and strong red is negative trend with $p < 0.05$.

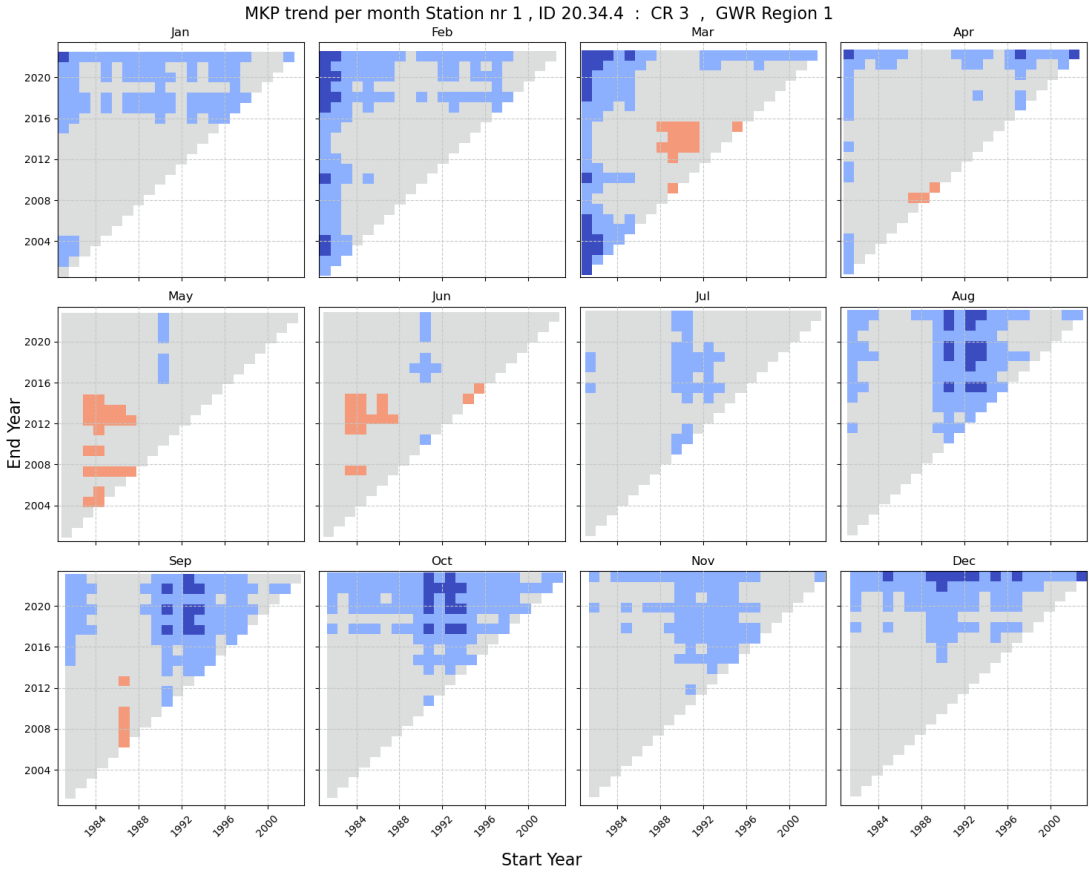

Figure 4.12: Same as figure 4.11 Mann-Kendall P-value plot, but for Birkenes station (1).

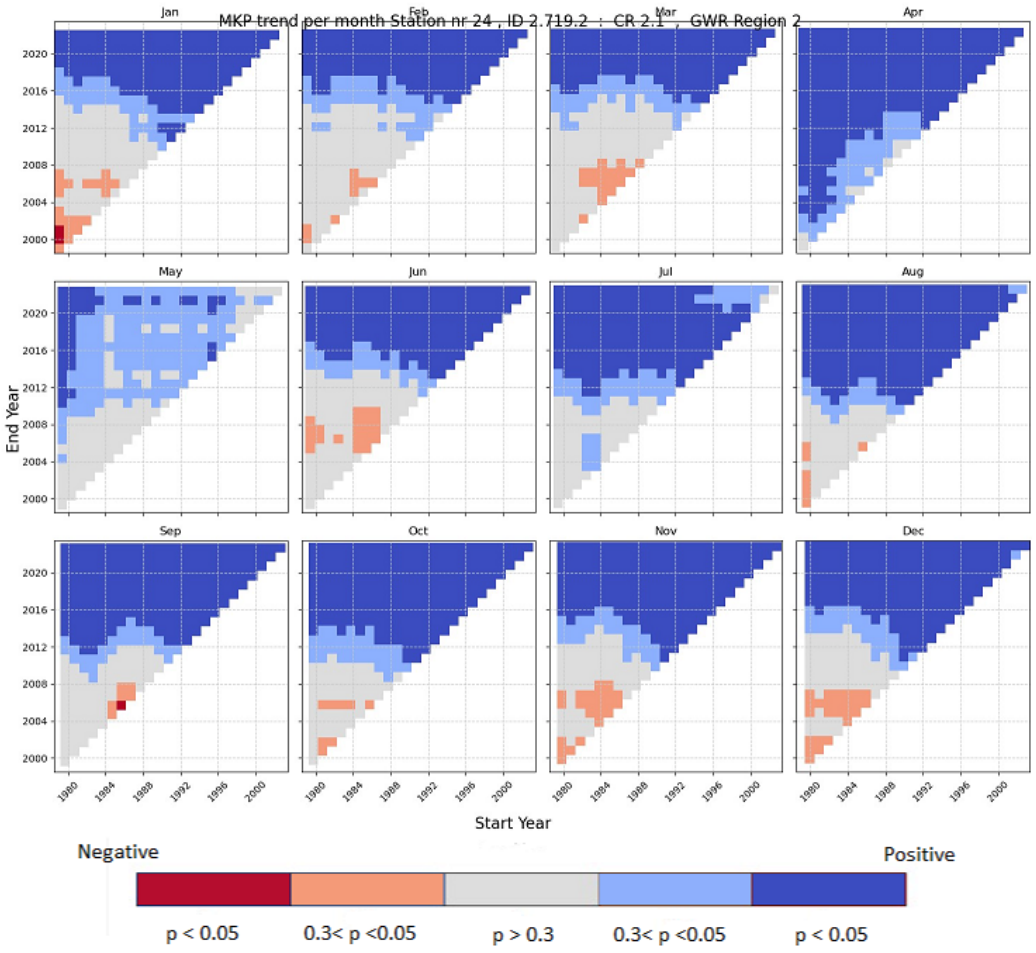

Figure 4.13: Same as figure 4.11 Mann-Kendall P-value plot, but for Øyangen station (24).

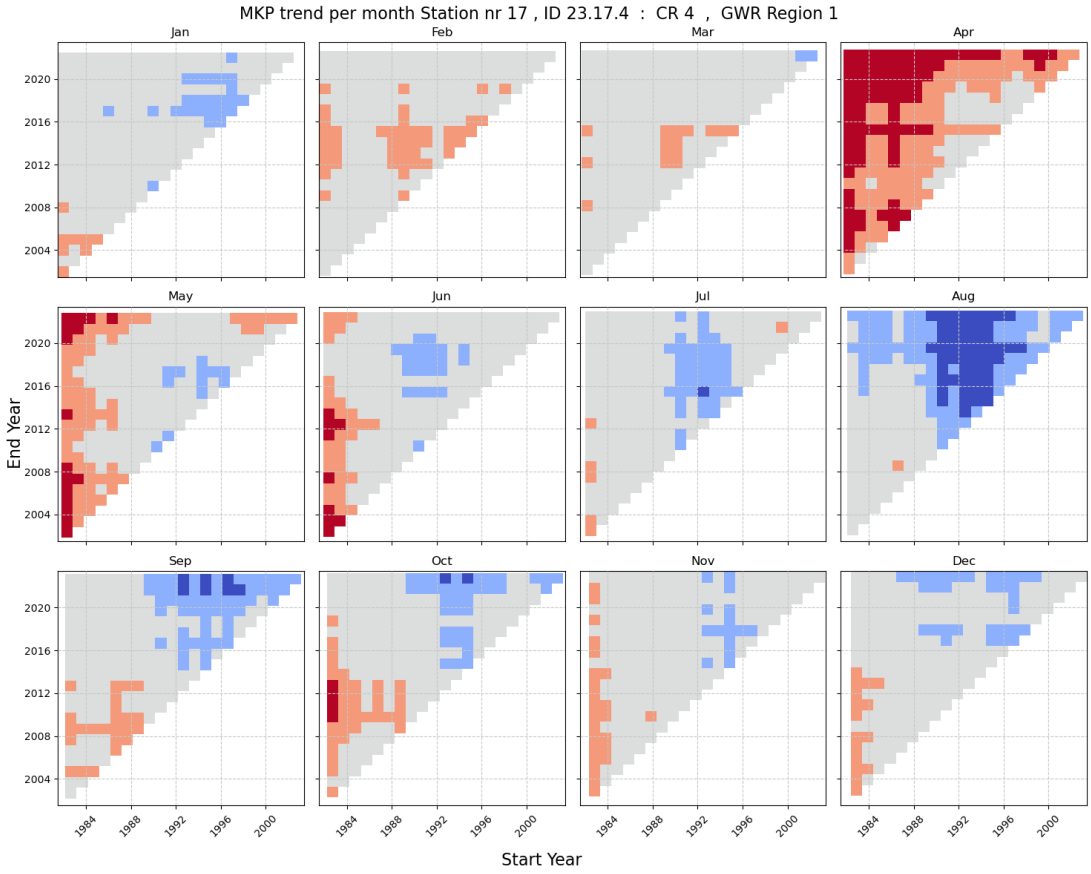

Figure 4.14: Same as figure 4.11 Mann-Kendall P-value plot, but for Eikamoen station (7)

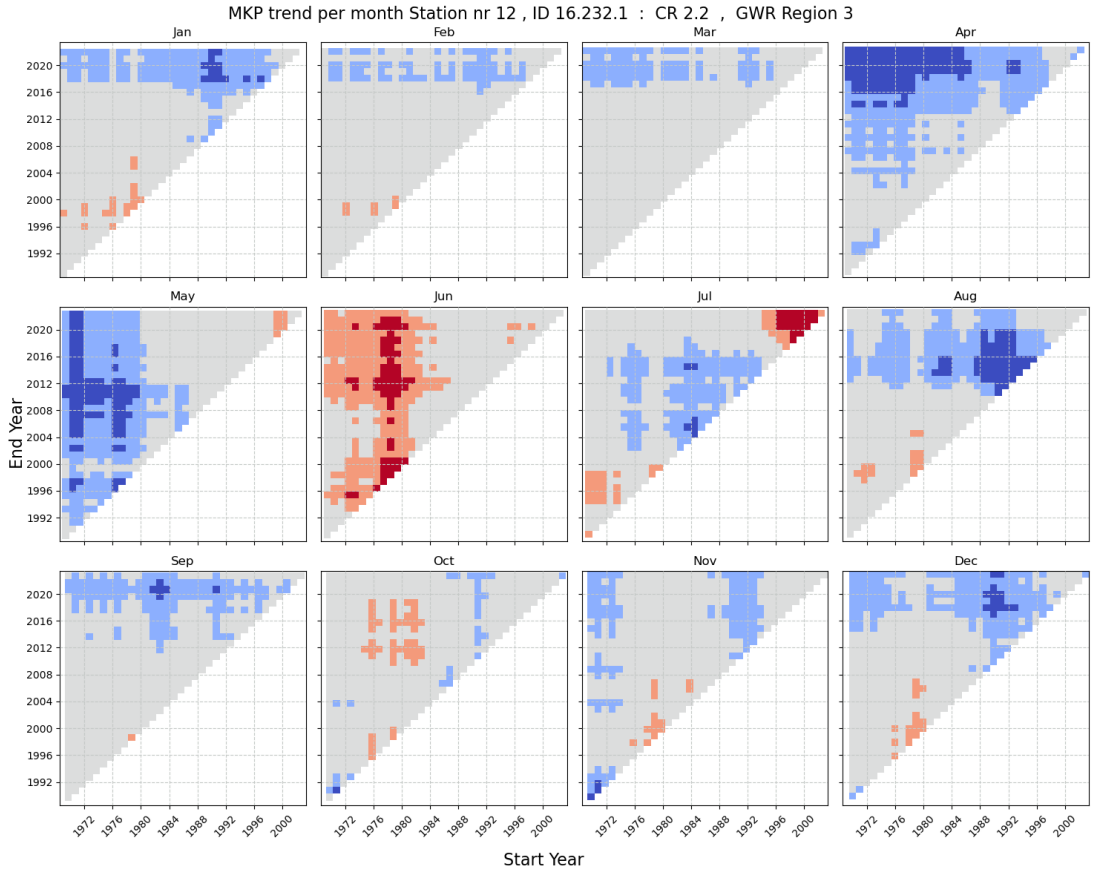

Figure 4.15: Same as figure 4.11 Mann-Kendall P-value plot, but for Groset station (12).

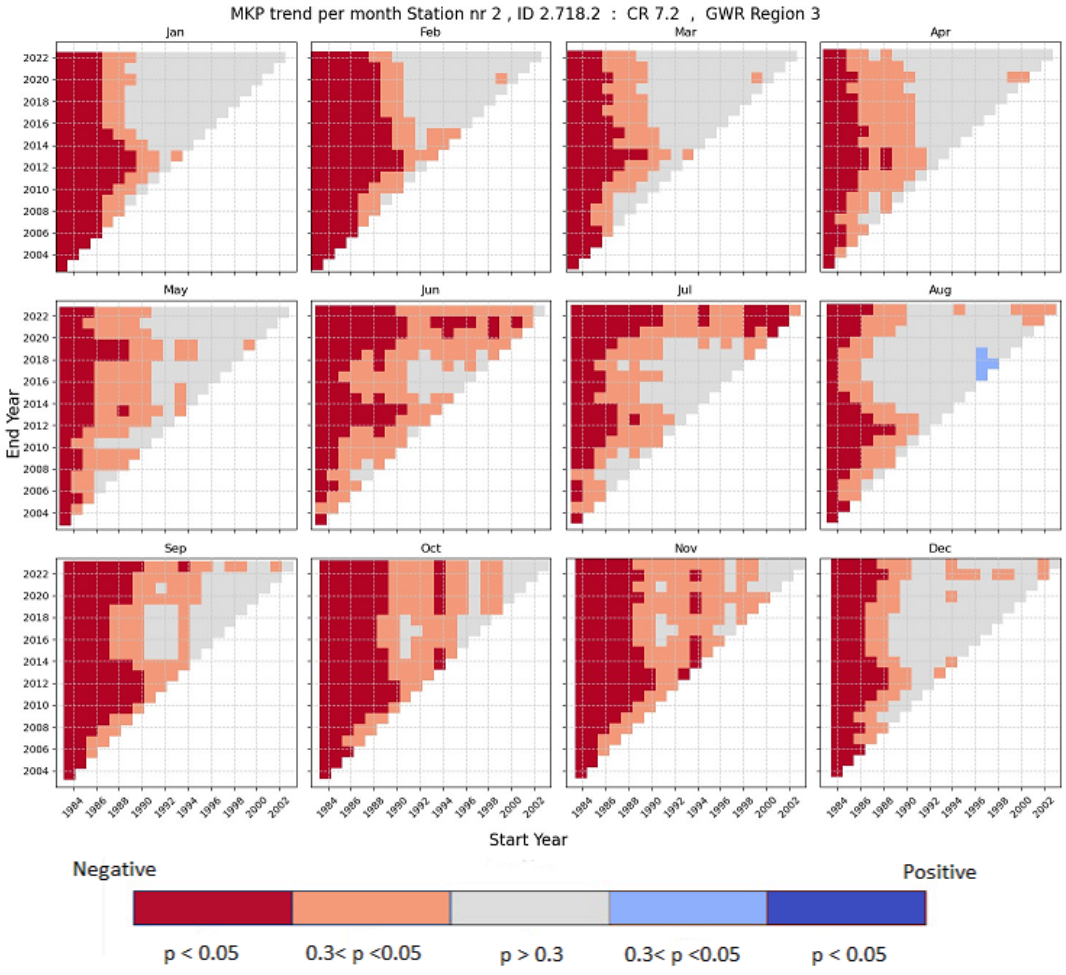

Figure 4.16: Same as figure 4.11 Mann-Kendall P-value plot, but for Dombås station (2).

4.5.2 Average annual GWL

The multi temporal trends for the average annual GWL are plotted for the different groundwater regimes in figures 4.17 -4.20. All stations within the regime are plotted relative to each other's time series. In Figure 4.17 we see the stations within the Atlantic regime. Here, the time series of all stations start around 1982. We see that Birkenes (1), Fana (9) and Jæren (15) stations have primarily positive trends, while Evje (8) and Lindesnes (17) stations have both positive and negative trends depending on the periods calculated. Førde/Moskog (11) and Nordfjordeid (20) stations have some negative trends, but mostly insignificant (grey).

In Figure 4.18 we see the stations within the transitional regime. Here, station Kise (3) has a much shorter time series as compared with the other stations in the regime. We also see that the Stigvassåi (6), Lykjestøylane (18), Magnor (19) and Øyangen (24) stations have several periods with a significant positive trend. Kise (3), Eikamoen (7) and Settalbekken (21) stations are more ambiguous with changing trends for different small clusters of periods, and with insignificant trends for most periods. Stenerseter (22) station is noteworthy since it has a pronounced period cluster with negative trend in the early to middle part of the time series (start periods before 1988), and a big period cluster with positive trends at the end of the time series (start periods after 1988).

Figure 4.19 shows the yearly average GWL trends for the stations in the Mountain regime. Here we see that Finnbølseter (10) and Kårvatn (16) stations have positive trends for almost all periods. At the same time, Abrahamsvoll (0), Skjomen (5) and Groset (12) stations have positive trends for most of the possible periods, with short period clusters of ether negative trends or insignificant trends. Dombås (2) station is an exception with general negative trends for almost all possible periods starting before 1996.

In Figure 4.20 we see the yearly average GWL trend for stations in the Mountain delayed regime. Here, we see that Haslemoen (13) and Hauerseter (14) stations have a primarily positive trend for the majority of the periods, whereas Modum (4) station has a generally positive trend for the periods that starts after 1990. We can see that for the periods that start between 1980-1992 and end before 2016, there are either negative or insignificant trends present for all stations.

4.5.3 Summary Table of drivers and GWL

The summary tables shown in figures 4.21 and 4.22, is showing the 41- and 31-year trends for yearly and monthly GWL for all stations covering the period. The trend is calculated for the last 31- and 41-years (e.i. 1992- and 1982- 2022), with most stations having the same start and end date. For stations with large autocorrelation (over 1 year), we calculate 2- or 3-year trends to ensure independence between the data points. This forces a different start date at some stations. These stations are shown in the table with its start date in the parentheses by the station number.

There are some changes in the trends between the two set periods. The 31-year trend table (Figure 4.21), we can see some general patterns within the groundwater regimes. Looking at the Atlantic regime, we see that there is a general positive trend in the Autumn and early winter months. At the same time, the trends in the summer are either insignificant or negative. The yearly trends are significant positive for 3 stations, weak significant positive for one station, insignificant for 2 stations and weak significant negative for one station.

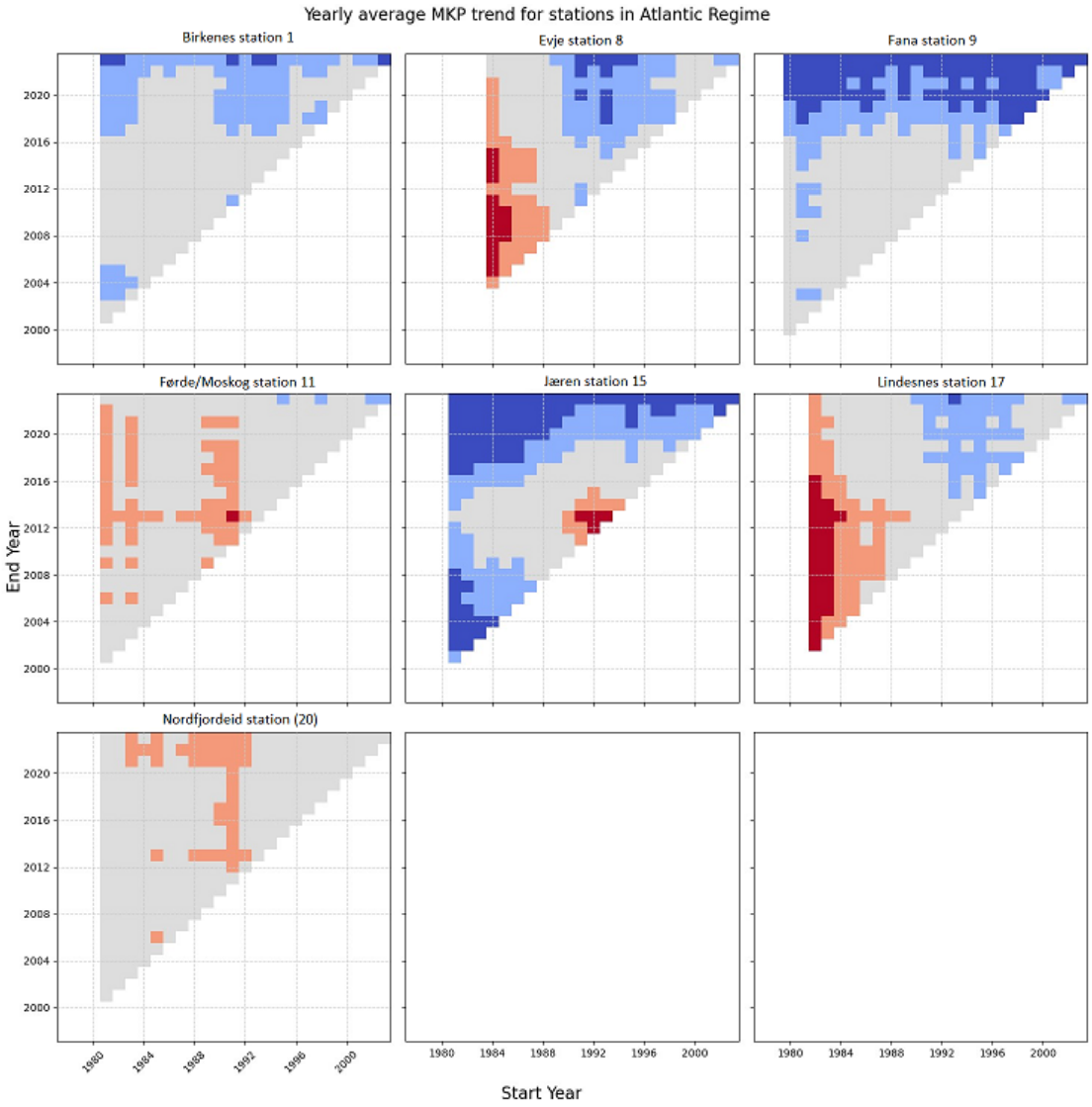

Figure 4.17: Here, the average yearly GWL is plotted for stations in the Atlantic regime. Here, the color scheme is the same as figure 4.11 Mann-Kendall P-value plot.

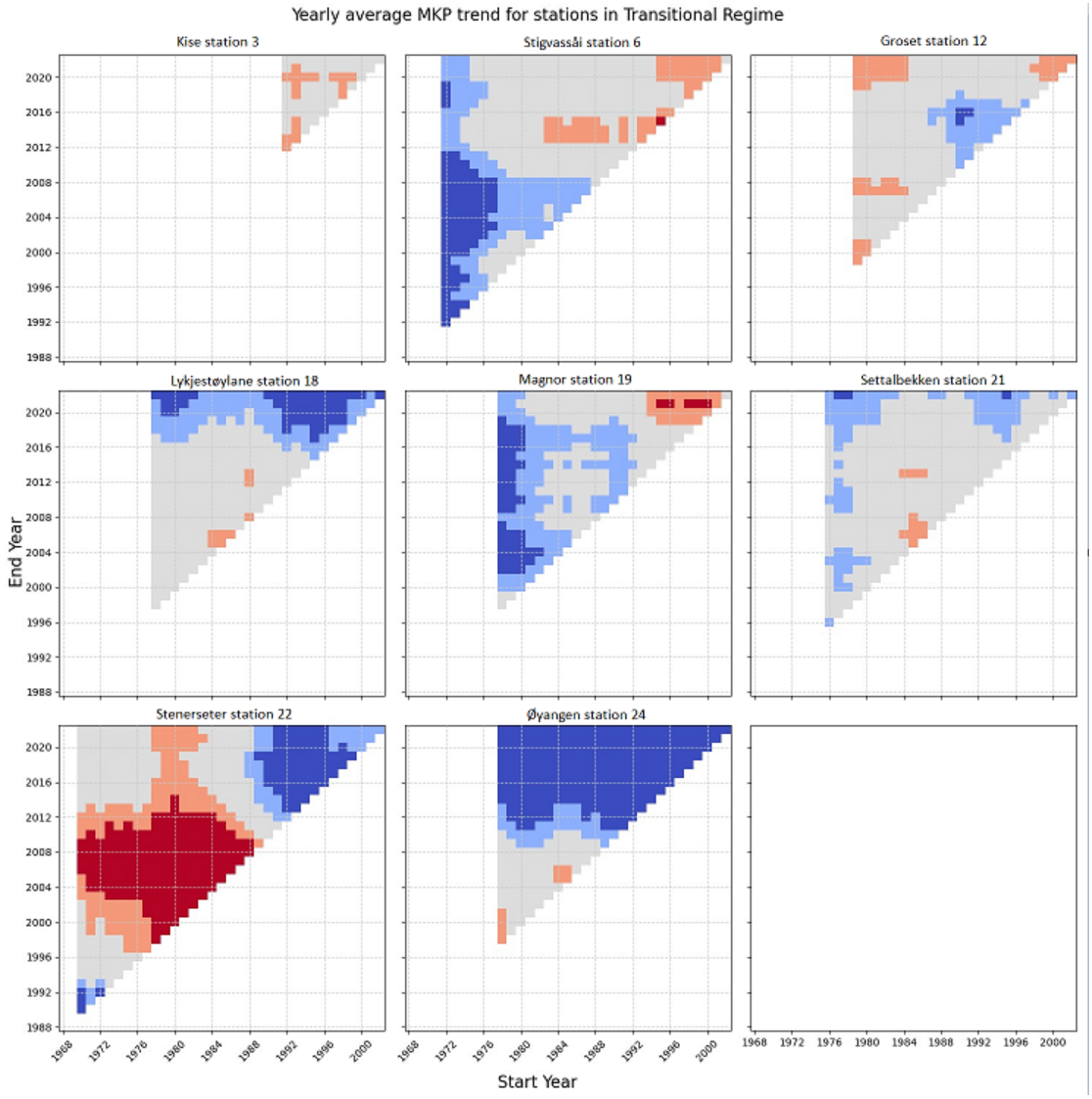

Figure 4.18: The same as in figure 4.17, but plotted for stations in the Transitional regime.

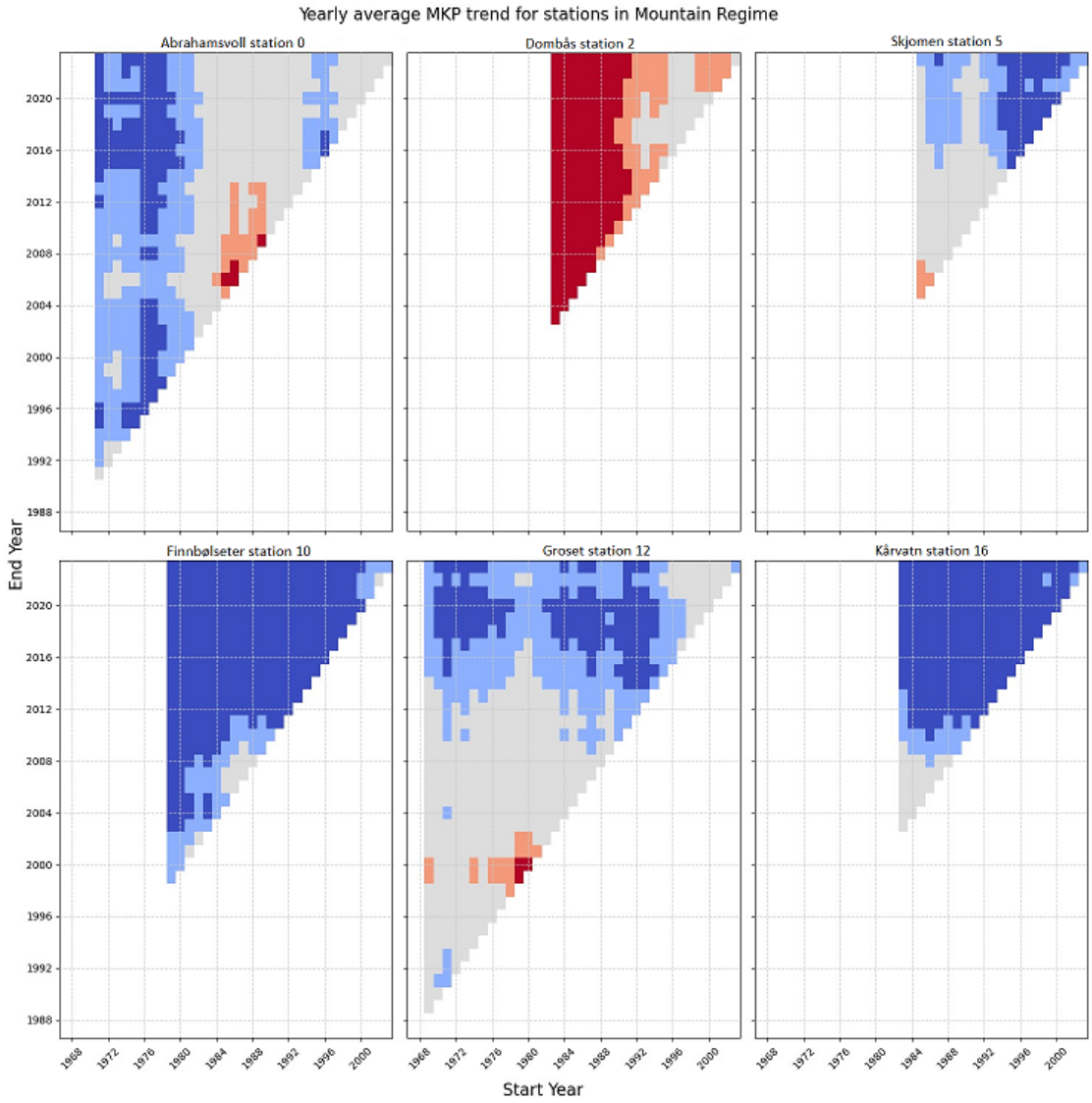

Figure 4.19: The same as in figure 4.17, but plotted for stations in the Mountain regime.

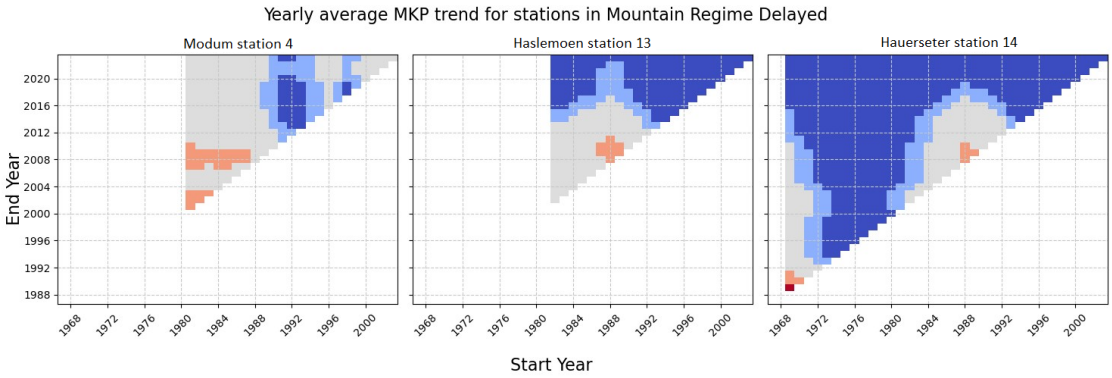

Figure 4.20: The same as in figure 4.17, but plotted for stations in the Mountain delayed regime.

The stations in the Transitional regime, the general patterns are more ambiguous. Generally, there are two patterns present. The first pattern is insignificant or significant negative trend in the summer and autumn months. The second pattern is insignificant or significant positive trends in the winter, early spring and late autumn. Here, Øyangen (24) station is an exception since it has strong significant, or weak significant positive trends in all months. The yearly trends are strong significant positive for 3 stations, weak significantly positive for one station, insignificant for 3 stations and weak significant negative for one station.

For the Mountain- and Mountain delayed- regime, there is a general wetting in the winter, spring and autumn months. The months January, February, March, April, September, October, November and December months have positive trends for all stations except Dombås (2) station. The yearly trends are significant positive for 5 stations, weak significantly positive for 2 stations, insignificant for one stations and weak significant negative for one station. Here we see that Haslemoen (13) and Hauerseter (14) stations have a significant positive GWL trend in all months and year average. While Haslemoen and Hauerseter station are located in the south-eastern Norway with a long auto correlation, Øyangen (24) station is located in the high mountainous region in the middle of southern Norway.

31-year trends on Groundwater levels calculated in the period 1992-2022

	Station Nr	Station ID	Year trend	Jan	Feb	Mar	Apr	May	Jun	Jul	Aug	Sep	Oct	Nov	Dec	AC (D)
Atlantic : Regime 1	9	56.3.2	0.03	0.66	0.92	0.63	0.61	0.68	0.61	0.45	0.02	0.02	0.04	0.15	0.41	73
	17	23.17.4	0.52	0.73	1.00	0.50	0.00	0.11	0.71	0.61	0.12	0.54	0.36	0.45	0.41	81
	11	84.25.3	0.41	0.45	0.28	0.54	0.31	0.32	0.38	0.50	0.71	0.05	0.03	0.01	0.59	88
	8	21.80.1	0.16	0.36	0.56	0.76	0.63	0.31	0.89	0.84	0.43	0.54	0.28	0.04	0.09	91
	15	28.14.2	0.01	0.01	0.10	0.22	0.79	0.34	0.20	0.07	0.00	0.01	0.03	0.01	0.02	93
	1	20.34.4	0.10	0.08	0.06	0.06	0.23	0.87	0.97	0.71	0.13	0.32	0.12	0.12	0.07	94
	20	89.3.1	0.26	0.89	0.66	0.29	0.13	0.08	0.04	0.06	0.08	0.36	0.54	0.34	0.54	96
Transitional : Regime 2	22	2.716.6	0.02	0.54	0.31	0.32	0.28	0.61	0.02	0.36	0.12	0.26	0.00	0.00	0.13	49
	3	2.727.0	0.15	0.43	0.41	0.97	0.68	0.07	0.43	0.63	1.00	0.10	0.29	0.92	0.71	59
	6	19.144.6	0.53	0.77	0.16	0.16	0.40	0.62	0.74	1.00	1.00	0.59	0.65	1.00	0.93	63
	24	2.719.2	0.00	0.00	0.00	0.00	0.00	0.13	0.00	0.01	0.00	0.01	0.00	0.00	0.00	64
	18	2.721.1	0.01	0.04	0.06	0.14	0.40	0.32	0.95	0.92	0.38	0.71	0.05	0.03	0.03	69
	21	2.723.4	0.15	0.16	0.84	0.36	0.05	1.00	0.12	0.87	0.50	0.52	0.13	0.04	0.34	75
	7	16.231.9	0.36	0.73	0.61	0.50	0.04	0.00	0.01	0.10	0.43	0.63	0.63	0.16	0.59	170
	19	313.12.7	0.89	0.39	0.44	0.22	0.34	0.89	0.75	0.50	0.50	0.05	0.03	0.44	0.19	424
Mountain : Regime 3	16	111.14.2	0.01	0.02	0.68	0.04	0.43	0.34	0.59	0.36	0.48	0.02	0.12	0.29	0.05	56
	12	16.232.1	0.38	0.10	0.23	0.28	0.10	0.50	0.87	0.21	1.00	0.59	0.56	0.08	0.21	62
	0	2.725.1	0.21	0.05	0.11	0.21	0.16	0.48	0.13	1.00	0.87	0.95	0.73	0.20	0.07	66
	10	2.722.1	0.00	0.00	0.01	0.00	0.01	0.92	0.54	0.66	0.22	0.73	0.92	0.03	0.01	74
	23	196.47.2	---	---	---	---	---	---	---	---	---	---	---	---	---	80
	5	173.28.1	0.02	0.18	0.61	0.17	0.02	0.04	0.12	0.22	0.61	0.08	0.10	0.13	0.10	80
	2	2.718.2	0.07	0.89	0.97	0.61	0.92	0.31	0.07	0.04	0.13	0.01	0.04	0.05	0.13	95
Mountain delay : Regime 3	4	12.343.12	0.12	0.03	0.03	0.04	0.12	0.16	0.14	0.26	0.44	0.69	0.89	0.92	0.84	399
	13 (1991)	2.724.9	0.00	0.02	0.01	0.01	0.01	0.01	0.01	0.01	0.01	0.00	0.00	0.00	0.00	645
	14	2.713.3	0.02	0.01	0.01	0.01	0.02	0.02	0.04	0.04	0.04	0.06	0.04	0.04	0.04	814

Figure 4.21: Table over the trend calculated by the Mann-Kendall test at a 95% confidence interval for the stations with data starting from 1992. Station 13 has different start date which is shown in parenthesis. Here the P value is shown in each cell with the blue color representing an increasing trend and red color representing decreasing trend. The color strength is representing the significance with; dark red and blue being significant ($p < 0.05$), light red and blue being strong ($0.05 < p\ 0.3$), and grey being no significant ($p > 0.3$). The stations are sorted according to their assigned GWL region. Within each region, the stations are sorted in ascending order of the AC.

If we look at the 41-year trend table in figure 4.22, we can see a divide between the regions in addition to a clear difference between the stations with positive and negative trends.

In the Atlantic region, we see Fana (9), Jæren (15) and Birkenes (1) stations having the significant positive yearly trend, along with several months with significantly or weakly significant positive trends. We also see Nordfjordeid (20) station, that has yearly, along with all months from May to December, weakly significant negative trend. Thirdly, we see at Lindesnes (17), Førde/Moskog (11) and Evje (8) stations, where the months April, May, June and July have mostly significantly or near significantly negative trends, while the yearly trend is insignificant.

In the Transitional regime, we see that only Eikamoen (7) station has a significant negative yearly trend. It also has weak significant negative trend in April and September, while May, June and July are significantly negative. In addition, Øyangen (24) station has a significant positive yearly trend, with all the months also having significant positive trend. The other stations within the transitional regime have months with weakly positive, weakly negative or insignificant trends. Noteworthy, station 2.721.1 has a weakly significant positive yearly trend, but with some months having weak negative and weak positive trends right after one another, despite having significant auto correlation of 69 days.

In the mountain regime, there is a general pattern of significant positive trend in the winter and spring months. The yearly trends are also all weak or significantly positive for 6 out of 9 stations. An exception to this is Dombås (2) station, where the yearly trend, and the trend in all months, is significantly negative. Noteworthy, April month is consistently significantly positive for all stations except Dombås (2) and Modum (4).

41-year trends on Groundwater levels calculated in the period 1982-2022

	Station Nr	Station ID	Year trend	Jan	Feb	Mar	Apr	May	Jun	Jul	Aug	Sep	Oct	Nov	Dec	AC (D)
Atlantic : Regime 1	9	56.3.2	0.02	0.15	0.06	0.22	0.09	0.69	0.39	0.28	0.02	0.26	0.17	0.07	0.58	73
	17	23.17.4	0.31	0.85	0.88	0.66	0.00	0.00	0.16	0.57	0.37	0.99	0.66	0.54	0.60	81
	11	84.25.3	1.00	0.80	0.74	0.74	0.88	0.13	0.28	0.87	0.25	0.61	0.47	0.88	0.81	88
	8 (1983)	21.80.1	0.38	0.62	0.63	0.88	0.04	0.00	0.19	0.08	0.46	0.75	0.92	0.86	0.27	91
	15	28.14.2	0.00	0.00	0.00	0.00	0.11	0.01	0.03	0.01	0.00	0.05	0.00	0.00	0.00	93
	1	20.34.4	0.21	0.12	0.04	0.02	0.41	0.48	0.54	0.97	0.45	0.66	0.29	0.31	0.08	94
	20	89.3.1	0.15	0.55	0.55	0.68	0.51	0.13	0.05	0.09	0.12	0.16	0.16	0.16	0.29	96
Transitional : Regime 2	22	2.716.6	0.35	0.04	0.00	0.05	0.92	0.48	0.39	0.48	0.83	0.31	0.68	0.33	0.34	49
	3	2.727.0	---	---	---	---	---	---	---	---	---	---	---	---	---	59
	6	19.144.6	0.57	0.65	0.72	0.46	0.42	0.07	0.78	0.82	0.86	0.50	0.99	0.61	0.75	63
	24	2.719.2	0.00	0.00	0.00	0.00	0.00	0.09	0.00	0.00	0.00	0.00	0.00	0.00	0.00	64
	18	2.721.1	0.05	0.06	0.19	0.32	0.16	0.22	0.36	0.35	0.09	0.30	0.81	0.21	0.15	69
	21	2.723.4	0.31	0.24	0.74	0.24	0.03	0.30	0.23	0.68	0.73	0.52	0.88	0.28	0.60	75
	7	16.231.9	0.04	0.48	0.32	0.37	0.05	0.00	0.00	0.00	0.04	0.29	0.55	0.87	0.99	170
	19 (1980)	313.12.7	0.88	0.45	0.26	0.11	0.26	0.93	0.53	0.41	0.45	0.49	0.41	0.93	0.65	424
Mountain : Regime 3	16	111.14.2	0.00	0.00	0.09	0.00	0.04	0.23	0.06	0.47	0.27	0.03	0.12	0.25	0.08	56
	12	16.232.1	0.16	0.15	0.29	0.30	0.05	0.99	0.39	0.71	0.61	0.58	0.92	0.44	0.21	62
	0	2.725.1	0.55	0.22	0.10	0.07	0.05	0.55	0.06	0.24	1.00	0.54	0.06	0.55	0.88	66
	10	2.722.1	0.00	0.00	0.00	0.00	0.00	0.74	0.34	0.06	0.01	0.17	0.34	0.00	0.00	74
	23	196.47.2	---	---	---	---	---	---	---	---	---	---	---	---	---	80
	5 (1984)	173.28.1	0.06	0.24	0.79	0.12	0.03	0.24	0.68	0.51	0.32	0.05	0.12	0.18	0.24	80
	2	2.718.2	0.00	0.00	0.00	0.01	0.01	0.00	0.00	0.00	0.00	0.00	0.00	0.00	0.00	95
Mountain delay : Regime 3	4	12.343.12	0.65	0.38	0.26	0.22	0.45	0.69	0.49	0.83	0.53	0.38	0.32	0.42	0.58	399
	13 (1981)	2.724.9	0.01	0.01	0.00	0.00	0.00	0.00	0.00	0.01	0.01	0.01	0.02	0.03	0.01	645
	14 (1980)	2.713.3	0.02	0.01	0.01	0.01	0.01	0.02	0.04	0.03	0.03	0.04	0.03	0.03	0.03	814

Figure 4.22: Table over the trend calculated by the Mann-Kendall test at a 95% confidence interval for the stations with data starting from 1982. Stations 5, 8, 13, 14 and 19 has different start date which is shown in parenthesis. The colors and sorting of stations is the same as in figure 4.21.

4.6 Trends in high and low groundwater levels

High and low GWL trends

In figures 4.23 - 4.28, we see the MKP plot for GWL highs and lows. The period at which the values is gathered for each regime is described in section 3.6. The selection of stations shown in here is to highlight two different types of patterns that are seen in the stations within the regimes. The GWL period highs and lows in GWL for Fana station (9) and Førde/Moskog station (11), both within the Atlantic regime. Here, the period where we gather the maximum head is between September-April, and the minimum value is gathered from April-November (Table 3.2). Here we see that Fana station (9) has prominent positive trends in the maximum GWL, while the minimum GWL has no prominent trends. Comparatively, Førde/Moskog station (11) has prominent negative trends in the maximum GWL, and like Fana station (9), no prominent trends in the minimum GWL.

The trends for minimum and maximum GWL at Stenerseter station (22) and Øyangen station (24), both within the Transitional regime. Here, the period where we gather the maximum head is between October-July, and the minimum value is gathered from July-May (Table 3.2). We see that Stenerseter station (22) has clusters of negative and positive trend periods in the maximum GWL. At the same time, the minimum GWL has a more prominently negative trend, but with two small clusters of positive trend periods. The positive trend clusters in the minimum GWL, correspond with the positive trend and insignificant trend periods in the maximum GWL. Øyangen station (24) shows prominent positive trends for both the maximum and minimum GWL. The maximum GWL has a negative trend cluster at the beginning of the earliest periods that correspond with the insignificant trends in the minimum GWL.

The trends for minimum and maximum GWL at Abrahamsvoll station (0) and Finnbølseter station (10), both within the Mountain regime. Here, the period where we gathered the maximum head is between March-October, and the minimum value is gathered from November-July (Table 3.2). We see at Abrahamsvoll station (0)1, that there is a prominent negative trend in the maximum GWL. At the same time, there is a prominent positive trend in the minimum GWL. For Finnbølseter station (10), we see that there is negative trend clusters in the maximum GWL along with generally insignificant trend periods. Comparatively, there is a prominent positive trend within the minimum GWL, with no seemingly correspondence with the maximum GWL.

Trends in the timing of snowmelt related max and min

Trend in the timing of the spring melt related recharge maximum, as well as the GWL minimum before the spring melt, was conducted on the stations within the Mountain regime (Section 4.6). The trends were calculated according to the periods in Table 3.3. In Figure 4.29 we can see an example of the test that was conducted for each station. Here, Groset station (12) has a significant negative trend in the spring maxima, and a weak significant negative trend in the spring minima. At each station, the whole time series were used to test for the trends and the process to test the timing is explained in section 3.6.

The maximum GWL for all stations were plotted along with the trends in timing, in a comparative MKP plot. In Figure 4.30 we see the trends in maximum GWL and how it compares with the timing (Figure 4.31) of the winter and spring maxima. Here we see that Abrahamsvoll (0), Dombås (2), Groset (12) and Finnbølseter (10) stations all have significant trends towards

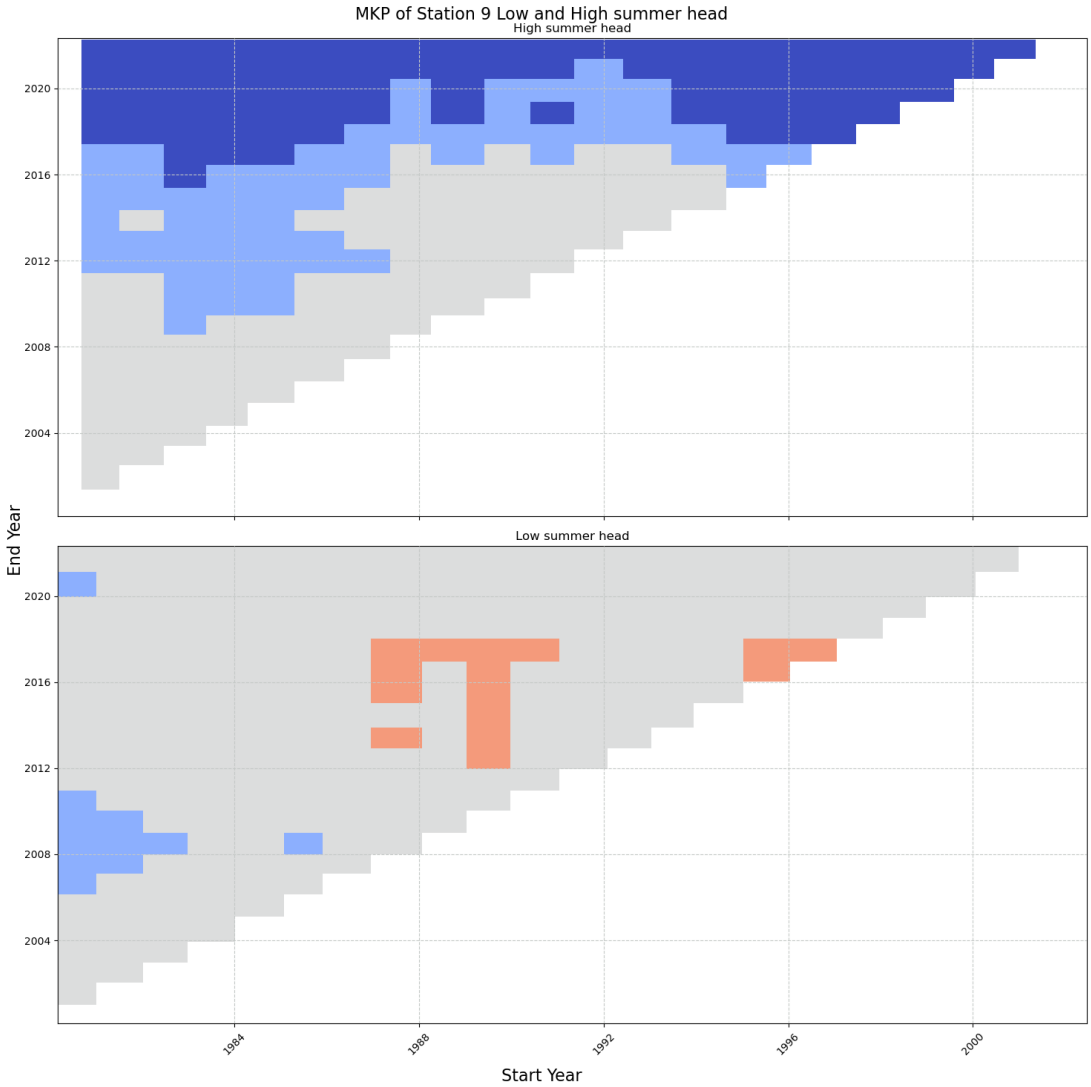

Figure 4.23: Multi temporal trend plot of the highest (top panel) and lowest (bottom panel) period highs at Fana station (9). Each color represents a significance level. Dark blue is positive trend with $p < 0.05$, light blue is positive trend with $0.05 < p < 0.3$, grey is $p > 0.3$, light red is negative trends with $0.05 < p < 0.3$ and dark red is negative trend with $p < 0.05$.

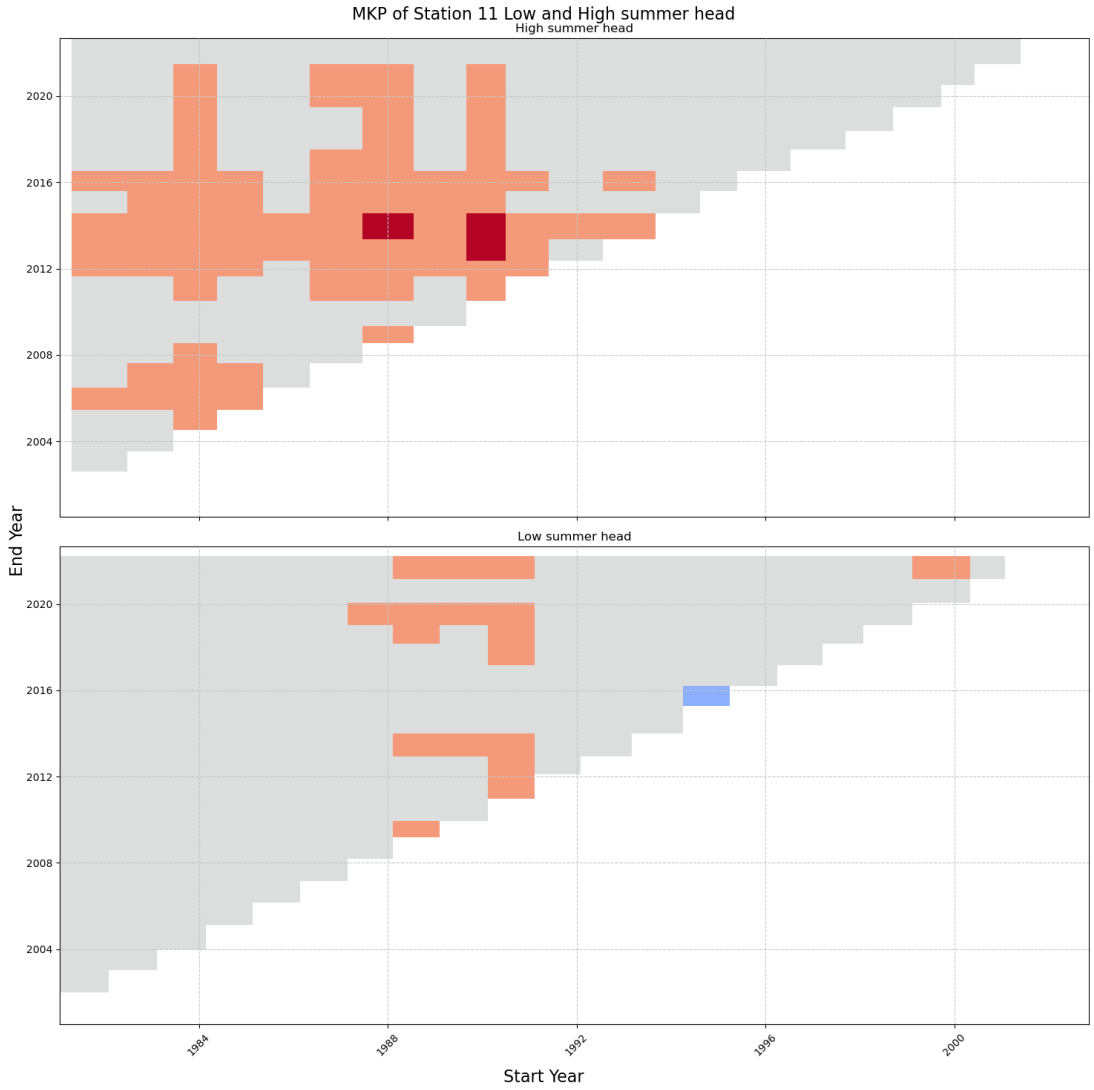

Figure 4.24: Same as figure 4.23, but for Førde/Moskog station (11).

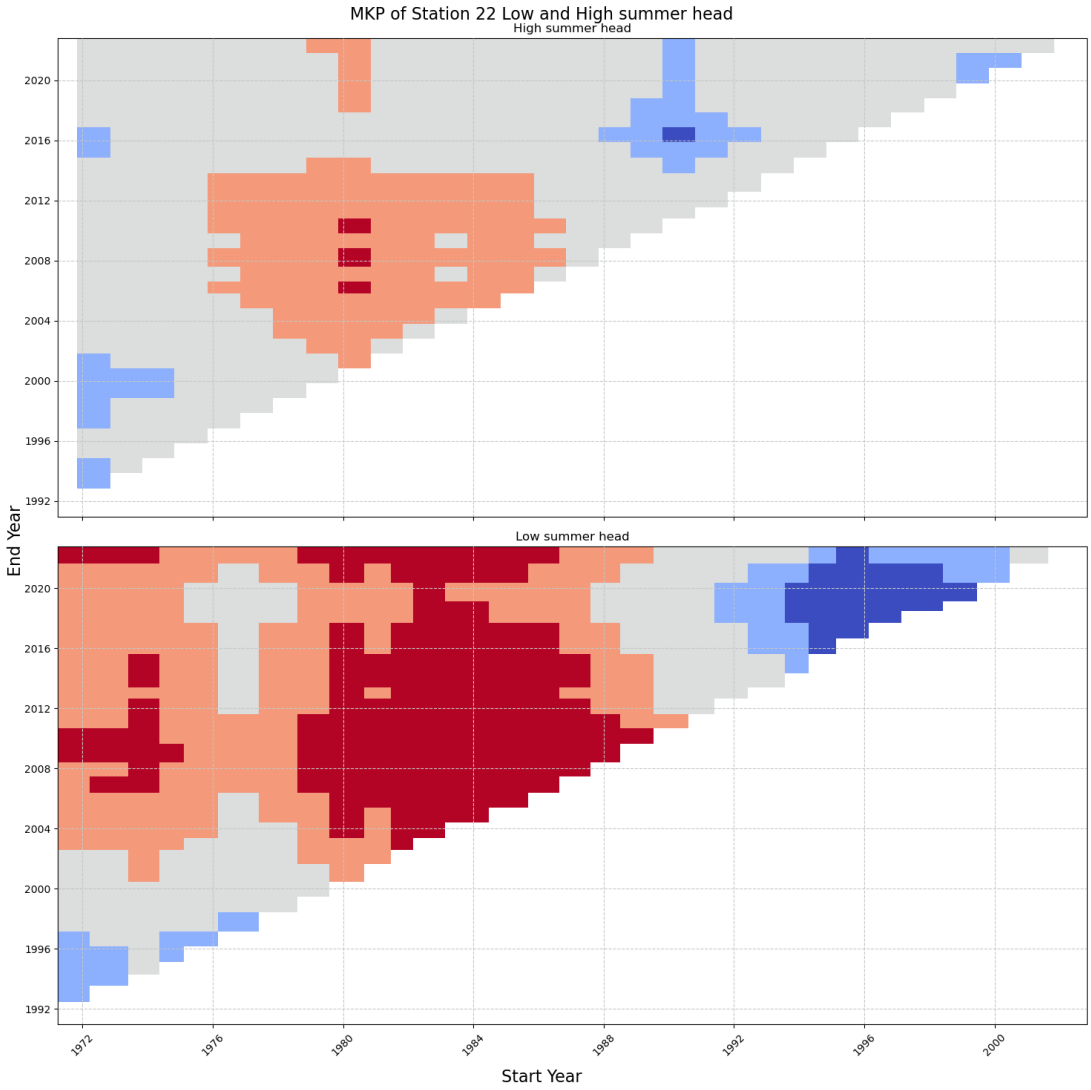

Figure 4.25: Same as figure 4.23, but for Stenerseter station (22).

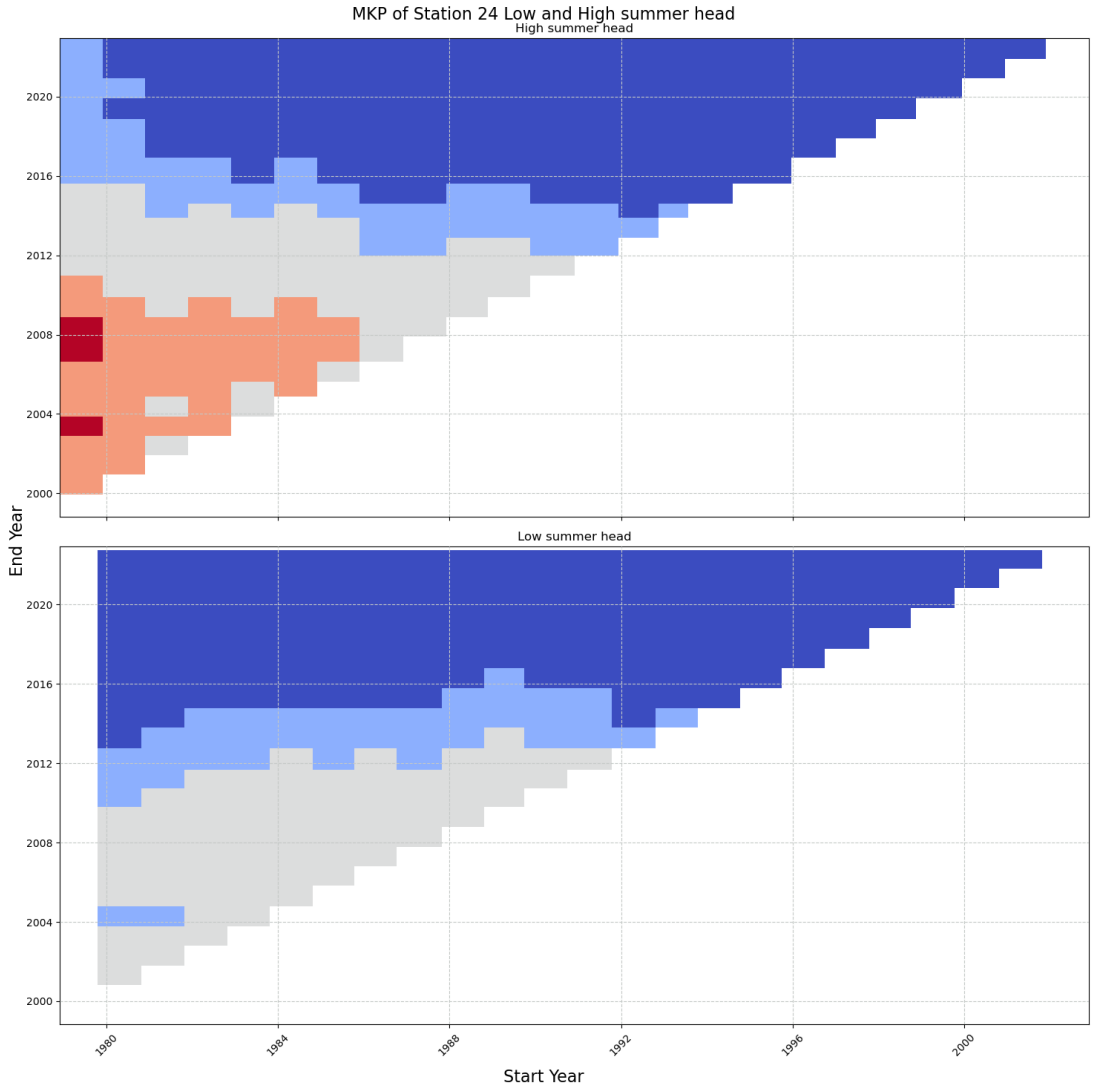

Figure 4.26: Same as figure 4.23, but for Øyangen station (24).

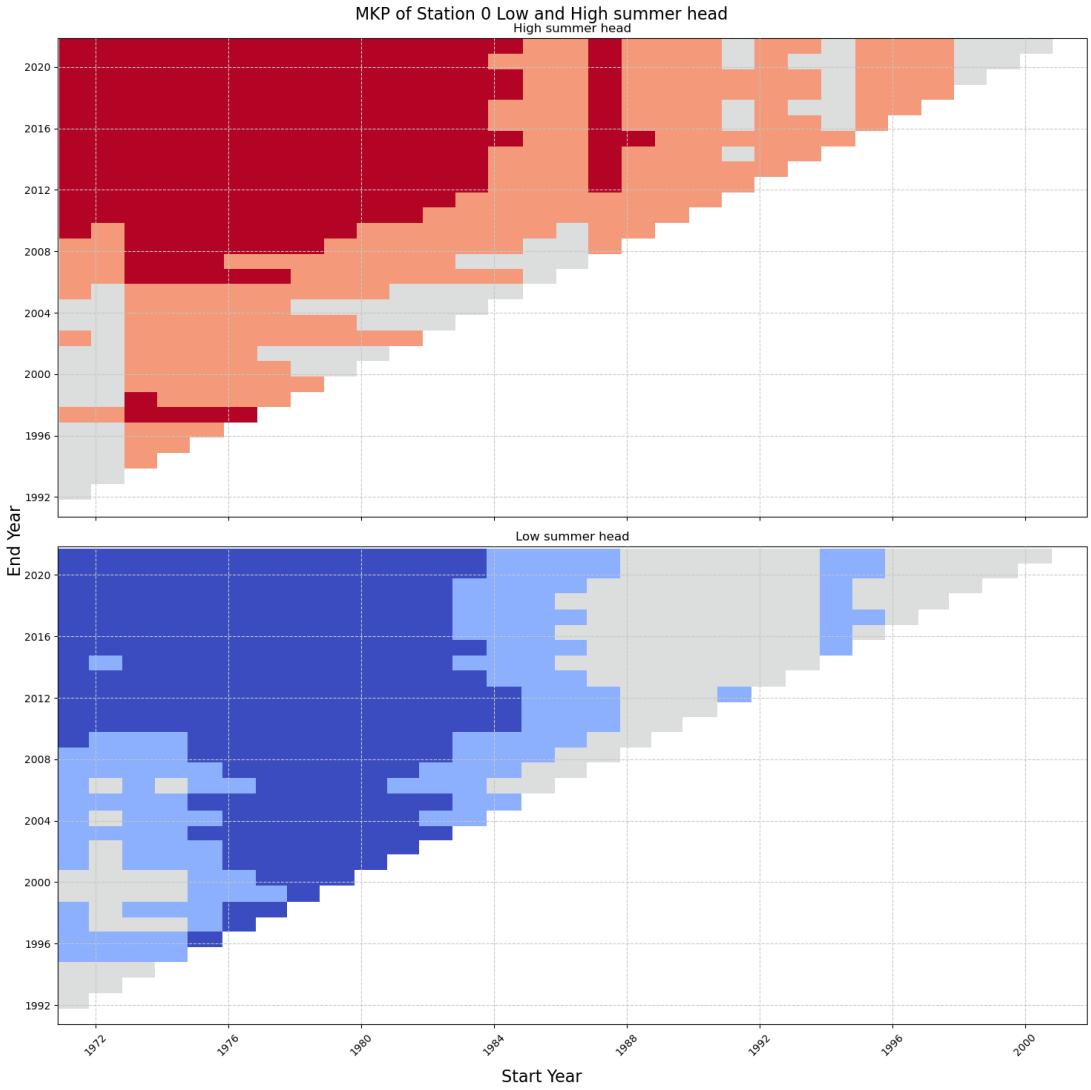

Figure 4.27: Same as figure 4.23, but for Abrahamsvoll station (0).

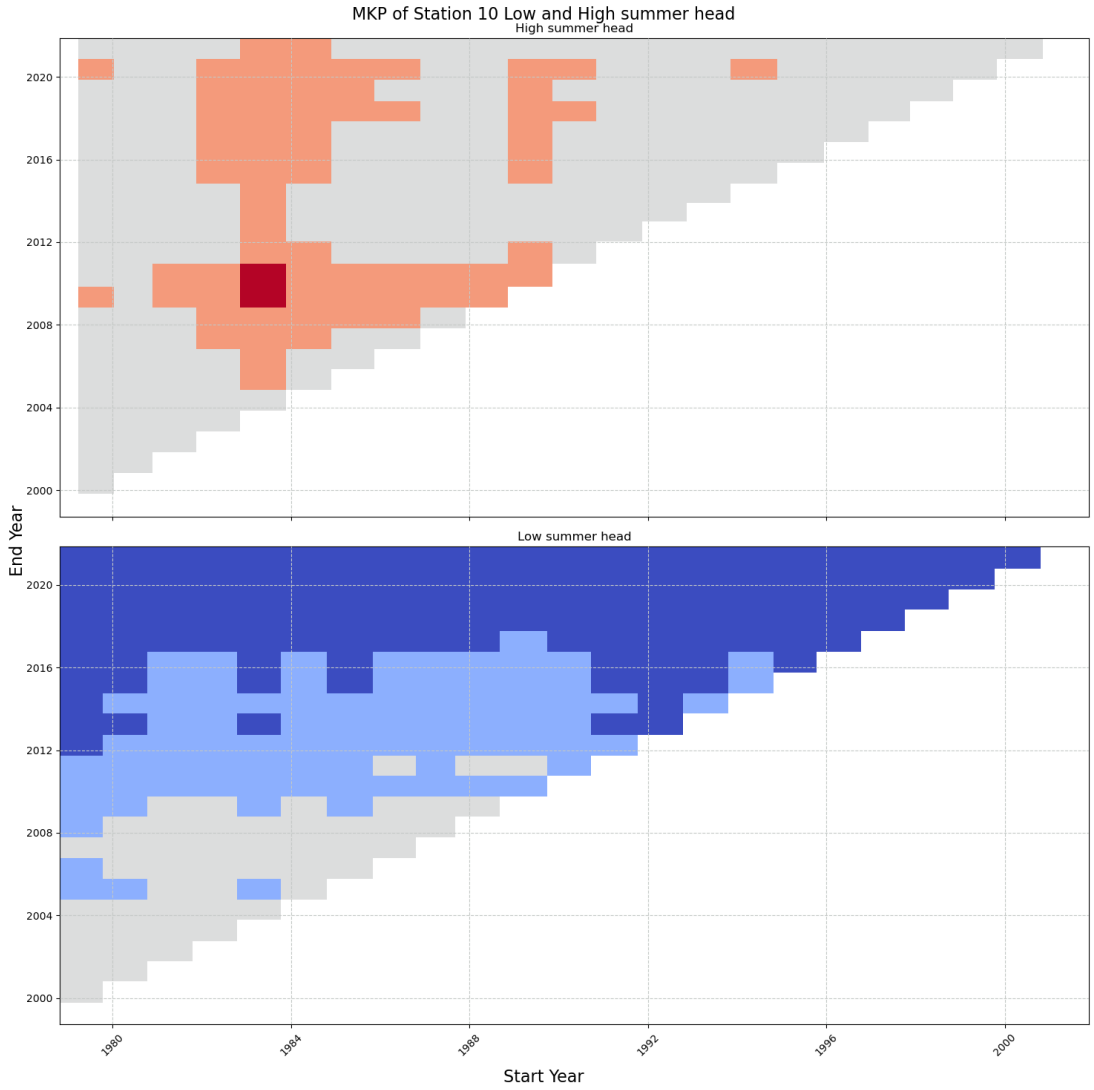

Figure 4.28: Same as figure 4.23, but for Finnbølseter station (10).

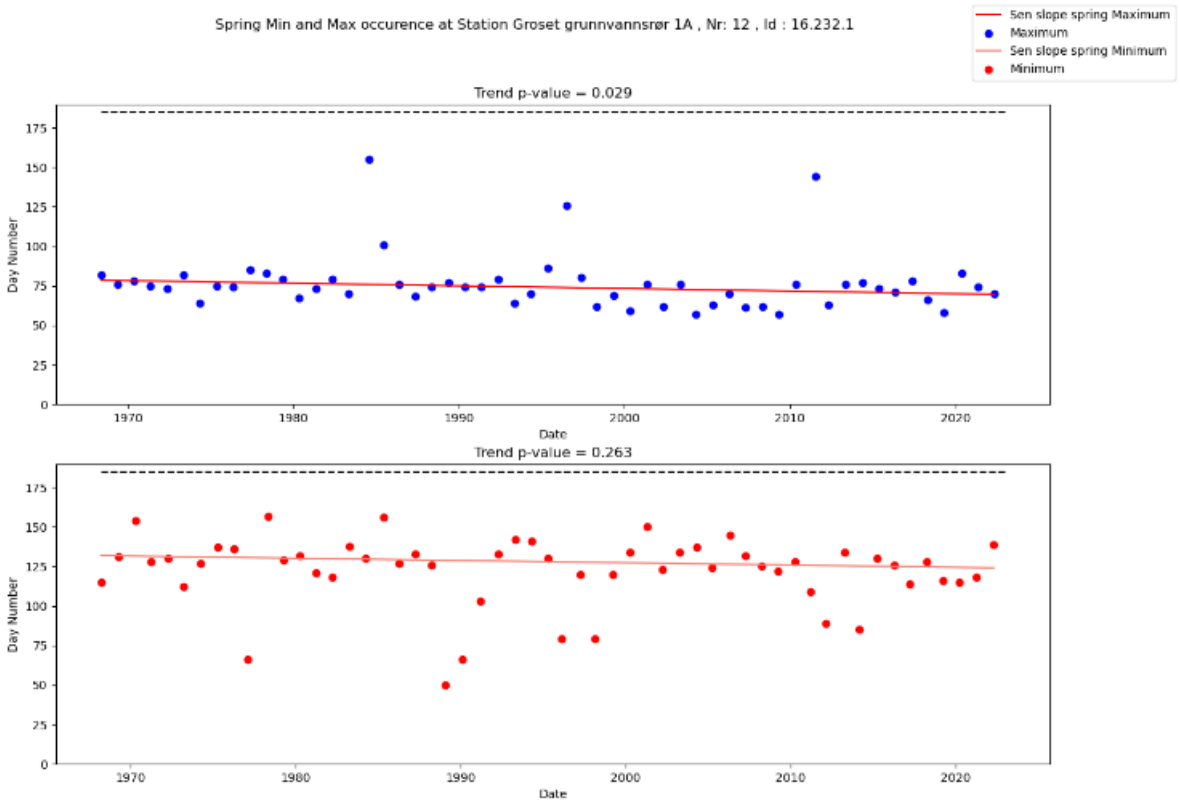

Figure 4.29: Trends in the timing of spring minima and maxima at Groset station (12). The upper graph shows the timing of the spring maxima (blue points) along with the Sen slope of the trend. The lower graph shows the spring timing of the minima (red points) along with its Sen slope of the trend. The x-axis shows the date of the given minima or maxima, while the y-axis is the day number within the period at which it occurred (period stated in section 3.6). The black dashed line (—) indicate the total length of the period, and the title of each graph states the trend p-value.

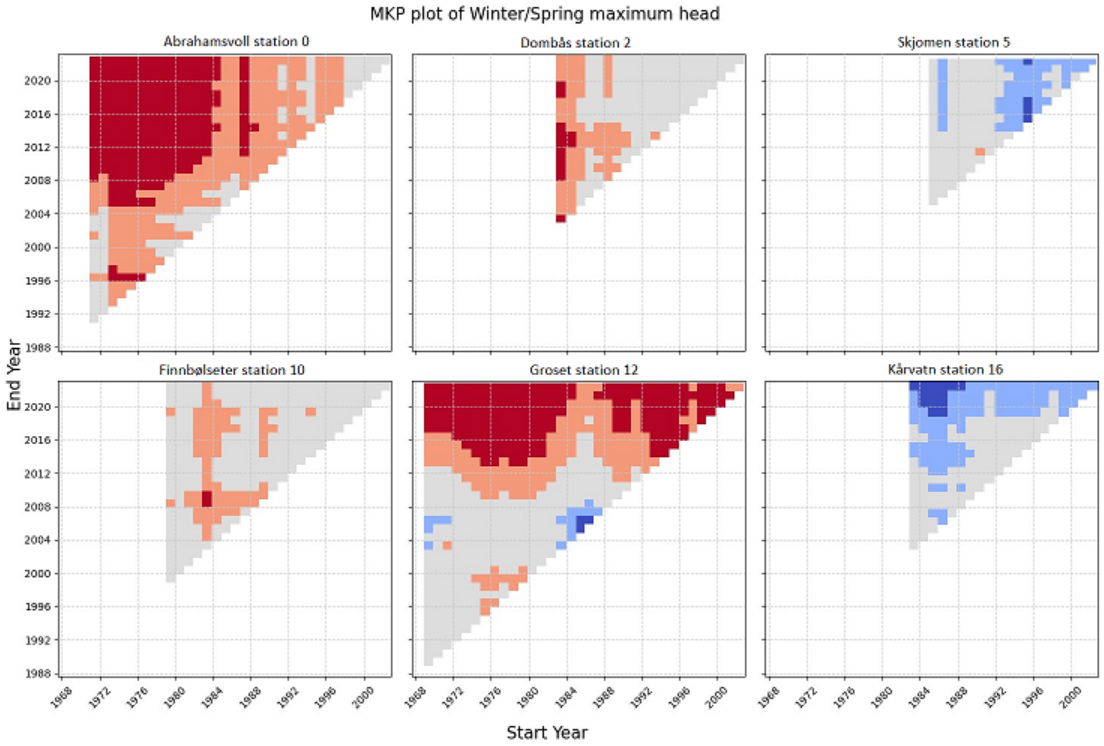

Figure 4.30: Multi temporal trends for the GWL maximum is shown for the stations within the Mountain regime. Here the stations are plotted with the relative start date according to the length of the stations. Dark blue is positive trend with $p < 0.05$, light blue is positive trend with $0.05 < p < 0.3$, grey is $p > 0.3$, light red is negative trends with $0.05 < p < 0.3$ and dark red is negative trend with $p < 0.05$.

drier conditions (negative), while Skjomen (5) and Kårvatn (16) stations have significant trends toward wetter conditions (positive). Simultaneously, the trends of the maximum GWL timing are negative, indicating moving towards earlier timing for Abrahamsvoll (0), Finnbølseter (10), Groset (12) and Kårvatn (16) stations. Here only Kårvatn (16) station shows trends of increasing maximum GWL and earlier timing. Overall, a trend towards an decrease in GWL corresponds with an earlier timing of the GWL maxima.

In Figure 4.32 we see the minimum of the winter and spring months plotted with the trends in timing (Figure 4.33). Here we see that there is a general positive trend of the minimum GWL. Abrahamsvoll (0), Finnbølseter (19) and Kårvatn (16) stations show that there is stable strong significant positive GWL trends, while Groset (12) and Skjomen (5) stations show weak significant positive GWL trends for a portion of the periods. Dombås (2) station is an exception to this, since it exhibits significant negative GWL trend. Looking at the trends in timing, Abrahamsvoll (0) and Finnbølseter (10) stations show general negative trends, indicating that the minima is occurring earlier in the period. Dombås (2), Kårvatn (16) and Skjomen (5) stations however, show general positive trends, indicating later timing. Groset (12) station is not so clear with no prominent trend in timing. Overall, a trend towards an increase GWL minima, corresponds with either an earlier or later timing.

Using all the data at each station in the Mountain regime, we calculate the trend of the timing of the maximum and minimum GWL. Table 4.34 shows the p-value of the trend with the colours indicating the trend direction of the trends. Here we see that the timing of the minimum GWL value has a strong and weak significant negative trend for Kårvatn (16), Groset (12) and Finnbøl-

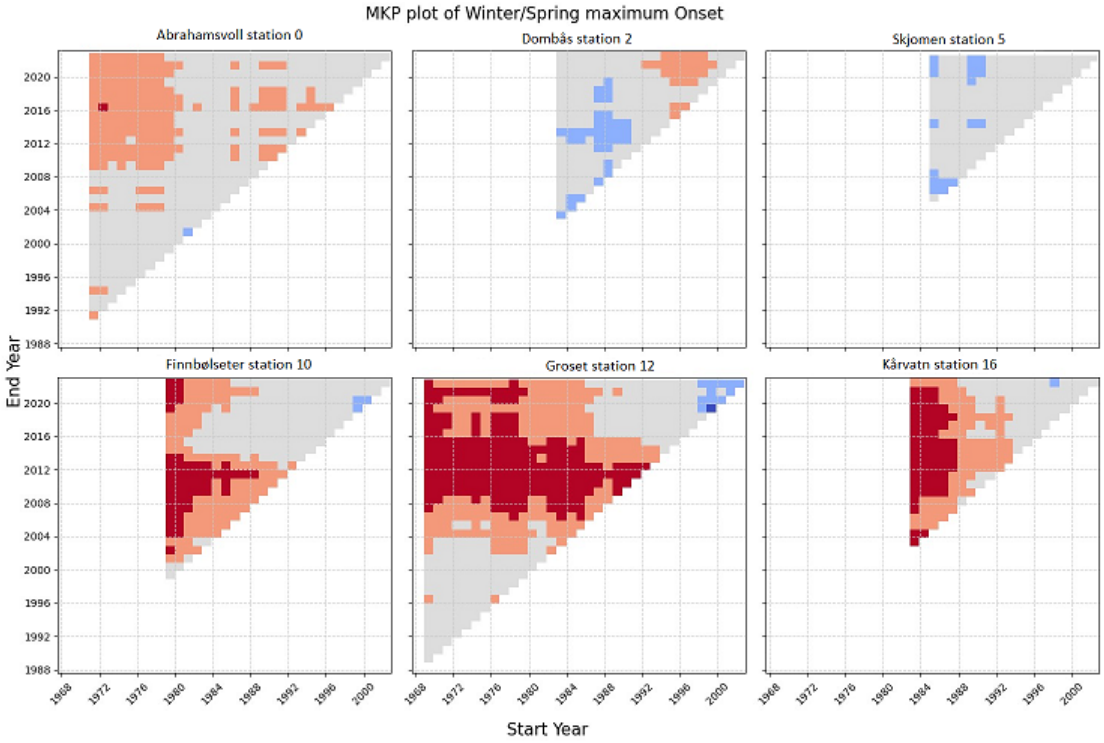

Figure 4.31: The multi temporal trends for the timing of the maximum GWL in the winter and spring months are shown for the stations within the Mountain regime. The coloring is as in Figure 4.30. The positive trends reflect a later timing, while the negative trends reflect to earlier timing.

Figure 4.32: The same as in Figure 4.30, but with the GWL minimum.

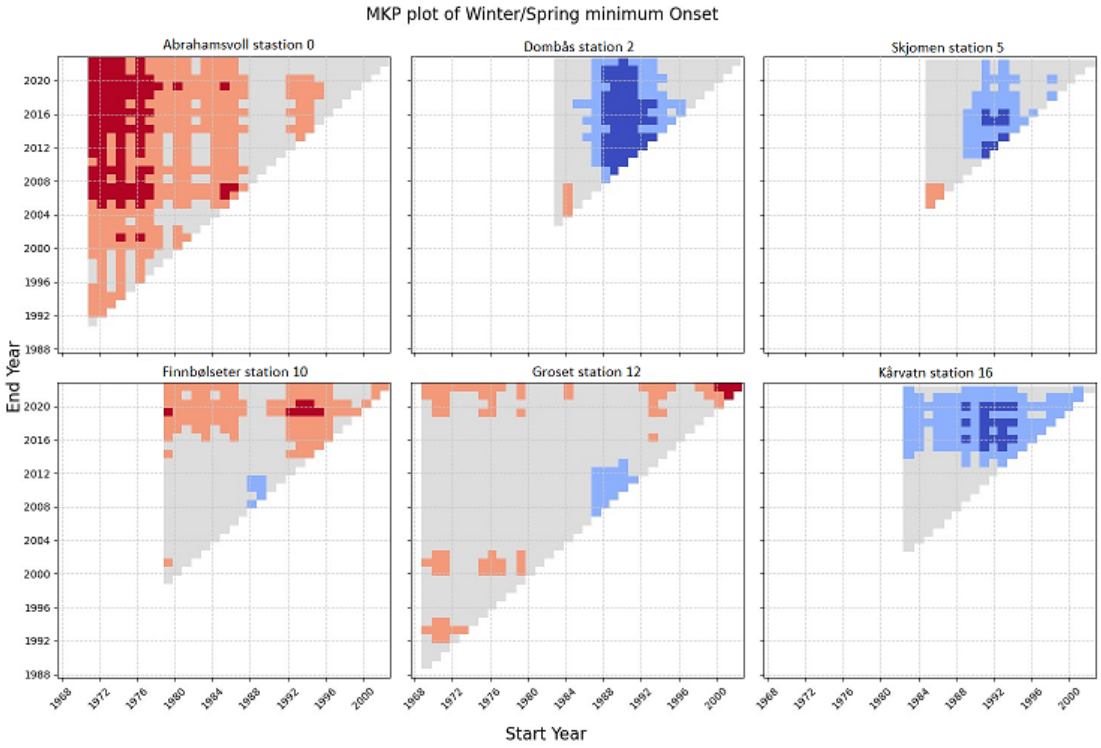

Figure 4.33: The same as in Figure 4.31, but with the GWL minimum.

seter (10) stations. This indicates that the timing of the GWL peak has a trend towards earlier dates. At the same time, we see that the minimum GWL has strong and weak negative trends for Abrahamsvoll (0), Finnbølseter (10), Groset (12) and Skjomen (5) stations. This indicates that the timing of the minimum GWL is also moving towards earlier periods on these stations.

4.7 Trends in annual and monthly hydrometorological drivers

To calculate the trends of the main drivers we use the data from E-OBS and SeNorge. This is the same data that were used as inputs in the Pastas models. A summary of the trends in rain + snow melt (R+SM) and the potential evapotranspiration (PET) is shown in Table 4.36. The stations are sorted according to the groundwater regimes shown in figure 4.5-4.8. Each station is shown with the trend in average annual R+SM and PET, in addition to the trends in average R+SM and PET for each month. The colors represent the same values as in Tables 4.22 and 4.21, with the addition that the green color is assigned if the months Sen slope is exactly $0.00 mm/yr$. This situation is highlighted in Figure 4.35. Here we see the average R+SM for the March month each year. It is apparent that the majority of the average R+SM value is exactly 0.00 mm/day, but in the later years the R+SM is increasing. Here, the Mann-Kendall test is giving a significantly value, while the Sen slope is exactly 0.00 mm/yr.

Overall, we find a generally positive trends in yearly PET for stations across all regimes. In addition, especially the March, April and September months have a significant positive trend in PET, while February, June, October and November have weak significant positive PET trends, seemingly across all regimes. Furthermore, there are 9 stations with weak significant or strong significant trends in yearly R+SM, whereas two are negative and 7 positives. Both stations with

Figure 4.34: Trends in timing of the minimum and maximum GWL during the late winter and spring for the stations in the mountain regime. The trend p-value is stated for each station with the color code indicating the trend direction. Here grey means insignificant trend (p-value > 0.3), red is weak significant trend towards earlier timing. The strength of the color is indicated by the p-value with light being $0.05 < p < 0.3$ and the dark color is $p < 0.05$.

Trend in timing using All Data				
Groundwater regime	Station Nr	Station ID	Minima	Maxima
Mountain : Regime 3	16	111.14.2	0.452	0.286
	12	16.232.1	0.263	0.029
	0	2.725.1	0.007	0.307
	10	2.722.1	0.199	0.090
	23	196.47.2	0.649	0.649
	5	173.28.1	0.255	0.439
	2	2.718.2	0.628	0.653

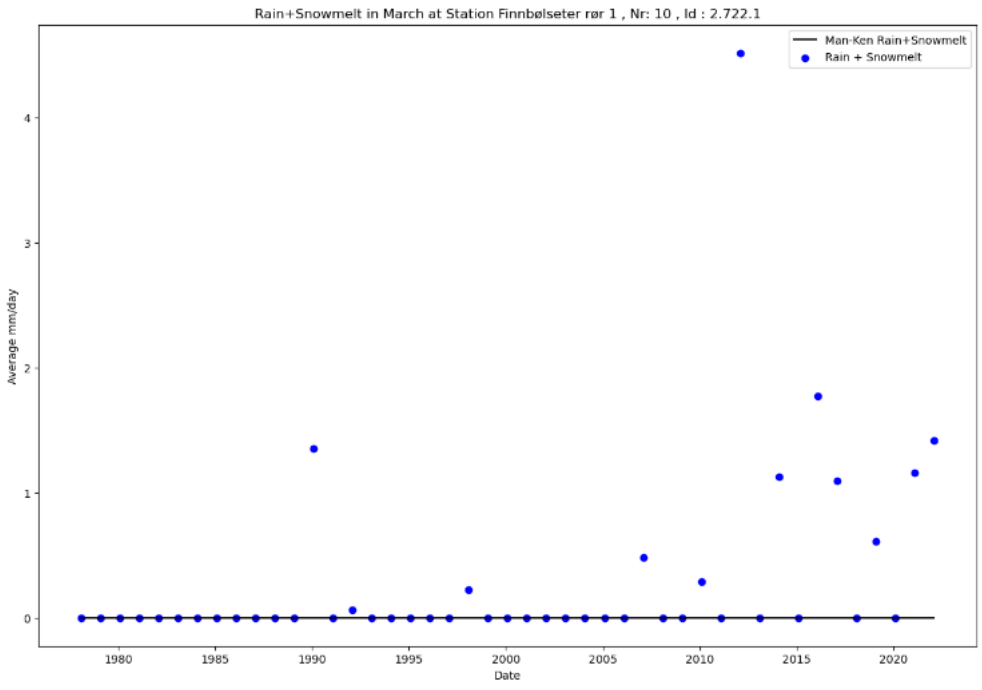

Figure 4.35: Here, we see the average monthly R+SM values for March month at station 2.722.1 plotted with the Sen slope.

negative trends are within the Mountain regime. For stations within the Transitional, Mountain and Mountain delayed regimes, several stations have significant positive trends and Sen slope of $0.00 mm/yr$ in December, January, February and March months. In addition, the negative R+SM trends seems to be primarily within the months between March to May, while there are some stations that have weak significant negative trends in June, July, September and October. The positive R+SM trends seems to be mainly in November, February, April, May, June and July, seemingly across all regimes.

	41-year trends on R+SM and PET calculated in the period 1982-2022																											
	Station Nr	Station ID	Year trend		Jan		Feb		Mar		Apr		May		Jun		Jul		Aug		Sep		Oct		Nov		Dec	
			R+SM	PET	R+SM	PET	R+SM	PET	R+SM	PET	R+SM	PET	R+SM	PET	R+SM	PET	R+SM	PET	R+SM	PET	R+SM	PET	R+SM	PET	R+SM	PET	R+SM	PET
Atlantic : Regime 1	9	56.3.2	0.49	0.97	0.78	0.63	0.43	0.25	0.27	0.54	0.69	0.10	0.77	0.49	0.32	0.43	0.31	0.39	0.83	0.60	0.75	0.16	0.39	0.05	0.34	0.03	0.59	0.41
	17	23.17.4	0.60	0.00	0.61	0.08	0.47	0.02	0.03	0.00	0.15	0.00	0.14	0.09	0.40	0.02	0.13	0.13	0.89	0.01	0.49	0.00	0.93	0.00	0.29	0.11	0.93	0.48
	11	84.25.3	0.87	0.01	0.68	0.32	0.45	0.33	0.96	0.20	0.56	0.04	0.49	0.76	0.16	0.55	0.02	0.26	0.88	0.22	0.68	0.04	0.94	0.10	0.90	0.07	0.73	0.61
	8	21.80.1	0.80	0.14	0.79	0.41	0.22	0.21	0.30	0.00	0.01	0.00	0.29	0.99	0.61	0.65	0.24	0.23	0.80	0.87	0.65	0.15	0.74	0.22	0.23	0.28	0.93	0.83
	15	28.14.2	0.03	0.54	0.69	0.28	0.14	0.18	0.75	0.13	0.88	0.06	0.21	0.36	0.47	0.99	0.04	0.71	0.95	0.31	0.21	0.04	0.67	0.11	0.27	0.36	0.90	0.80
	1	20.34.4	0.04	0.00	0.37	0.45	0.05	0.15	0.85	0.00	0.14	0.00	0.21	0.13	0.15	0.02	0.33	0.85	0.91	0.07	0.79	0.02	0.68	0.01	0.15	0.28	0.28	0.47
	20	89.3.1	0.96	0.08	0.73	0.92	0.41	0.92	0.68	0.88	0.96	0.20	0.67	0.71	0.31	0.49	0.51	0.34	0.73	0.71	0.57	0.07	0.76	0.57	0.88	0.49	0.90	0.34
Transitional : Regime 2	22	2.716.6	0.98	0.12	0.17	0.57	0.94	0.04	0.02	0.01	0.33	0.00	0.03	0.66	0.37	0.20	0.51	0.66	0.19	0.69	0.54	0.02	0.89	0.29	0.03	0.26	0.68	0.74
	3	2.727.0	0.24	0.01	0.78	0.87	0.16	0.15	0.79	0.01	0.01	0.00	0.18	0.69	0.36	0.09	0.17	0.66	0.33	0.16	0.69	0.02	0.55	0.09	0.22	0.35	0.10	0.85
	6	19.144.6	0.14	0.00	0.36	0.52	0.03	0.20	0.74	0.00	0.01	0.00	0.41	0.36	0.20	0.20	0.27	0.54	0.92	0.58	0.77	0.15	0.93	0.07	0.17	0.37	0.61	0.73
	24	2.719.2	0.51	0.05	0.02	0.99	0.43	0.52	0.01	0.01	0.03	0.01	0.01	0.94	0.94	0.13	0.60	0.85	0.47	0.39	0.42	0.02	0.44	0.24	0.04	0.18	0.04	0.73
	18	2.721.1	0.31	0.05	0.01	0.78	0.16	0.55	0.16	0.03	0.05	0.06	0.47	0.88	0.12	0.14	0.39	0.97	0.65	0.40	0.70	0.00	0.57	0.05	0.02	0.12	0.03	0.83
	21	2.723.4	0.05	0.00	0.18	0.88	0.68	0.07	0.32	0.01	0.51	0.00	0.27	0.17	0.66	0.01	0.51	0.06	0.51	0.01	0.58	0.00	0.27	0.04	0.20	0.00	0.42	0.49
	7	16.231.9	0.80	0.04	0.81	0.57	0.28	0.14	0.49	0.00	0.01	0.00	0.46	0.81	0.32	0.32	0.31	0.76	0.66	0.76	0.94	0.07	0.89	0.32	0.79	0.48	0.60	0.87
	19	313.12.7	0.57	0.01	0.34	0.37	0.29	0.13	0.84	0.00	0.02	0.00	0.09	0.87	0.87	0.07	0.18	0.81	0.98	0.69	0.40	0.02	0.87	0.09	0.50	0.10	0.16	0.83
Mountain : Regime 3	16	111.14.2	0.23	0.00	0.56	0.47	0.13	0.22	0.01	0.00	0.72	0.00	0.00	0.14	0.67	0.01	0.15	0.13	0.54	0.02	0.39	0.00	0.88	0.04	0.68	0.05	0.74	0.76
	12	16.232.1	0.04	0.01	0.00	0.48	0.43	0.10	0.00	0.01	0.02	0.00	0.00	0.32	0.15	0.17	0.37	0.61	0.46	0.19	0.48	0.00	0.86	0.05	0.05	0.07	0.05	0.85
	0	2.725.1	0.83	0.00	0.01	0.88	0.67	0.15	0.21	0.02	0.49	0.01	0.67	0.90	0.06	0.06	0.89	0.35	0.37	0.06	0.27	0.00	0.59	0.41	0.79	0.06	0.27	0.49
	10	2.722.1	0.71	0.02	0.01	0.88	0.17	0.37	0.00	0.00	0.33	0.00	0.08	0.57	0.74	0.12	0.52	0.97	0.66	0.30	0.45	0.04	0.69	0.55	0.12	0.39	0.11	0.61
	23	196.47.2	---	---	---	---	---	---	---	---	---	---	---	---	---	---	---	---	---	---	---	---	---	---	---	---	---	---
	5	173.28.1	0.02	0.00	0.85	0.57	0.88	0.28	0.07	0.19	0.31	0.00	0.67	0.03	0.05	0.55	0.89	0.06	0.44	0.05	0.57	0.04	0.39	0.11	0.98	0.09	0.84	1.00
	2	2.718.2	0.48	0.00	0.12	0.85	0.08	0.30	0.03	0.01	0.45	0.00	0.16	0.57	0.74	0.06	0.15	0.37	0.33	0.13	0.36	0.00	0.28	0.05	0.48	0.03	0.94	0.71
Mountain delay : Regime 3	4	12.343.12	0.00	0.00	0.35	0.96	0.10	0.15	0.49	0.00	0.08	0.00	0.12	0.78	0.06	0.04	0.01	0.52	0.63	0.06	0.56	0.05	0.46	0.22	0.33	0.19	0.22	0.78
	13	2.724.9	0.92	0.01	0.51	0.54	0.24	0.14	0.86	0.00	0.00	0.00	0.24	0.97	0.45	0.22	0.64	1.00	0.39	0.60	0.46	0.04	0.50	0.30	0.32	0.44	0.49	0.90
	14	2.713.3	0.44	0.08	0.42	0.54	0.06	0.14	0.29	0.00	0.00	0.00	0.63	0.97	0.28	0.22	0.17	1.00	0.88	0.60	0.47	0.04	0.43	0.30	0.38	0.44	0.31	0.90

Figure 4.36: Trends in the table are calculated in the same way as in Table 4.22, but for the Input. Here the colors are in set in relation to the impact on the groundwater recharge, with blue indicating increasing GWL recharge and red indicating decrease GWL recharge. Therefore, a positive R+SM trend is given a blue color, and a positive trend in PET is given a red color.

Chapter 5

Discussion

5.1 Model performance

To determine which type of recharge model is the best, and if they are acceptable to use for the infilling, we compare each model type R^2-score. A high score would mean that the model is simulating the variations of the groundwater accurately and thus, would be a good model to use in the infilling.

In Table 4.2, we see that the "Threshold model" and the "Non-linear model with a snow scheme" are performing the best across almost all stations. Since the precipitation input data we use in the models is the sum of the rain and snowmelt, it alone should be able to account for the rain and snowmelt water contribution to the groundwater recharge. We therefore expect a similar performance between the Non-linear and Non-linear models with a snow scheme. From Table 4.1, we see that the difference in R^2-score between the two model types is less than 0.4 for 17 out of 25 stations. There are no apparent similarities between the 8 stations with a larger difference, but 6 of the stations are within the Mountain or Mountain delayed regime, and one in the Transitional regime where the snow is a considerable factor. Only Fana station (2) is in the Atlantic regime, located by the coast with high average temperatures and where the number of potential snow days is low.

An explanation for the difference between the Non-linear model and the Non-linear model with snow scheme, could be in the difference between the method NVE is using to calculate the rain and snowmelt data (section 2.2), and the inbuilt snow scheme in the model (section 3.2.4). If this is the chase, there would be a miss match between what is considered rain and what is considered snow. In addition, since the rain and snowmelt data are using an energy balance to estimate the snowmelt, and the model is using the degree-day method, there would presumably be a mismatch between when the snowpack is considered melted in the input data and the model snow scheme. This could give rise to a scenario when the model has almost no snow in the winter (because the input data estimate no effective precipitation), but during the early spring months, the model estimate snowfall instead of precipitation, because of the mismatch in temperature. Noteworthy, the earliest point the model can estimate positive groundwater recharge is when the rain and snowmelt input data is positive (e.i. when NVEs model has estimated that the snowpack is melted). Therefore, the difference in performance between the Non-linear model and the Non-linear model with a snow scheme, is most likely due to the time lag of recharge, created by the model snowmelt scheme.

It is also noteworthy that the threshold model is preforming the best at most stations. As described in section 3.2.4, this recharge model type is fitting two response functions to the recharge. Therefore, it is able to capture if there is a natural boundary or change in dynamics of the recharge. Such natural threshold levels could be if the GWL reaches the surface or an impermeable lower boundary, or it could be the root-zone, where the dynamic of the surface to subsurface changes.

In addition, Hauerseter station (14) was the only one where the linear recharge model preformed the best. Noteworthy, this is the station with the deepest GWL and highest AC. An explanation to why the linear recharge model preformed the best could be that the deposits, soil type and structure, vegetation cover etc create a linear relationship between the surface water and the recharge.

5.2 Gap-filling

The gap-filling is based on using the simulated values from the best model at each station. From Table 2.2 we see that the majority of the gaps are under 31 days. There are 36 gaps with lengths between 3 and 12 months, and 9 gaps over 12 months. The difference between the gap-filled value and the actual GWL is minimal in the short gaps, while the potential difference increases with the length of the gap. If we look at Figure 4.3, we see a zoom-in of the infilled values for Nordfjordeid station (20). Her, we see a short gap in the observations, and the infilled values is realistic. However, if the gap had been much longer (for example several months), then this would not necessarily be the case.

Therefore, for gaps lasting several months or years, the model ability to estimate the groundwater accurately plays an important role in how good the infilled values are. For the stations that contains gaps in the observation data over 1 year, the best model R^2 performance ranges between 0.50 to 0.90. However, only Kise (3), Kårvatn (16) and Settalbekken (21) stations have a R^2 score lower than 0.75. This could lead us to be more sceptical to the infilled values within the long gap in these stations, and an improvement of the model, through better parameter calibration or input data, could give a meaningful improvement of the time series.

In addition, because we set the boundary of the gap-filled values according to the maximum and minimum observations, new extreme observations could affect a new gap-filling by allowing for higher or lower values. To minimize this effect, one could use natural upper- and lower-boundaries. An example could be using depth to bedrock and surface level instead of the maximum and minimum observation. This would require more information about each station, and using surface level, or maximum- with minimum-observation value as a boundary is a easy way to confine the infilling values to a realistic value. One such example of this is shown in Figure 4.4. Here we see that the infilled values (green) is more or less fitting with the observations, with few outliers. We can also see that there is one peak (ca. 1983), and one low (ca. 2004) which is restricted to the boundary of maximum and minimum observations. Hence, new extreme observations in the future could enable us to fit higher or lower simulated values to the time series.

5.3 Groundwater trends

The trends in groundwater level were preseuted in two ways; Multi Temporal p-value (MKP) plot and set period table. The set period tables, figures 4.21 and 4.22, shows the 31-year and 41-year trends respectively. Only Øverbygd station (23) has too short time series to be calculated trend for both periods, while Kise station (3) is only calculated for the 31-year period. Trends are shown for each month and the year GWL average.

Whereas the set period tables could give us an understanding of how the long-term trends (31- and 41-year) are, the MKP plot give us a understanding on how the trends change, and how different "drying" or "wetting" periods are affecting the trends. Some stations have a significant auto correlation between 52-1026 days, the significance of the trend in one month is expected to transfer over to the next month. This way, positive or negative trends can be seen in months where the meteorological drivers is not actual changing. Therefore, in order to interpret the significance of the change in each month, we need not only look at the p-value of the Mann-Kendall test, but also how the trend changes from one month to another in relation to the auto correlation. This way, if the trend is highly significant in April but insignificant in May, there could be a shift in yearly peak value from May to April, even though we don't see a negative trend in the later months.

5.3.1 31- and 41- year set periods

In the table shown in Figure 4.21 we see the 31-year trend over the period 1992-2022. The table is sorted in according to the groundwater regime, and within the regimes, according to the auto correlation. each regime shows different general patterns in trends. This is also done for with the 41-year period (1982-2023 in the table in Figure 4.22.

If we compare the 31- and 41-year trend tables, the trends present in the 31-year periods tend to become more significant in the 41-year trends. For Evje (8), Førde/Moskog (11), Stenerseter (21), Lykjestøylane (17), Settalbekken (21), Magnor (19), Finnbølseter (10) and Modum (4) stations, trends became less significant or even changed directions (stations Abrahamsvoll (0) and Finnbølseter (10)). This could be because there is a general positive or negative trend present at each station. If this is the case, it would be expected that adding the 10 years between 1982 and 1992 would make the trend more significant.

However, it could also be the case that the trends are affected by particular wet or dry periods between 1982 and 1992. This could be the case for station Abrahamsvoll (0) and Finnbølseter (10), where we see that the trends, in July and August respectively, change direction. If we examine the time series for these two periods (In appendix B) we see that Abrahamsvoll (0) station has especially low values in 2016 and 2018. This could lead us to believe that the 31-year trend is more effected by this than the 41 year trend. For Finnbølseter (10) station, the values in 1982 and 1983 is particularly low, while the value in 1993 is particularly high. This may indicate that the change in direction of the trends in the different periods, is affected by these values.

The effect of having a few years changing the significance of the trend is proportional with the number of observations. Since we are dealing with 31 and 41 data points when calculating the trends, we expect that the significance of the trends might be influenced by years with particular high or low values. However, the more data points we have, the less is this effect. This is also the advantage of the MKP plot since we can see how prominent the trend is.

5.3.2 Groundwater regimes

Analysing the set period tables we see a general pattern within the different regions. In the Atlantic regime, all stations are located along the coast, with a relatively high yearly average temperature. From the 31- and 41-year trends, we see that the regime has two general patterns. First, we see positive trends in the winter, spring and autumn months while the summer months are insignificant. Secondly, negative trends in the summer months along with insignificant or weak significant positive trends in the other months. The typical drivers of the seasonal variations for the Atlantic regime stations are peaks driven by precipitation events and lows driven by PET and grow rates. Looking at the trends in drivers, it is apparent that there is a general positive trend in PET in the spring an autumn. Positive PET trends in combination with negative R+SM trends are seen in Fana (9), Lindesnes (17), Evje (8) and Birkenes (1) stations. Looking at the MKP figures, station Evje (8) and Lindesnes (17), and in a small degree station Birkenes (1), seem to show an effect of this. March, April and May months in Evje (8) and Lindesnes (17) stations have prominent negative trends as expected. Likewise, the stations that have significant positive yearly R+SM trend, show generally positive trends in their GWL (MKP figures in Appendix C for Birkenes (1) and Jæren (15) stations). An exception is Fana (9) station, which show negative R+SM trends in March, with no other positive trends in R+SM in the other months, but still has generally positive GWL trends in almost all months (MKP figures in Appendix C fro Fana (9)).

There are no apparent geographical similarities between the stations following the different patterns. However, the stations with negative trends in the summer are located on sandy glacial fluvial deposits, with a forest cover between 38% to 84% around the station. In contrast, the stations with the positive trends are located on sandy moraine or marine sand deposits, with a forest cover between 19% to 74% around the stations. The different deposit types combined with vegetation density could indicate a different surface-to-subsurface interaction which might explain the different trend patterns within the regime.

For the stations within the mountain regimes, there is little to no recharge to the groundwater in the winter because of the stable cold temperatures resulting in frost and snow cover. When we see that there is a significant increase in groundwater level in the winter months at these stations, then we can assume that the frost and snow cover is discontinuous and enabling recharge. The resulting recharge is small, but it is a significant change from past conditions. This small change can be seen in the 41-year trends in drivers for these stations where we see that the trends are significant according to Mann-Kendall, but the Sen slope is exactly $0.00 mm/yr$. What this could point towards, is that the small positive change in groundwater level we see at several of the mountain regime stations is indicating the start of a shift towards earlier spring melt related GWL increase.

Another scenario could also be that there is a general temperature increase leading to an increase in winter GWL, but in combination with an increase in general precipitation, not necessarily result in a shift timing in spring melt related GWL increase. However, as seen in the seasonal variation patterns (Figure 4.7), the snow melt is a much larger contribution to the groundwater recharge than the precipitation. This is because prolonged snowmelt creates fully soil saturated conditions for long periods, and groundwater recharge is high.

Looking at the 41-year trends in drivers, we can see that for all the stations the yearly PET has a significant positive trend. Since PET is a function of temperature, indicates this that the temperature at the stations could also be increasing. This is again supported by the findings in [Hanssen-Bauer et al., 2015] and is shown in map 2.4, were the temperature has shown to be

increasing. It is also worth noting that, with higher temperatures comes potentially higher grow rates and earlier start of the growing season for the vegetation in the area.

In addition to the trends in PET, we see that there is also trends in R+SM. Here, there is a general positive trend in February and March, along with negative trends in April and May. For the yearly trends, two stations have positive trends and two negative trends. The two stations that have a significant (Groset station (12)) and weak significant (Kårvatn station (16)) negative trend, there is overall less R+SM through the year mainly due to the negative trends in May. This is typically the month of, or before, the spring GWL peak, and thus might indicate decreasing peak.

For Groset station (12), this is supported by the negative trends in spring maxima (Figure 4.30). In contrast, Kårvatn station (16) seems to have positive spring maximum trends (Figure 4.30), despite having a significant decrease in R+SM in the month before the peak. A lower amount of R+SM, would lead us to believe it should result in negative trends in the groundwater level in the typical spring melt related months. However, we see from the monthly MKP figures, that the trends in these months are significant or weak significant positive (in addition to more prominent positive trends in the month before the typical spring peak month, supporting the findings in trends in timing, Figure 4.31).

An explanation to this could be that during the spring melt, the soil is fully saturated and the groundwater recharge is restricted by the spatial distribution of the frost, and the hydraulic conductivity of the soil. Here, excess water, that cannot infiltrate through the soil, will then drain on the surface as overland flow. In such a scenario, the deciding factor of the amount of recharge is the time duration of the spring melt. Because of this, there is not necessarily a direct correlation of decreasing trends in the R+SM and the groundwater level, if the soil is fully saturated over approximately the same time span. With temperatures in the early spring fluctuating around 0 ^{o}C, the melt and freeze processes of the ground and snowpack can contribute to a prolonged "spring melt infiltration period", and therefore contribute to increasing GWL recharge. As we see in table 2.5 and 4.4, the stations within the Mountain regime, Mountain delayed regime and the majority within the Transitional regime have had a increase in number of days with daily average temperature between -1.5 to 1 ^{o}C. However, if after a while, there is less snow accumulated during winter, the time the it takes to melt the snow in spring, would also presumably be shortened. Therefore, negative trends in spring and summer GWL would become apparent after a sufficient change in snow accumulation has occurred.

The Transitional regime more ambiguous. The stations within this regime have two annual peaks; one that is linked to the snowmelt and one to the rainfall. The stations located at high altitudes (Settalbekken (21), Lykjestøylane (18) and Øyangen (24)) have similar seasonal variations to the Mountain regime. In addition, examining the seasonal variations, Magnor (19) station seems to get the biggest contribution from what could be the spring melt. However, this station also has a deep groundwater table and a high autocorrelation.

All stations within the Transitional regime that resembles the mountain regime, have similar positive trends for the winter and spring months. The monthly MKP plots for each station show that the for some of the winter, spring and autumn months, several or majority, of the possible periods have positive trends. Here Lykjestøylane (18) and Settalbekken (21) stations differ somewhat from the patterns with prominent negative trends for some of the spring and autumn months. Both stations are differing from the other stations within the Mountain regime by having peat as the dominant land cover, or peat in combination with mountain. Dominant peat and mountain

could affect the surface to subsurface dynamic differently than other vegetation types and therefore explain difference. Looking at the yearly average MKP, most prominently Lykjestøylane (18), Øyangen (24) and Magnor (19) stations, and station Settalbekken (21) in a lesser extent, seem to have positive trends resembling the general patterns in the Mountain regime.

5.3.3 Groundwater minima and maxima

The GWL minima and maxima is calculated for two different periods (Table 3.2 and 3.3). The MKP plot shows us how prominent the trends are and how they change depending on the periods. The GWL minima and maxima plots of the stations within the Atlantic regime show that there is a both negative and positive prominent trends. It seems like there is a similarity between stations that is located in generally the same region. Førde/Moskog (11) and Nordfjordeid (20) stations, which is located in the Northern part of the Western coast, has both negative trends in the maxima and minima GWL. In contrast, station Førde (9) and Jæren (15) (located in the southern part of the western coast) have prominent positive trends in the maxima (and minima in Jæren (15) station). The rest of the stations in the Atlantic regime (Evje (8), Lindesned (17) and Birkenes (1) stations) are located in the Eastern part of the southern coast. They have all prominent positive trends in the GWL minima. For all stations, dominant driver of the groundwater seasonal pattern is the precipitation. With the typical GWL minima occurring in the early autumn, the positive trend in Birkenes (1), Lindesnes (17), Evje (8) and Jæren (15) stations, can be attributed to more precipitation in the autumn. In addition, GWL maxima occurs in the winter, and only for stations Jæren (15) and Fana (9) it has a positive trend. There is therefore, seemingly a geographical divide between these stations indicating:

- Wetter winter and summer in the south-western part of Norway
- Wetter summer in the south-eastern part of Norway
- Drier winter and summer in the north-western part of Norway

When examining the maxima and minima trends for stations within the Transitional regime, we see that there is no clear pattern between the stations. Only two stations (Lykjestøylane (18) and Øyangen (24)) showed similarities in the trends, but this is most likely due to their close proximity to each other. The wide range of different trends in minima and maxima could partly be explained by the geographical extent of the station's locations. In addition, the stations are varying in how dominant the precipitation or snowmelt recharge contribution (or lack thereof) is to the yearly GWL maxima and minima. Another factor one has to take into account is the different geological conditions and vegetation cover. The different deposits and soil material in combination to winter snow cover, could impact the frost propagation in winter. In addition, the difference between the vegetation types (peat, mountain and forest) impacts the interception from precipitation, root extraction and surface runoff. While this is true for all stations, the different conditions might make it harder to determine any overarching patterns between the Transitional regime stations.

From the MKP figures showing the trends in minimum and maximum occurrence and GWL of the stations within the Mountain regime, we can infer three patterns:

1. Stations with an increasing minima on an earlier date combined with a decreasing maxima on an earlier date (Abrahamsvoll (0), Groset (12) and Finnbølseter (10) stations).

2. Stations with an increasing minima on a later date, combined with an increasing maxima on the same or earlier date (Skjomen (5) and Kårvatn (16) station).

3. Stations with decreasing minima on a later date, combined with decreasing maxima on the same date (Dombås (2) station).

Pattern 1; the groundwater minima is increasing in tandem with a decreasing trend in GWL maxima. This could come in relation to a lower amount of total snow accumulation during winter, and or earlier snowmelt in the spring. The earlier snowmelt would lead to a higher GWL in the months before the primary spring melt, and with less snow in the late spring, a lower spring GWL maxima.

Patterns 2; the timing of the spring GWL minima and maxima is approaching each other while both the minima and maxima are increasing. This could happen if there is a general increase in winter groundwater recharge combined with an increase in spring melt. From the station map (Figure 2.2), we see that both Skjomen (5) station and Kårvatn (16) station are located by the coast. The coastal climate keeps the yearly temperature variation stable as compared with the inland regions. Therefore, even though if the average temperature is low, the winter and spring temperature could be fairly warm. Varying temperatures around 0 degrees could increase GWL recharge through the winter and spring, thus increasing the overall GWL. In addition, with fairly warm winter temperatures, the soil frost depth propagation could also be limited, making early and more recharge possible.

Pattern 3; shows a later and decreasing spring minima combined with a decreasing spring maxima. This indicates that the spring melt timing is later, prolonging the winter frost cover, and thus, making the GWL minima just before the spring melt to decrease even further. The GWL is then on a lower level when the spring melt occurs, making the spring maxima lower under normal circumstances. Here, only Dombås (2) station fits this pattern.

5.4 Future studies

In order to improve the models, additional model calibration with the implementation of noise models could be applied. It could better the parameter calibration and model performance, and therefore, also the infilling of the time series. In addition, more observation data will be available in the future, particularly daily data, could improve both the infilling and the models. With more data, more stations could qualify for a trend study and give a better picture of the spatial extent of, and changes to, the groundwater regimes.

We also see the need to analyze how different weather systems impact the groundwater. Possible changes in large scale meteorological systems could lead to more intensive and frequent weather systems. In addition, through the spatiotemporal difference of weather systems impacting Norway, we could maybe see regional changes of the areas with different groundwater regimes.

This study used modeled meteorological gridded data with a spatial resolution of 1x1km and 11x11km. Future studies should look at the possibility of using meteorological data with a higher spatial resolution. Due to high topological gradients, especially in the south-western part, modeled temperature data can be inaccurate. Furthermore, additional data of the geology and terrain around the stations could give important information on hydraulically properties and

natural thresholds levels for the infilling. In addition, there is a need for examining how different types of vegetation covers impacts the seasonal recharge to the groundwater.

For future studies, it could be useful to implement a more robust method for estimating the trend in timing of the spring melt. With the method used here, the estimation of the changing timing is limited to very regular variation patterns with one regular occurring dominant GWL minimum and maximum. This is why it was only the stations within the Mountain regime that were tested. Utilizing circular statistics to determine the shift of the timing would in theory be a more universal approach. This could possibly enable testing stations with irregular occurring or multiple maximum and minimums, like stations within the Transitional regime.

Chapter 6

Conclusion

The Aim of this study is to examine the groundwater variations in Norway. In particular, we want to see if it is possible to identify trends in the groundwater levels. Further, if there is a trend, how does this relate to possible changes in drivers, and could this change the groundwater seasonality. We formulated three hypotheses, and tested them by comparing trends in:

- Annual GWL
- Monthly GWL
- High and low GWL
- Timing of high and low GWL
- 41-year trends in drivers

From comparing the results, we answer the following hypothesis.

Hypothesis 1 Stations where the seasonal variation is heavily influenced by snow accumulation and snowmelt, will experience increasing trends of groundwater levels in the winter months, and no significant increase or a decrease in the summer months.

Stations where the seasonal groundwater variation is influenced by snowmelt is primarily stations within the Mountain regime, in addition to some of the stations within the transitional regime (Lykjestøylane (18), Magnor (19), Settalbekken (21) and Øyangen (24) stations). We see from the tables 4.21 and 4.22, as well as for the MKP figures that for stations within the Mountain regime, there are general positive trends in the winter and spring months preceding the spring melt for 9 out of 10 stations. The exception being Dombås station (2), with significant negative trends in all months. In addition, the stations within the transitional regime, which the seasonal variation seem to be mostly influenced by spring snowmelt, also share these patterns. Based on this, the hypothesis seems to be in agreement with the findings. In addition, the trends in the drivers for these stations, particularly rain and snowmelt, show positive trends in the winter and early spring months, in combination with negative trends in the April and May month. This also seem to be in agreement of the hypothesis.

Hypothesis 2 Stations with a snowmelt related groundwater peak in the spring, will have a change towards earlier GWL peak timing.

Only the stations within the Mountain regime were conducted spring peak timing trend test on. The result was that 3 out of 7 stations showed a significant or weak significant trend in timing. This meant that the GWL maxima related to snowmelt was moving towards earlier periods. In addition, the same test was conducted on the GWL winter/spring minima. Here, 4 out of 7 stations showed a significant or weak significant negative trend in timing. This also meaning that the GWL winter/spring minima was moving toward earlier timing. This meant that most stations (5 out of 7 station) showed sign of a shifting timing of either winter/spring GWL minima or maxima, supporting the hypothesis.

Hypothesis 3 Stations where the seasonal variations are mainly driven by rain events, will experience a decreasing trend in groundwater levels in the summer months, and an increasing trend in the early winter months.

The stations where rainfall evens are a dominant factor in the seasonal groundwater variation is mostly within the Atlantic groundwater regime, but also includes some stations in the Transitional regime (Stenerseter (22), Kise (3), Stigvassåi (6), Eikamoen (7) stations). Here we see a comparatively more negative trends in the summer months, than in the Mountain regime stations. However, 3 out of 11 stations has positive trends in all months, or in the autumn, winter and spring months. In addition, only two stations show signs of positive trends in the autumn and winter months, in contrary of the hypothesis. Therefore, the findings is ambiguous and only partly in agreement of hypothesis 3.

We recommend that similar studies should be conducted in the future when more data is available. Trends found here suggest that there is a general GWL increase at 11 of 25 stations, and 15 stations showing increasing trends in the winter months (December-February). With this study showing change in PET and R+SM, and other studies showing a change temperatures, precipitation, and snowfall, we see clear impacts on the GWL. Stations in the Atlantic regime, and where the snowmelt input is potentially low, shows generally more negative GWL trends than the stations where snowmelt input is high.

In addition, several stations within the Mountain regime seem to exhibit a trend towards earlier spring melt related GWL maxima, along with increasing trend in winter GWL minima. This is in addition to a general increase in winter, spring and autumn GWL, as well as yearly GWL. These positive GWL trends could be in relation to more resent changes in generally wetter winters. With prolonged changes in higher temperatures and lower winter snowfall, there is a possibility that the Mountain regime might shift towards Transitional or Atlantic regimes.

Bibliography

[Allen et al., 1994] Allen, R., Smith, M., Perrier, A., Pereira, L. S., et al. (1994). An update for the definition of reference evapotranspiration. *ICID bulletin*, 43(2):1–34.

[Bakke et al., 2020a] Bakke, S. J., Ionita, M., and Tallaksen, L. M. (2020a). The 2018 northern european hydrological drought and its drivers in a historical perspective. *Hydrology and Earth System Sciences*, 24(11):5621–5653.

[Bakke et al., 2020b] Bakke, S. J., Ionita, M., and Tallaksen, L. M. (2020b). The 2018 northern european hydrological drought and its drivers in a historical perspective. *Hydrology and Earth System Sciences*, 24(11):5621–5653.

[Bakker and Schaars, 2019] Bakker, M. and Schaars, F. (2019). Solving groundwater flow problems with time series analysis: you may not even need another model. *Groundwater*, 57(6):826–833.

[Besbes and De Marsily, 1984] Besbes, M. and De Marsily, G. (1984). From infiltration to recharge: use of a parametric transfer function. *Journal of Hydrology*, 74(3):271–293.

[Collenteur et al., 2019] Collenteur, R. A., Bakker, M., Caljé, R., Klop, S. A., and Schaars, F. (2019). Pastas: Open source software for the analysis of groundwater time series. *Groundwater*, 57(6):877–885.

[Collenteur et al., 2021] Collenteur, R. A., Bakker, M., Klammler, G., and Birk, S. (2021). Estimation of groundwater recharge from groundwater levels using nonlinear transfer function noise models and comparison to lysimeter data. *Hydrology and Earth System Sciences*, 25(5):2931–2949.

[Collenteur et al., 2023] Collenteur, R. A., Moeck, C., Schirmer, M., and Birk, S. (2023). Analysis of nationwide groundwater monitoring networks using lumped-parameter models. *Journal of Hydrology*, 626:130120.

[Dingman, 2015] Dingman, S. L. (2015). *Physical hydrology*. Waveland press.

[Dyrrdal et al., 2012] Dyrrdal, A. V., Isaksen, K., Hygen, H. O., and Meyer, N. K. (2012). Changes in meteorological variables that can trigger natural hazards in norway. *Climate Research*, 55(2):153–165.

[Döll et al., 2012] Döll, P., Hoffmann-Dobrev, H., Portmann, F., Siebert, S., Eicker, A., Rodell, M., Strassberg, G., and Scanlon, B. (2012). Impact of water withdrawals from groundwater and surface water on continental water storage variations. *Journal of Geodynamics*, 59-60:143–156. Mass Transport and Mass Distribution in the System Earth.

[Engeset, 2016] Engeset, R. (2016). Hvordan lages vær-og snødata for senorge. no og xgeo. no. *Norges vassdrags- og energidirektorat*.

[Fleig et al., 2013] Fleig, A. K., Andreassen, L., Barfod, E., Haga, J., Haugen, L., Hisdal, H., Melvold, K., and Saloranta, T. (2013). Norwegian hydrological reference dataset for climate change studies. *NVE report*, pages 19–21, 34–37.

[Gottschalk et al., 1979] Gottschalk, L., Jensen, J. L., Lundquist, D., Solantie, R., and Tollan, A. (1979). Hydrologic regions in the nordic countries. *Hydrology Research*, 10(5):273–286.

[Hannaford et al., 2013] Hannaford, J., Buys, G., Stahl, K., and Tallaksen, L. (2013). The influence of decadal-scale variability on trends in long european streamflow records. *Hydrology and Earth System Sciences*, 17(7):2717–2733.

[Hanssen-Bauer and Førland, 1998] Hanssen-Bauer, I. and Førland, E. (1998). Annual and seasonal precipitation variation in norway 1896-1997. norwegian meteorological institute. Technical report, DNMI Report.

[Hanssen-Bauer et al., 2015] Hanssen-Bauer, I., Førland, E., Haddeland, I., Hisdal, H., Mayer, S., Nesje, A., Nilsen, J., Sandven, S., Sandø, A., Sorteberg, A., et al. (2015). Klima i norge 2100. nccs report no. 2/2015.

[Hanssen-Bauer and Nordli, 1998] Hanssen-Bauer, I. and Nordli, P. (1998). Annual and seasonal temperature variations in norway 1876-1997. *DNMI report*, 25:98.

[Jackson et al., 2019] Jackson, E. K., Roberts, W., Nelsen, B., Williams, G. P., Nelson, E. J., and Ames, D. P. (2019). Introductory overview: Error metrics for hydrologic modelling–a review of common practices and an open source library to facilitate use and adoption. *Environmental Modelling & Software*, 119:32–48.

[Kendall, 1975] Kendall, M. G. (1975). *Rank correlation methods*. Griffin.

[Kirkhusmo, 1988] Kirkhusmo, L. (1988). Groundwater fluctuation patterns in scandinavia. *NHP Rapport*, 23:32–35.

[Knotters and De Gooijer, 1999] Knotters, M. and De Gooijer, J. G. (1999). Tarso modeling of water table depths. *Water Resources Research*, 35(3):695–705.

[Mann, 1945] Mann, H. B. (1945). Nonparametric tests against trend. *Econometrica*, 13:245.

[Moeletsi et al., 2013] Moeletsi, M. E., Walker, S., and Hamandawana, H. (2013). Comparison of the hargreaves and samani equation and the thornthwaite equation for estimating dekadal evapotranspiration in the free state province, south africa. *Physics and Chemistry of the Earth, Parts A/B/C*, 66:4–15.

[NVE, 2019] NVE (11.01.2019/ 11.01.2019). Tørke- og flomåret 2018.

[Nygren, 2022] Nygren, M. (2022). Impact of climate variability on dynamic groundwater storage in mid-to high latitude countries.

[Önöz and Bayazit, 2012] Önöz, B. and Bayazit, M. (2012). Block bootstrap for mann–kendall trend test of serially dependent data. *Hydrological Processes*, 26(23):3552–3560.

[Sen, 1968] Sen, P. K. (1968). Estimates of the regression coefficient based on kendall's tau. *Journal of the American Statistical Association*, 63(324):1379–1389.

[Tallaksen and van Lanen, 2023] Tallaksen, L. M. and van Lanen, H. A. J. (2023). *Hydrological drought: Processes and Estimation Methods for streamflow and groundwater*. Elsevier.

[Tveito, 2021] Tveito, O. (2021). Norwegian standard climate normal 1991–2020–the methodological approach (met-report 05-2021). *Meteorological Institute*.

[UNESCO World Water Assessment Programme, 2022] UNESCO World Water Assessment Programme (2022). *"The United Nations World Water Development Report 2022: groundwater: making the invisible visible"*. "United Nations Educational, Scientific and Cultural Organization", "7, place de Fontenoy, 75352 Paris 07 SP, France".

[van der Schrier, 2023] van der Schrier (2023). The climate data guide: E-obs: High-resolution gridded mean/max/min temperature, precipitation and sea level pressure for europe northern africa. https://climatedataguide.ucar.edu/climate-data/e-obs-high-resolution-gridded-meanmaxmin-temperature-precipitation-and-sea-level.

[von Asmuth and Bierkens, 2005] von Asmuth, J. R. and Bierkens, M. F. (2005). Modeling irregularly spaced residual series as a continuous stochastic process. *Water Resources Research*, 41(12).

[von Asmuth et al., 2002] von Asmuth, J. R., Bierkens, M. F., and Maas, K. (2002). Transfer function-noise modeling in continuous time using predefined impulse response functions. *Water Resources Research*, 38(12):23–1.

[Yoosefdoost et al., 2022] Yoosefdoost, I., Bozorg-Haddad, O., Singh, V. P., and Chau, K. W. (2022). *Hydrological Models*, pages 283–329. Springer Nature Singapore, Singapore.

Appendix A

Pastas model simulations and Parameters

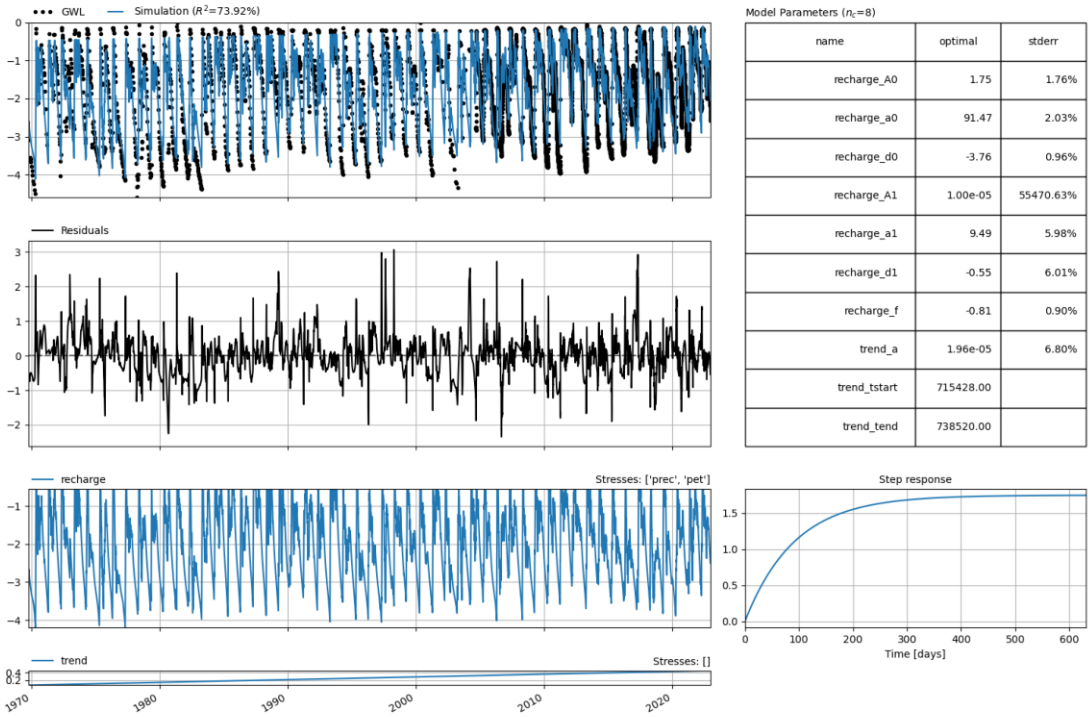

name	optimal	stderr
recharge_A0	1.75	1.76%
recharge_a0	91.47	2.03%
recharge_d0	-3.76	0.96%
recharge_A1	1.00e-05	55470.63%
recharge_a1	9.49	5.98%
recharge_d1	-0.55	6.01%
recharge_f	-0.81	0.90%
trend_a	1.96e-05	6.80%
trend_tstart	715428.00	
trend_tend	738520.00	

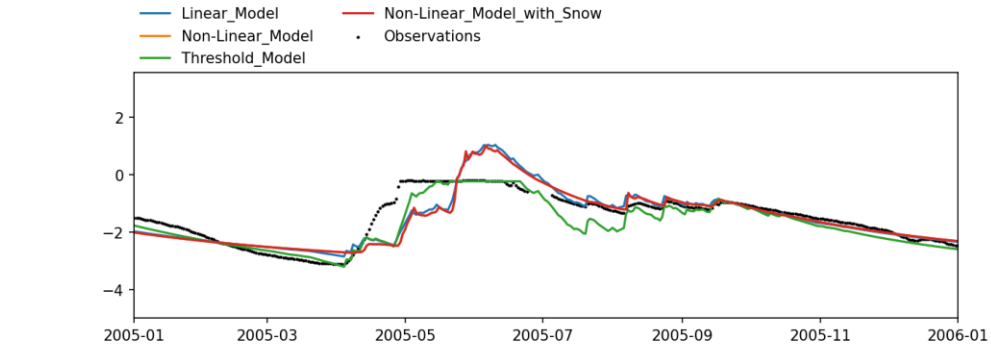

Figure show the same as in Figure 4.2, but for Abrahamsvoll station (0). Here, the Threshold model is the best preforming model, and the parameters shown here is for that model.

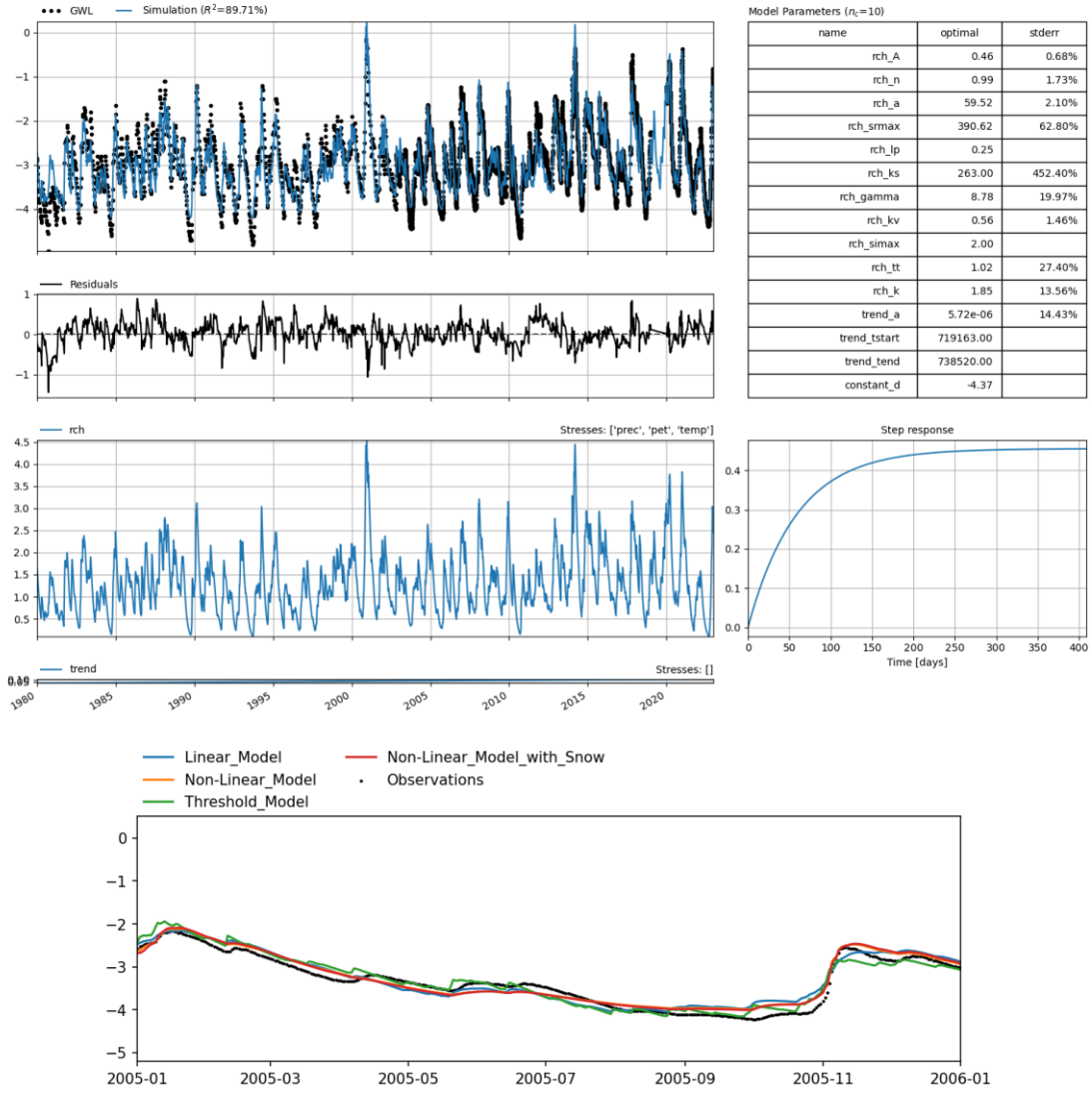

name	optimal	stderr
rch_A	0.46	0.68%
rch_n	0.99	1.73%
rch_a	59.52	2.10%
rch_srmax	390.62	62.80%
rch_lp	0.25	
rch_ks	263.00	452.40%
rch_gamma	8.78	19.97%
rch_kv	0.56	1.46%
rch_simax	2.00	
rch_tt	1.02	27.40%
rch_k	1.85	13.56%
trend_a	5.72e-06	14.43%
trend_tstart	719163.00	
trend_tend	738520.00	
constant_d	-4.37	

Figure show the same as in Figure 4.2, but for Birkenes station (1). Here, the Non-linear model with snow scheme is the best preforming model, and the parameters shown here is for that model.

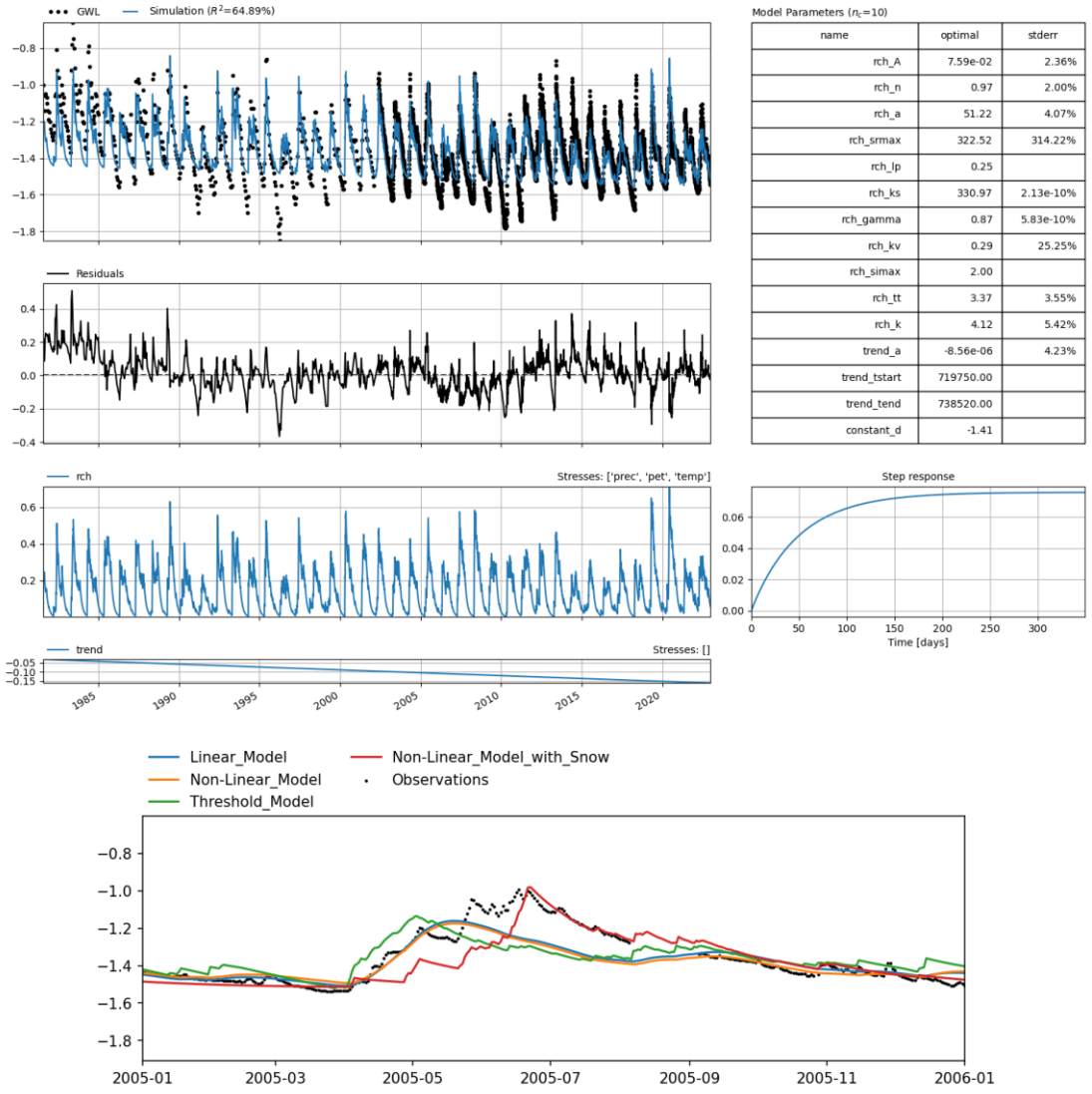

Figure show the same as in Figure 4.2, but for Dombås station (2). Here, the Non-linear model with snow scheme is the best preforming model, and the parameters shown here is for that model.

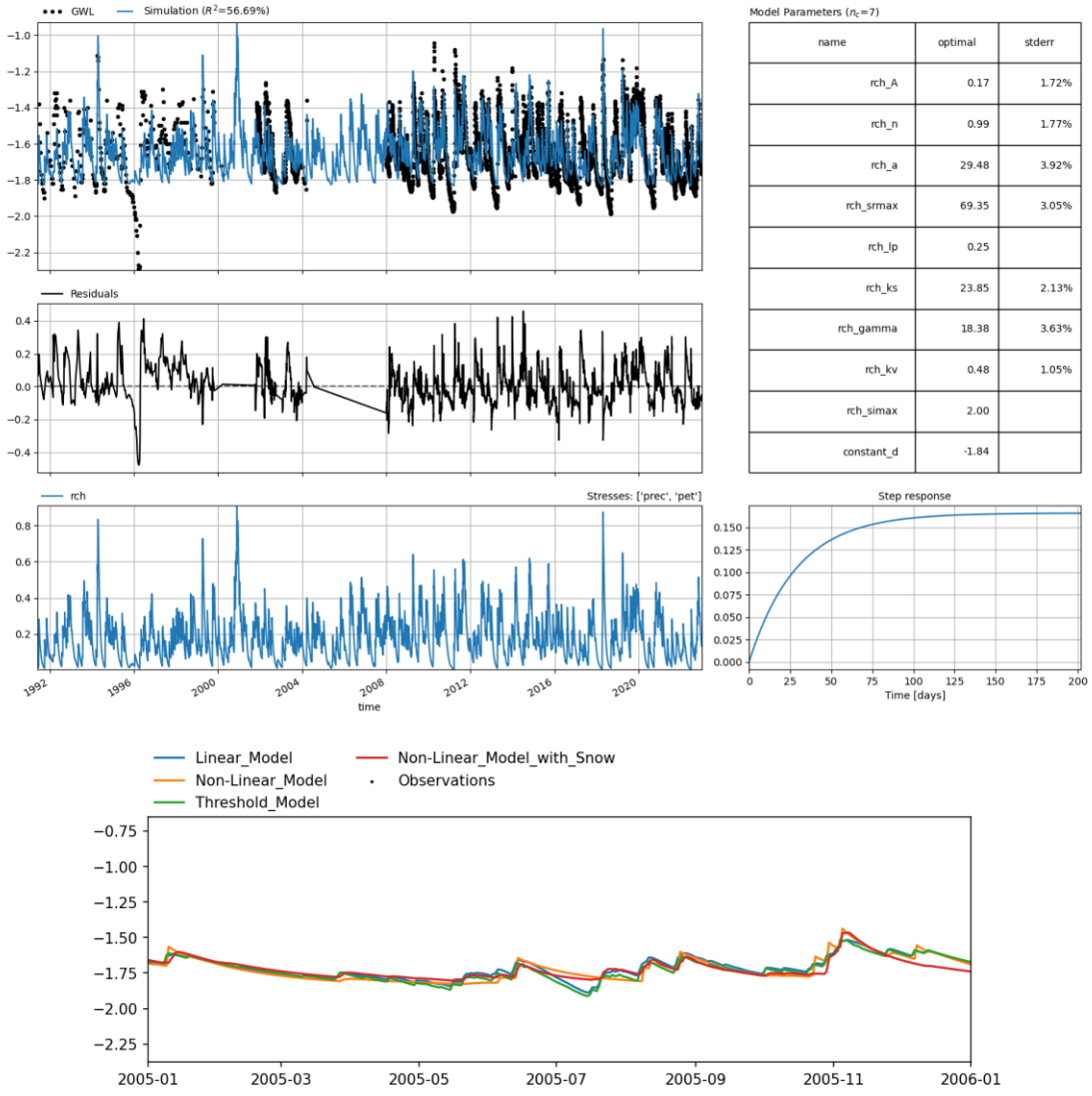

Figure show the same as in Figure 4.2, but for Kise station (3). Here, the Non-linear model is the best preforming model, and the parameters shown here is for that model.

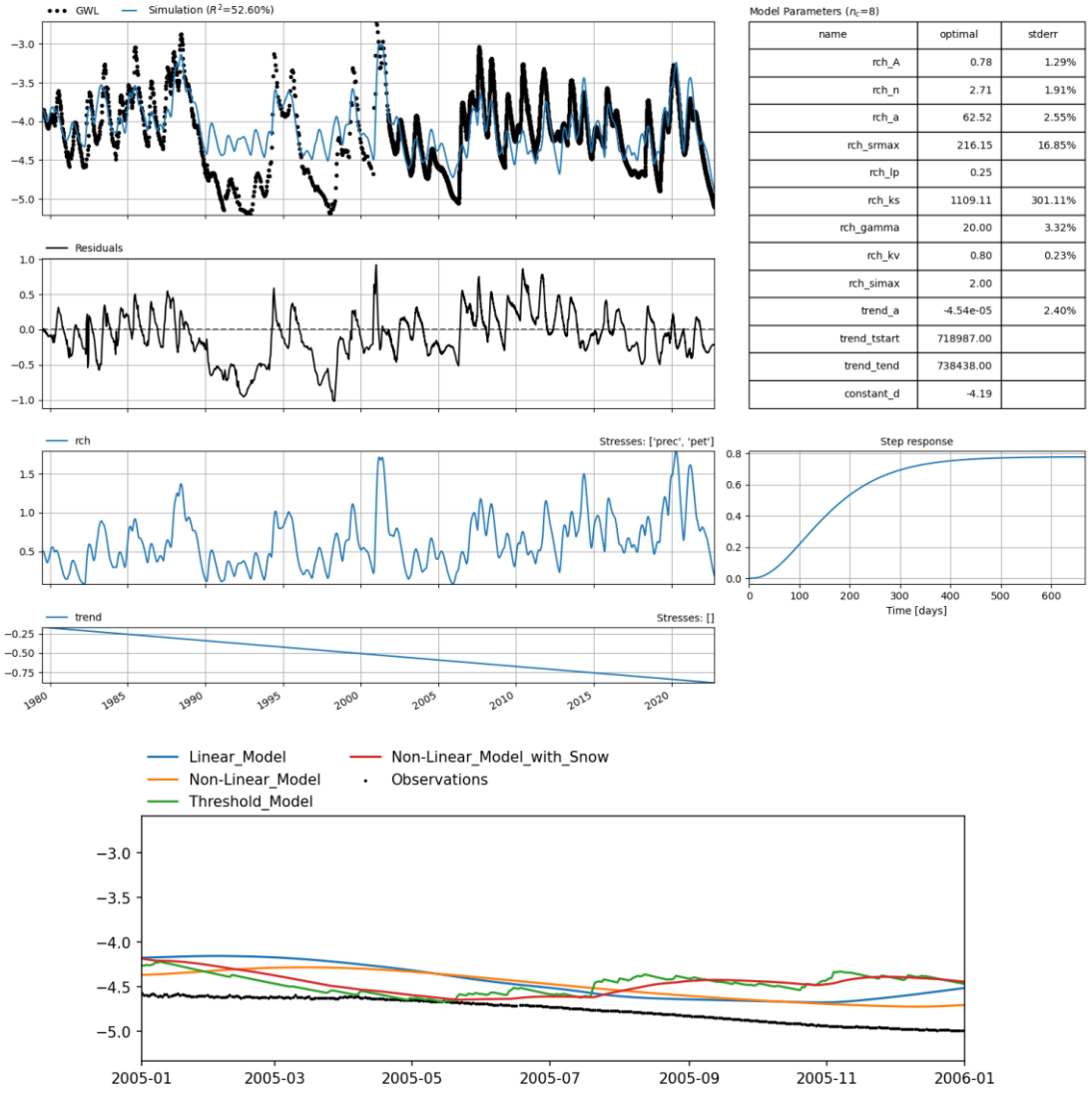

Figure show the same as in Figure 4.2, but for Modum station (4). Here, the Non-linear model is the best preforming model, and the parameters shown here is for that model.

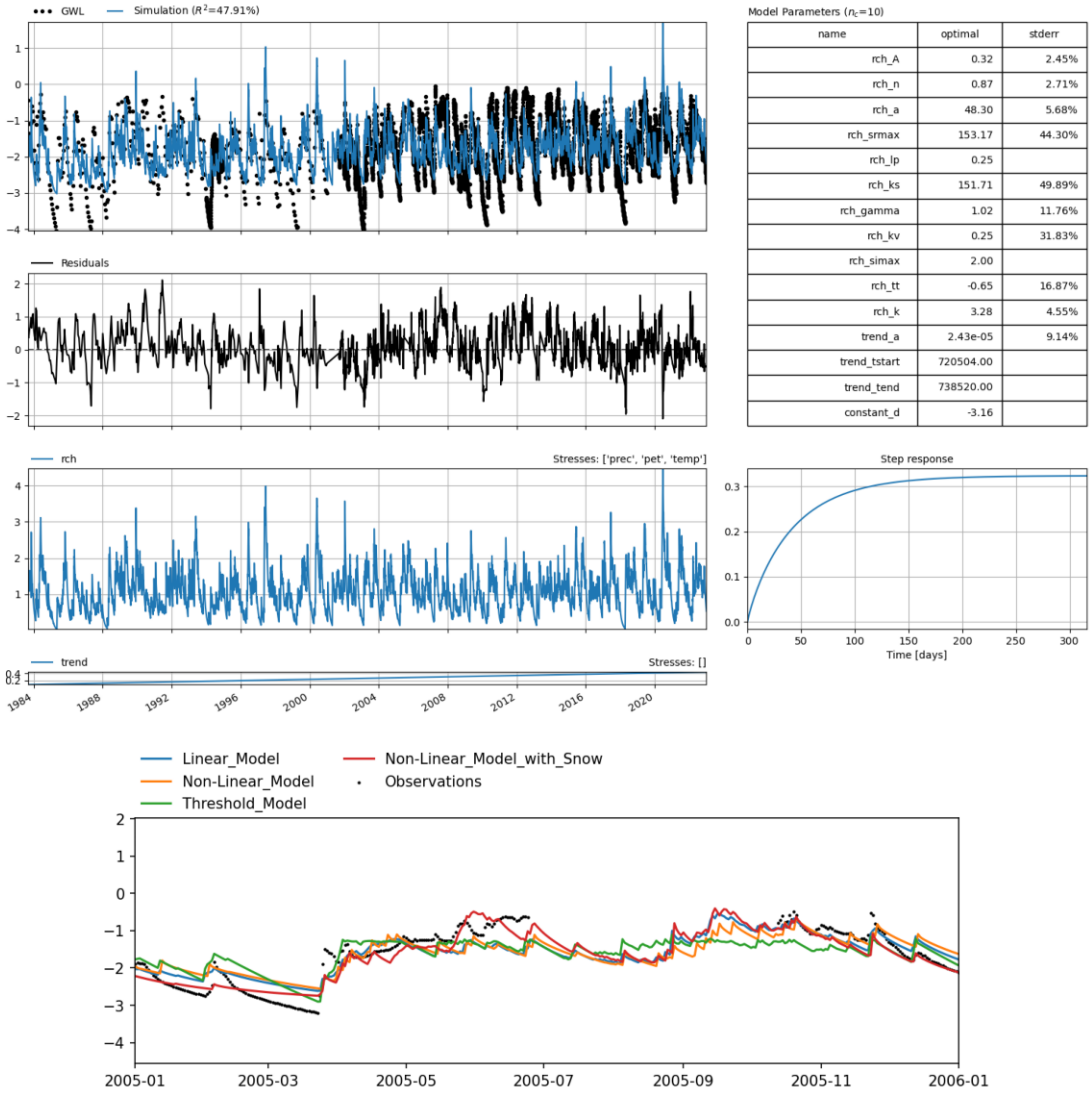

Figure show the same as in Figure 4.2, but for Skjomen station (5). Here, the Non-linear model with snow scheme is the best preforming model, and the parameters shown here is for that model.

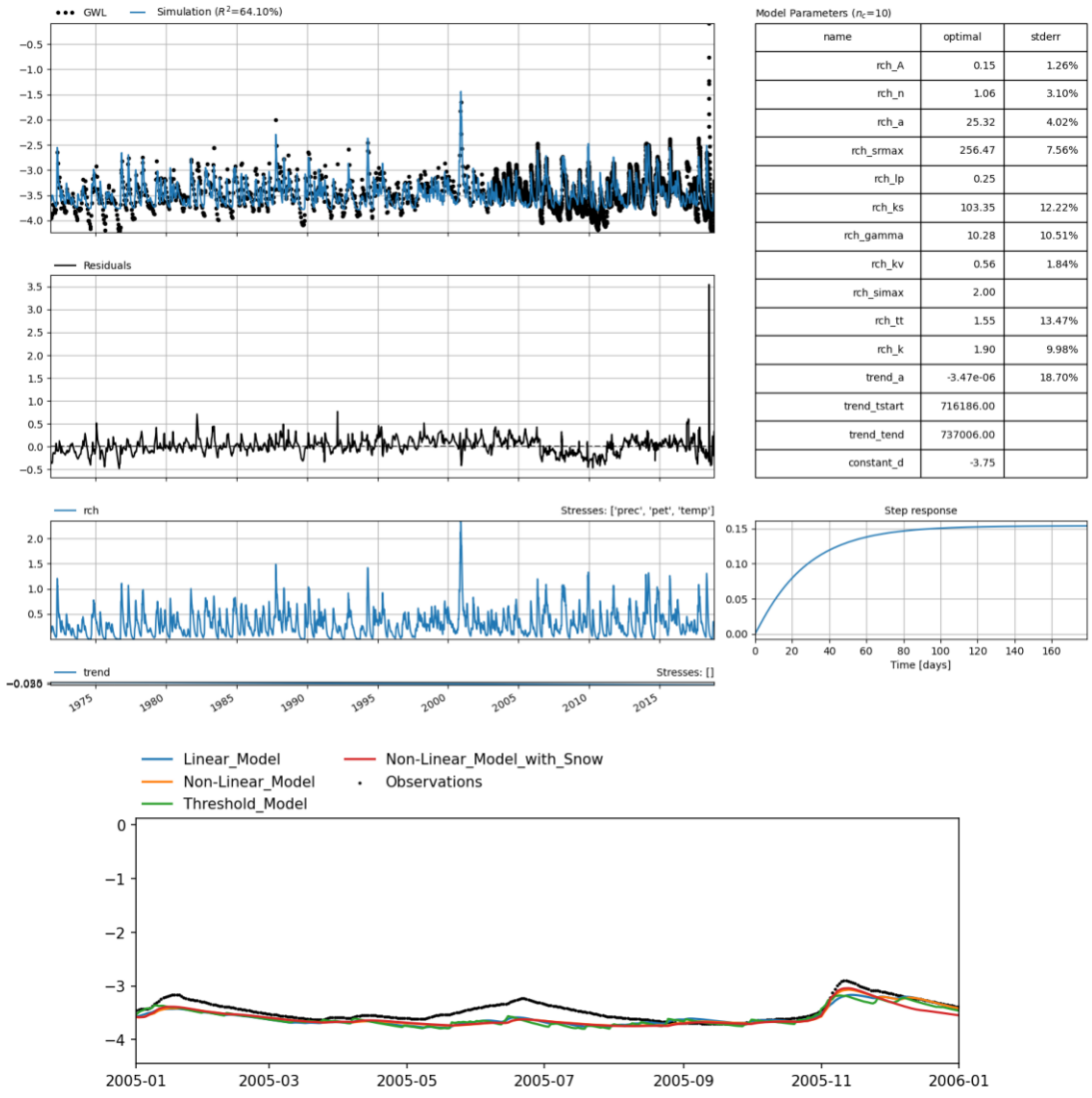

Figure show the same as in Figure 4.2, but for Stigvassåi station (6). Here, the Non-linear model with snow scheme is the best preforming model, and the parameters shown here is for that model.

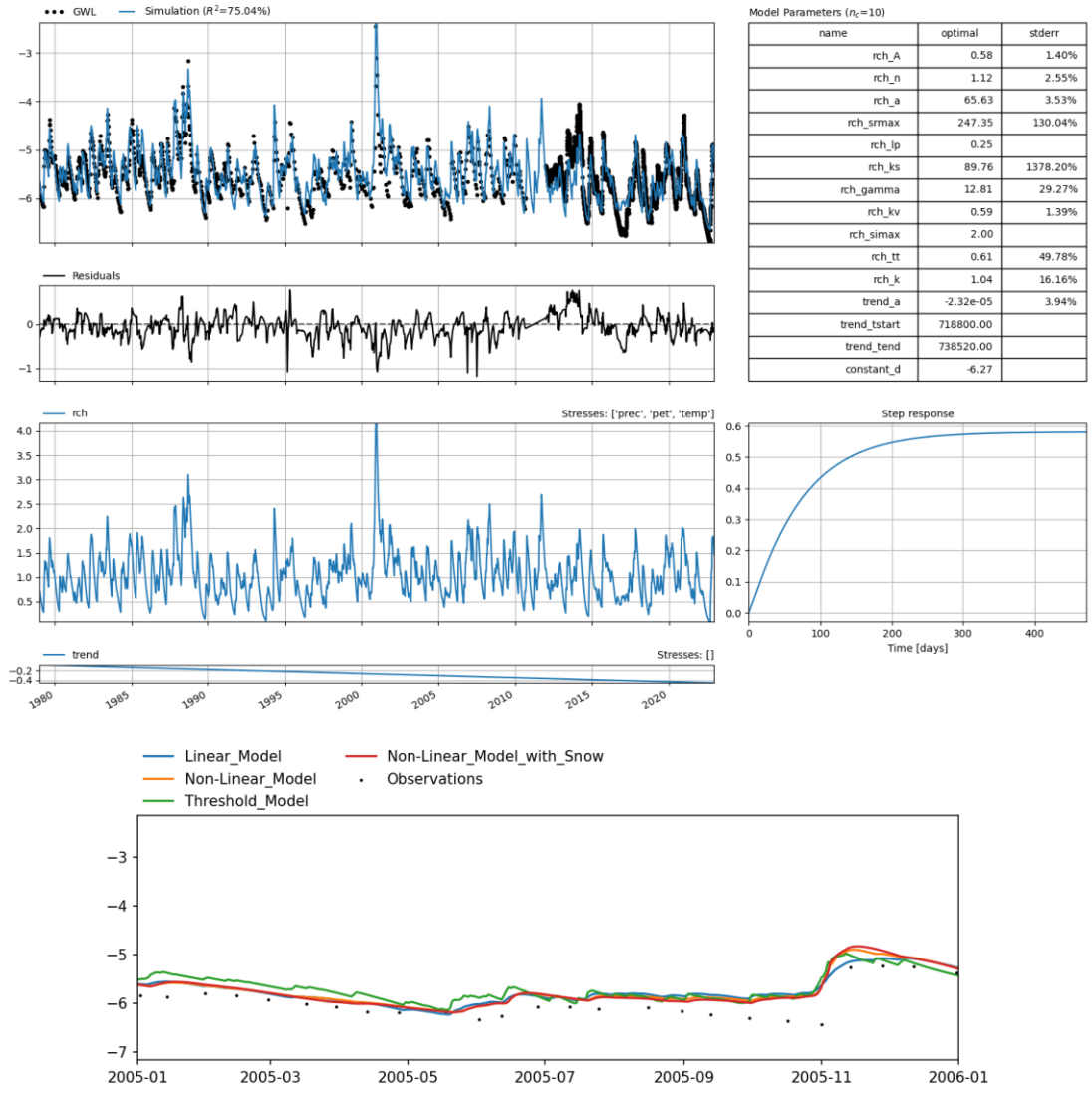

name	optimal	stderr
rch_A	0.58	1.40%
rch_n	1.12	2.55%
rch_a	65.63	3.53%
rch_srmax	247.35	130.04%
rch_lp	0.25	
rch_ks	89.76	1378.20%
rch_gamma	12.81	29.27%
rch_kv	0.59	1.39%
rch_simax	2.00	
rch_tt	0.61	49.78%
rch_k	1.04	16.16%
trend_a	-2.32e-05	3.94%
trend_tstart	718800.00	
trend_tend	738520.00	
constant_d	-6.27	

Figure show the same as in Figure 4.2, but for Eikamoen station (7). Here, the Non-linear model with snow scheme is the best preforming model, and the parameters shown here is for that model.

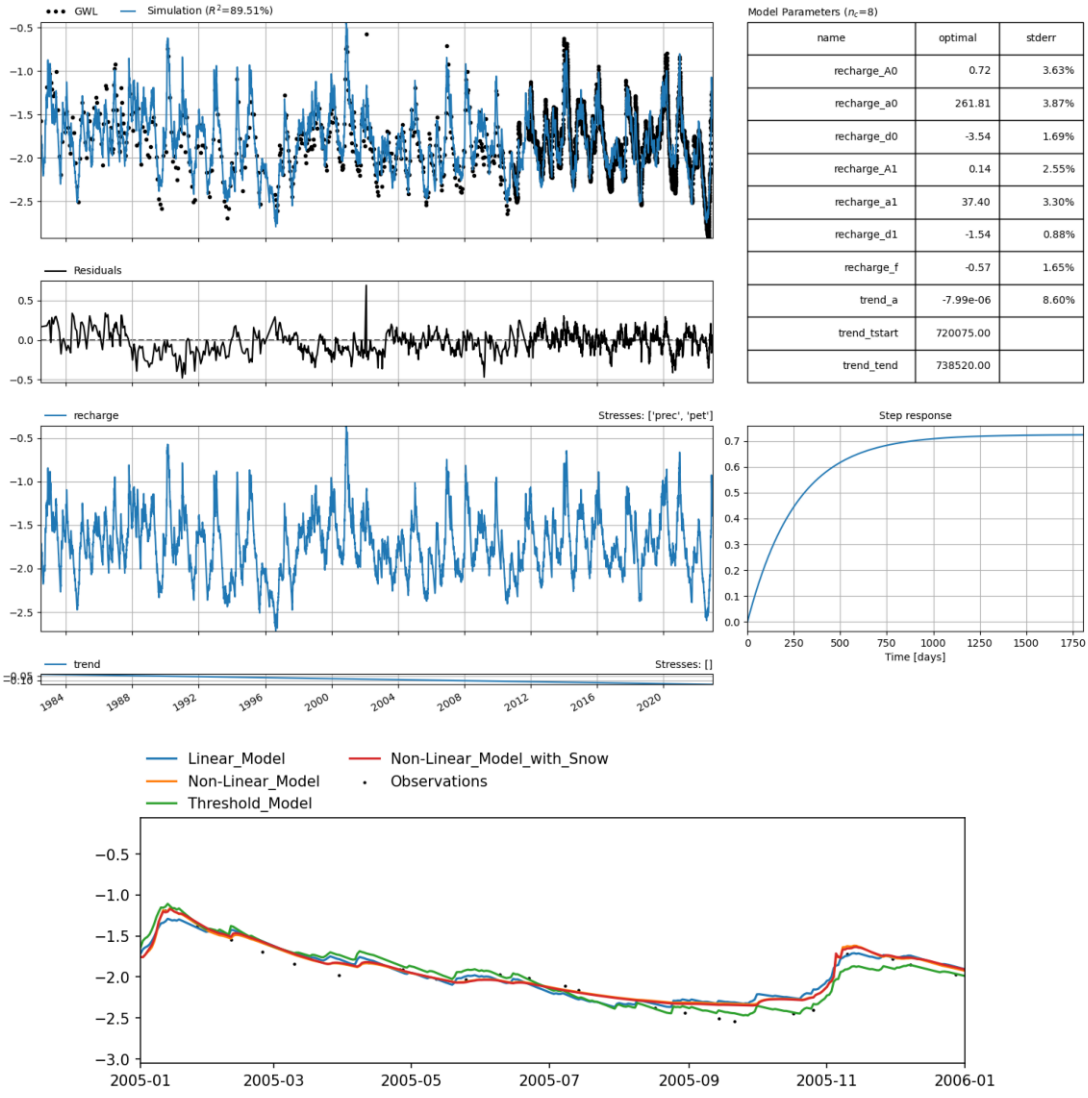

Figure show the same as in Figure 4.2, but for Evje station (8). Here, the Threshold model is the best preforming model, and the parameters shown here is for that model.

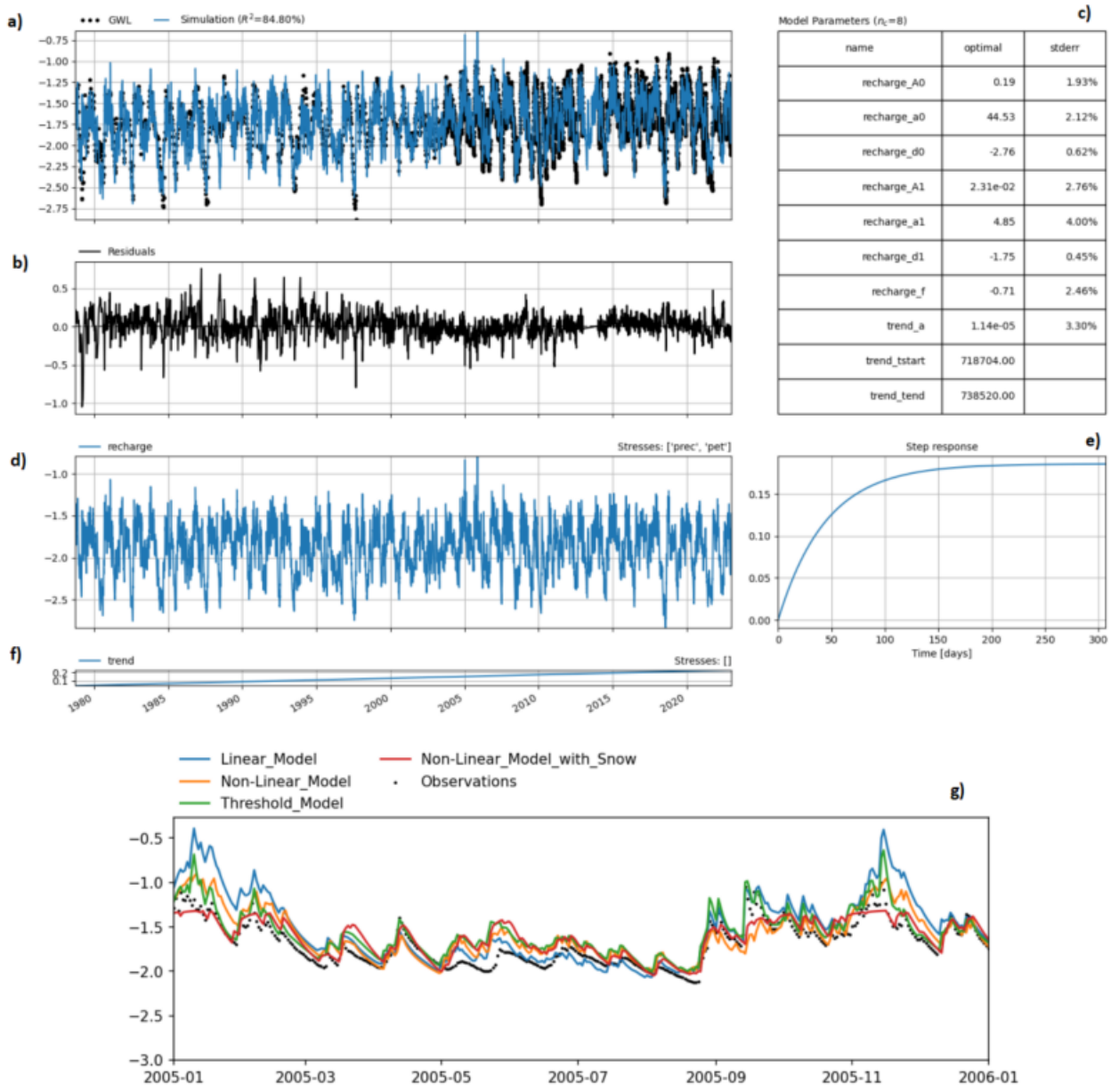

Figure show the same as in Figure 4.2, but for Fana station (9). Here, the Threshold model is the best preforming model, and the parameters shown here is for that model.

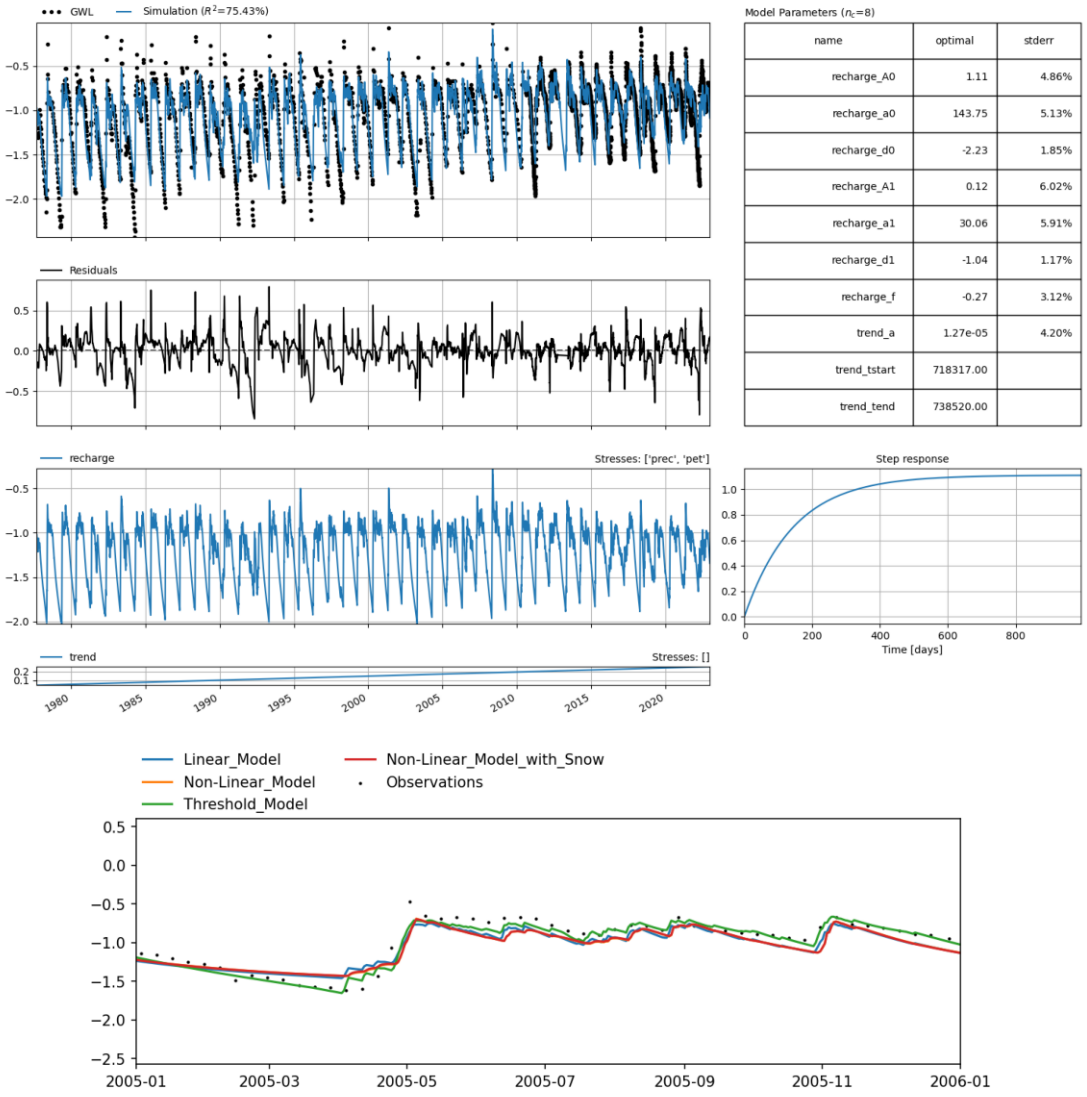

Figure show the same as in Figure 4.2, but for Finnbølseter station (10). Here, the Threshold model is the best preforming model, and the parameters shown here is for that model.

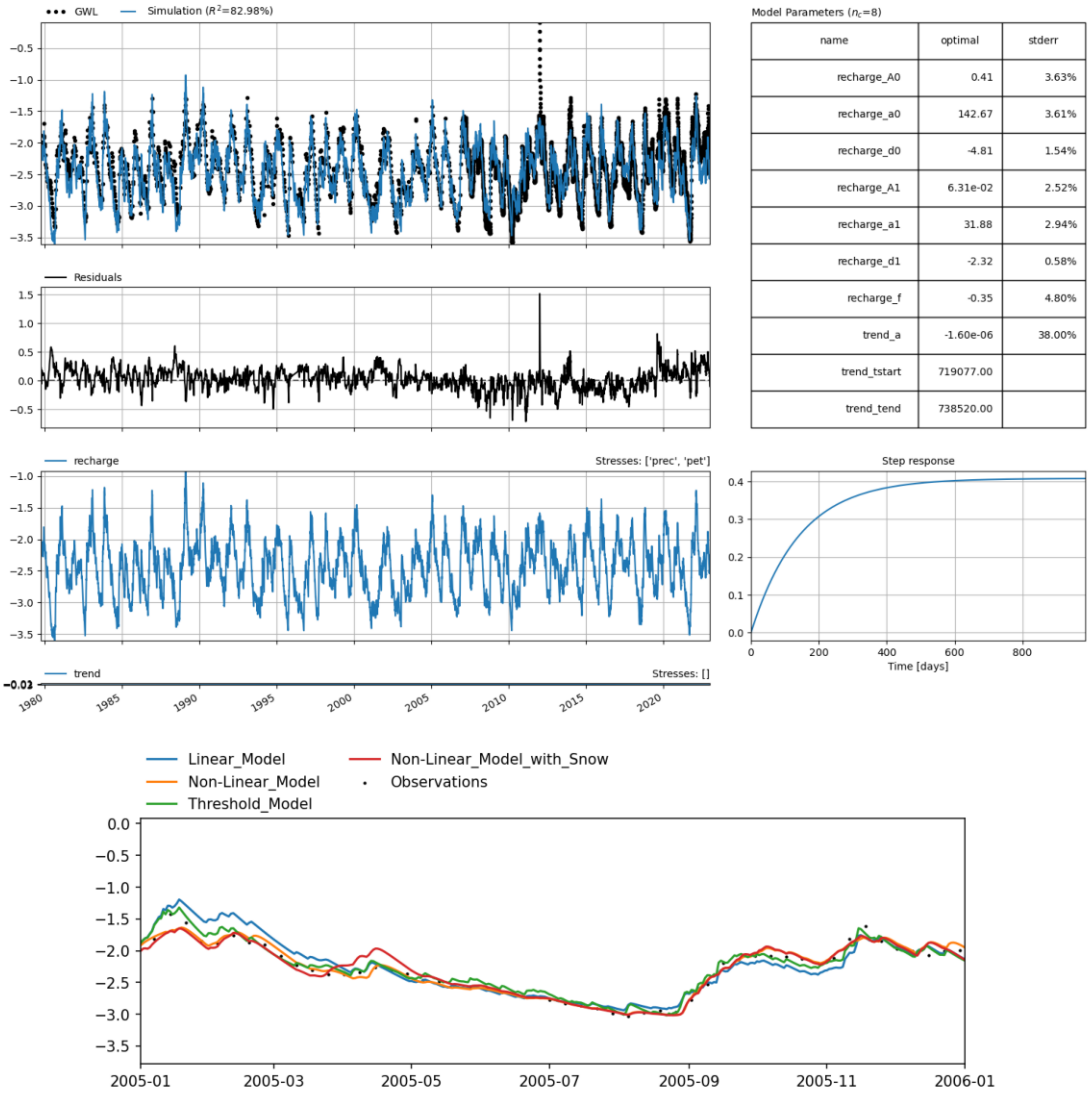

Figure show the same as in Figure 4.2, but for Førde/Moskog station (11). Here, the Threshold model is the best preforming model, and the parameters shown here is for that model.

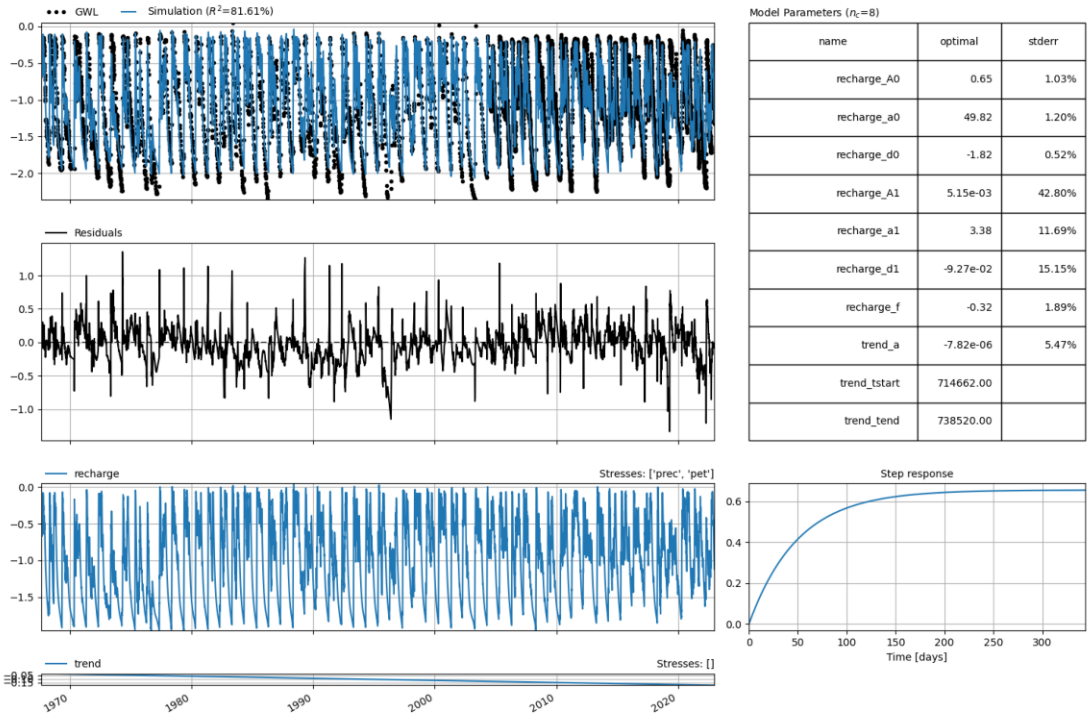

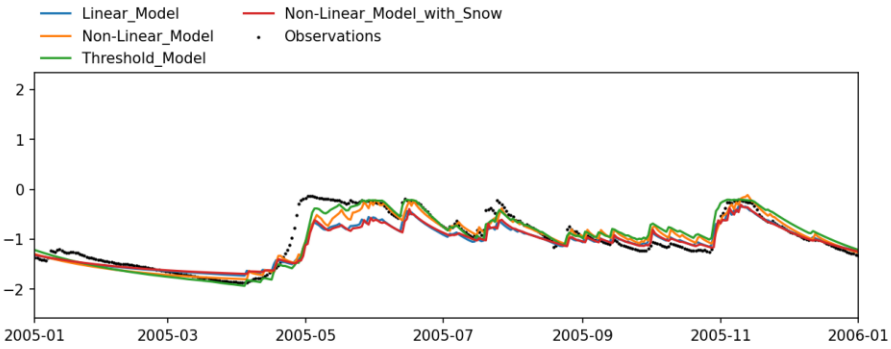

Figure show the same as in Figure 4.2, but for Groset station (12). Here, the Threshold model is the best preforming model, and the parameters shown here is for that model.

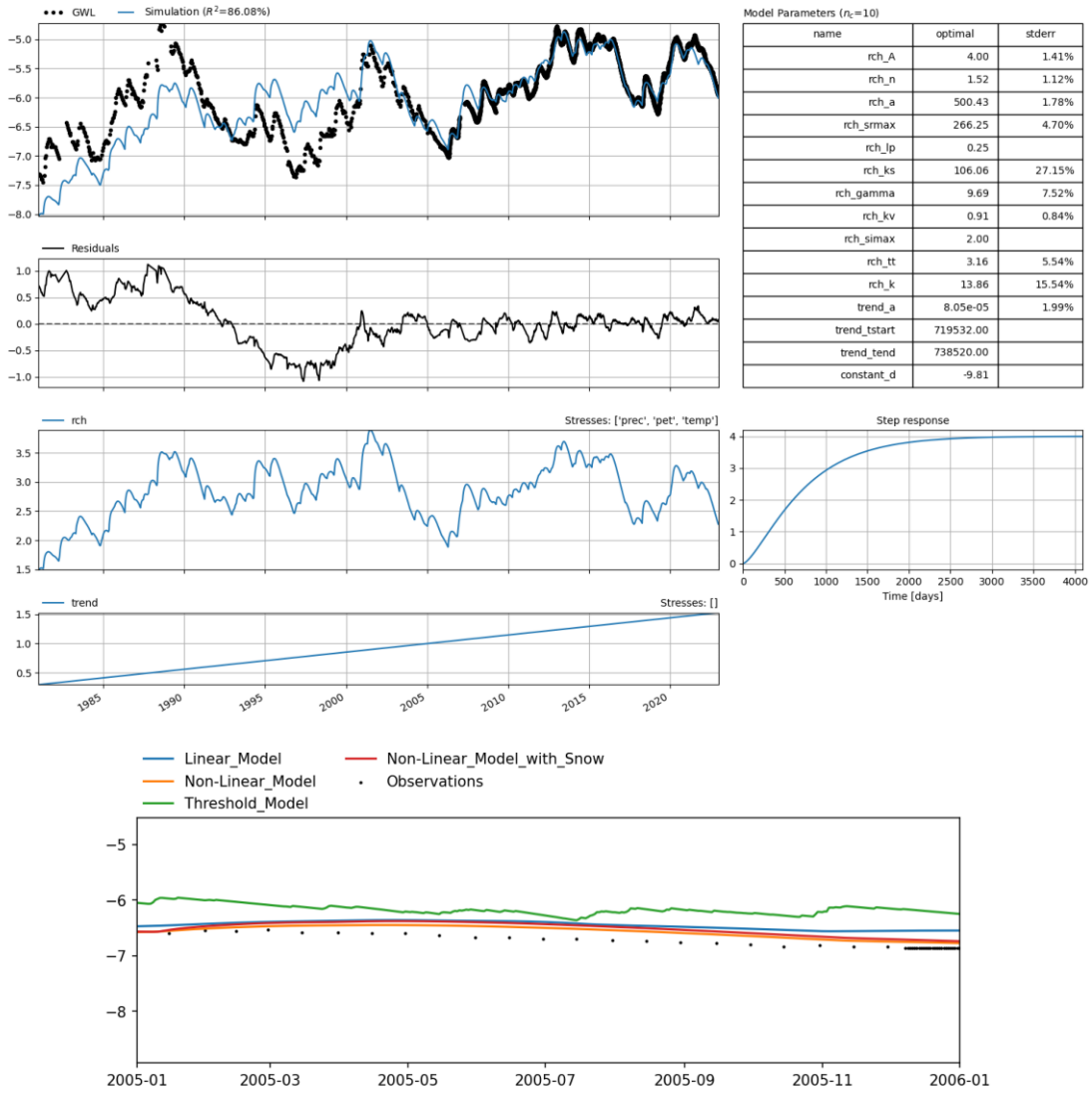

Model Parameters (n_c=10)

name	optimal	stderr
rch_A	4.00	1.41%
rch_n	1.52	1.12%
rch_a	500.43	1.78%
rch_srmax	266.25	4.70%
rch_lp	0.25	
rch_ks	106.06	27.15%
rch_gamma	9.69	7.52%
rch_kv	0.91	0.84%
rch_simax	2.00	
rch_tt	3.16	5.54%
rch_k	13.86	15.54%
trend_a	8.05e-05	1.99%
trend_tstart	719532.00	
trend_tend	738520.00	
constant_d	-9.81	

Figure show the same as in Figure 4.2, but for Haslemoden station (13). Here, the Non-linear model with snow scheme is the best preforming model, and the parameters shown here is for that model.

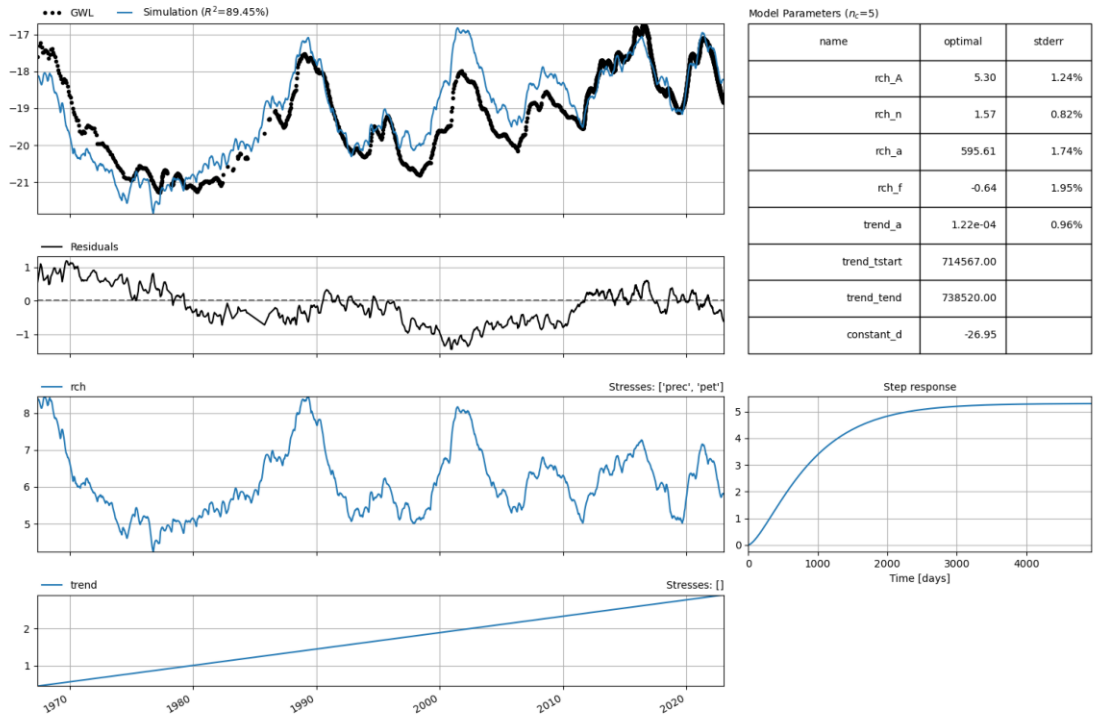

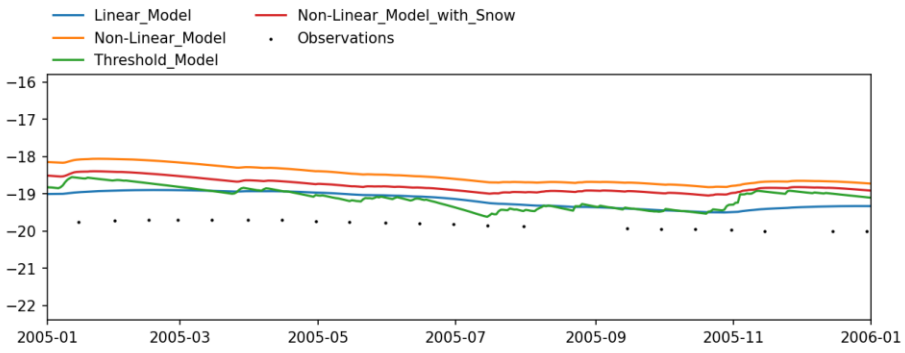

Figure show the same as in Figure 4.2, but for Hauerseter station (14). Here, the Linear model is the best preforming model, and the parameters shown here is for that model.

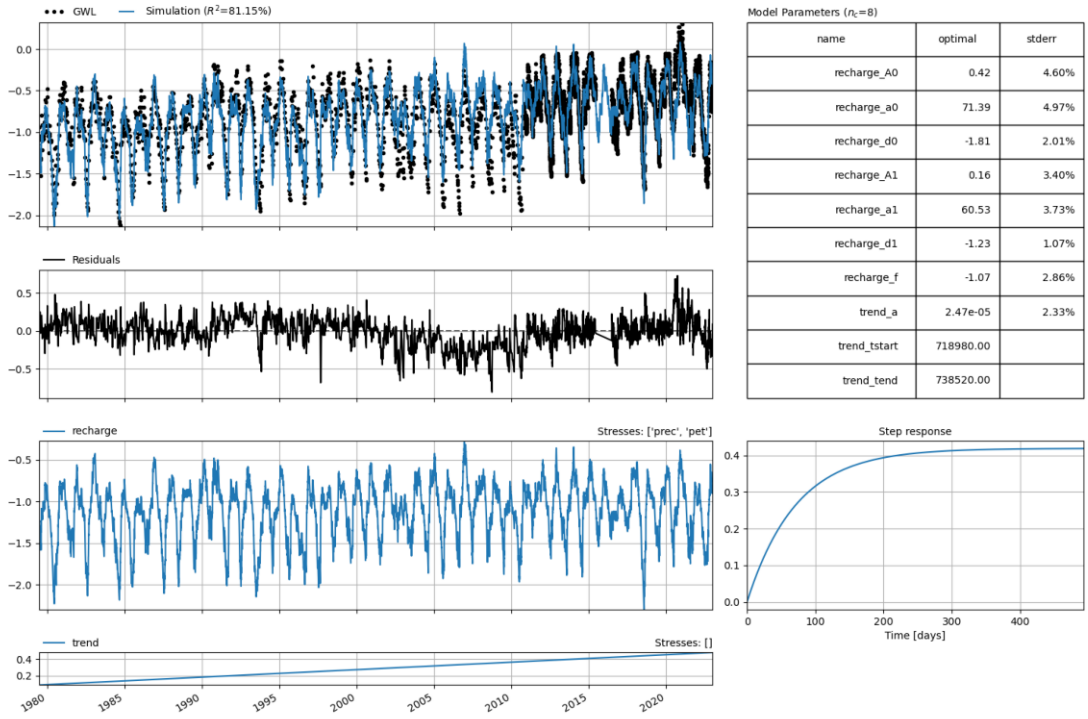

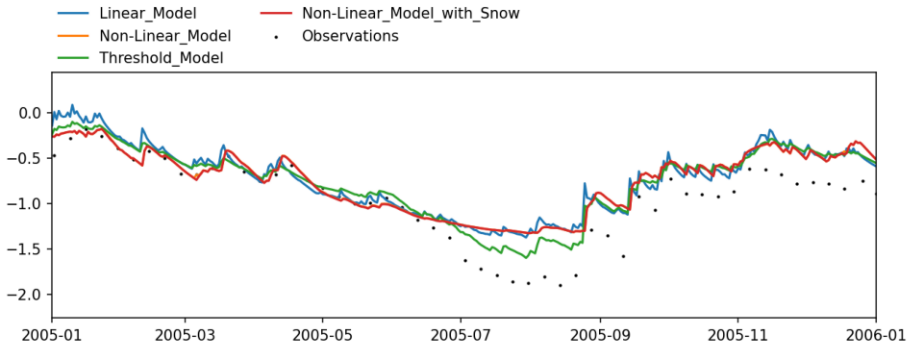

Figure show the same as in Figure 4.2, but for Jæren station (15). Here, the Threshold model is the best preforming model, and the parameters shown here is for that model.

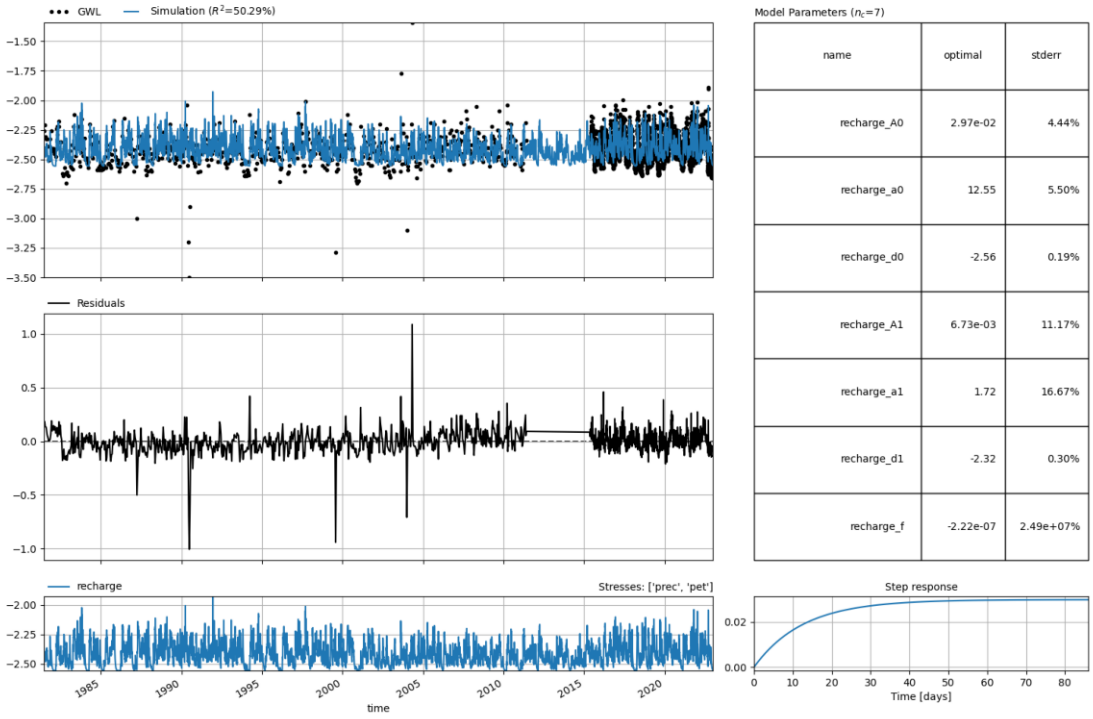

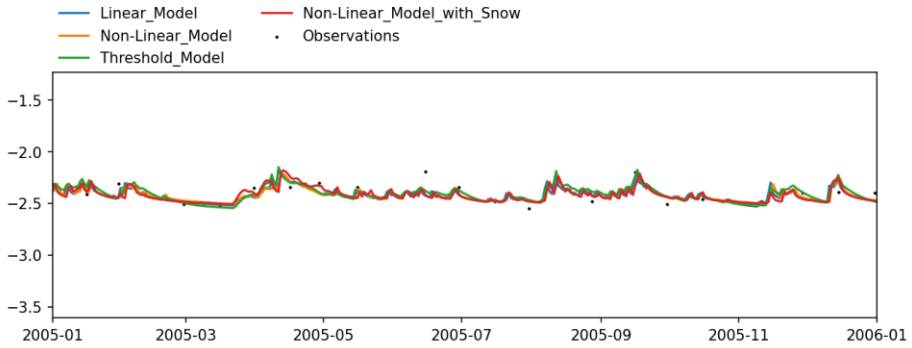

Figure show the same as in Figure 4.2, but for Kårvatn station (16). Here, the Threshold model is the best preforming model, and the parameters shown here is for that model.

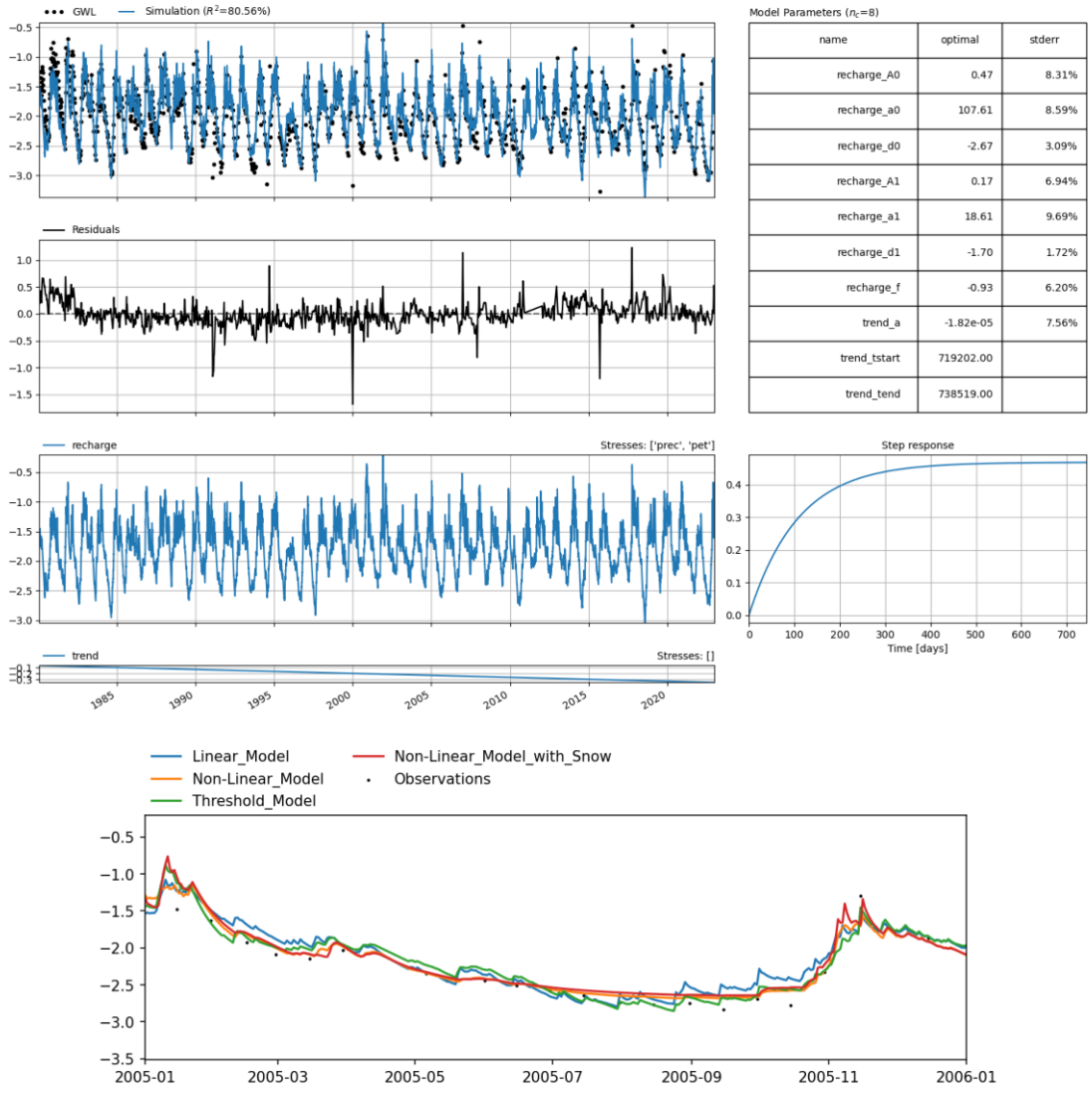

Figure show the same as in Figure 4.2, but for Lindesnes station (17). Here, the Threshold model is the best preforming model, and the parameters shown here is for that model.

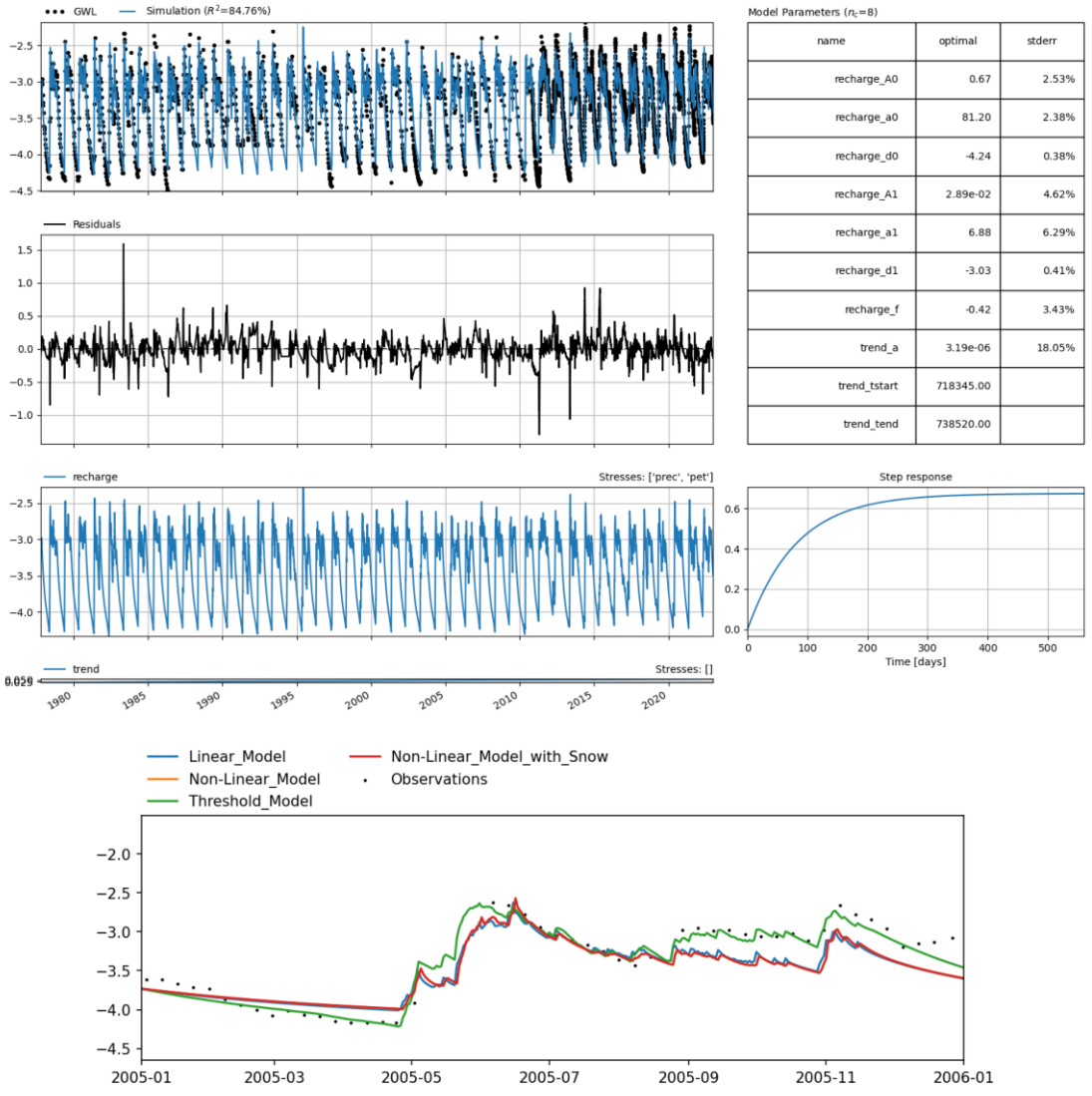

Figure show the same as in Figure 4.2, but for Lykjestøylane station (18). Here, the Threshold model is the best preforming model, and the parameters shown here is for that model.

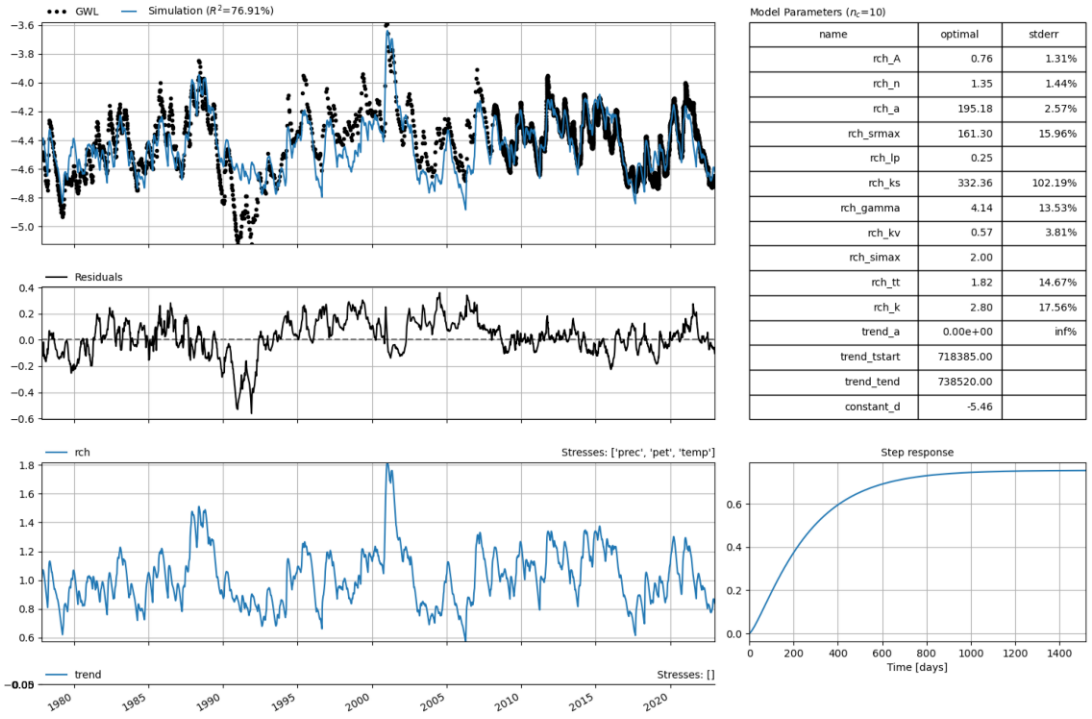

name	optimal	stderr
rch_A	0.76	1.31%
rch_n	1.35	1.44%
rch_a	195.18	2.57%
rch_srmax	161.30	15.96%
rch_lp	0.25	
rch_ks	332.36	102.19%
rch_gamma	4.14	13.53%
rch_kv	0.57	3.81%
rch_simax	2.00	
rch_tt	1.82	14.67%
rch_k	2.80	17.56%
trend_a	0.00e+00	inf%
trend_tstart	718385.00	
trend_tend	738520.00	
constant_d	-5.46	

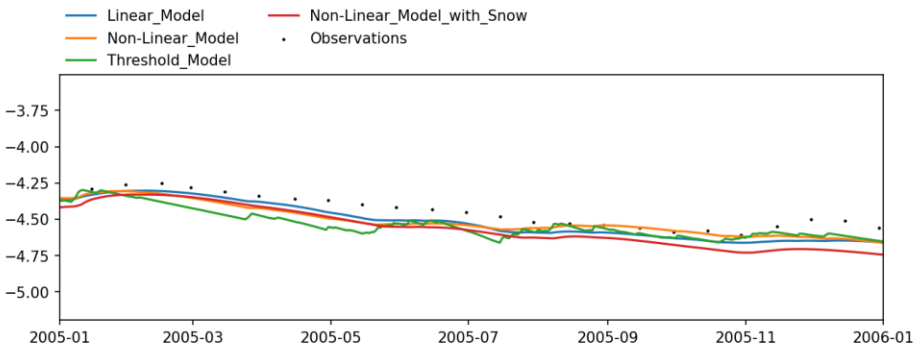

Figure show the same as in Figure 4.2, but for Magnor station (19). Here, the Non-linear model with snow scheme is the best preforming model, and the parameters shown here is for that model.

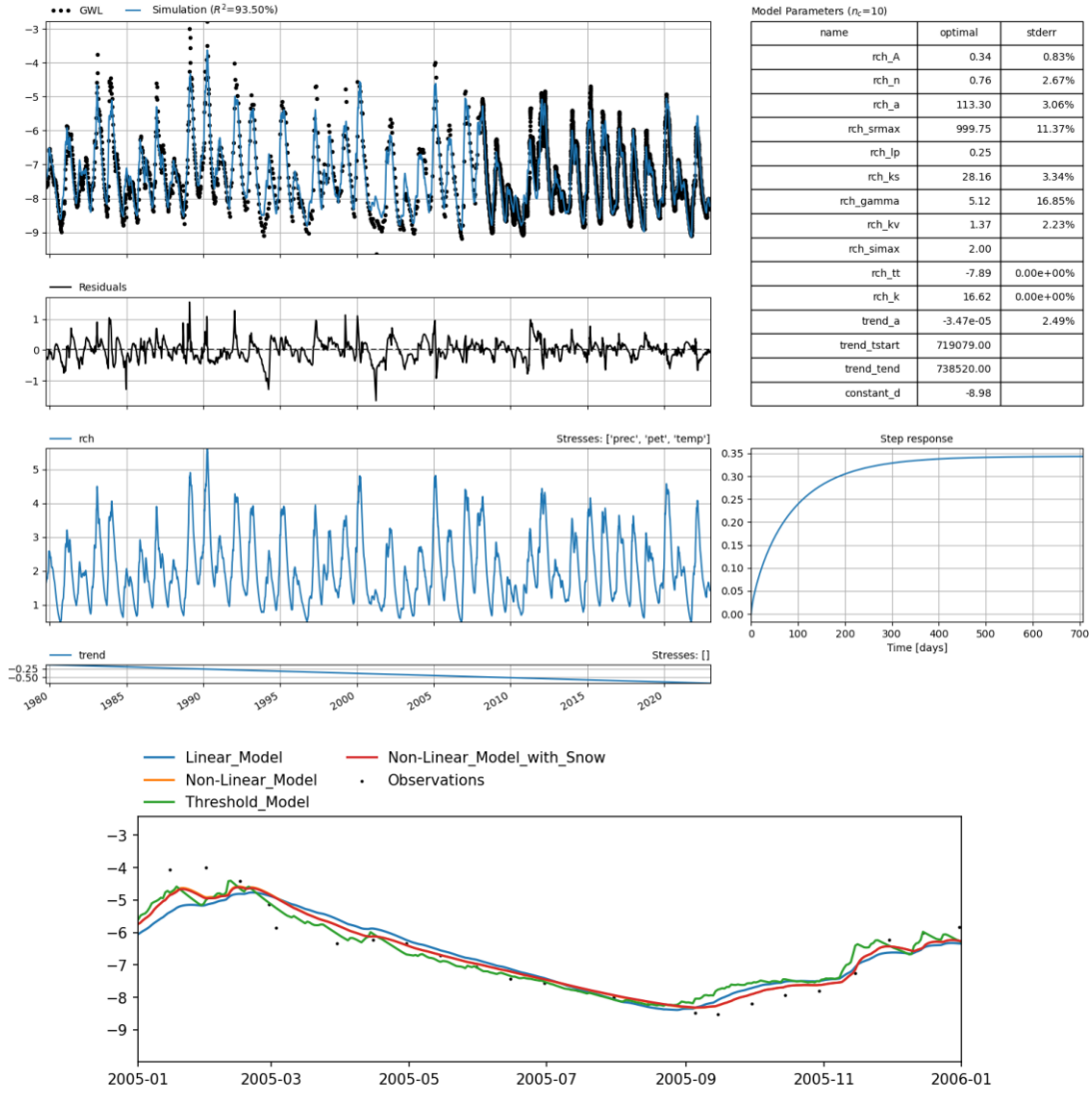

name	optimal	stderr
rch_A	0.34	0.83%
rch_n	0.76	2.67%
rch_a	113.30	3.06%
rch_srmax	999.75	11.37%
rch_lp	0.25	
rch_ks	28.16	3.34%
rch_gamma	5.12	16.85%
rch_kv	1.37	2.23%
rch_simax	2.00	
rch_tt	-7.89	0.00e+00%
rch_k	16.62	0.00e+00%
trend_a	-3.47e-05	2.49%
trend_tstart	719079.00	
trend_tend	738520.00	
constant_d	-8.98	

Figure show the same as in Figure 4.2, but for Nordfjordeid station (20). Here, the Non-linear model with snow scheme is the best preforming model, and the parameters shown here is for that model.

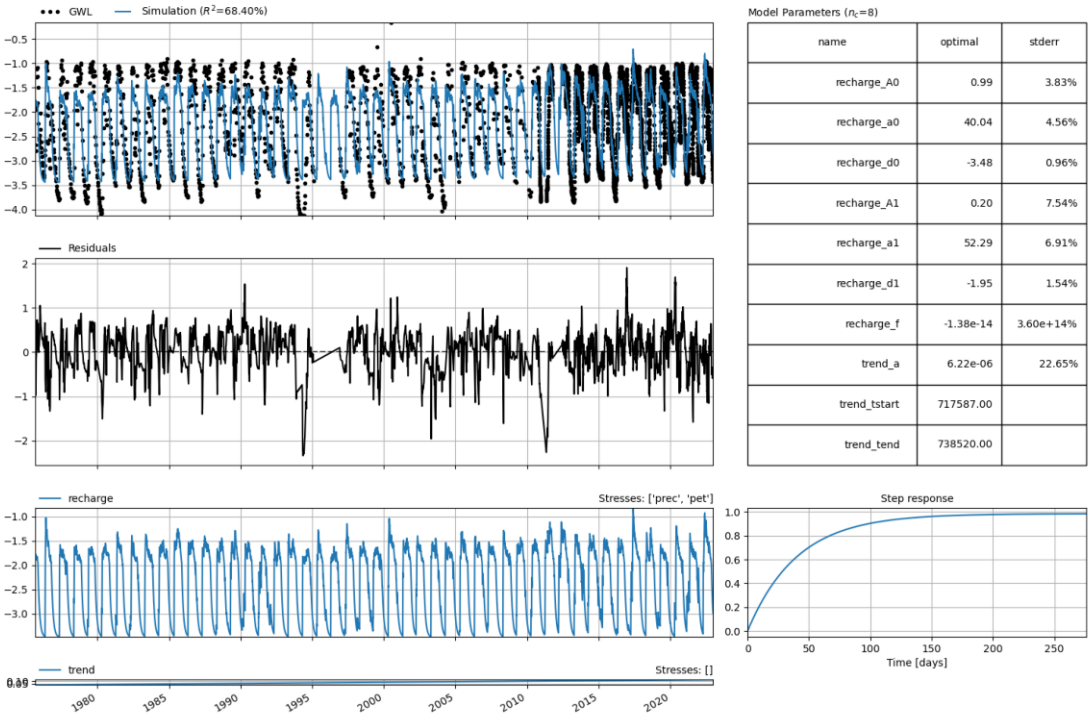

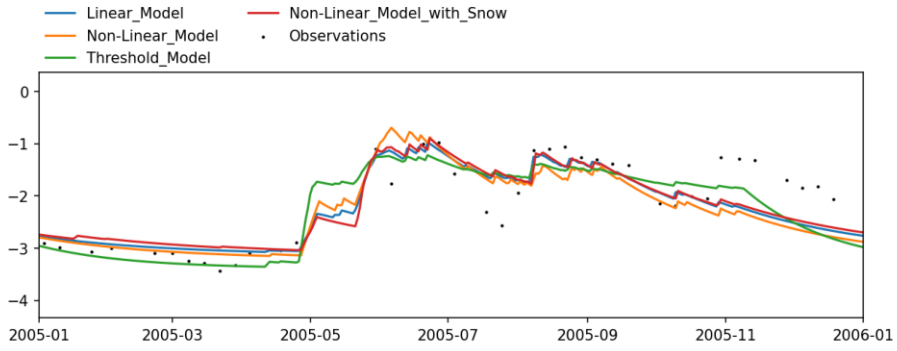

Figure show the same as in Figure 4.2, but for Settalbekken station (21). Here, the Threshold model is the best preforming model, and the parameters shown here is for that model.

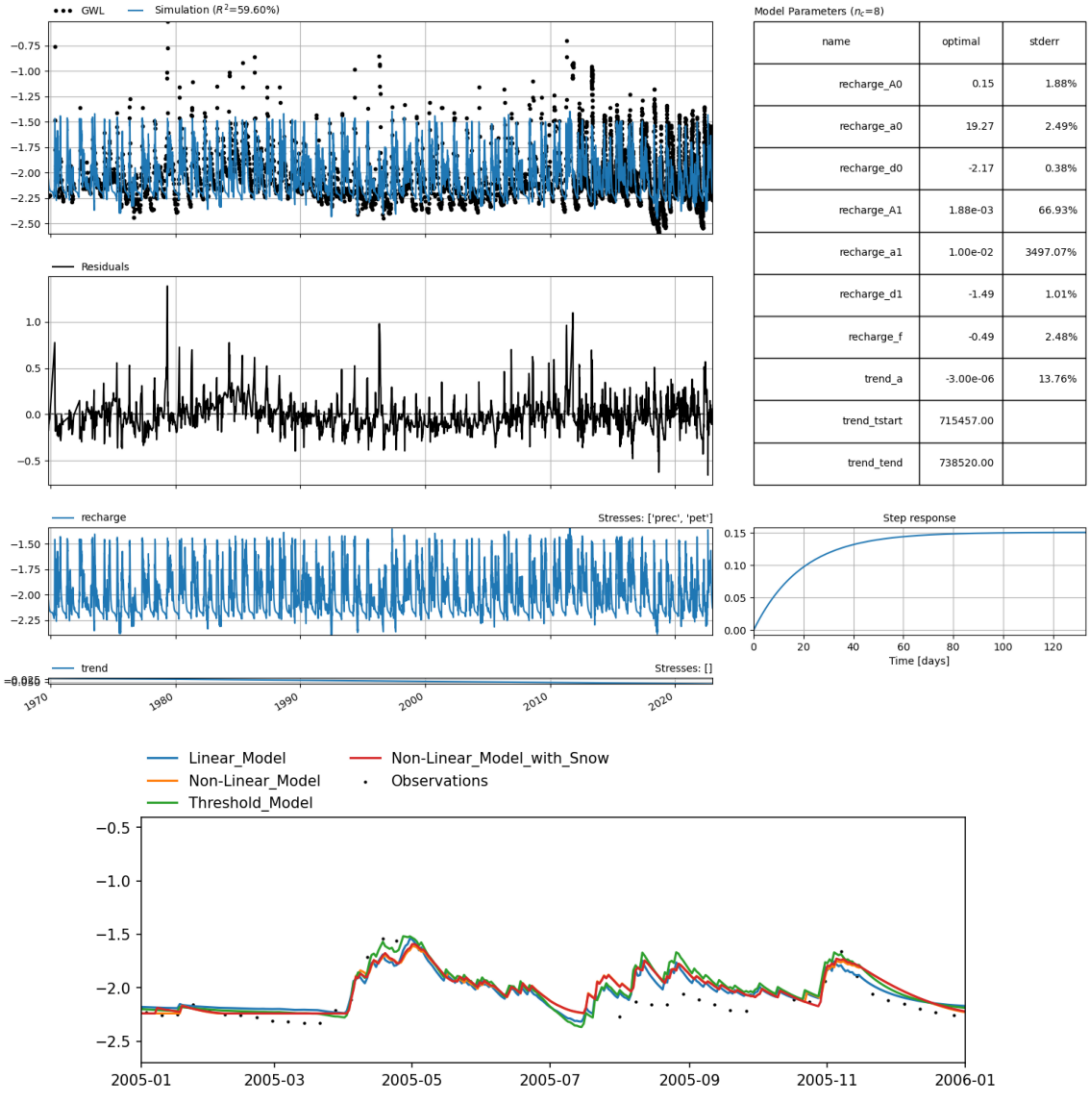

name	optimal	stderr
recharge_A0	0.15	1.88%
recharge_a0	19.27	2.49%
recharge_d0	-2.17	0.38%
recharge_A1	1.88e-03	66.93%
recharge_a1	1.00e-02	3497.07%
recharge_d1	-1.49	1.01%
recharge_f	-0.49	2.48%
trend_a	-3.00e-06	13.76%
trend_tstart	715457.00	
trend_tend	738520.00	

Figure show the same as in Figure 4.2, but for Stenerseter station (22). Here, the Threshold model is the best preforming model, and the parameters shown here is for that model.

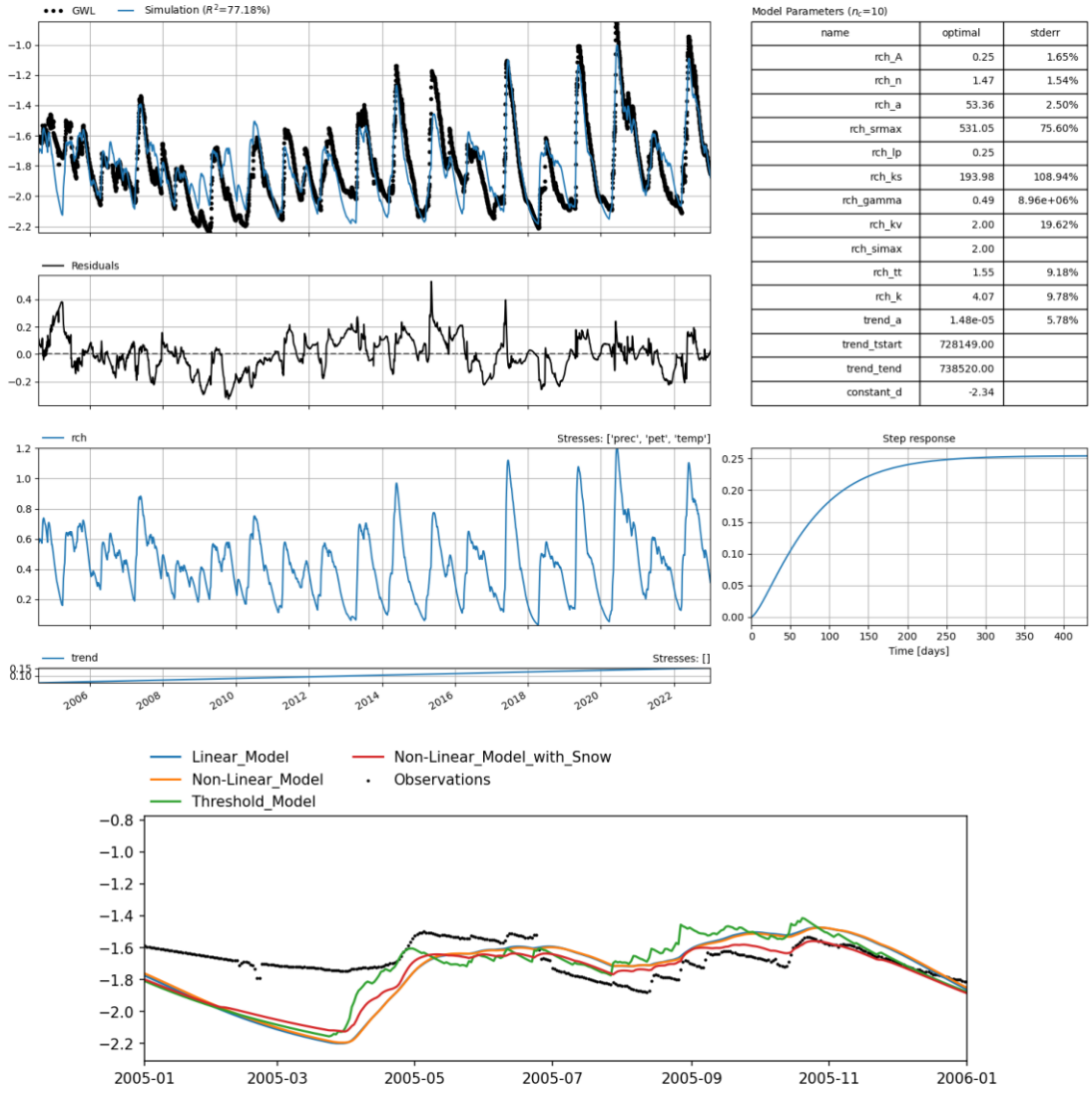

name	optimal	stderr
rch_A	0.25	1.65%
rch_n	1.47	1.54%
rch_a	53.36	2.50%
rch_srmax	531.05	75.60%
rch_lp	0.25	
rch_ks	193.98	108.94%
rch_gamma	0.49	8.96e+06%
rch_kv	2.00	19.62%
rch_simax	2.00	
rch_tt	1.55	9.18%
rch_k	4.07	9.78%
trend_a	1.48e-05	5.78%
trend_tstart	728149.00	
trend_tend	738520.00	
constant_d	-2.34	

Figure show the same as in Figure 4.2, but for Øverbygd station (23). Here, the Non-linear model with snow scheme is the best preforming model, and the parameters shown here is for that model.

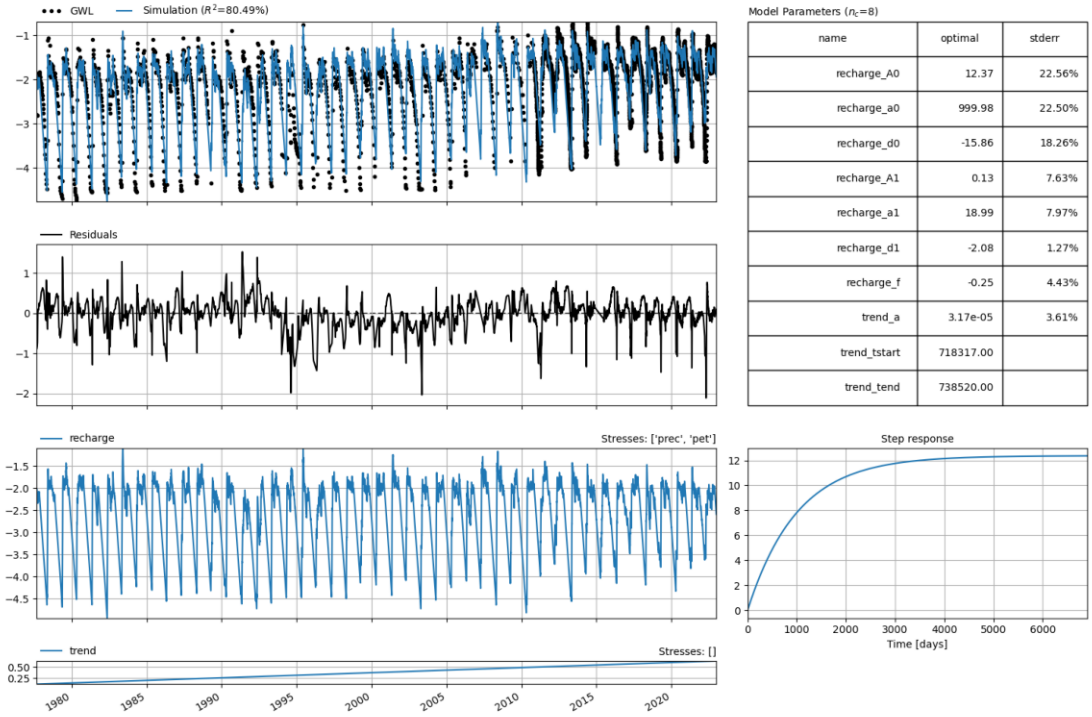

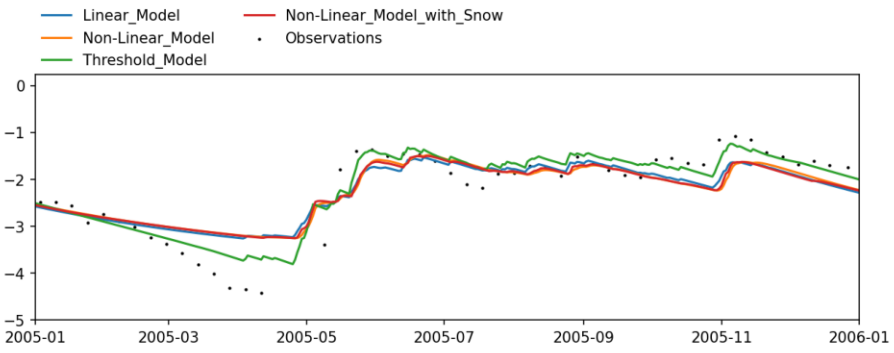

Figure show the same as in Figure 4.2, but for Øyangen station (24). Here, the Threshold model is the best preforming model, and the parameters shown here is for that model.

Appendix B

Linear infilled time series

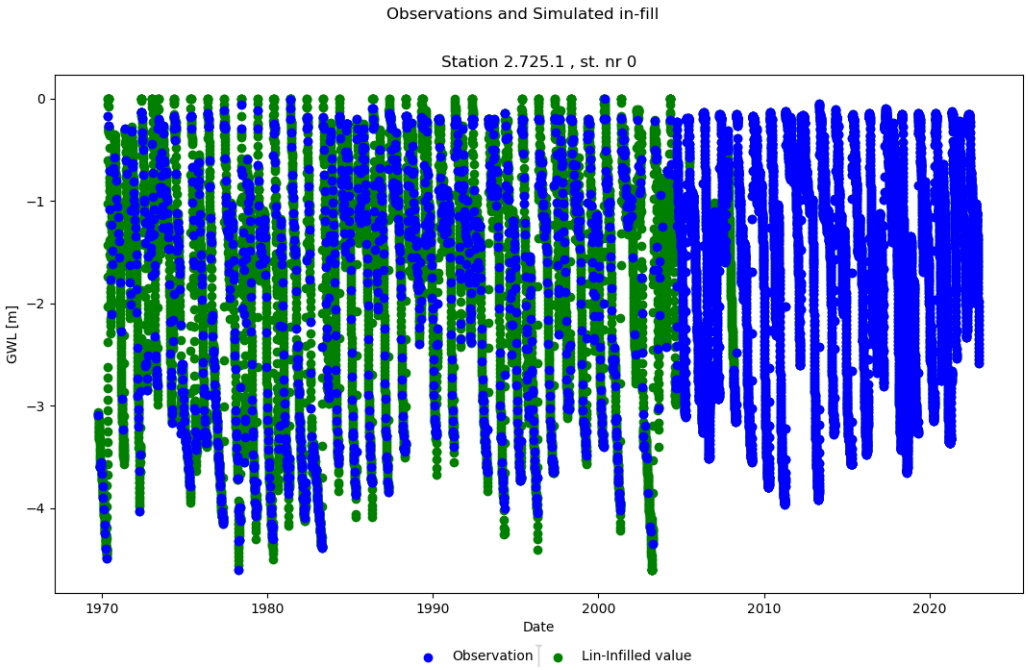

Gap-filled time series for Abrahamsvoll station (0).

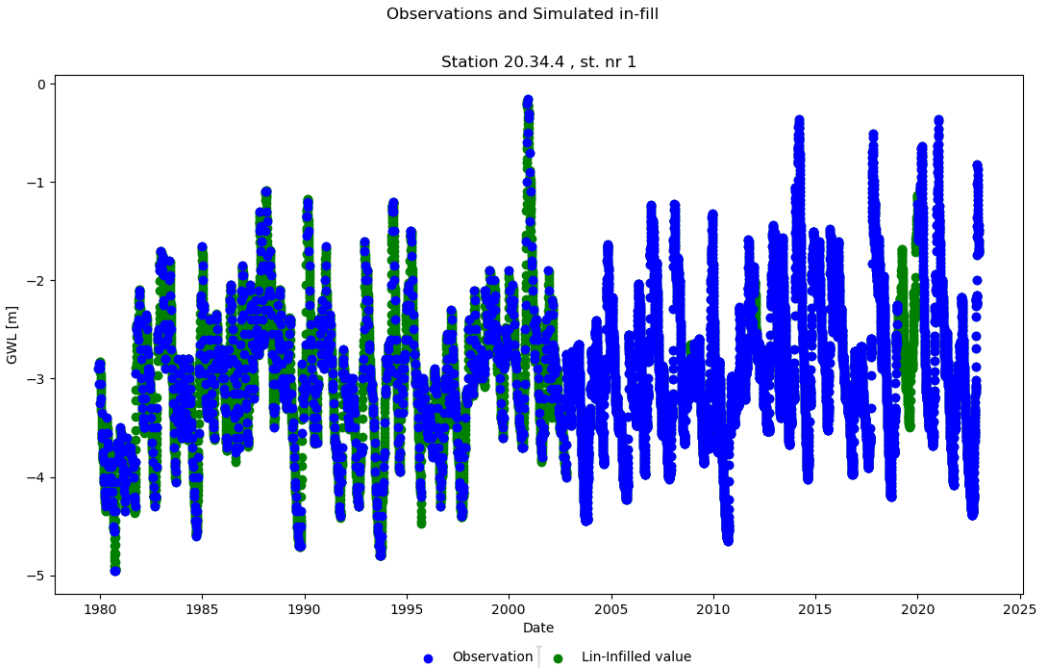

Gap-filled time series for Birkenes station (1).

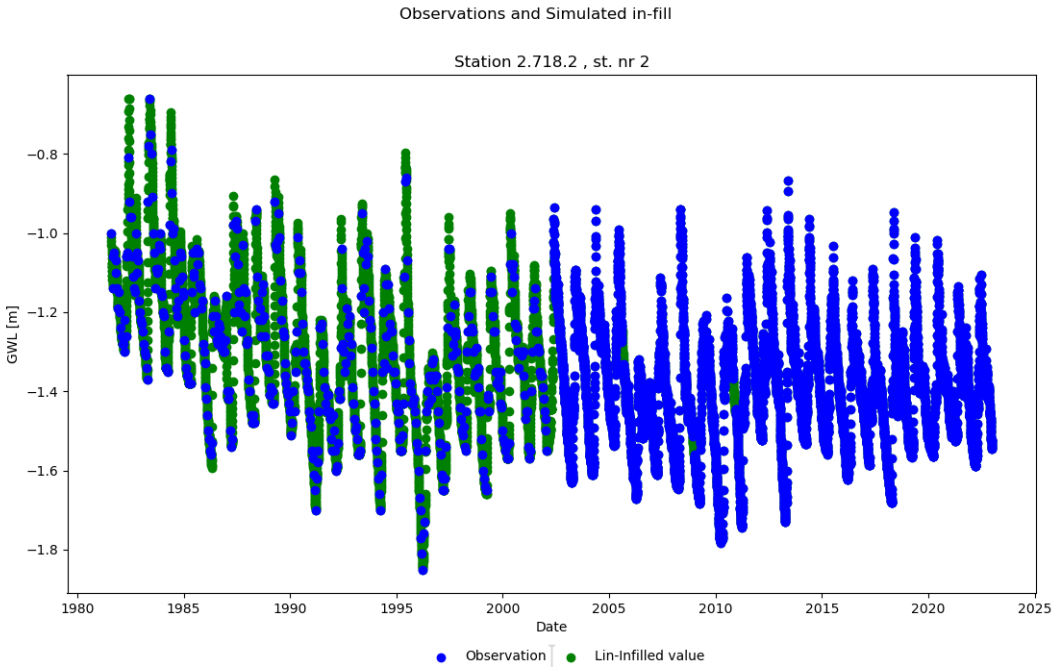

Gap-filled time series for Dombås station (2).

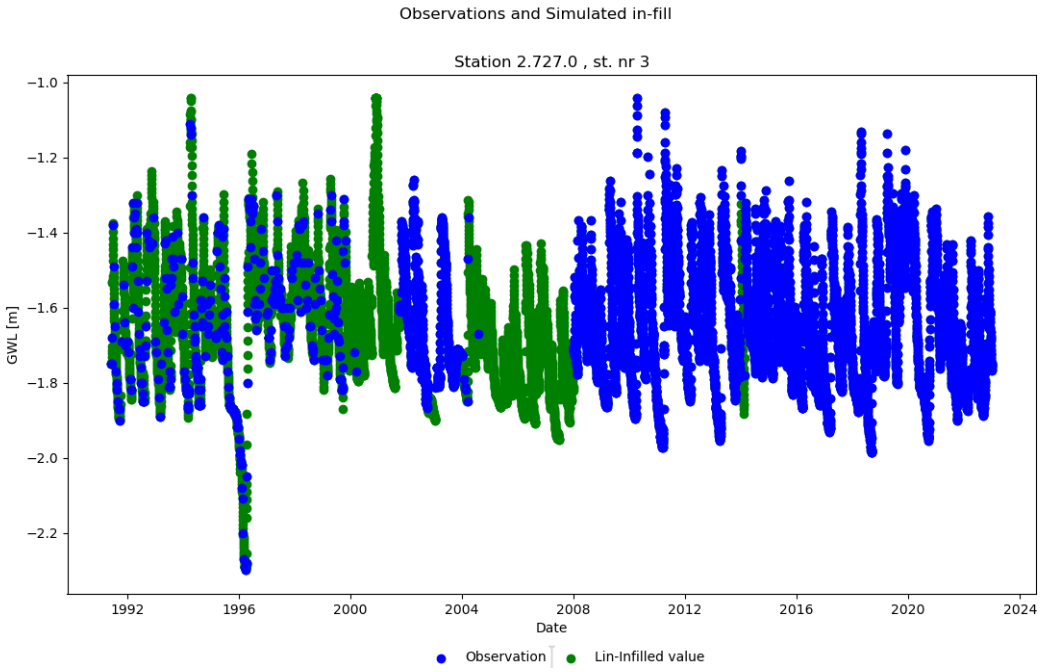

Gap-filled time series for Kise station (3).

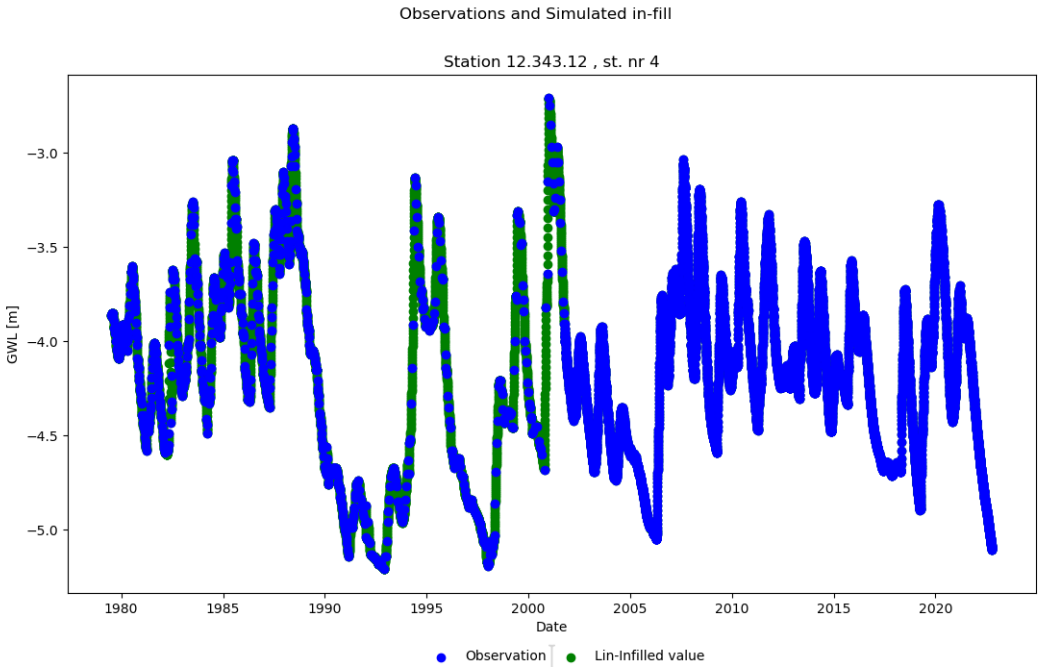

Gap-filled time series for Modum station (4).

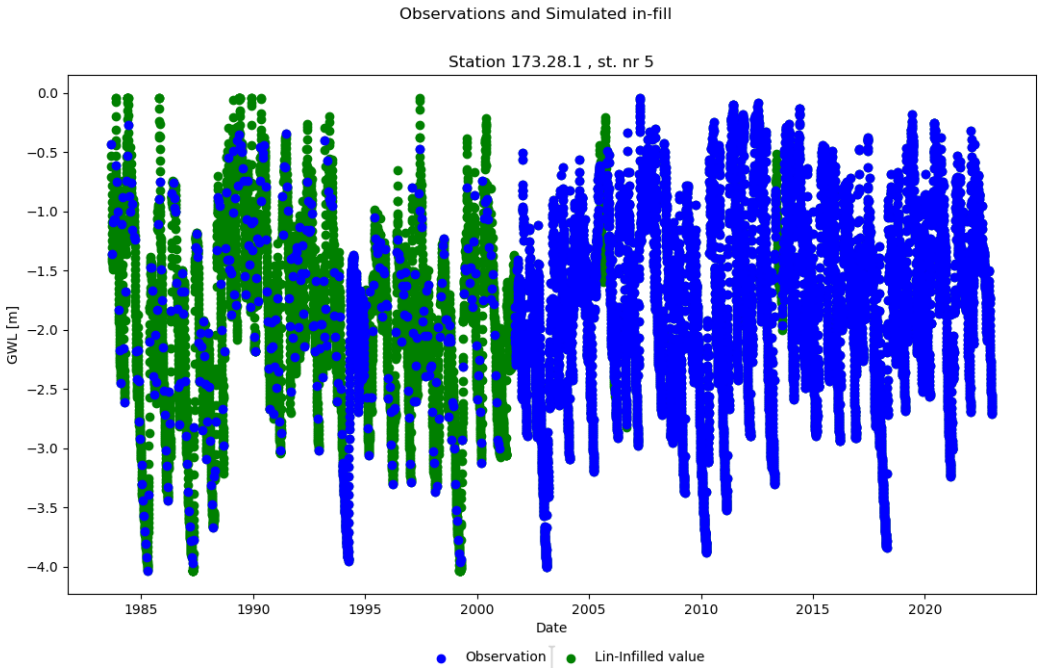

Gap-filled time series for Skjomen station (5).

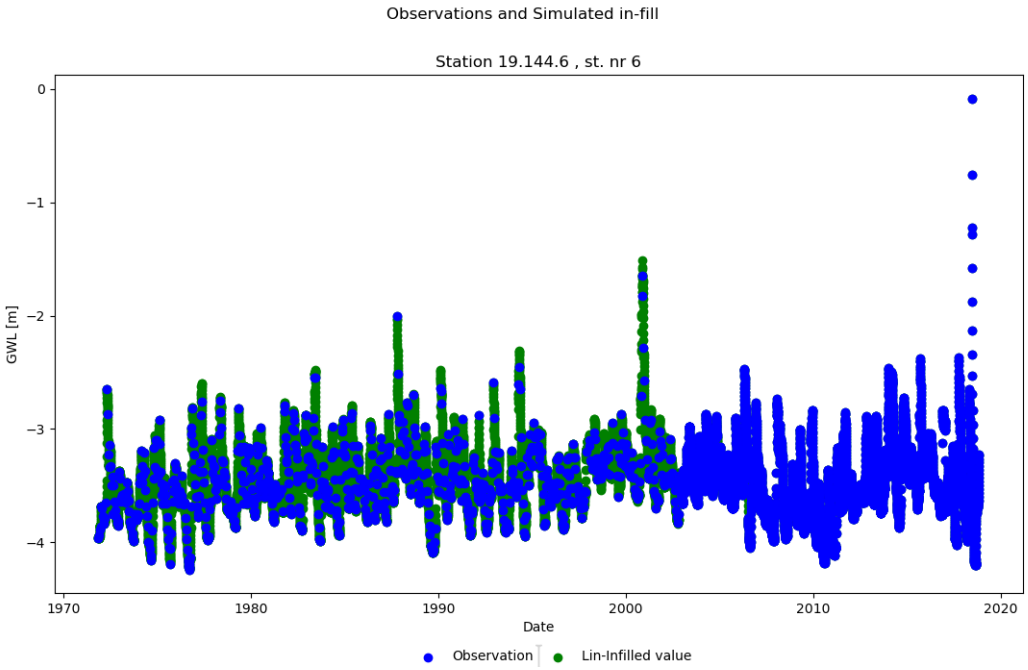

Gap-filled time series for Stigvassåi station (6).

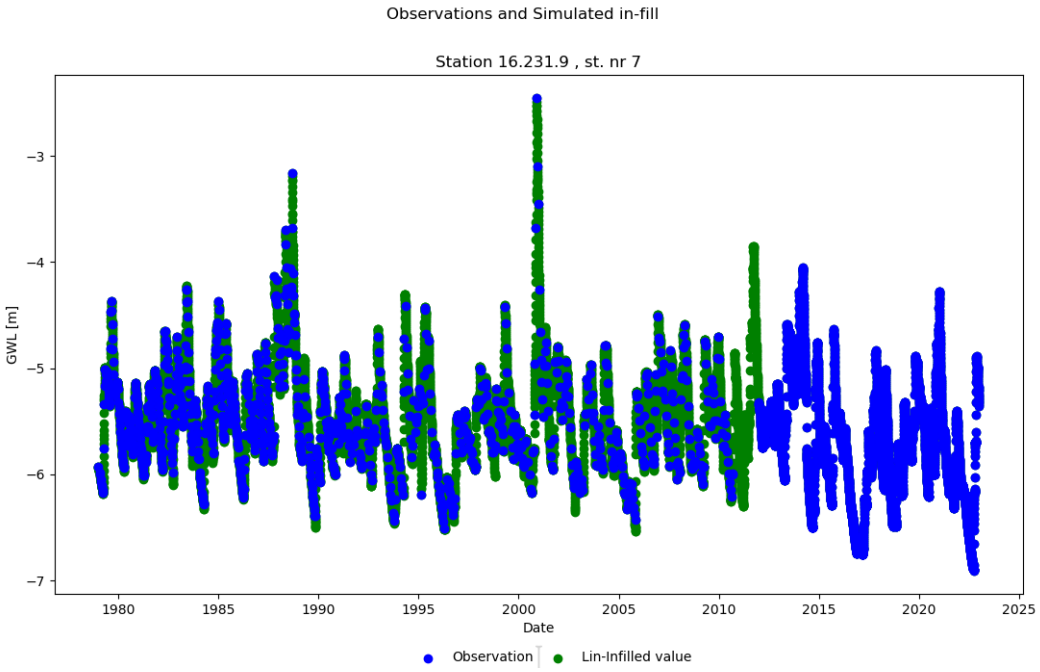

Gap-filled time series for Eikamoen station (7).

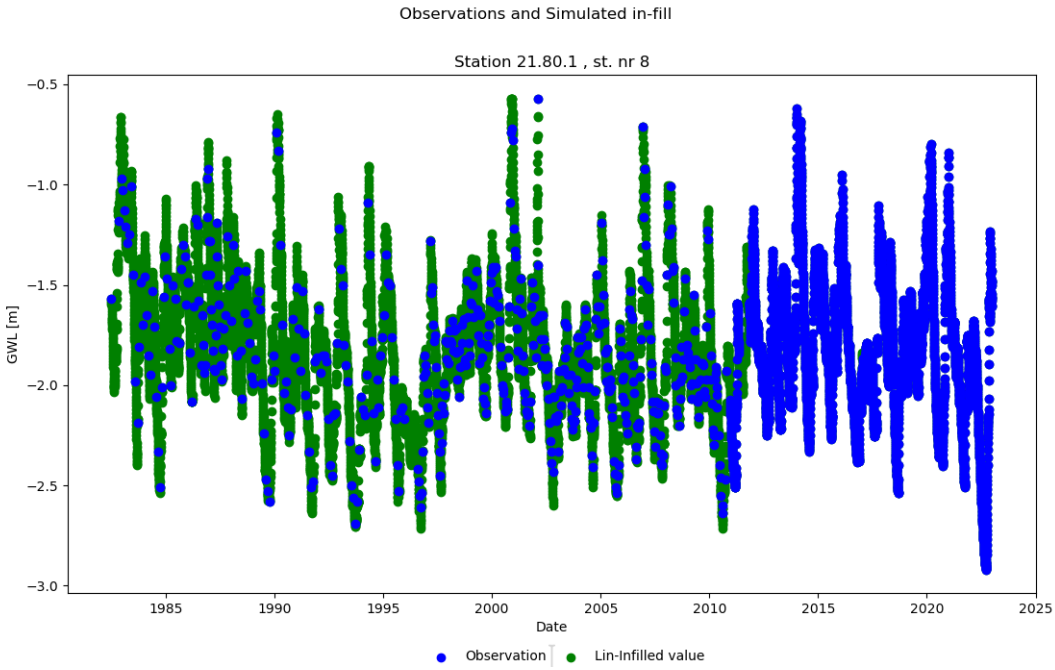

Gap-filled time series for Evje station (8).

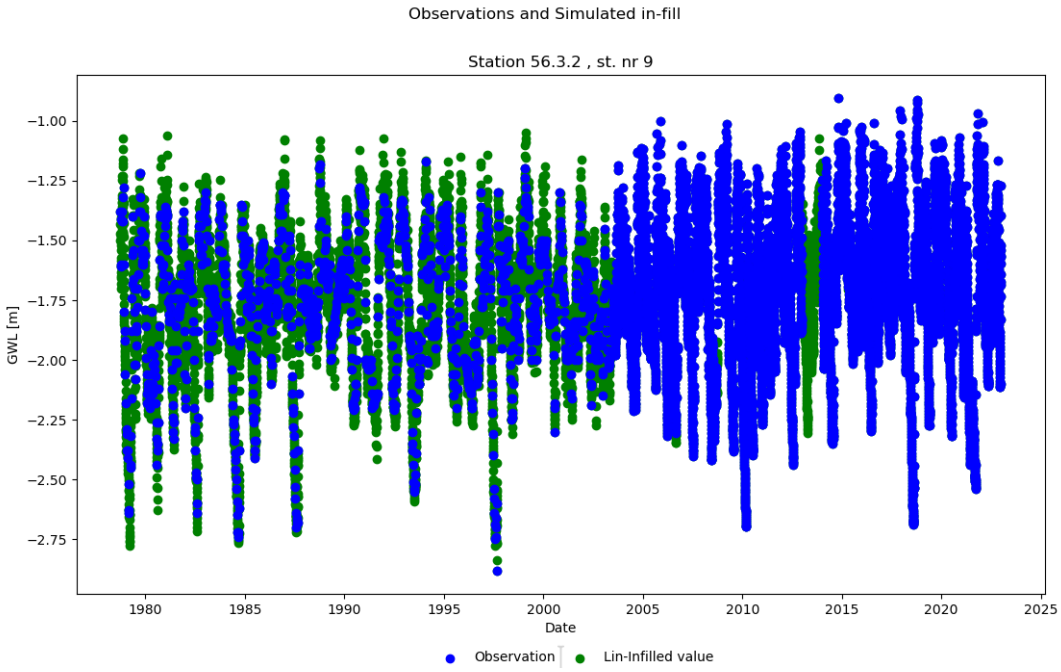

Gap-filled time series for Fana station (9).

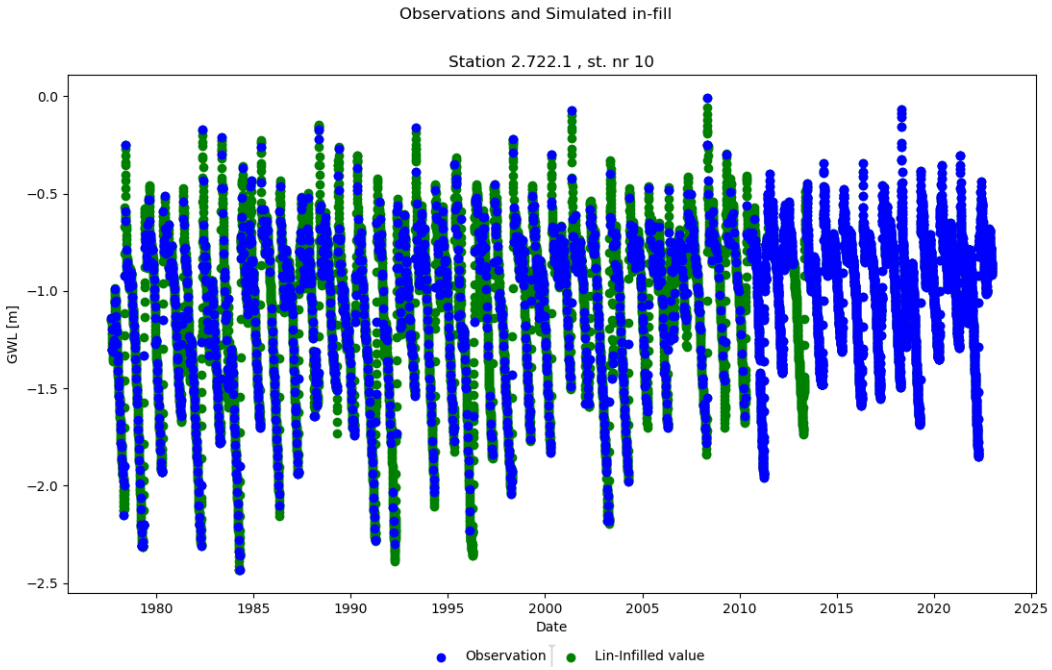

Gap-filled time series for Finnbølseter station (10).

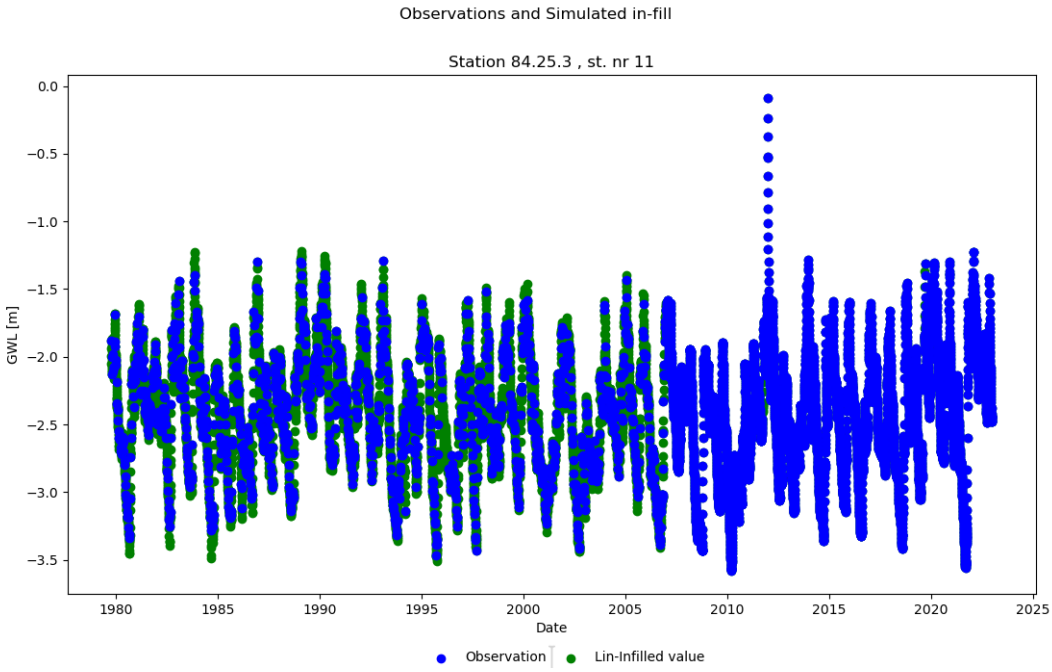

Gap-filled time series for Førde/Moskog station (11).

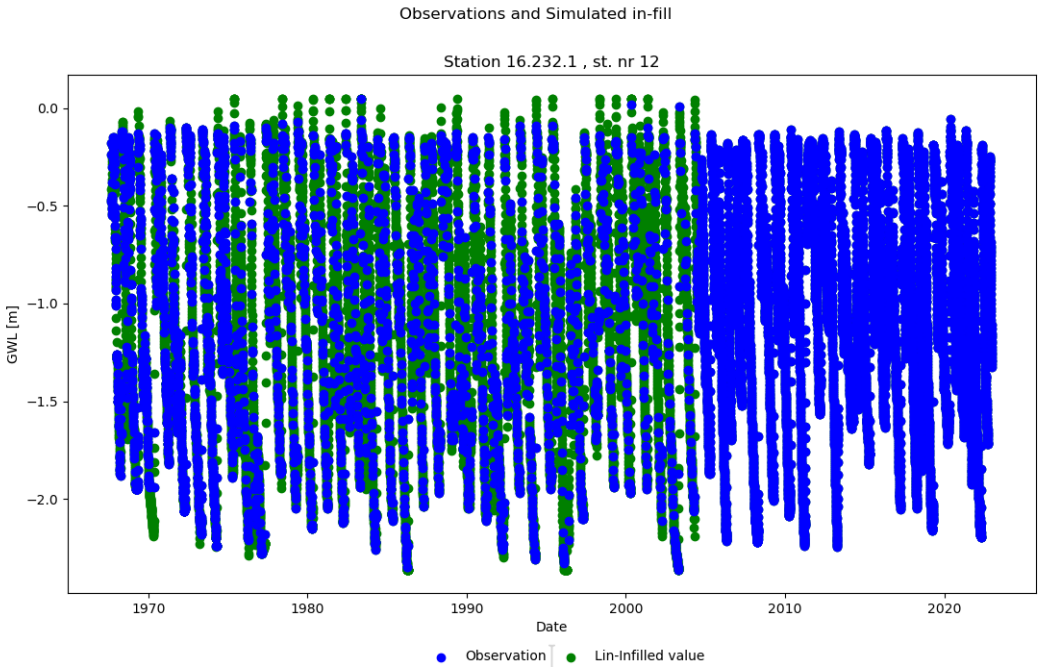

Gap-filled time series for Groset station (12).

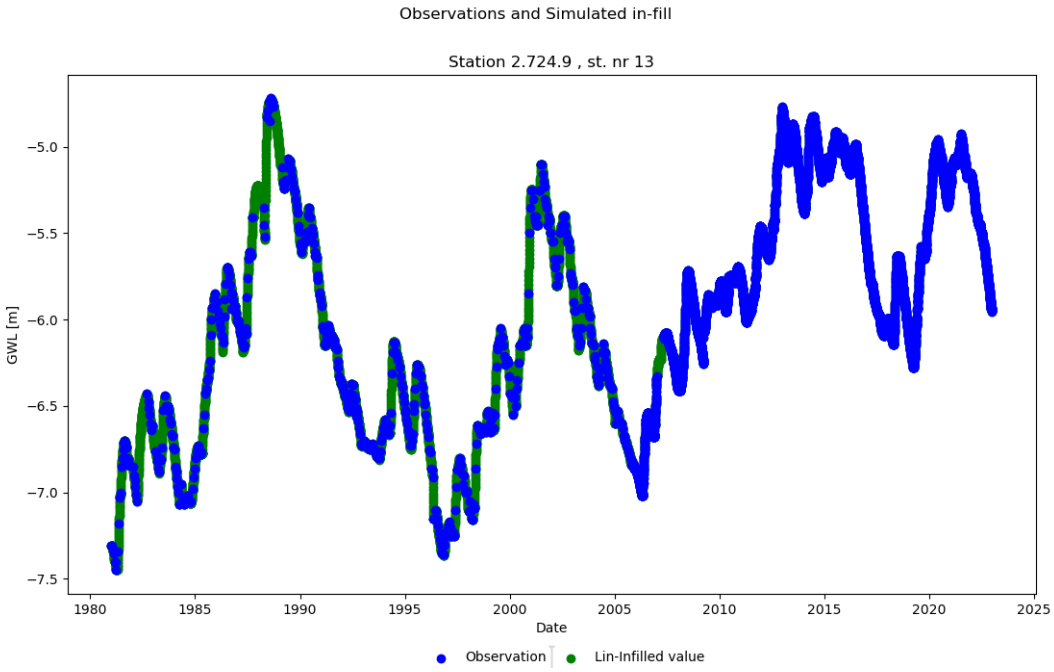

Gap-filled time series for Haslemoen station (13).

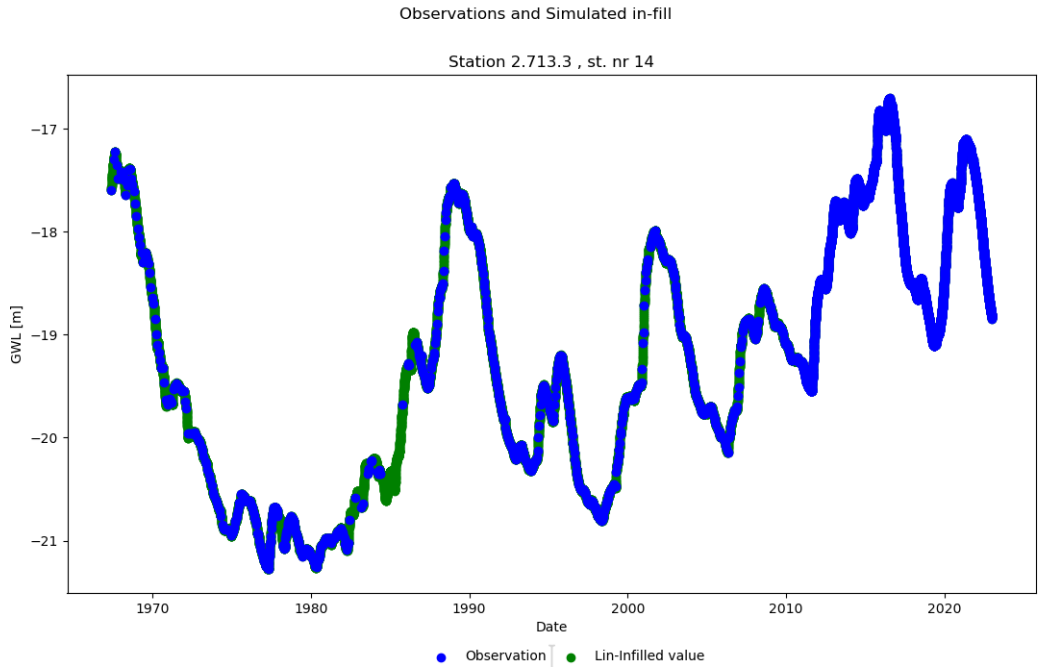

Gap-filled time series for Hauerseter station (14).

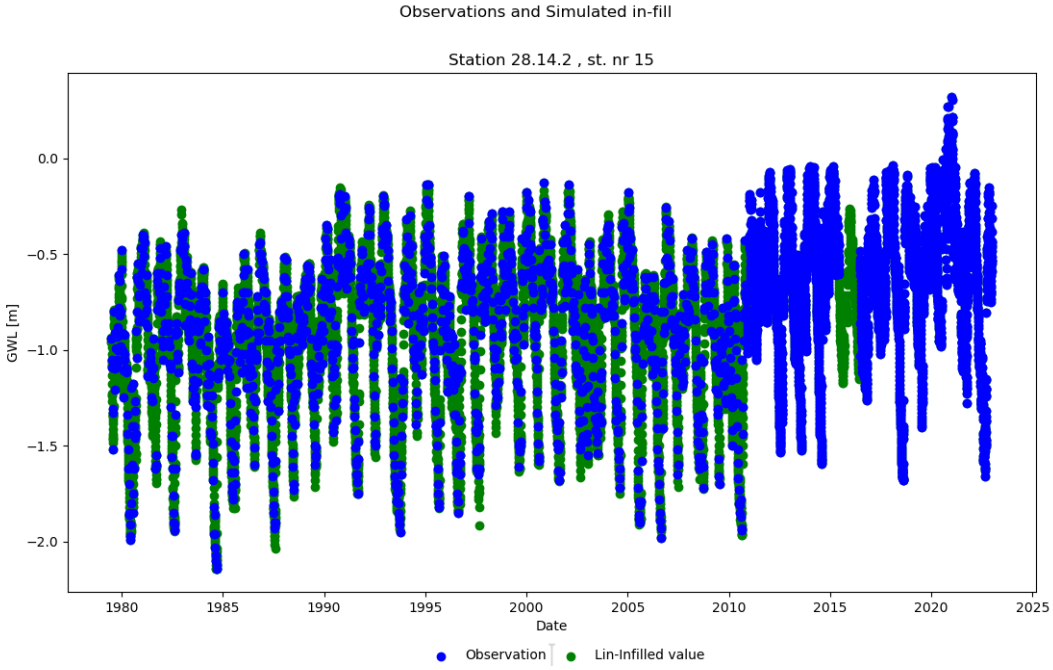

Gap-filled time series for Jæren station (15).

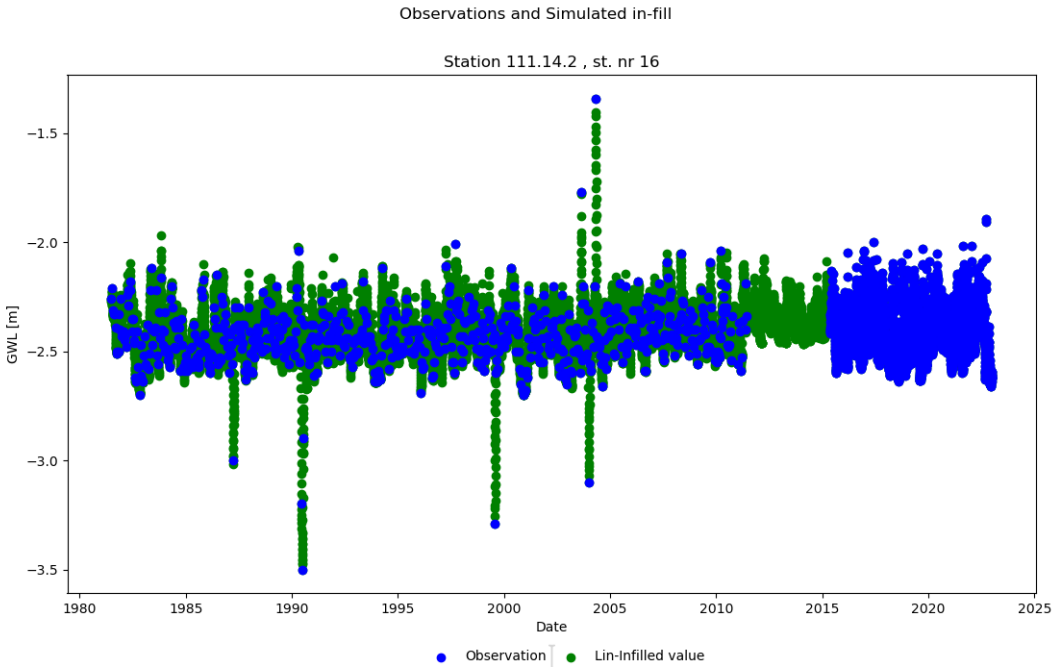

Gap-filled time series for Kårvatn station (16).

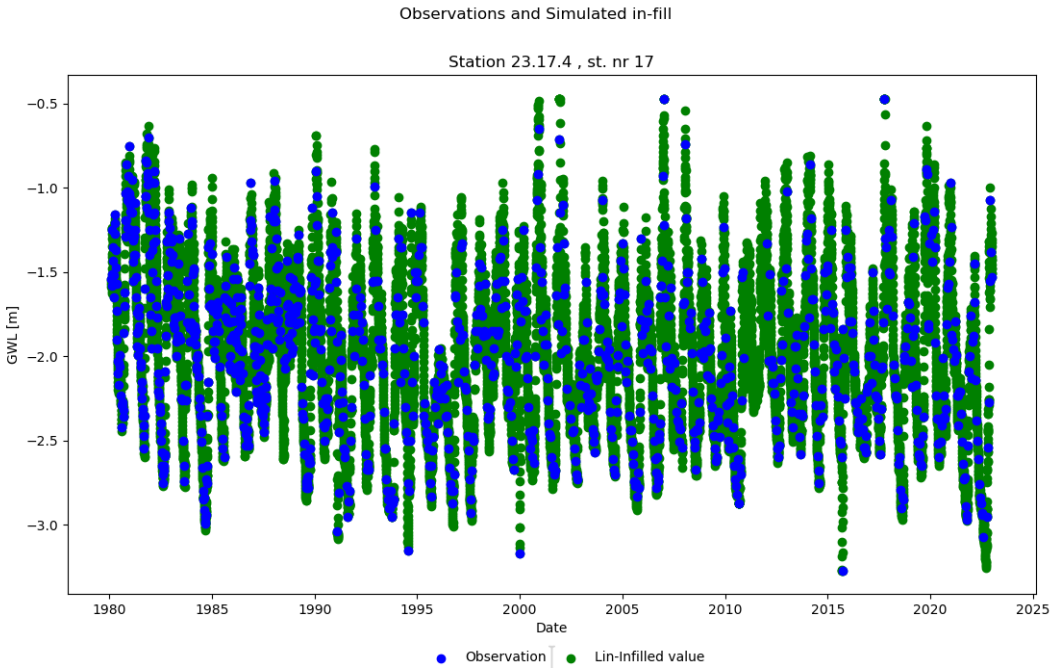

Gap-filled time series for Lindesnes station (17).

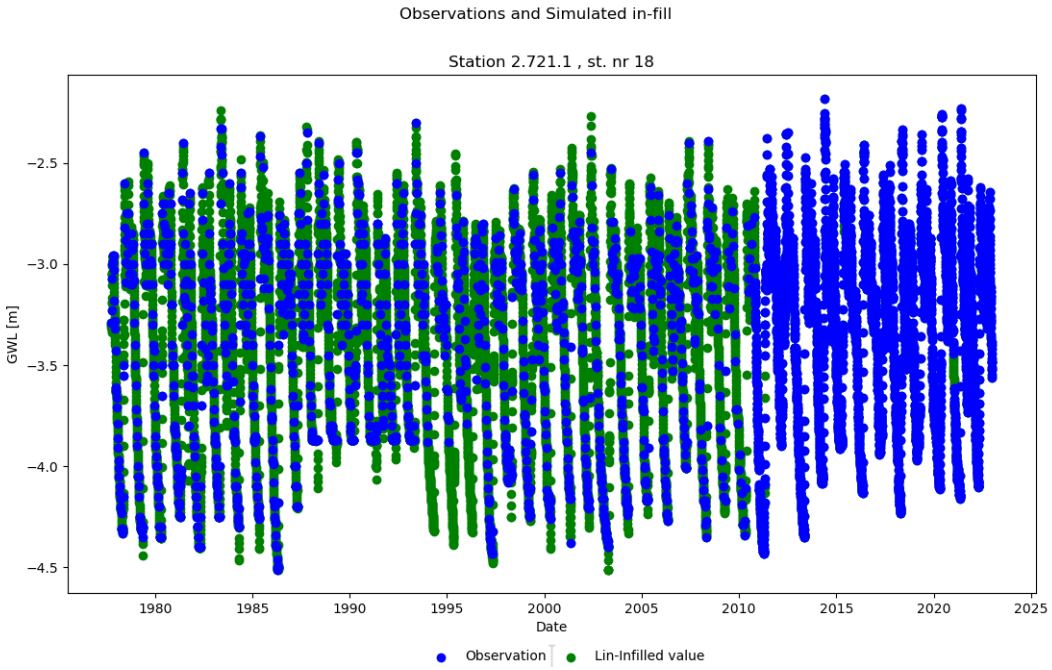

Gap-filled time series for Lykjestøylane station (18).

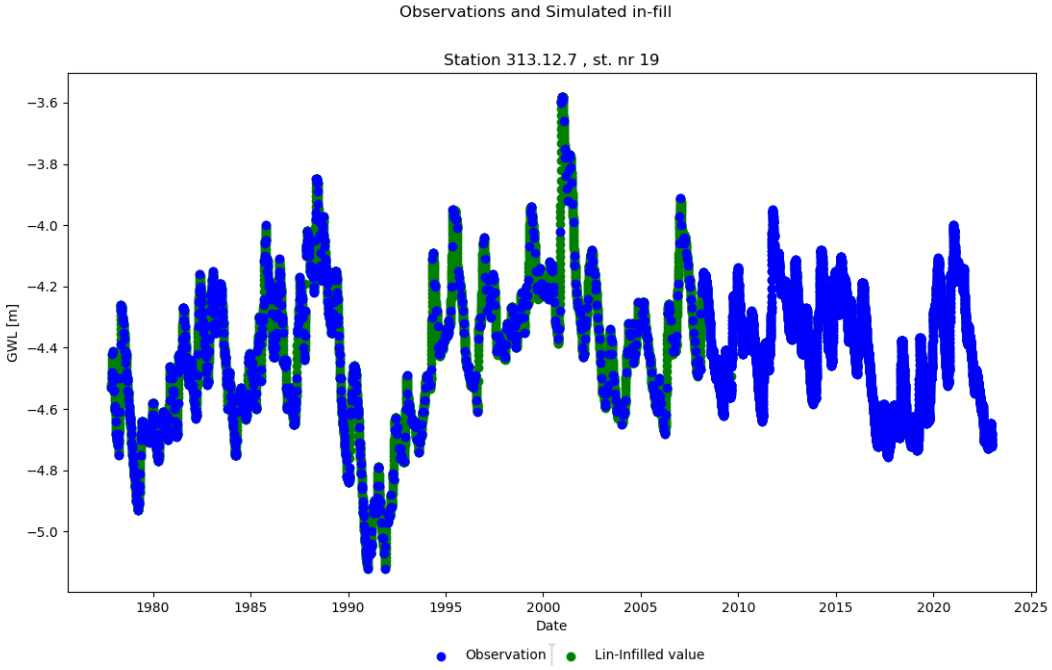

Gap-filled time series for Magnor station (19).

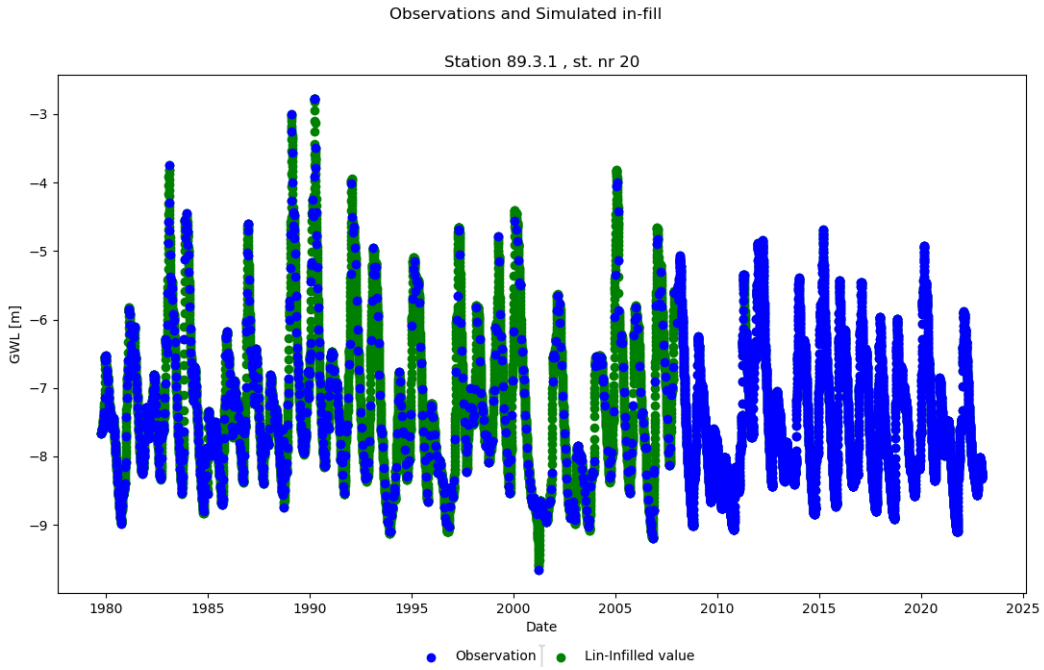

Gap-filled time series for Nordfjordeid station (20).

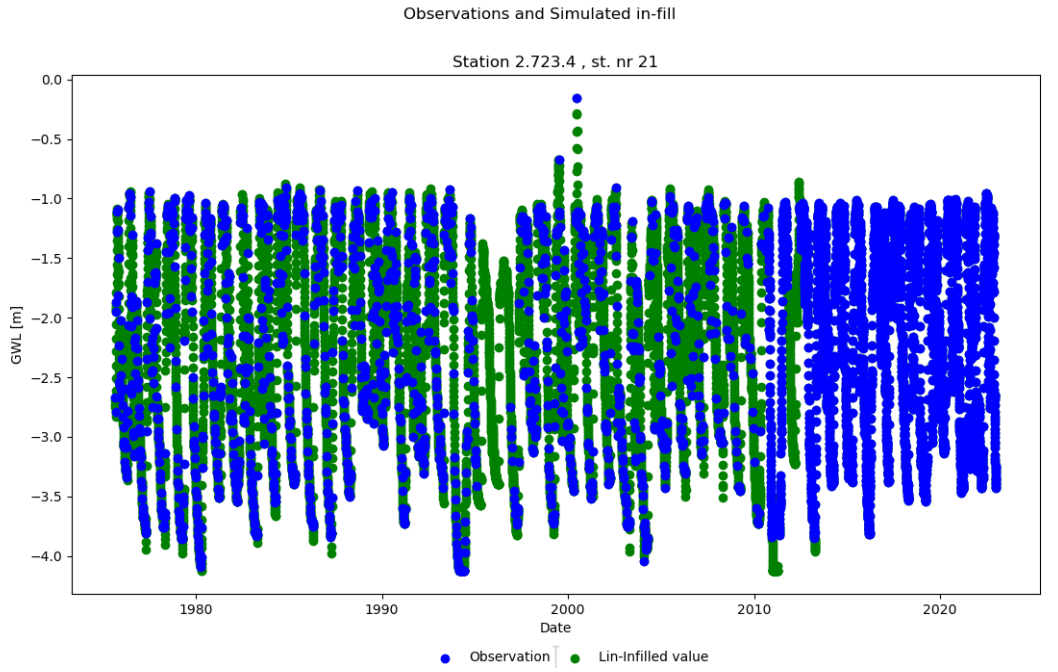

Gap-filled time series for Settalbekken station (21).

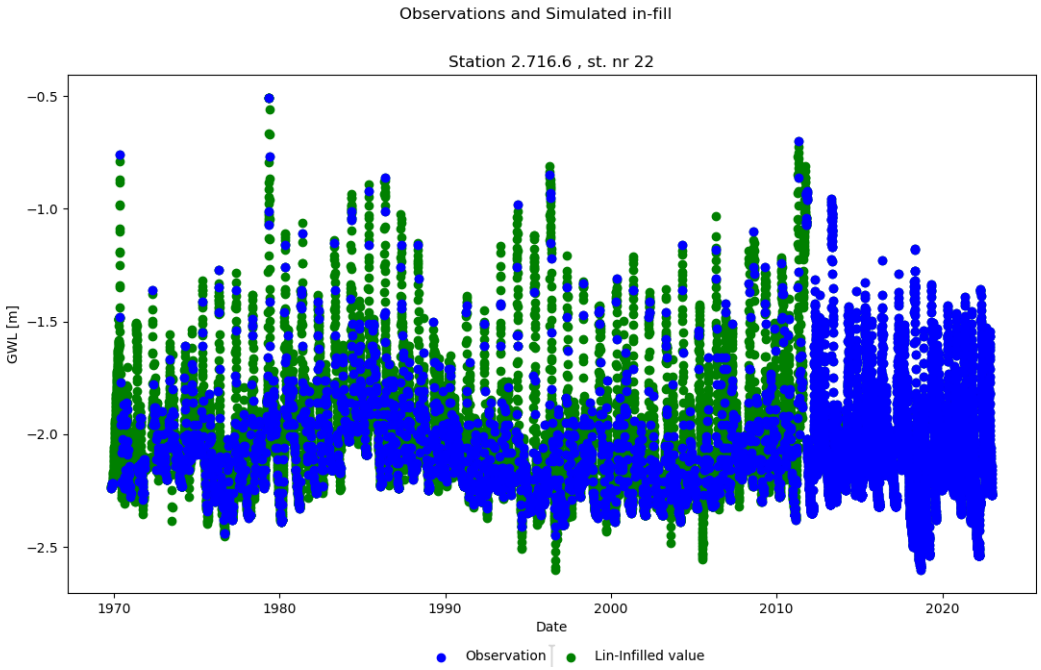

Gap-filled time series for AStenerseter station (22).

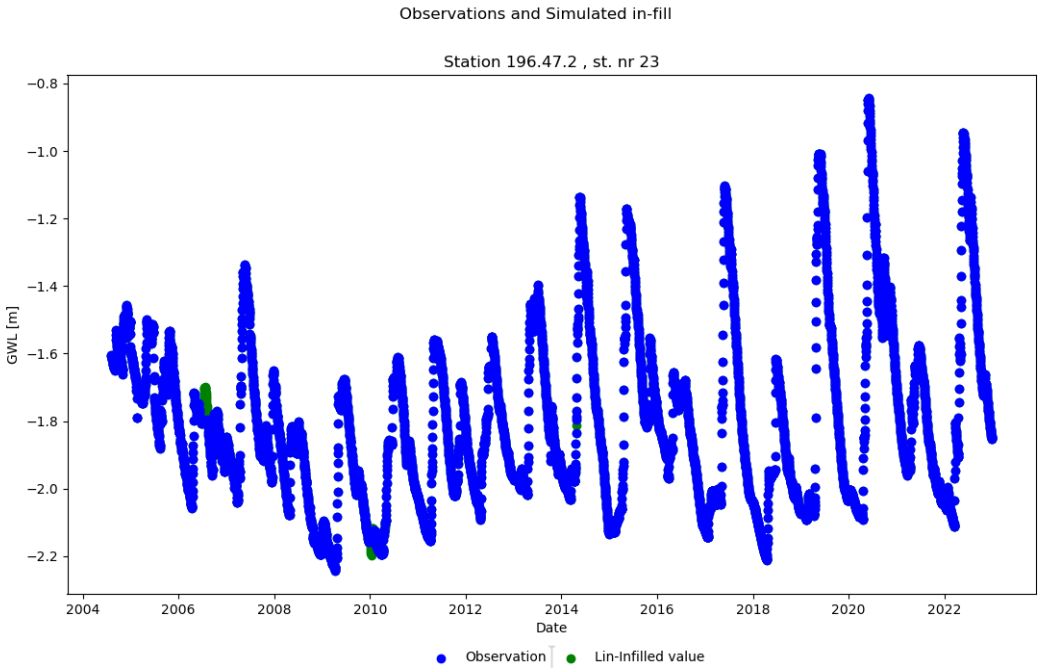

Gap-filled time series for Øverbygd station (23).

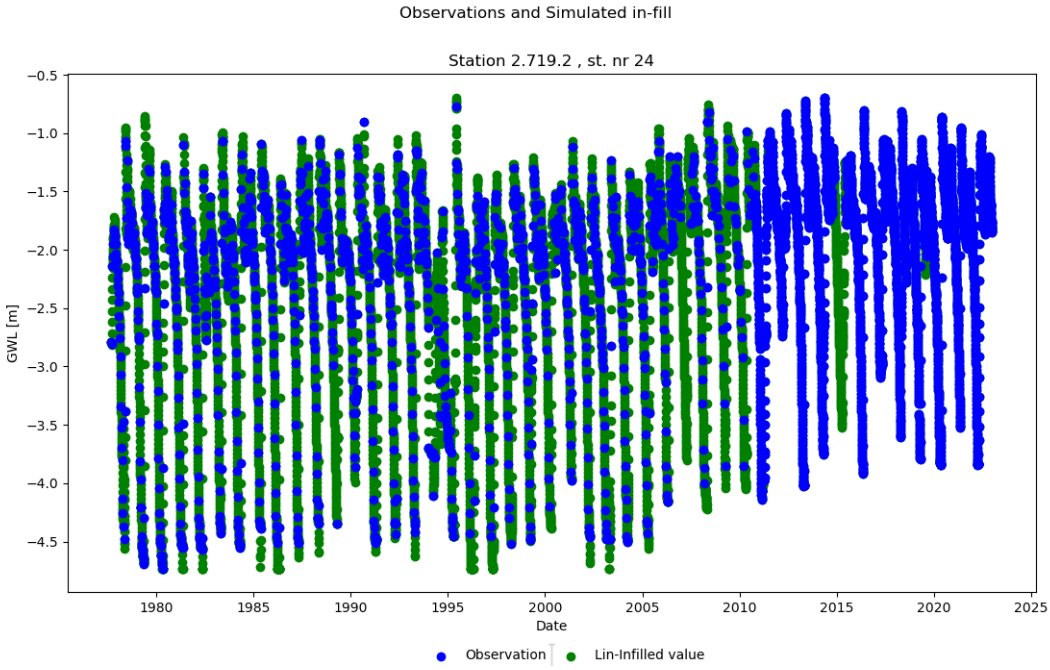

Gap-filled time series for Øyangen station (24).

Appendix C

Monthly multi temporal trend plots

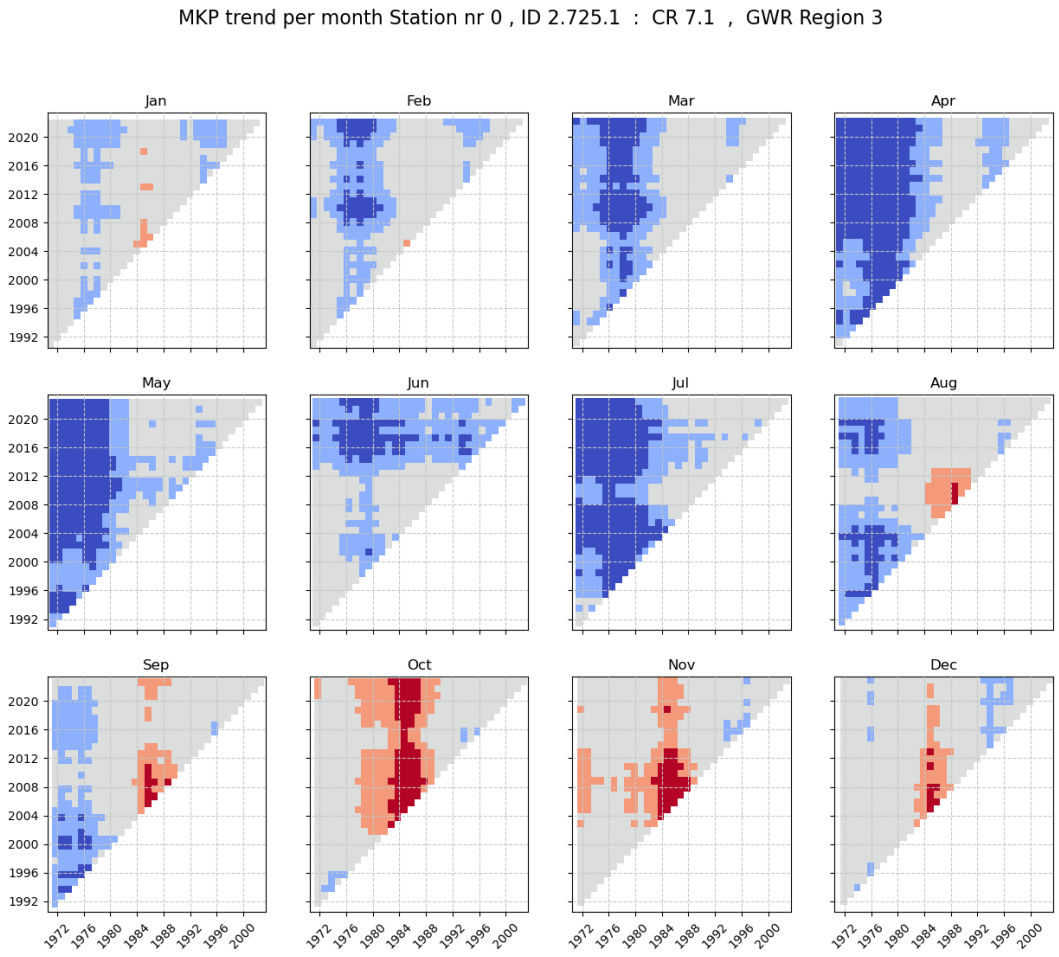

Same as in figure 4.11, but for Abrahamsvoll station (0).

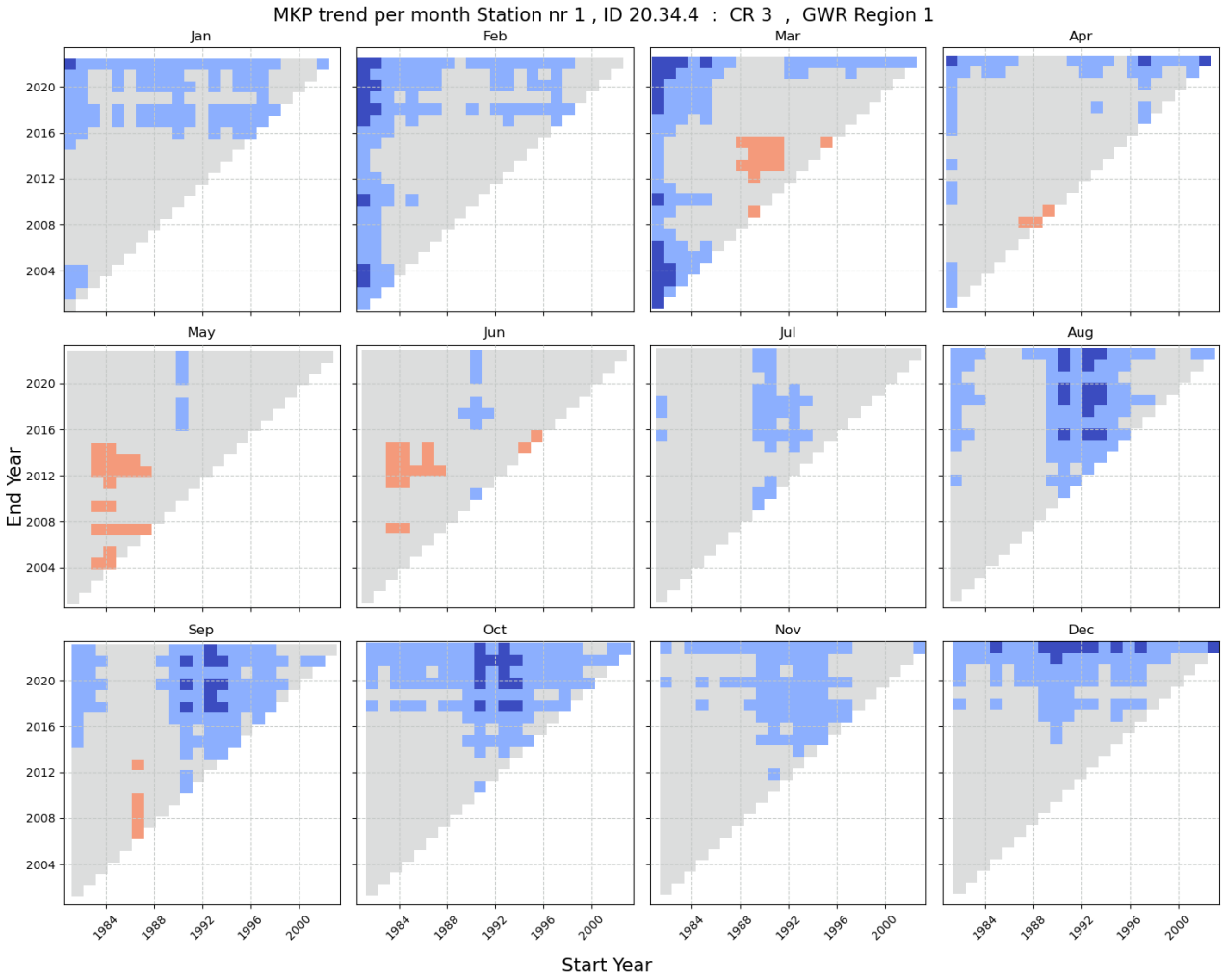

Same as in figure 4.11, but for Birkenes station (1).

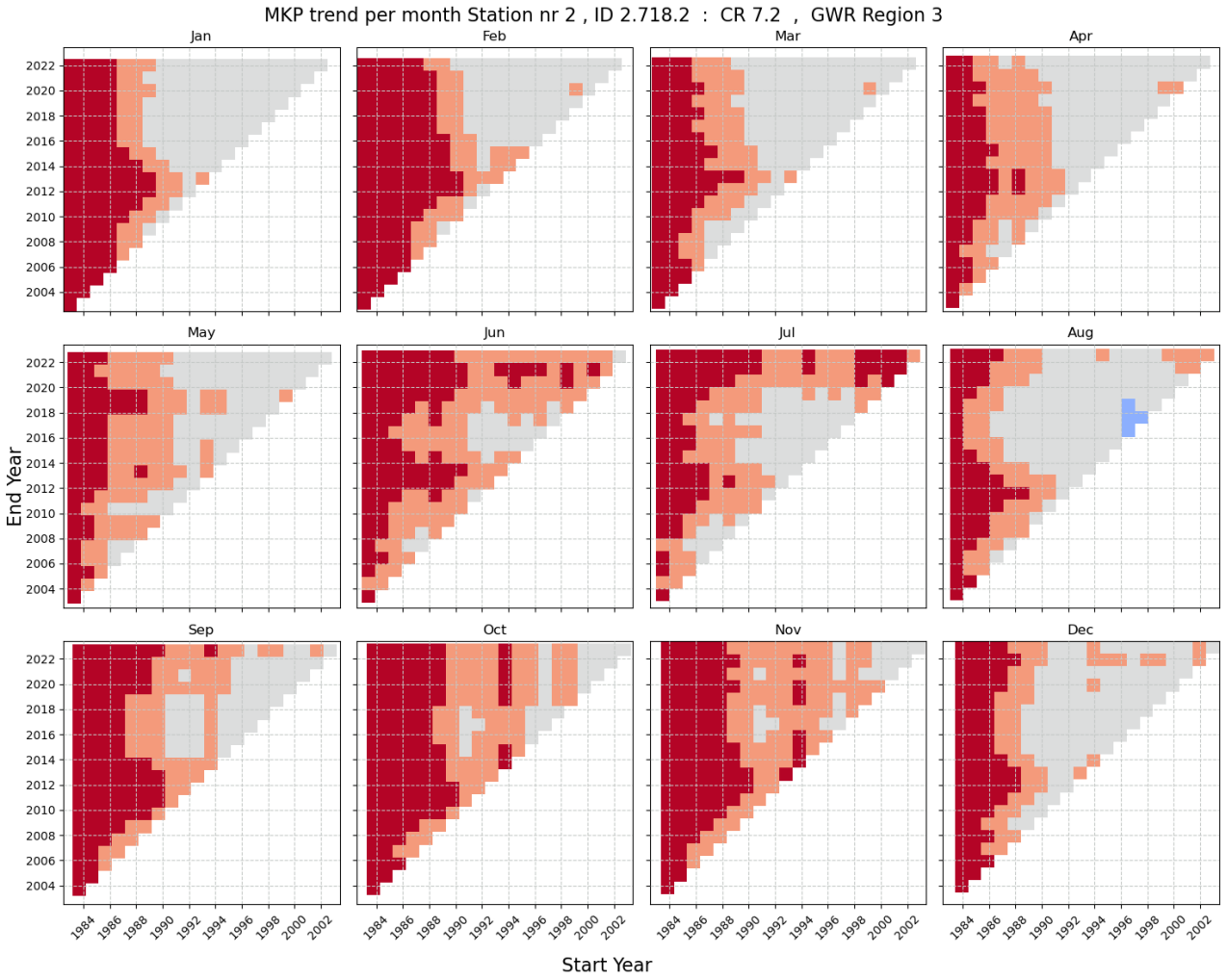

Same as in figure 4.11, but for Dombås station (2).

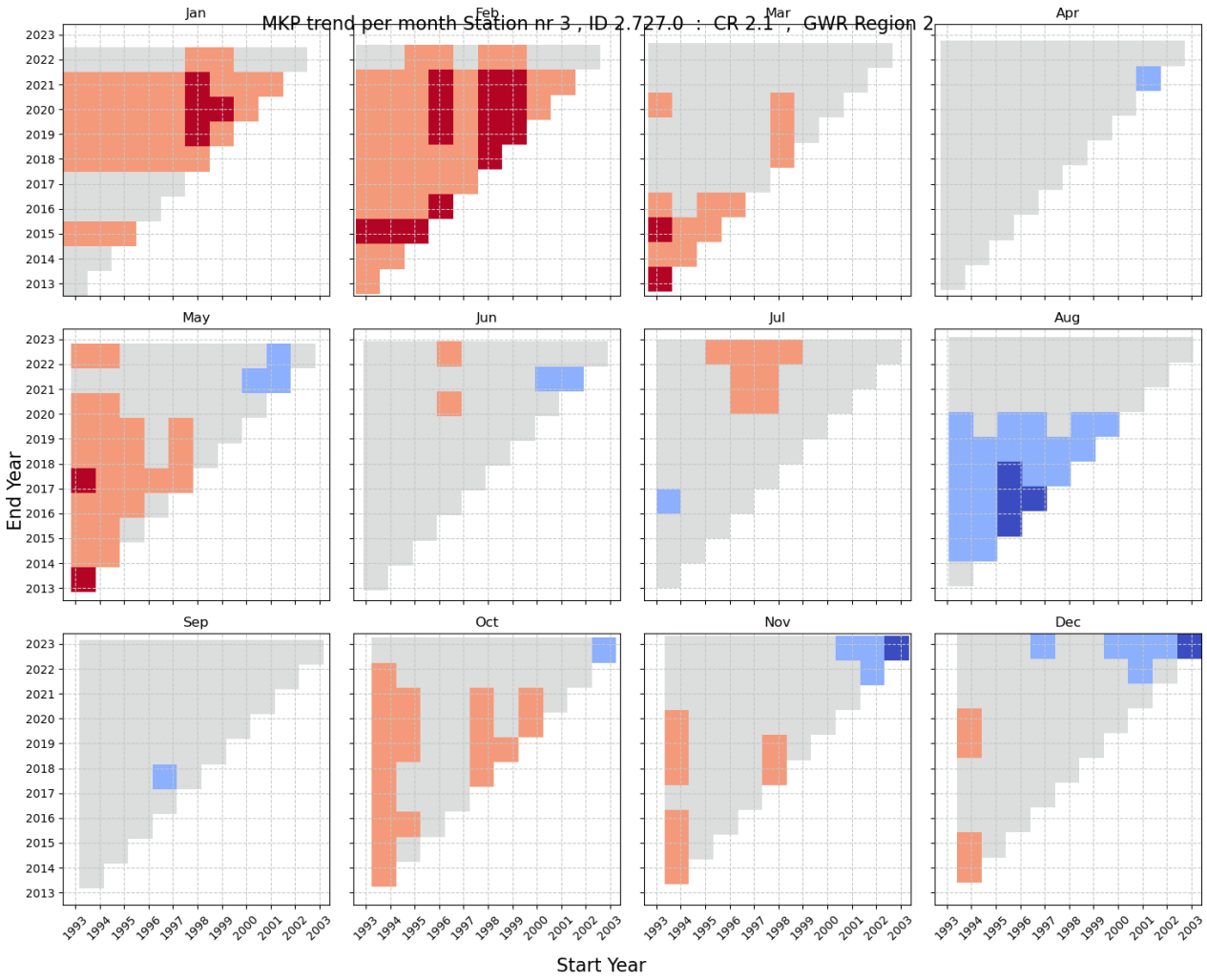

Same as in figure 4.11, but for Kise station (3).

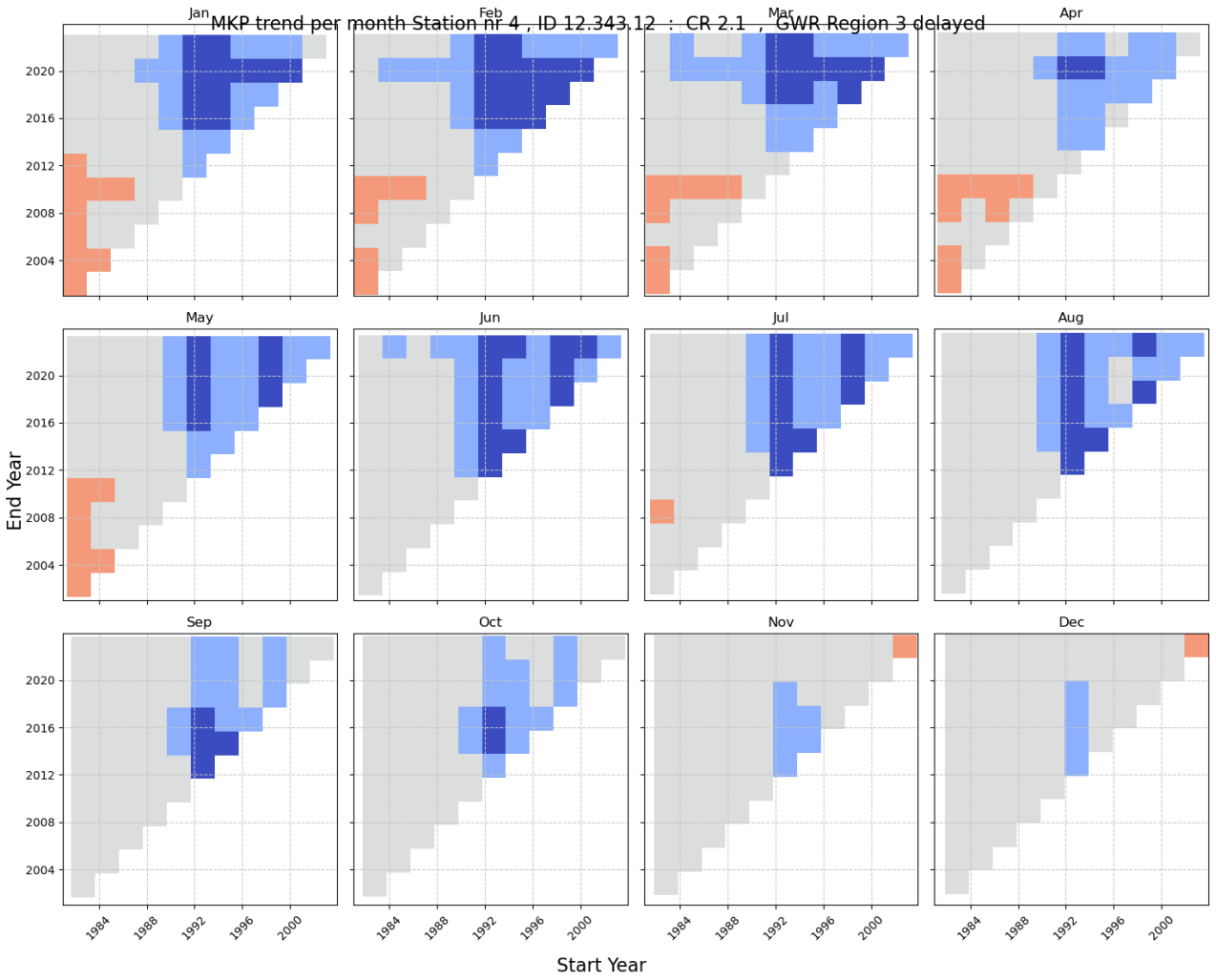

Same as in figure 4.11, but for Modum station (4).

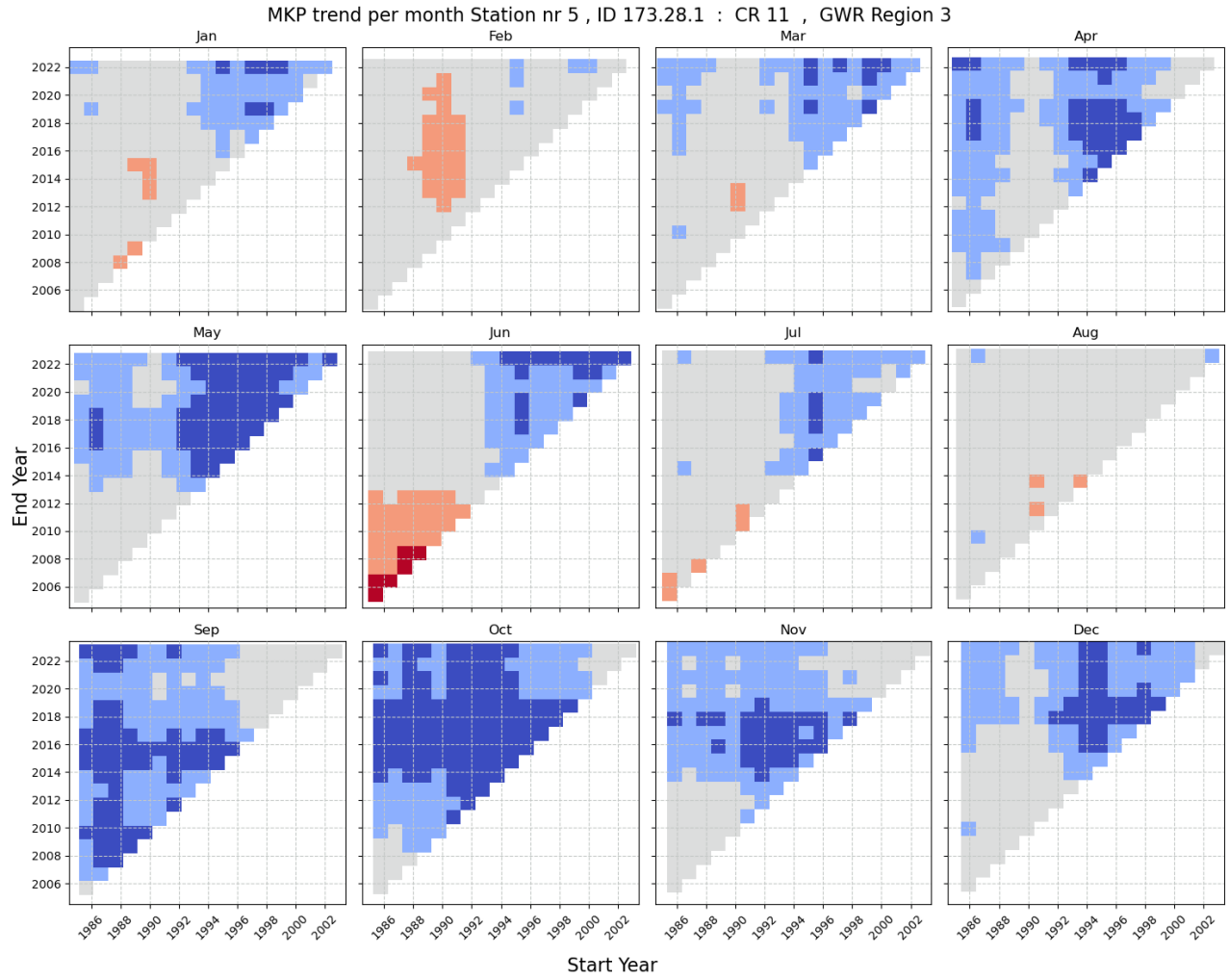

Same as in figure 4.11, but for Skjomen station (5).

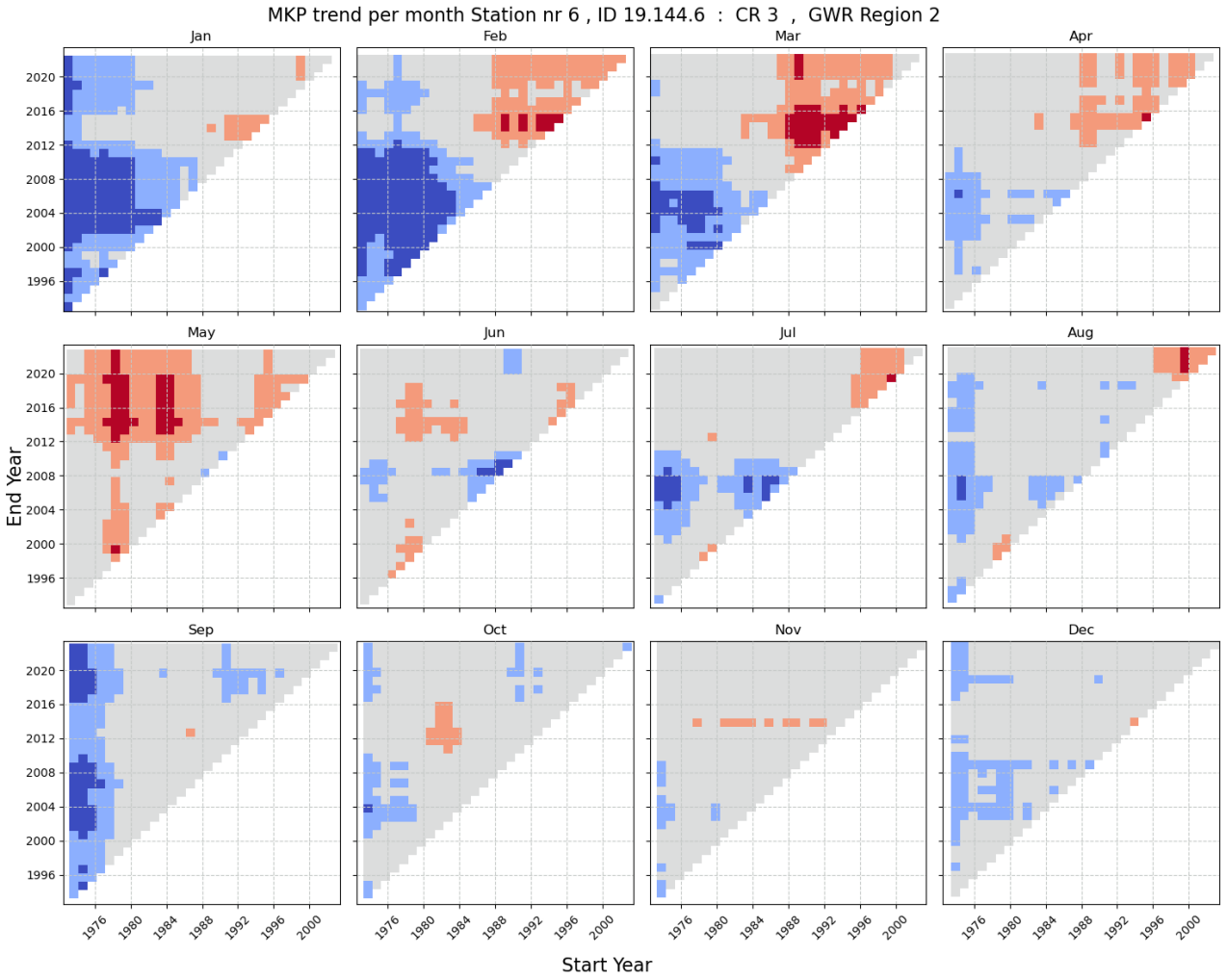

Same as in figure 4.11, but for Stigvassåi station (6).

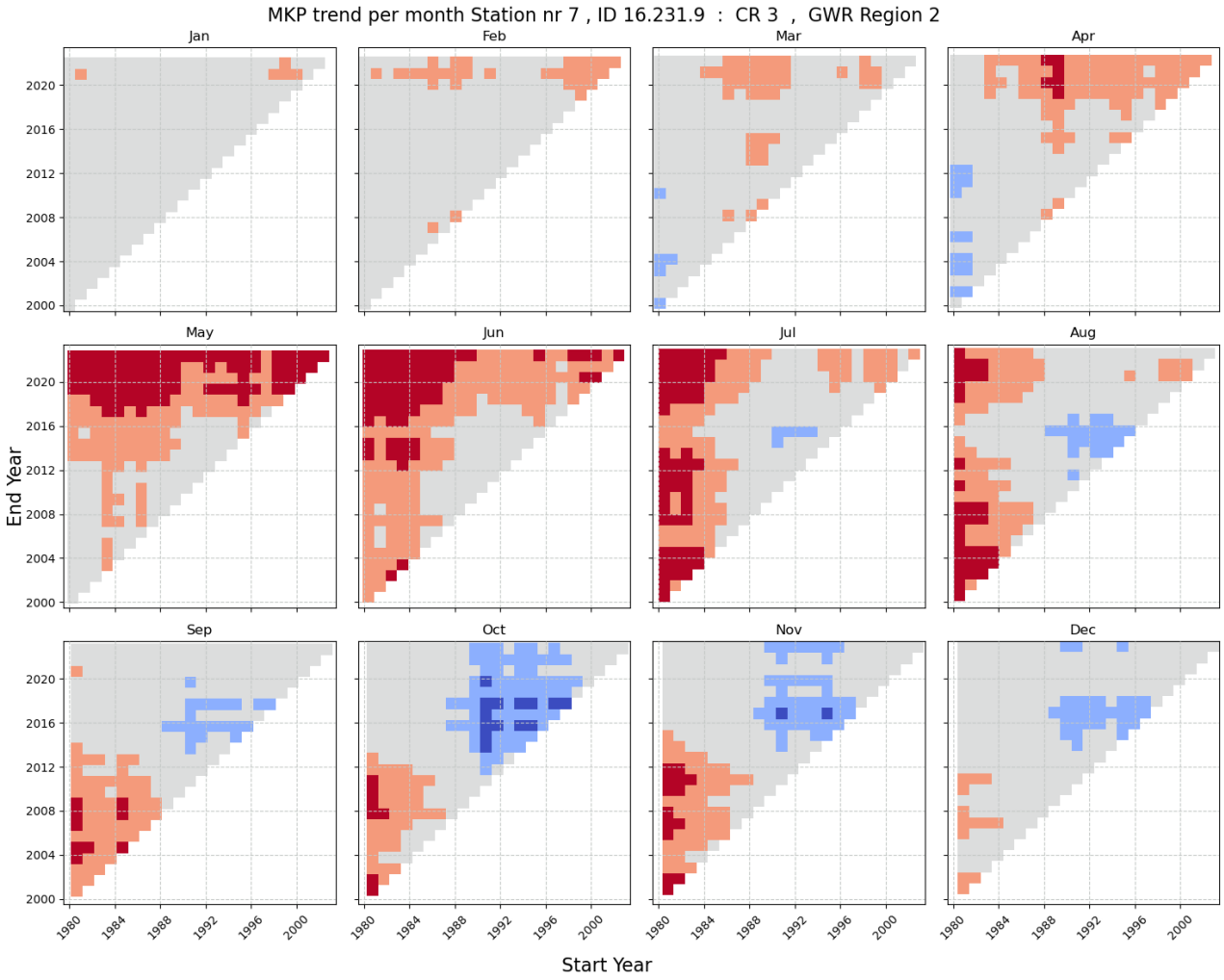

Same as in figure 4.11, but for Eikamoen station (7).

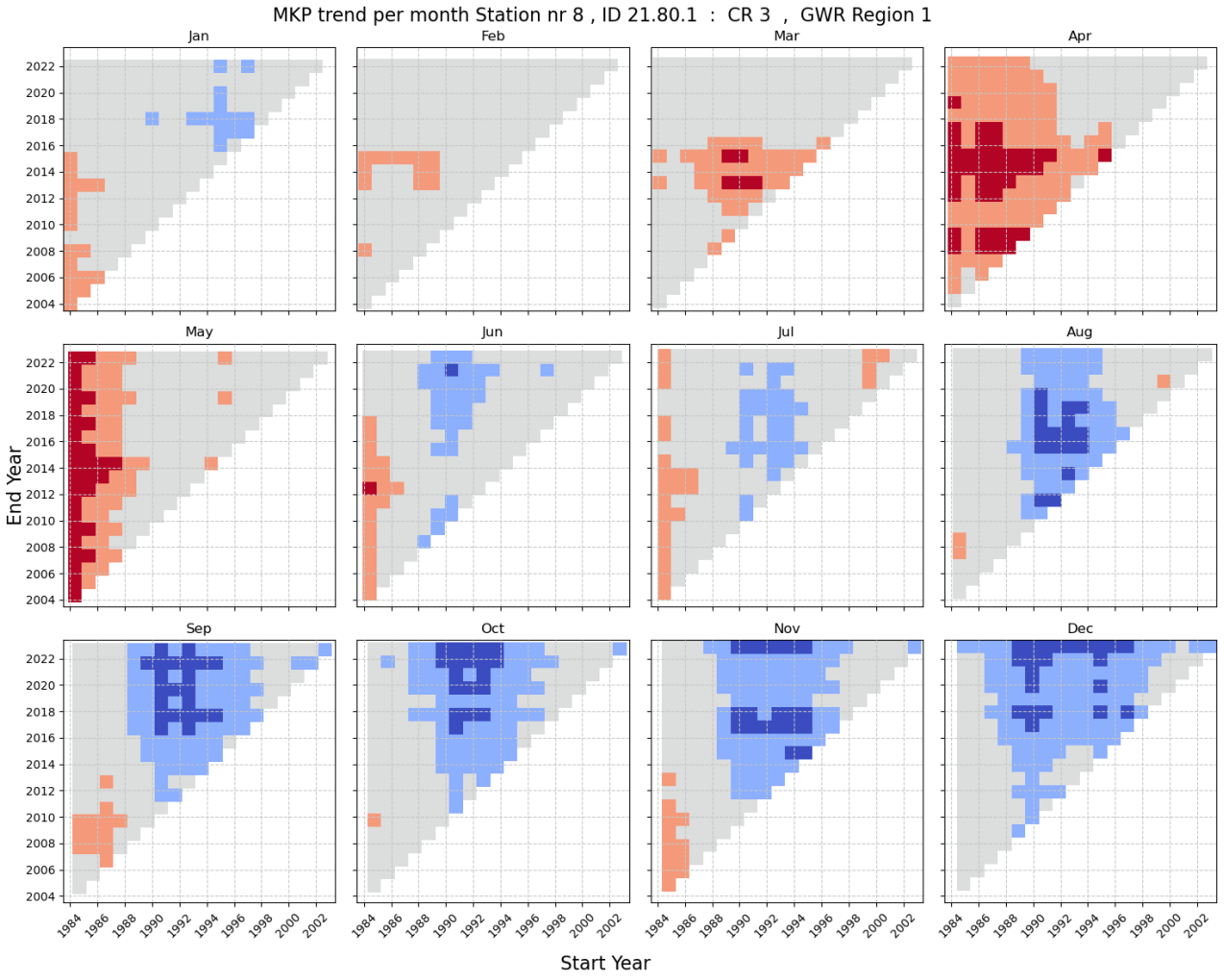

Same as in figure 4.11, but for Evje station (8).

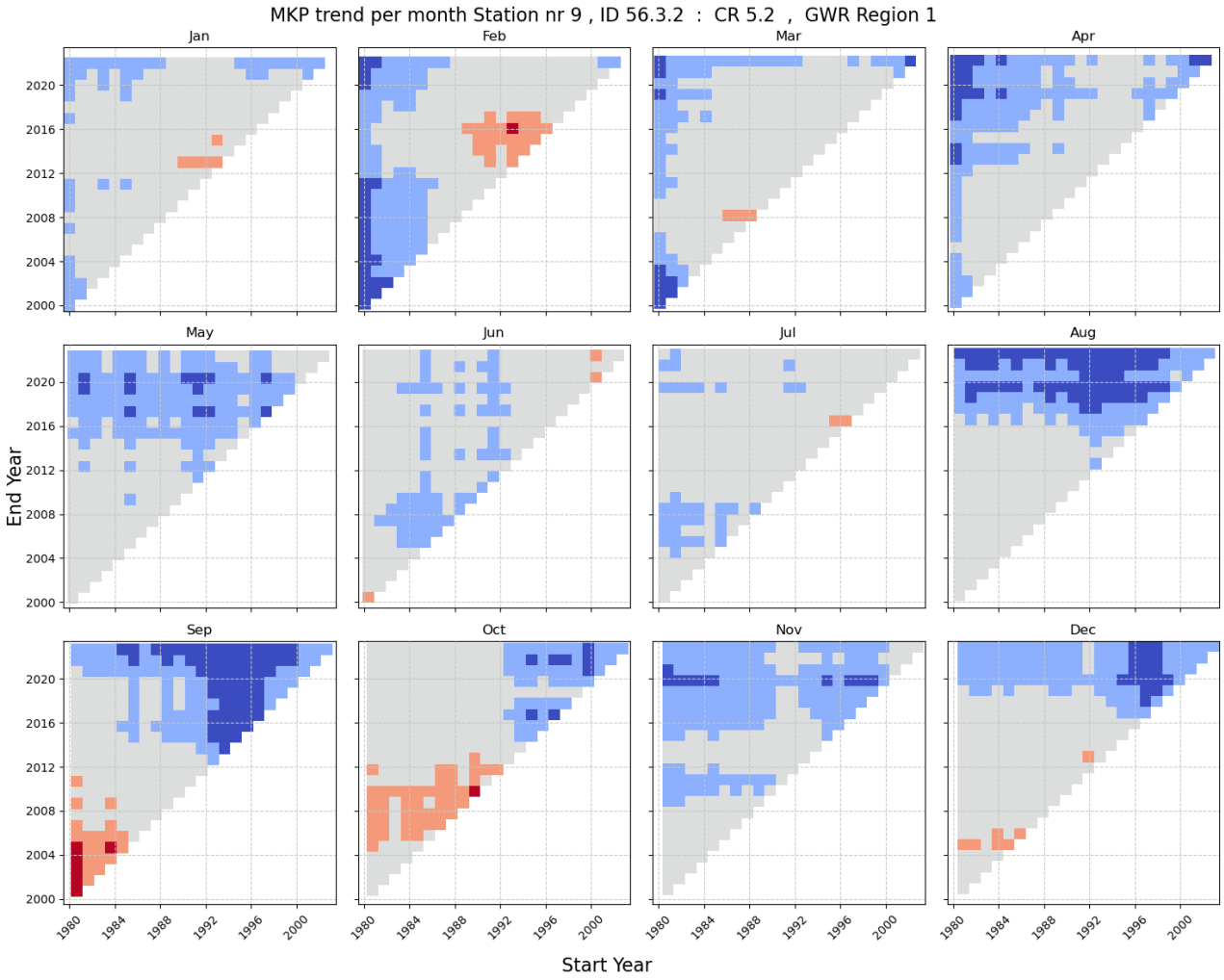

Same as in figure 4.11, but for Fana station (9).

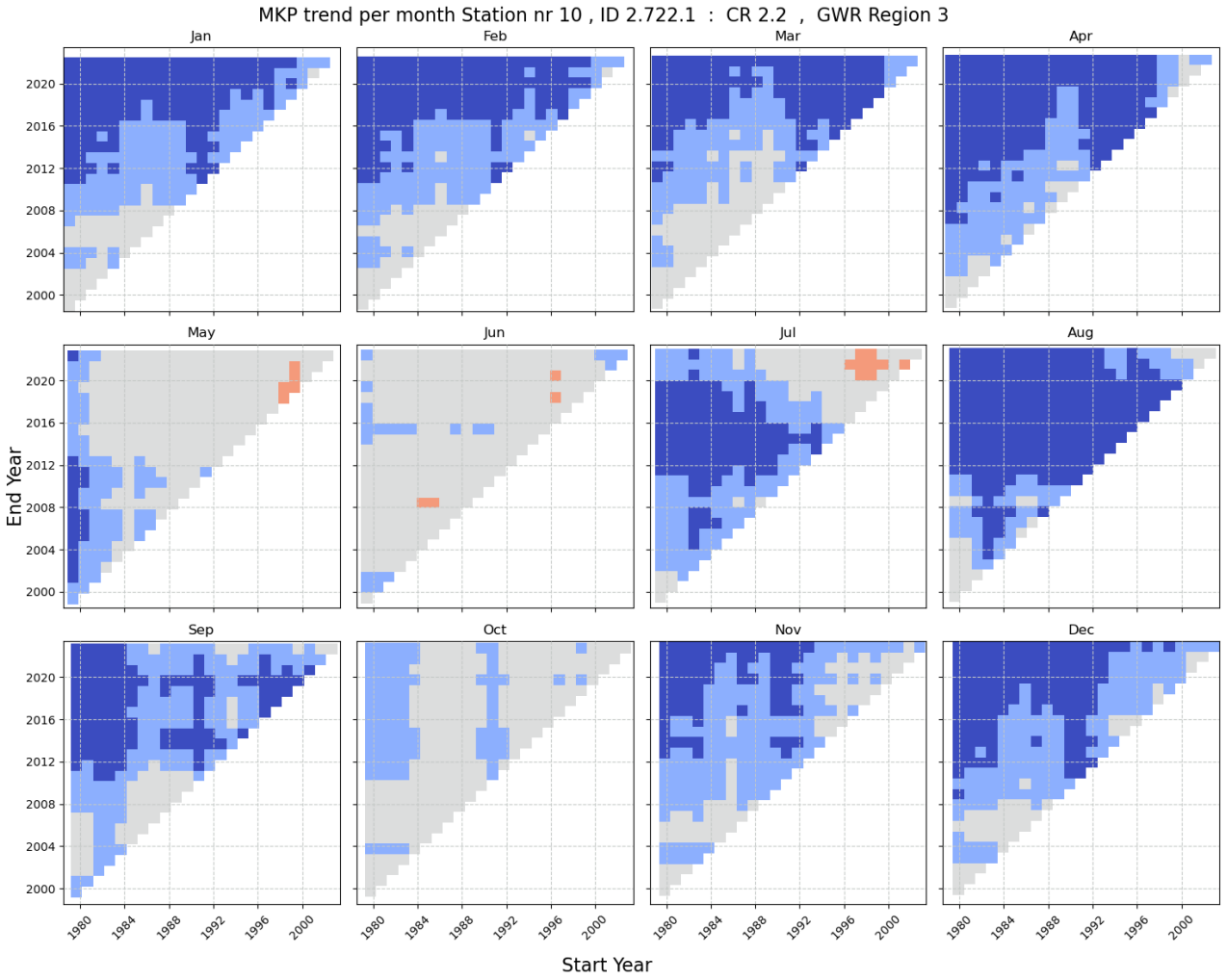

Same as in figure 4.11, but for Finnbølseter station (10).

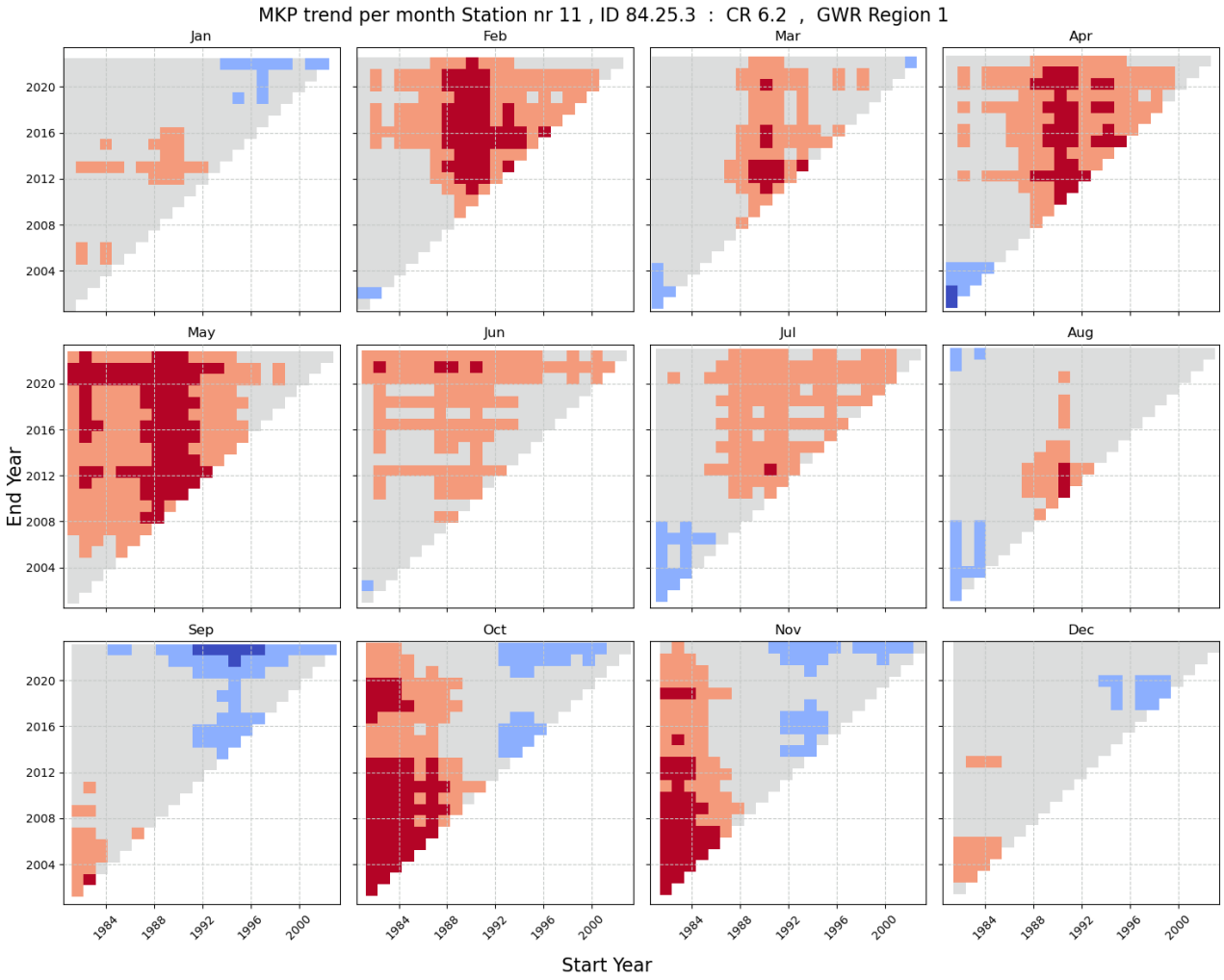

Same as in figure 4.11, but for Førde/Moskog station (11).

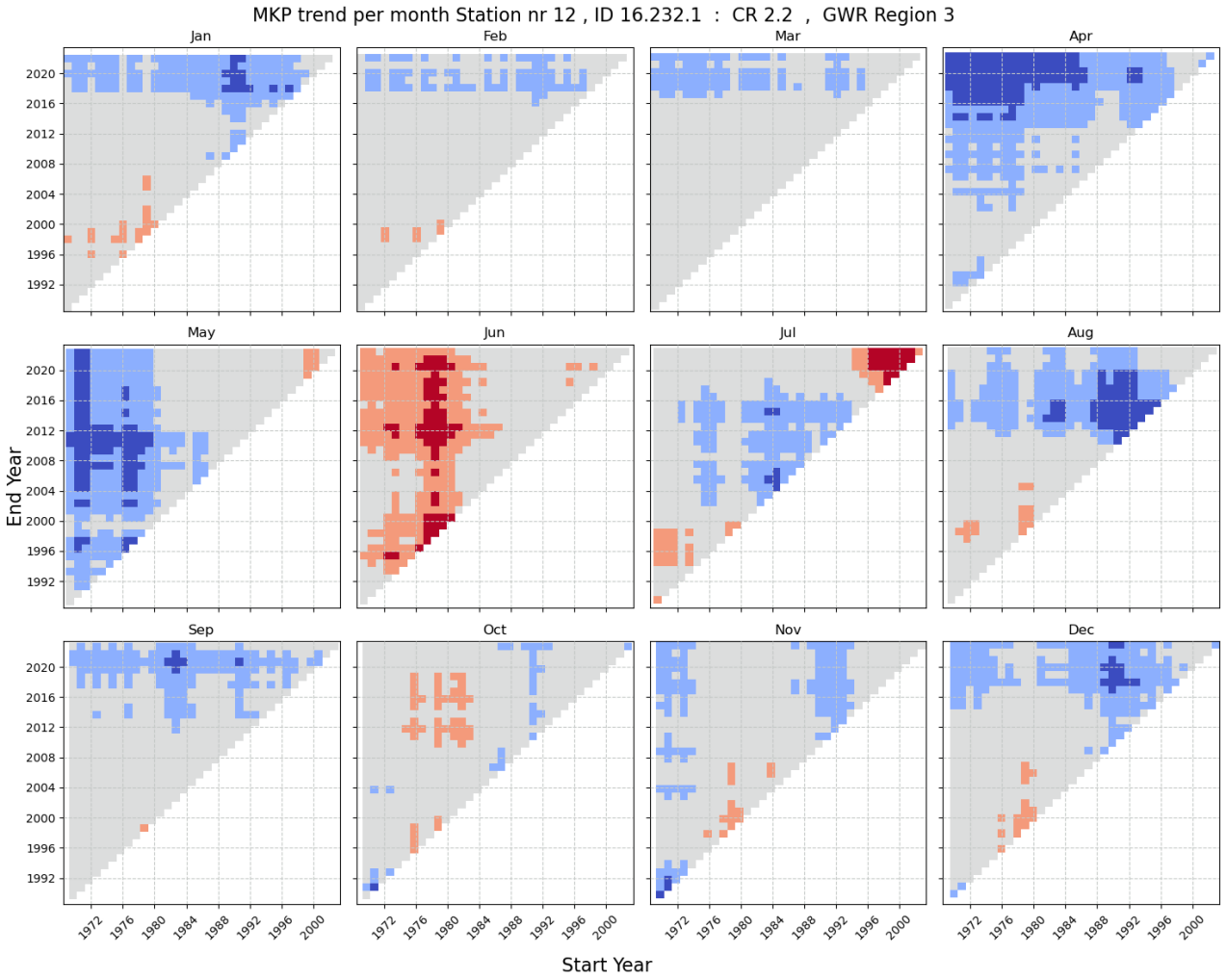

Same as in figure 4.11, but for Groset station (12).

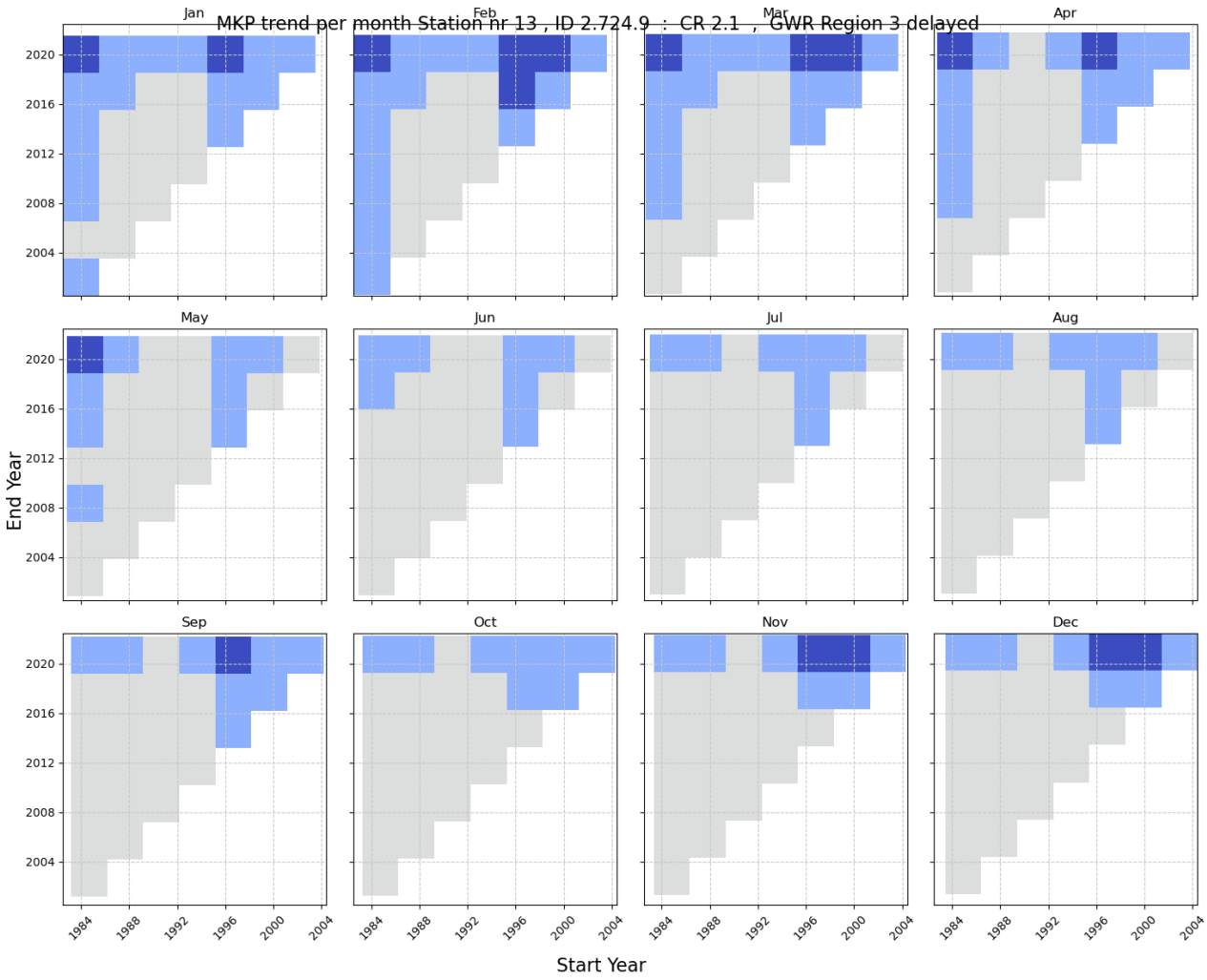

Same as in figure 4.11, but for Haslemoen station (13).

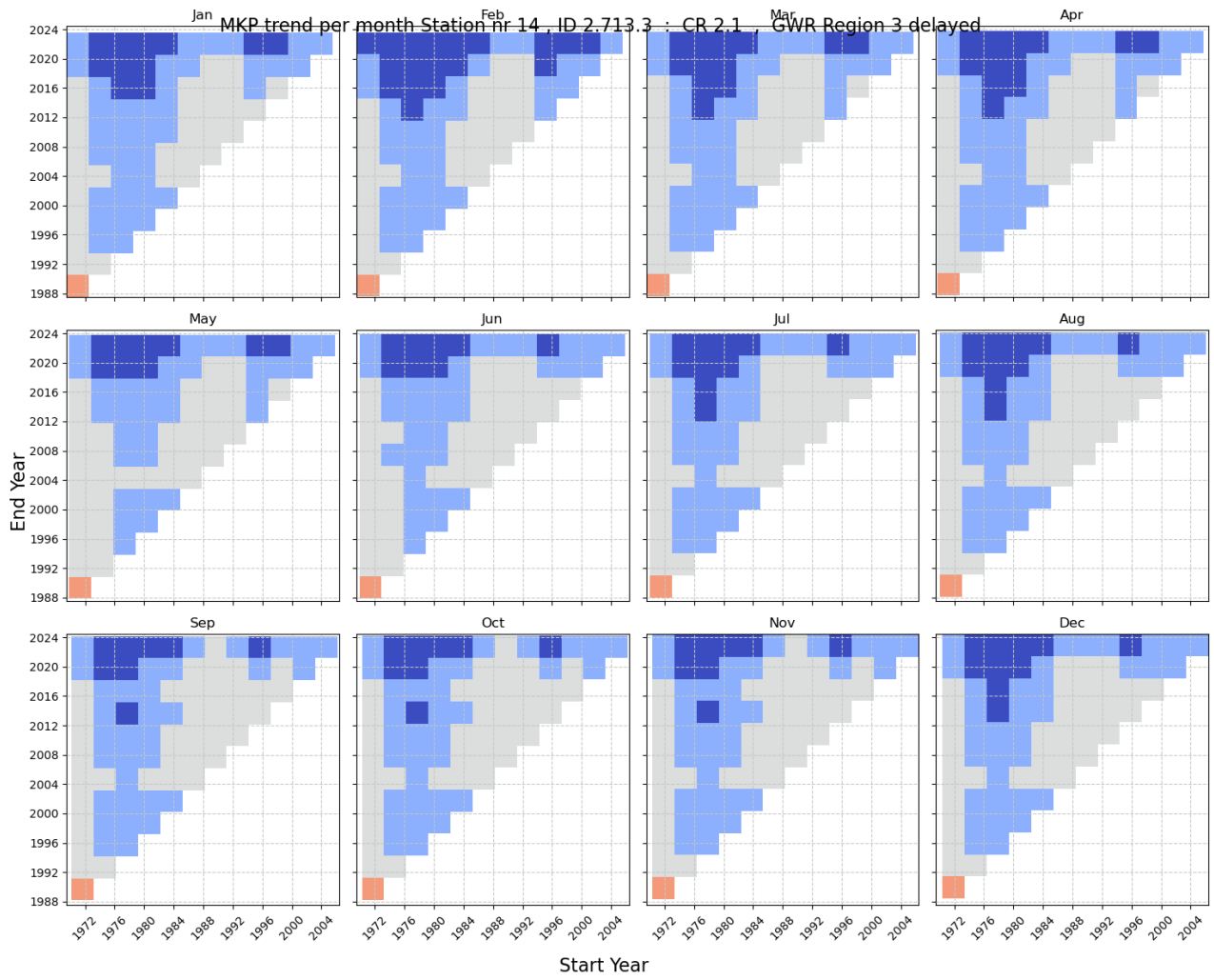

Same as in figure 4.11, but for Hauerseter station (14).

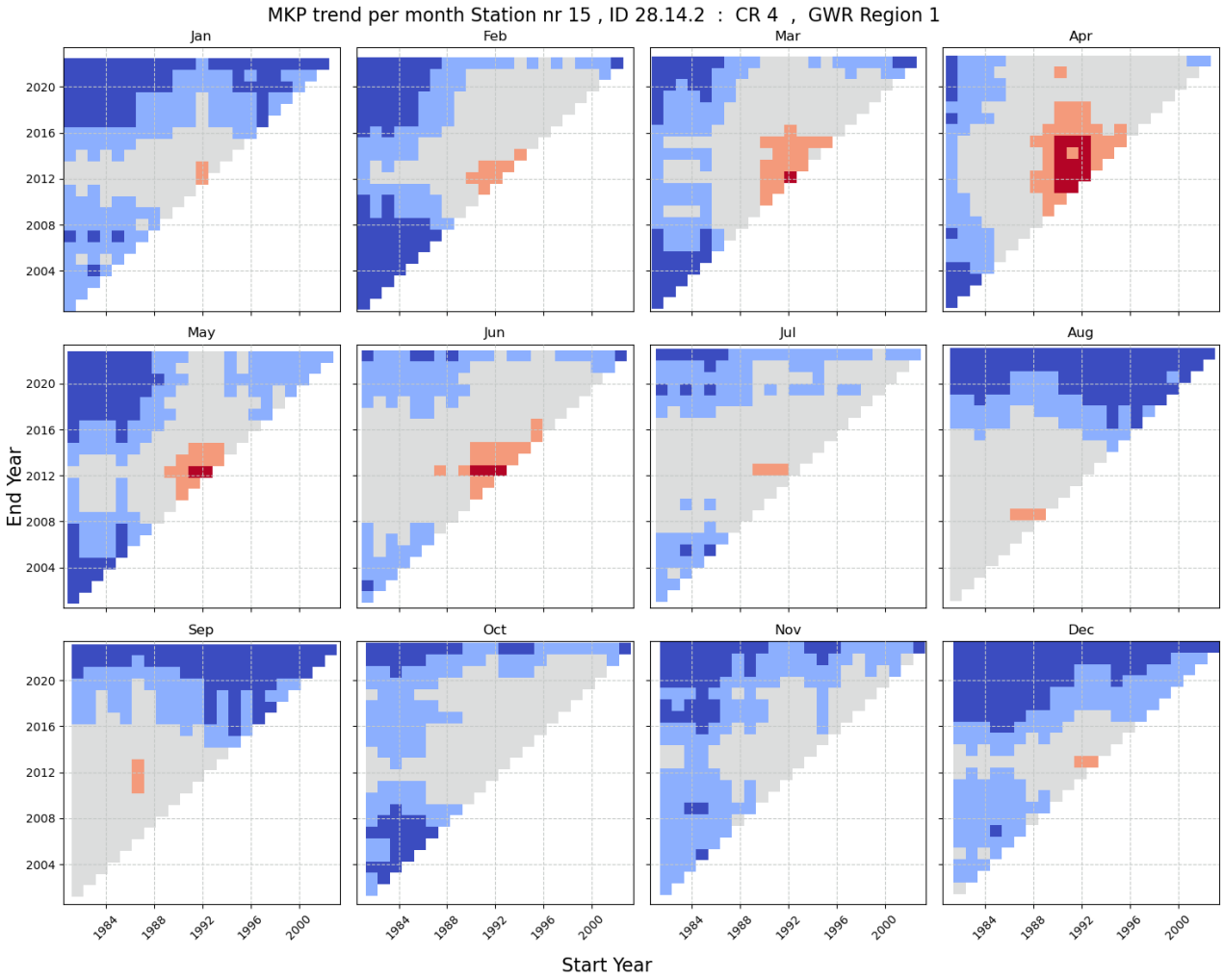

Same as in figure 4.11, but for Jæren station (15).

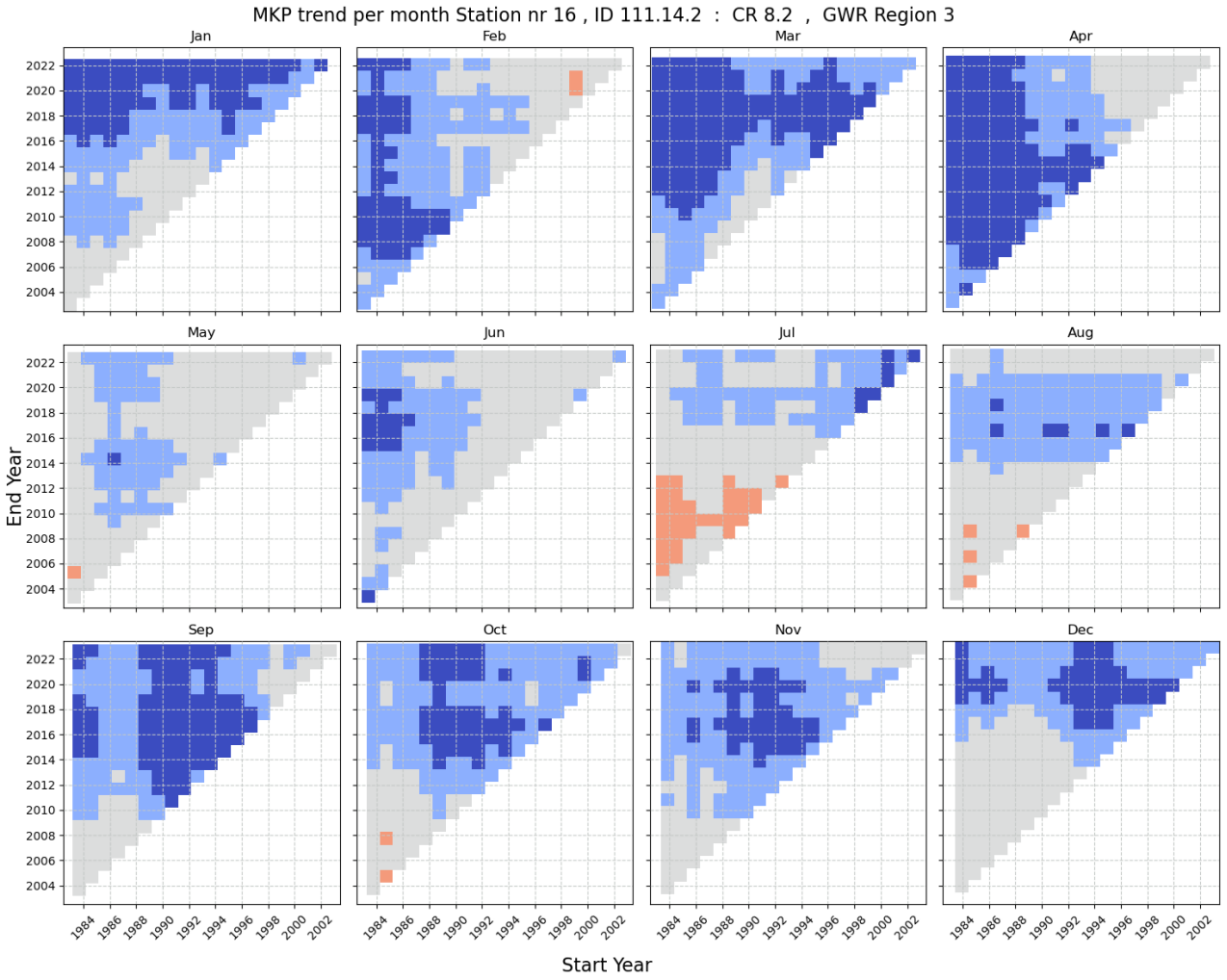

Same as in figure 4.11, but for Kårvatn station (16).

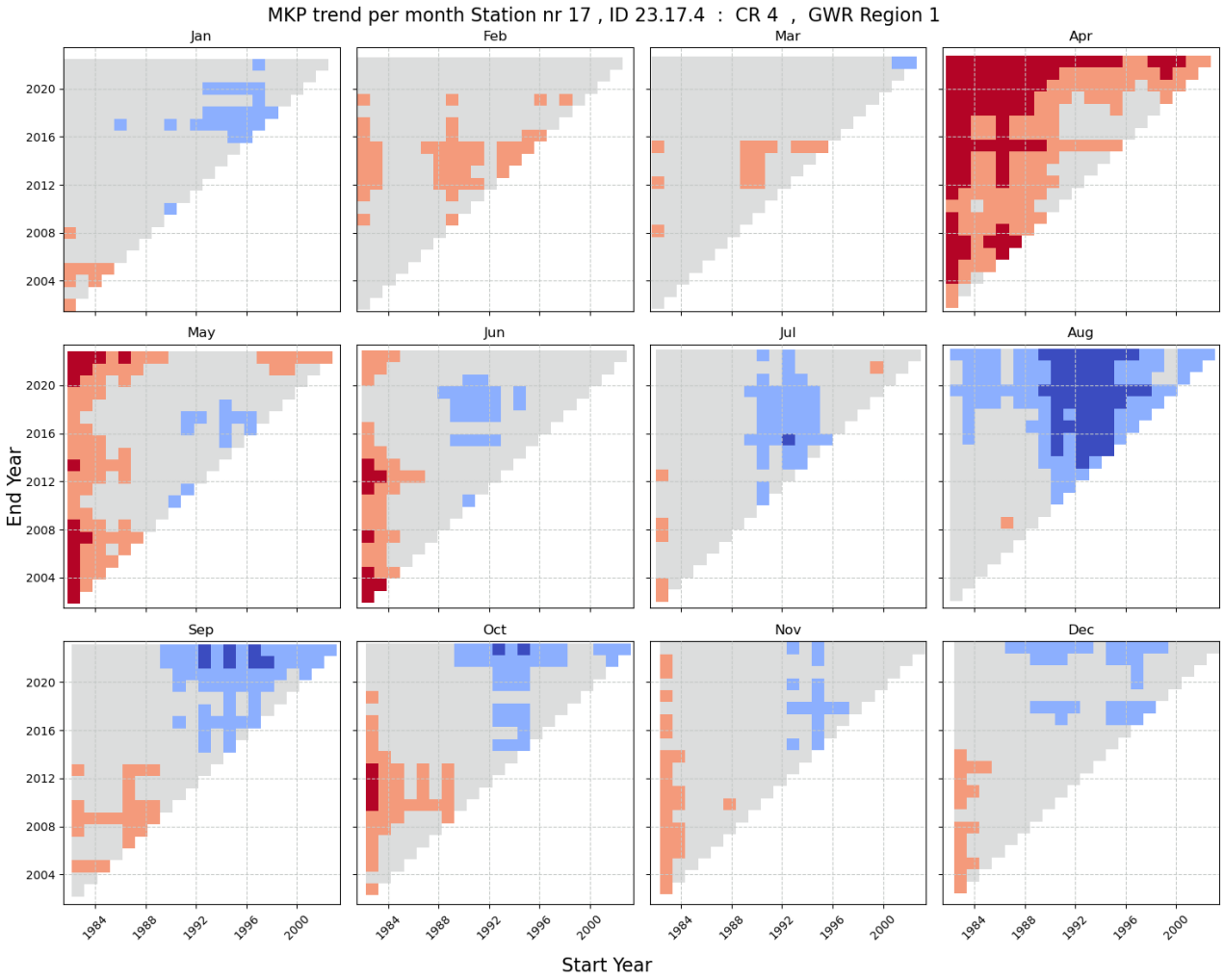

Same as in figure 4.11, but for Lindesnes station (17).

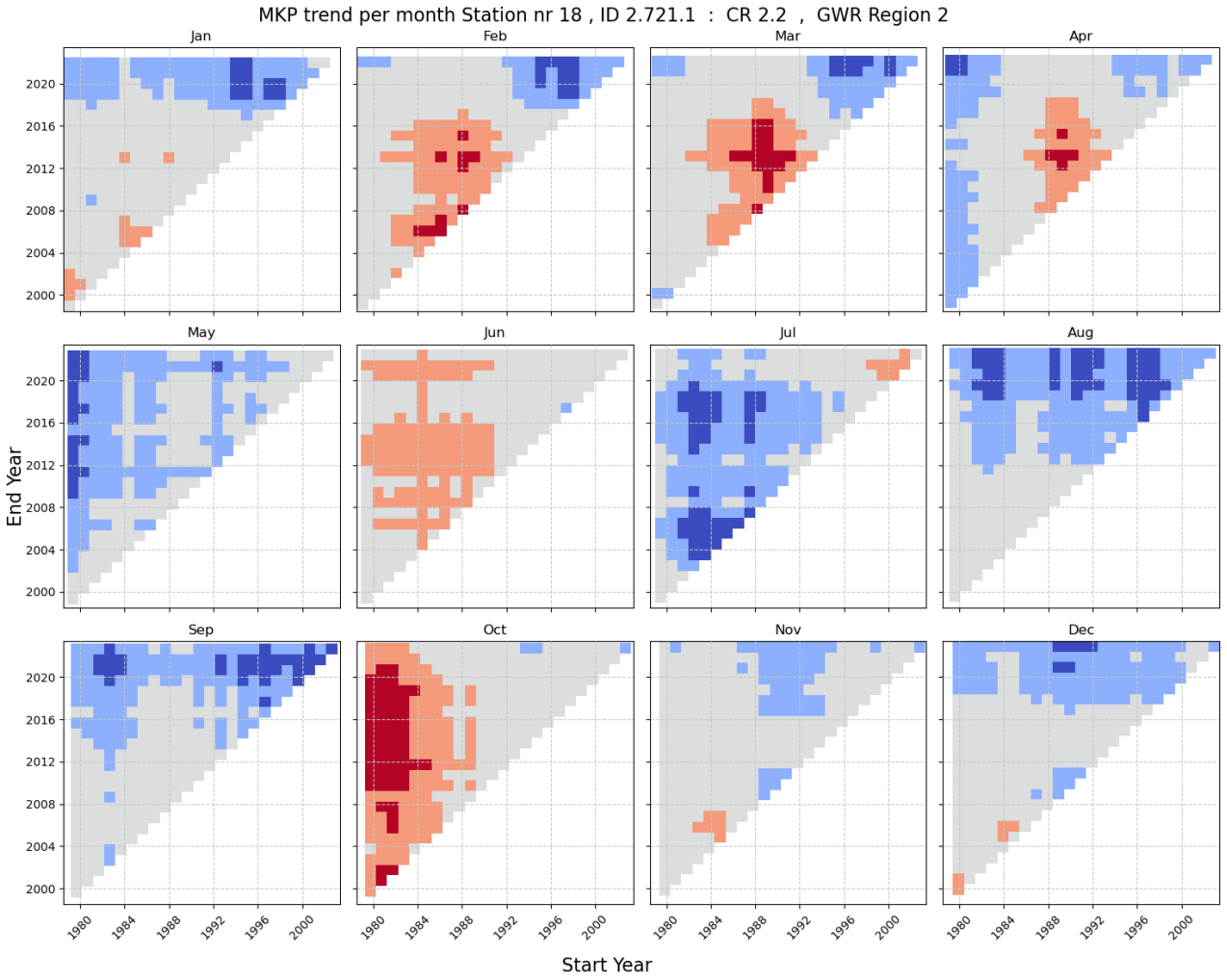

Same as in figure 4.11, but for Lykjestøylane station (18).

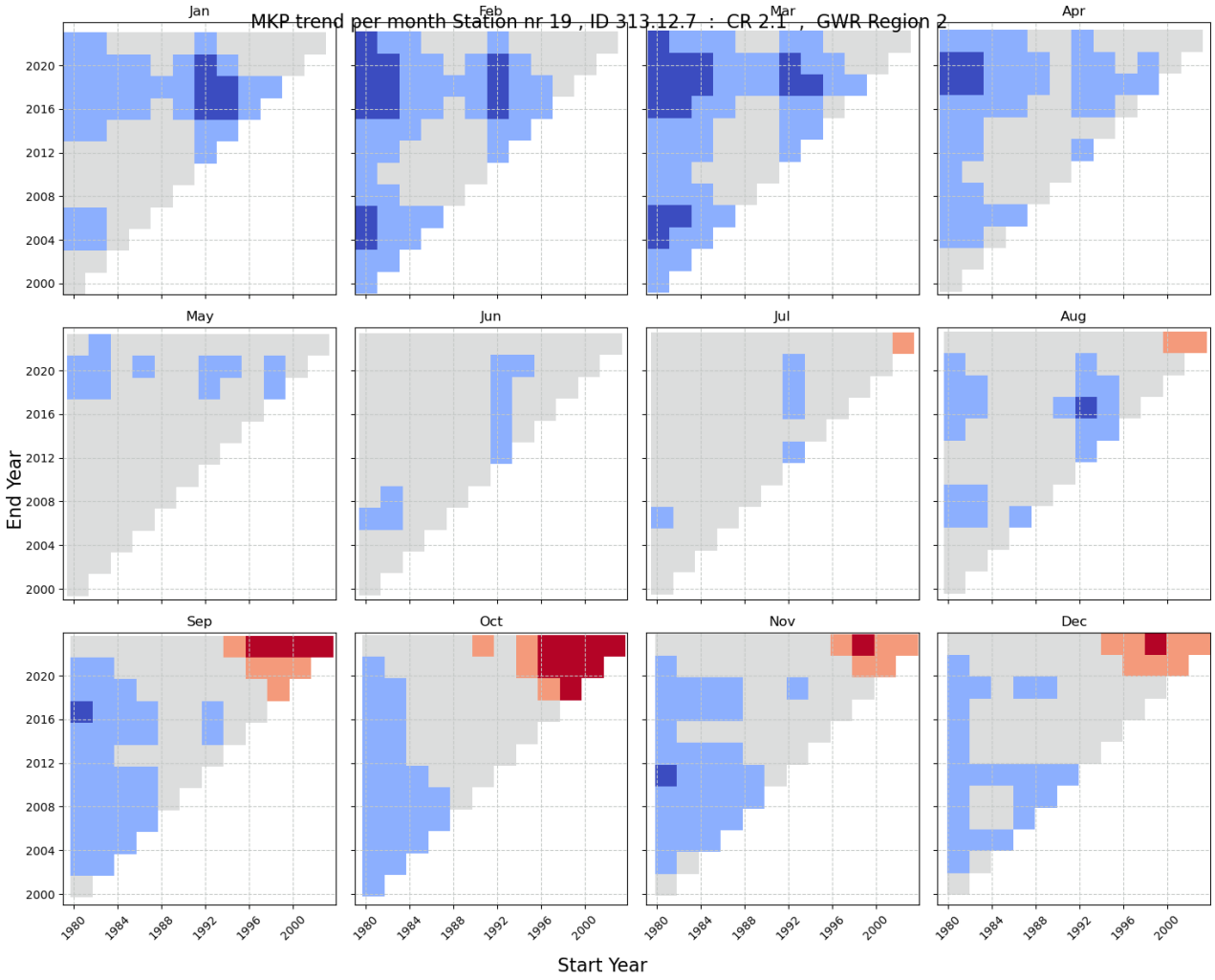

Same as in figure 4.11, but for Magnor station (19).

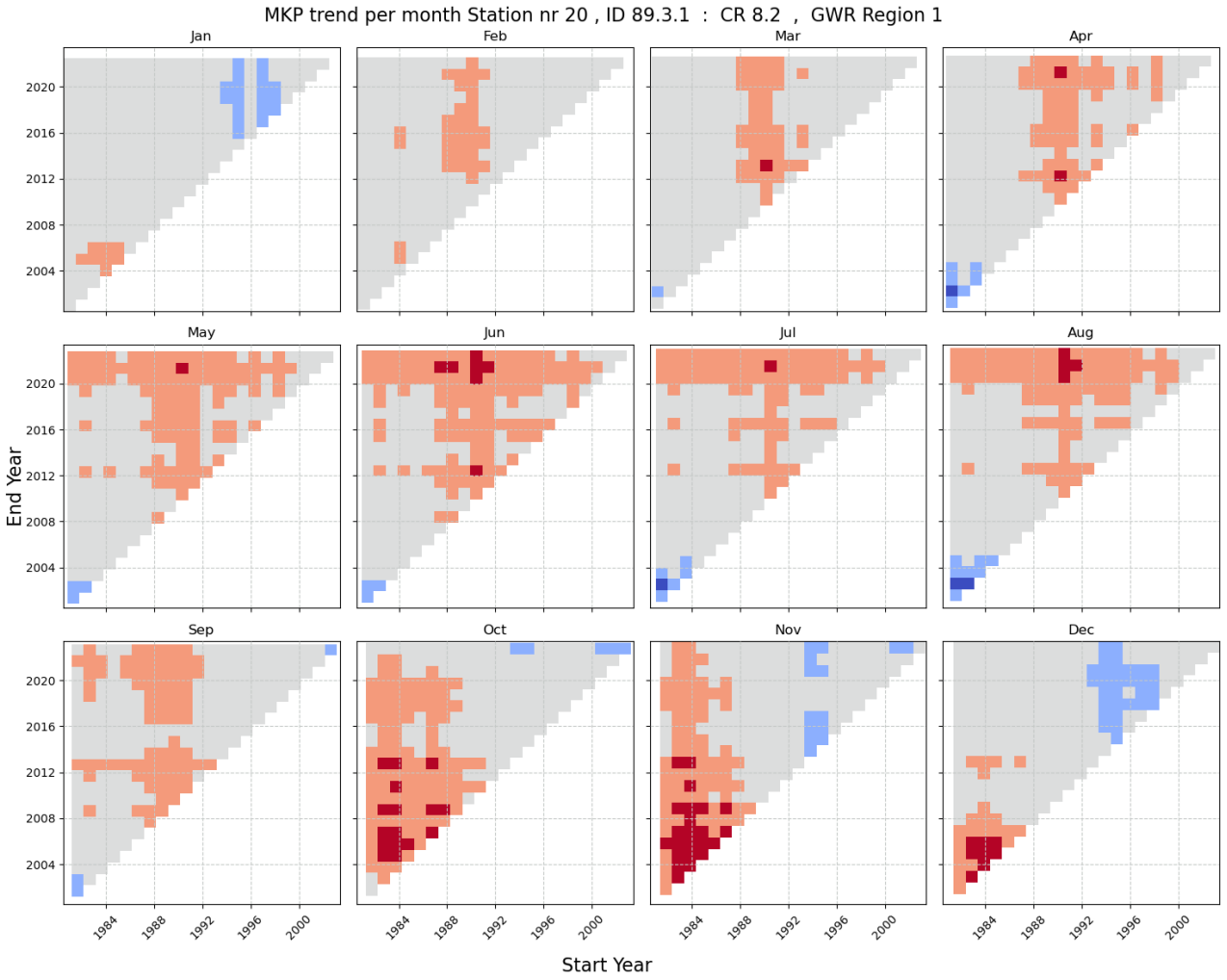

Same as in figure 4.11, but for Nordfjordeid station (20).

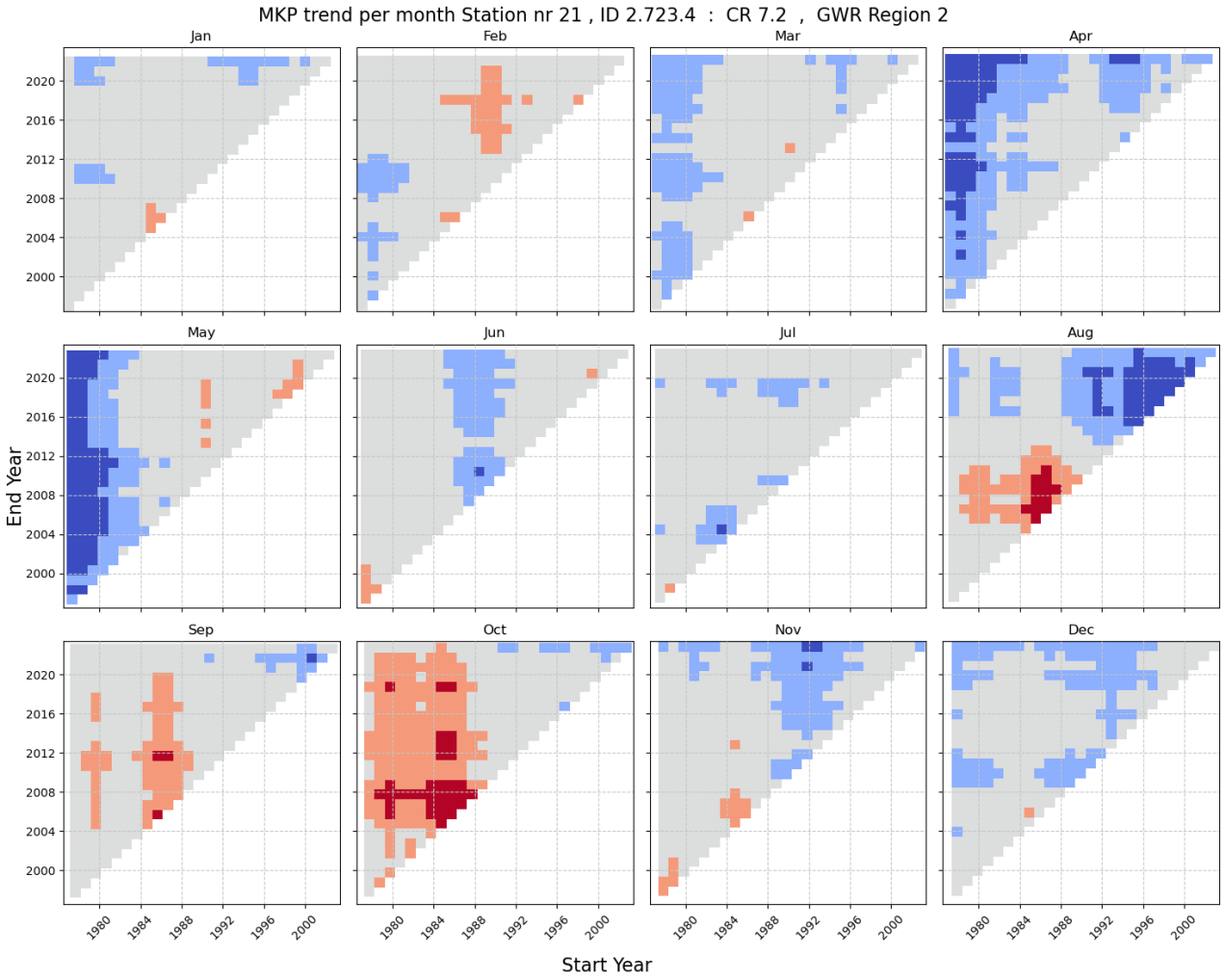

Same as in figure 4.11, but for Settalbekken station (21).

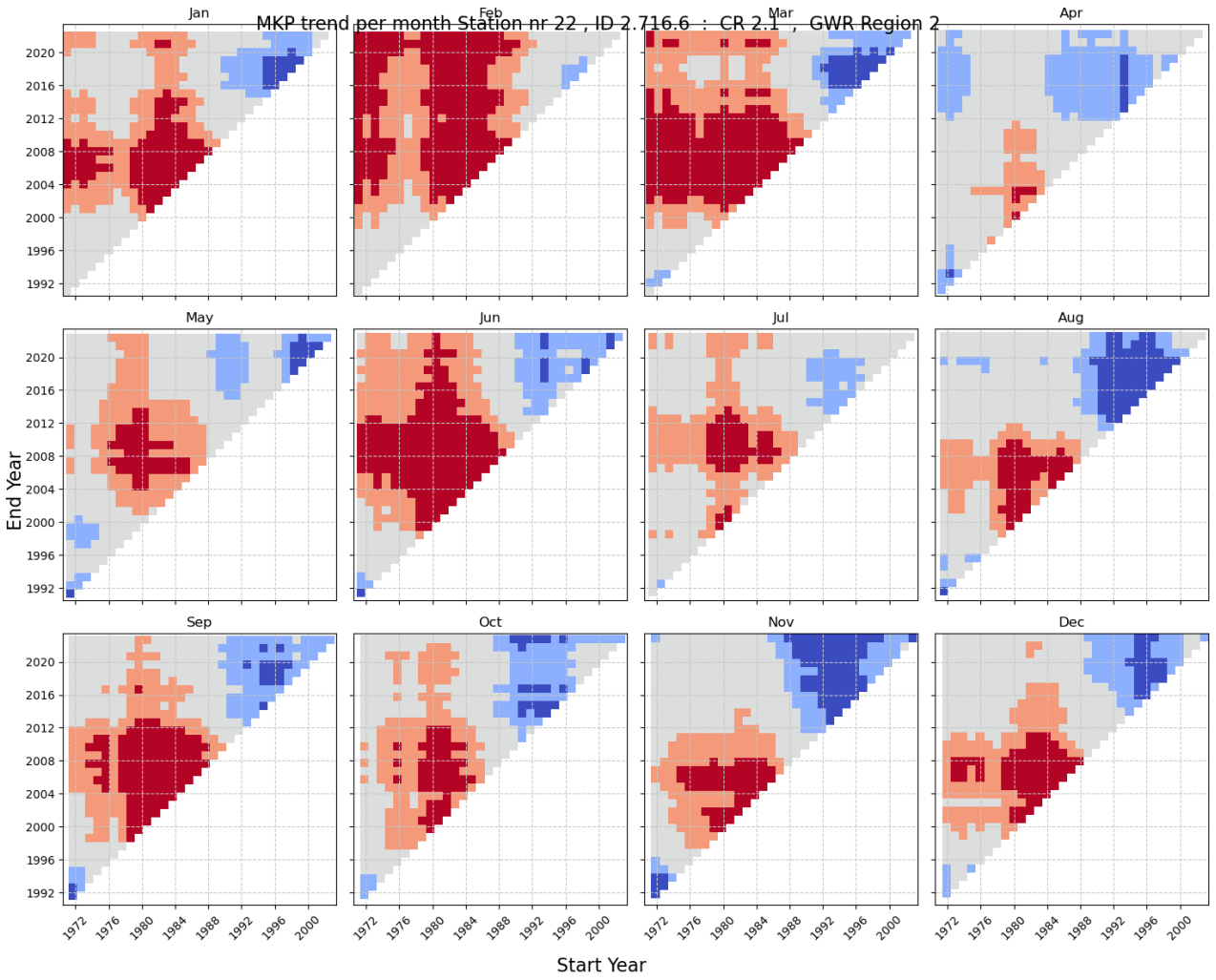

Same as in figure 4.11, but for Stenerseter station (22).

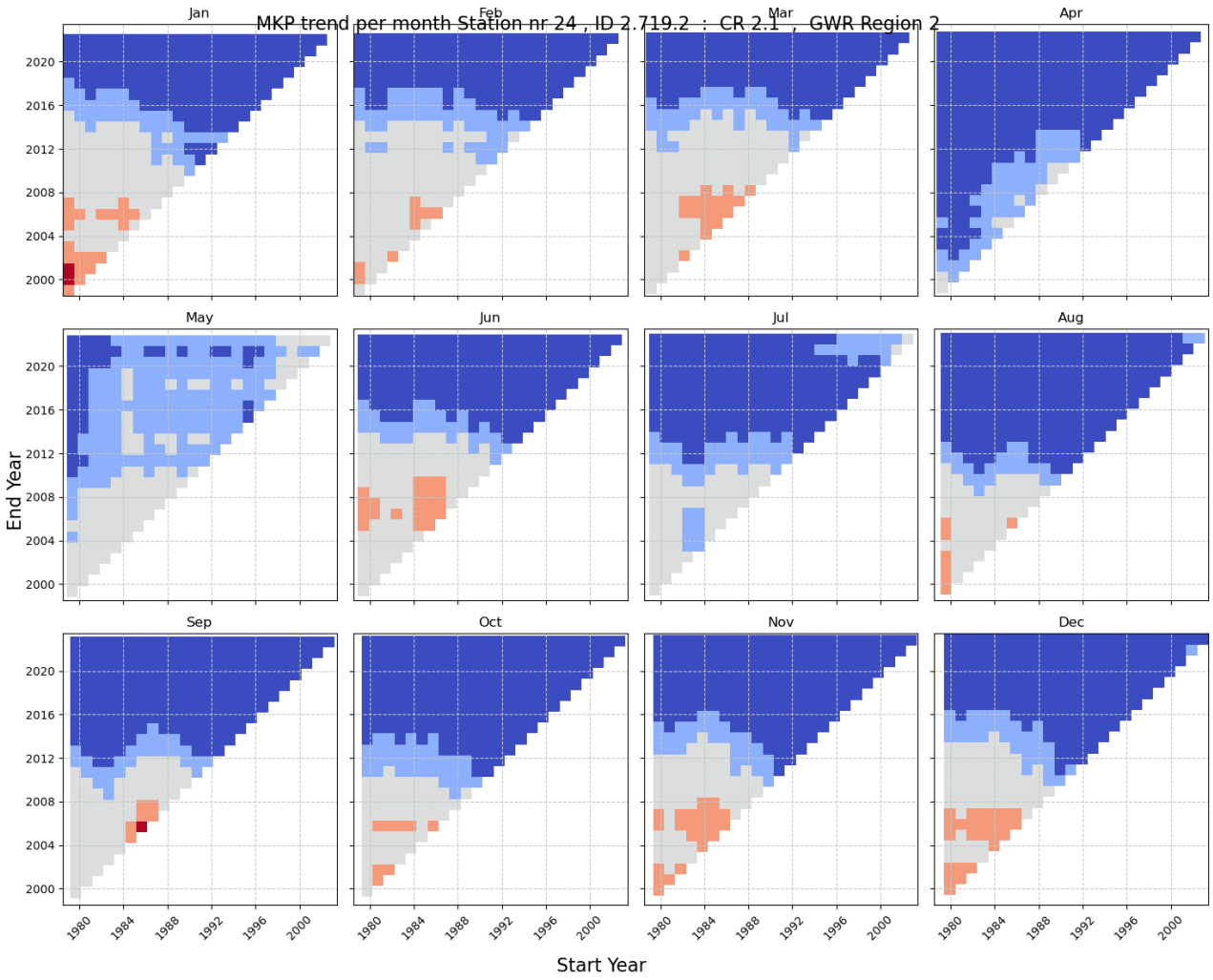

Same as in figure 4.11, but for Øyangen station (24).

Appendix D

Yearly multi temporal trend plot

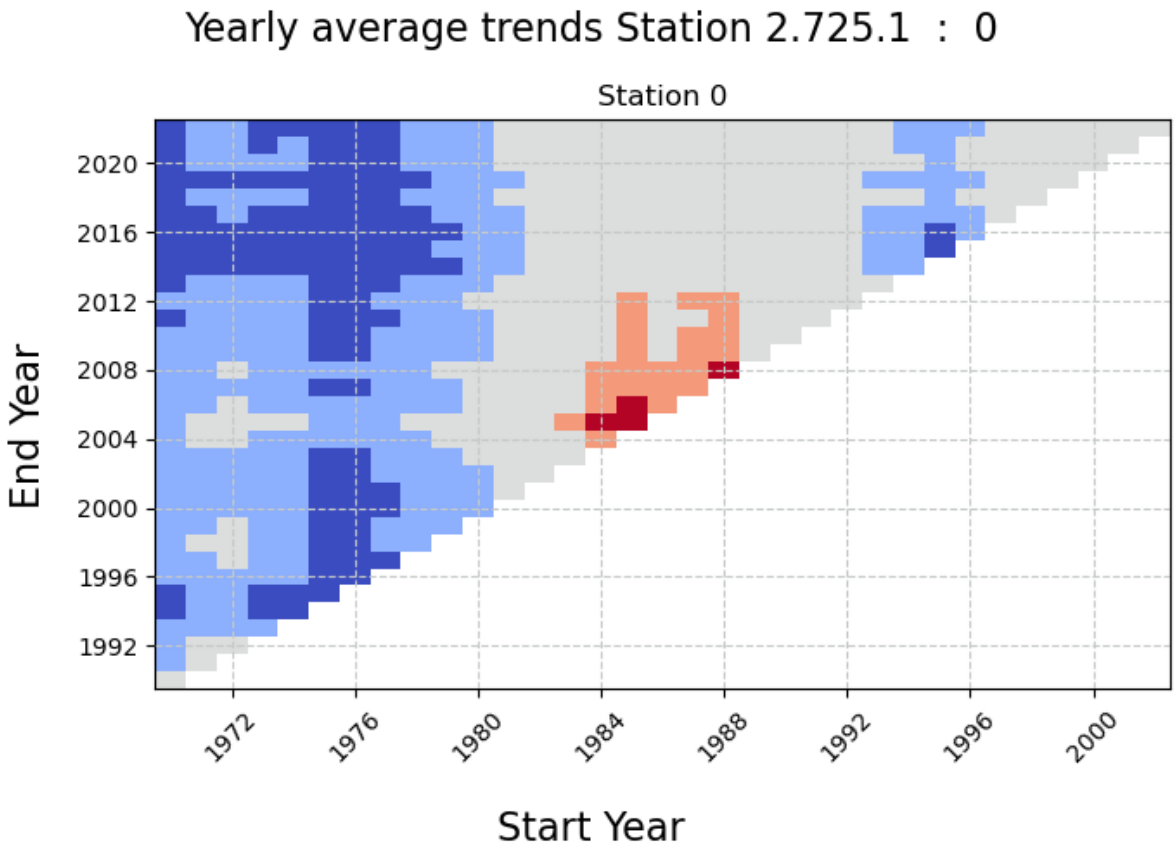

Multi temporal trends for annual GWL at Abrahamsvoll station (0).

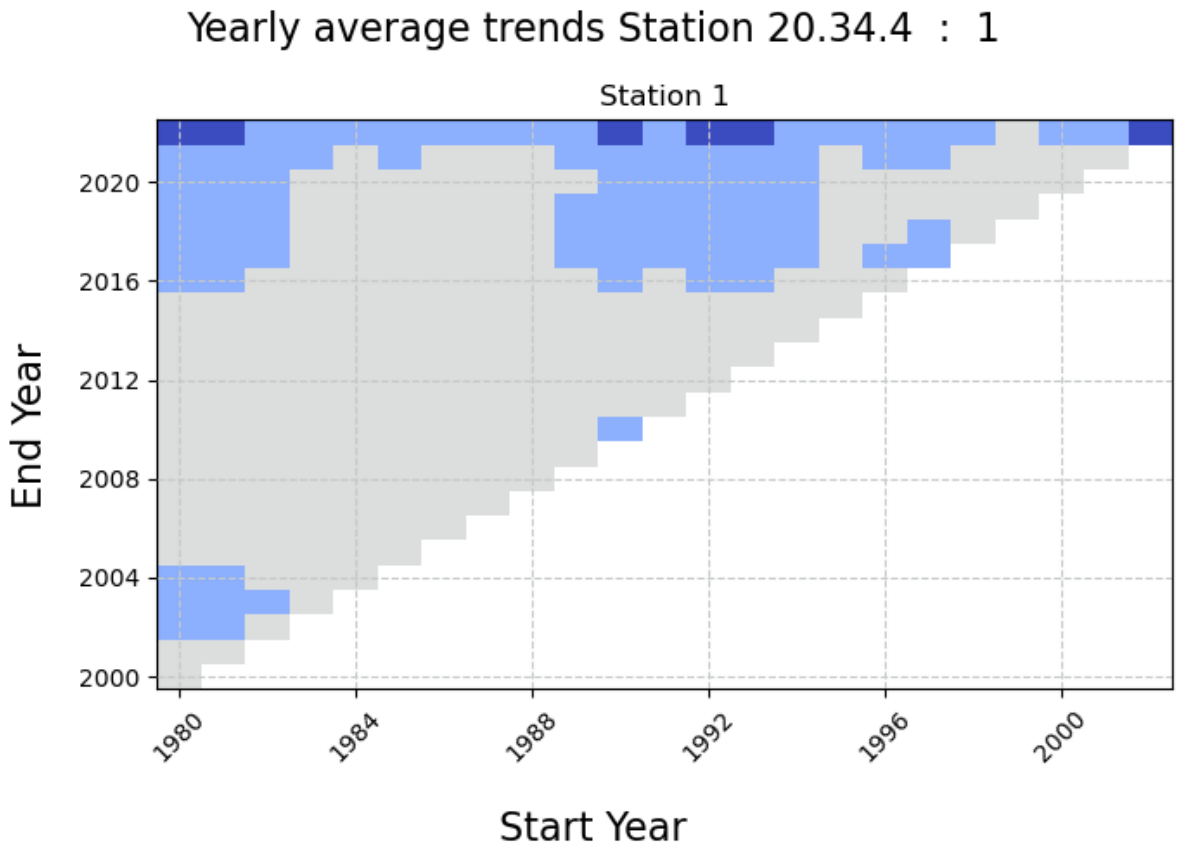

Multi temporal trends for annual GWL at Birkenes station (1).

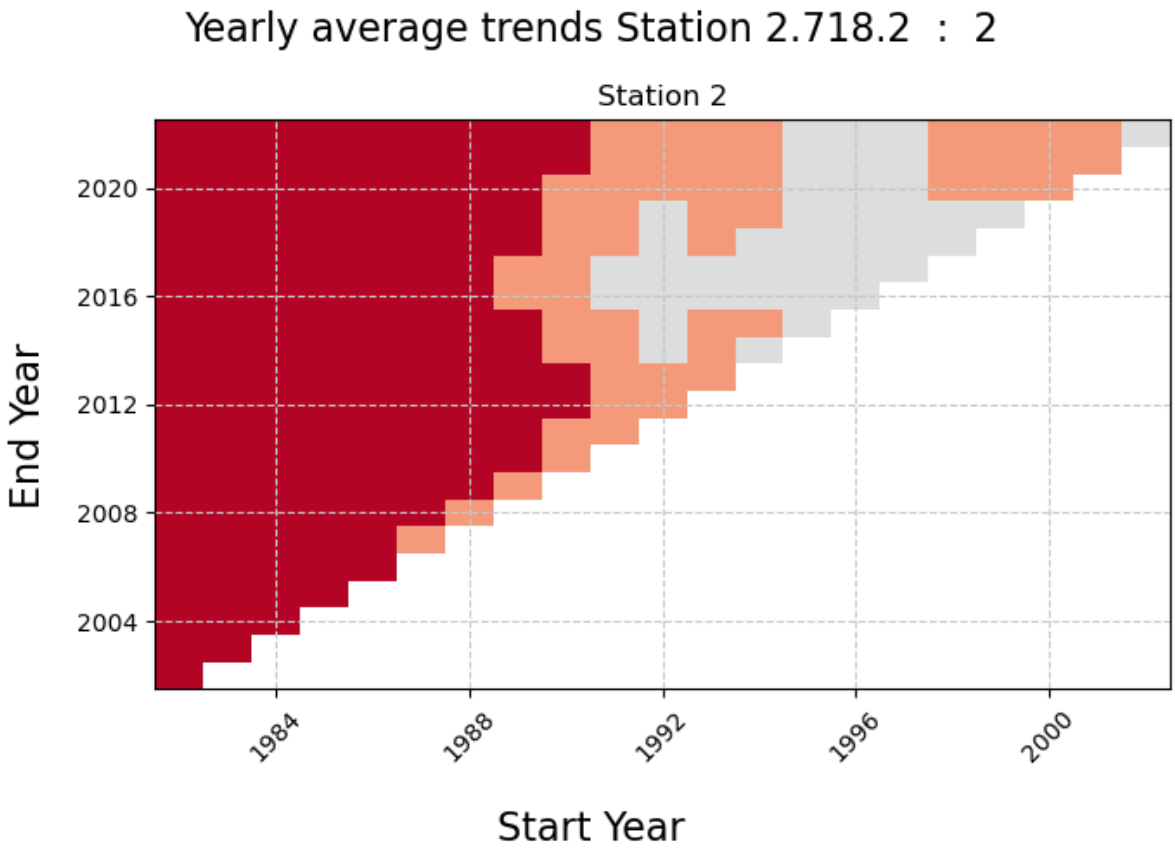

Multi temporal trends for annual GWL at Dombås station (2).

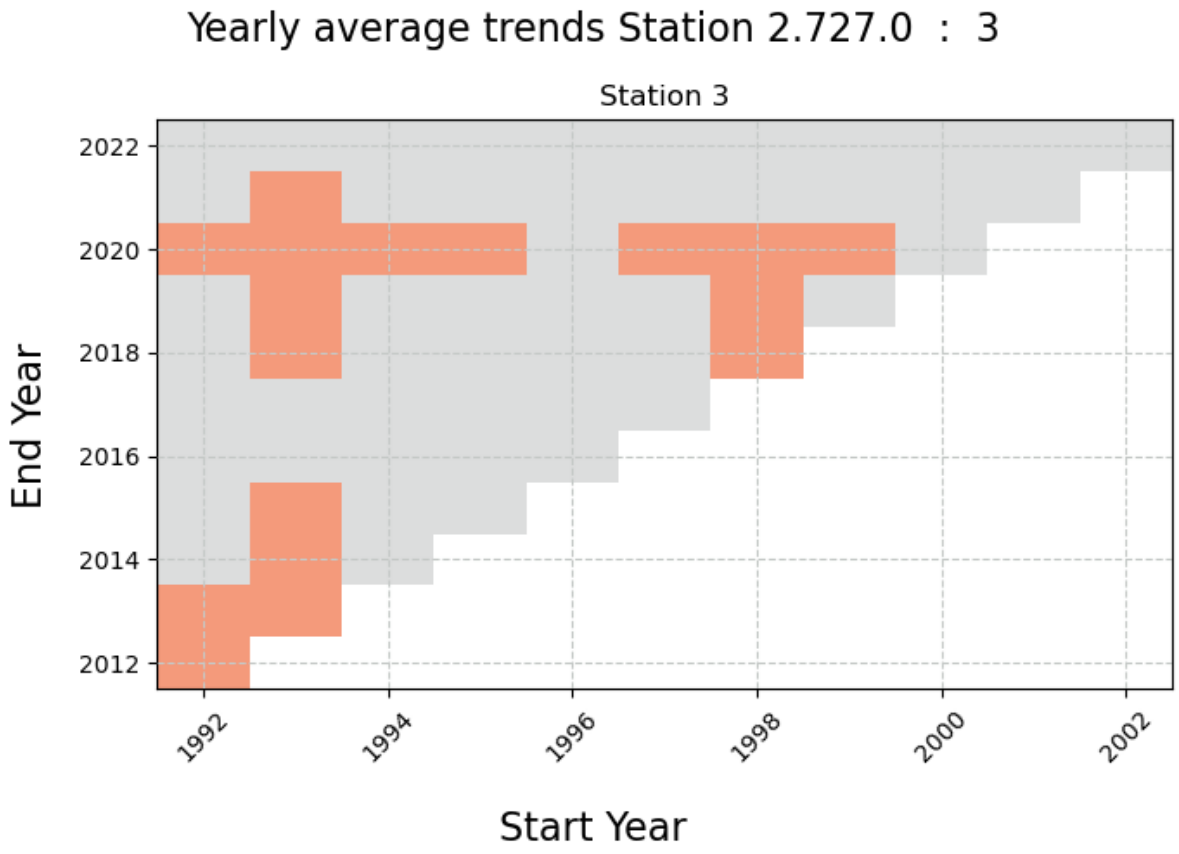

Multi temporal trends for annual GWL at Kise station (3).

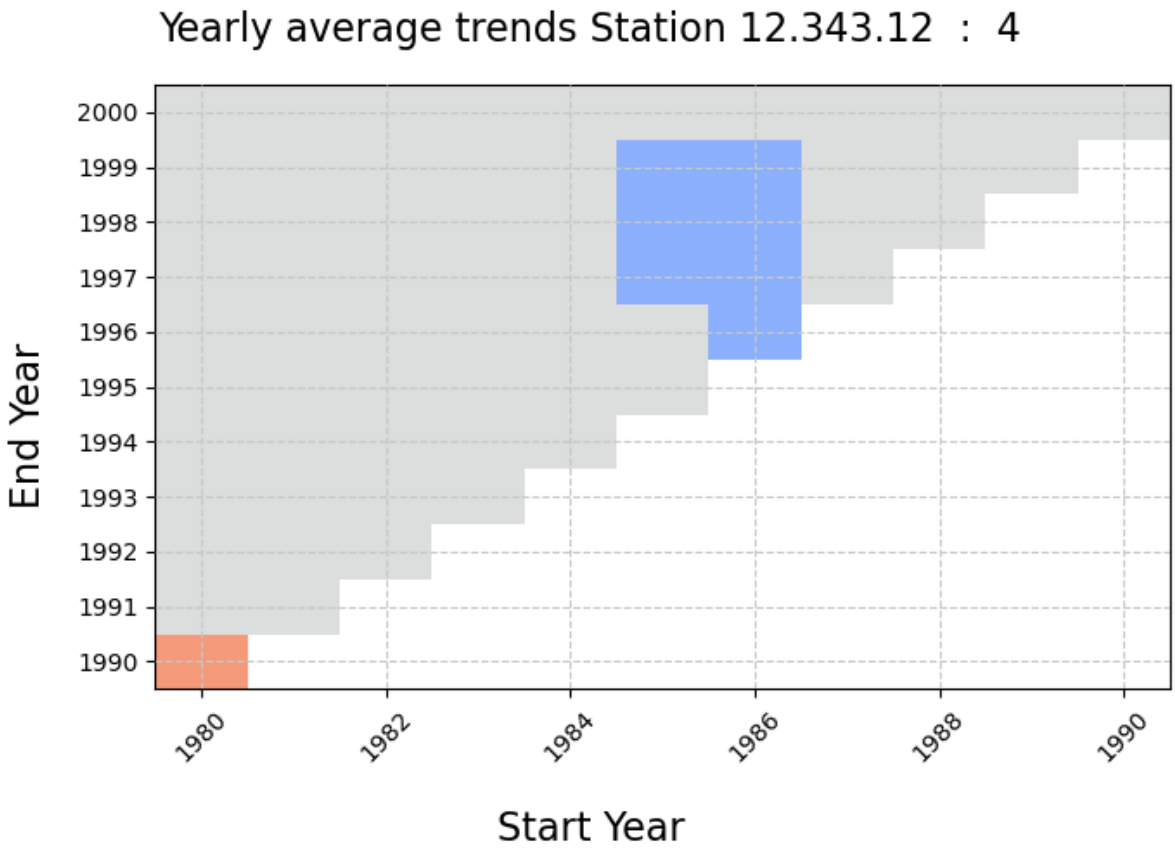

Multi temporal trends for annual GWL at Modum station (4).

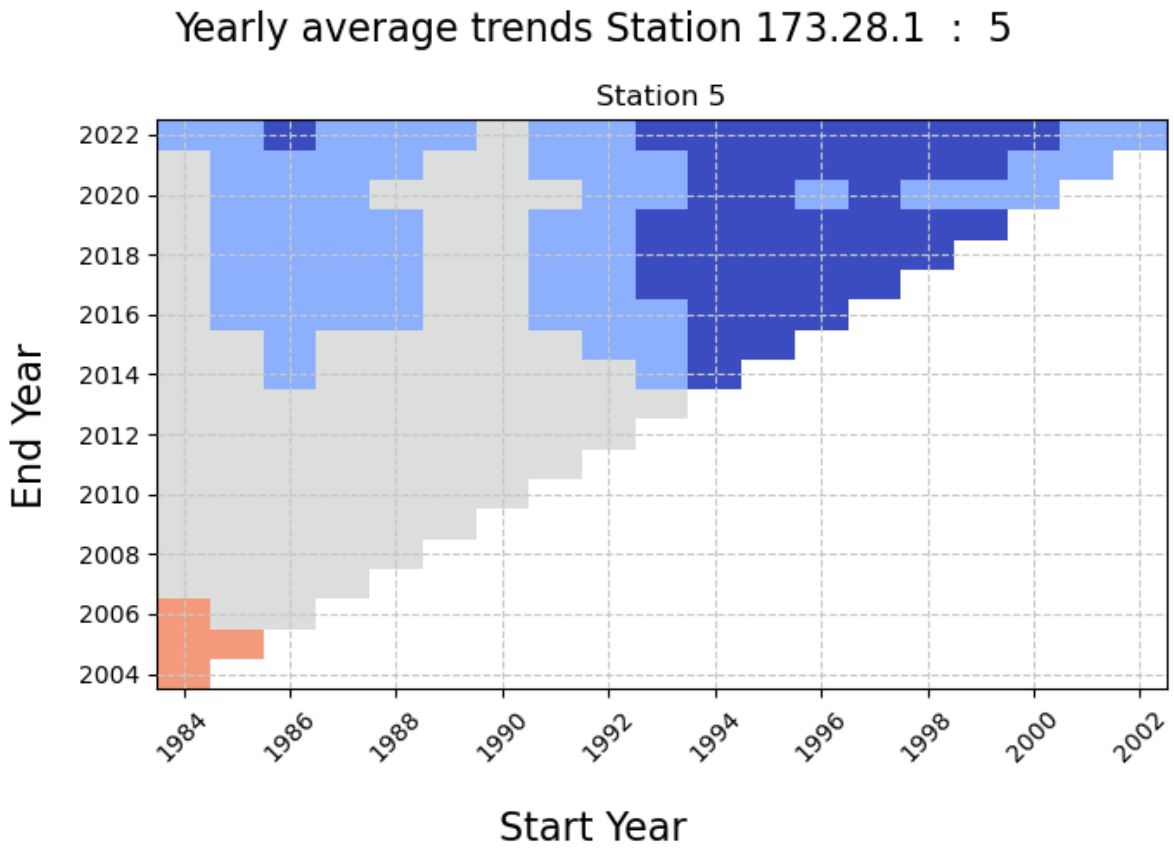

Multi temporal trends for annual GWL at Skjomen station (5).

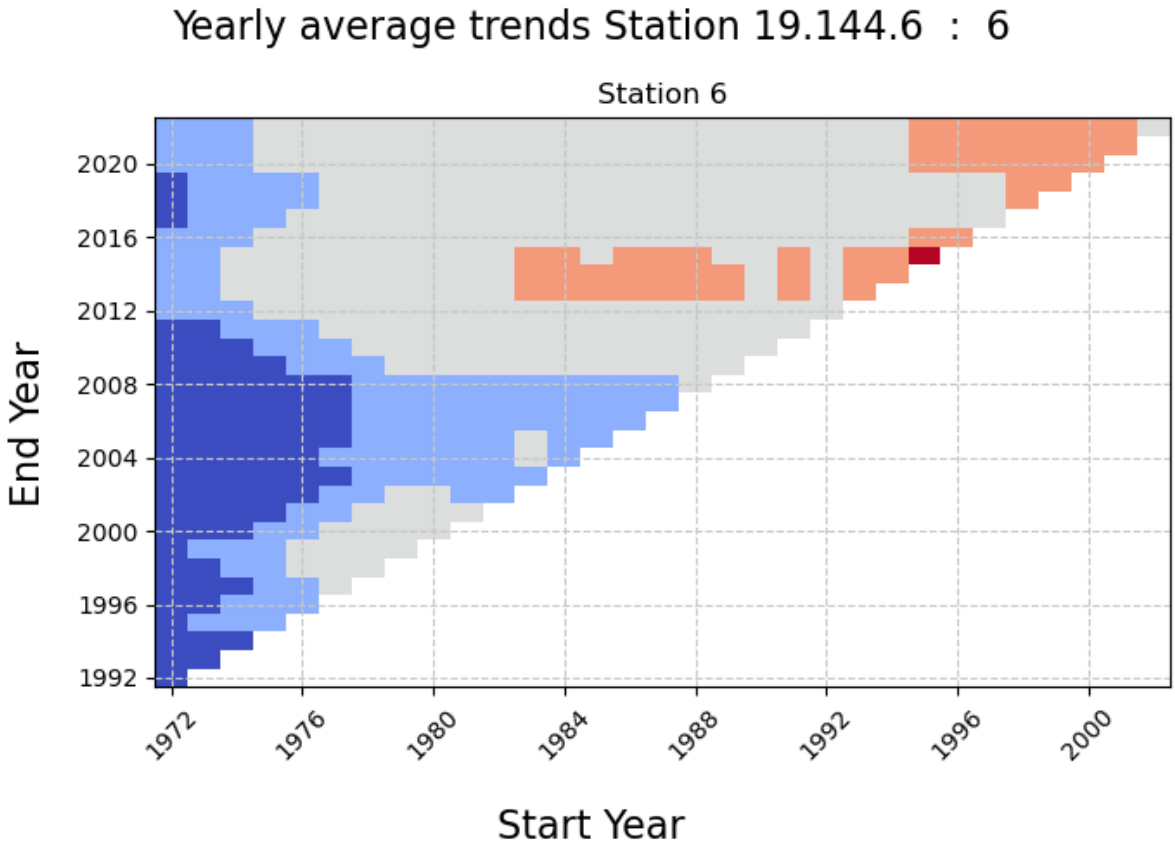

Multi temporal trends for annual GWL at Stigvassåi station (6).

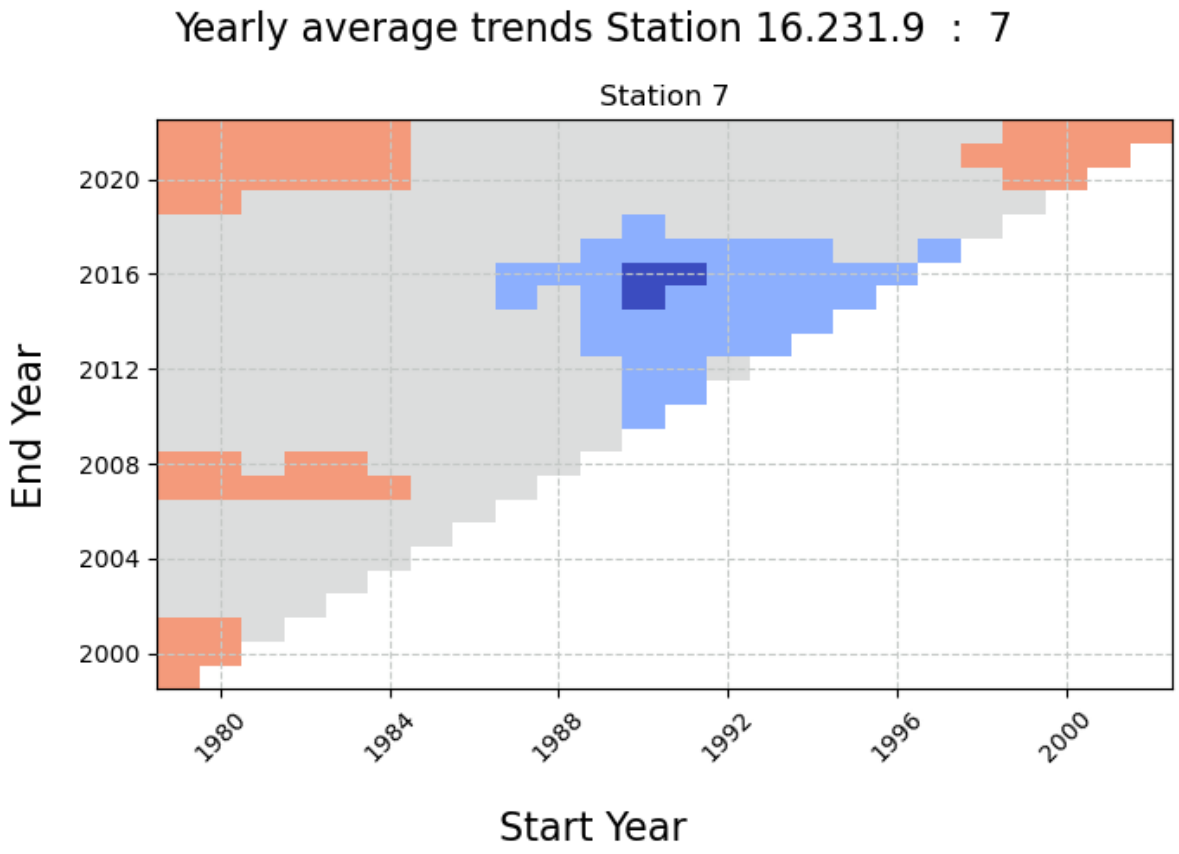

Multi temporal trends for annual GWL at Eikamoen station (7).

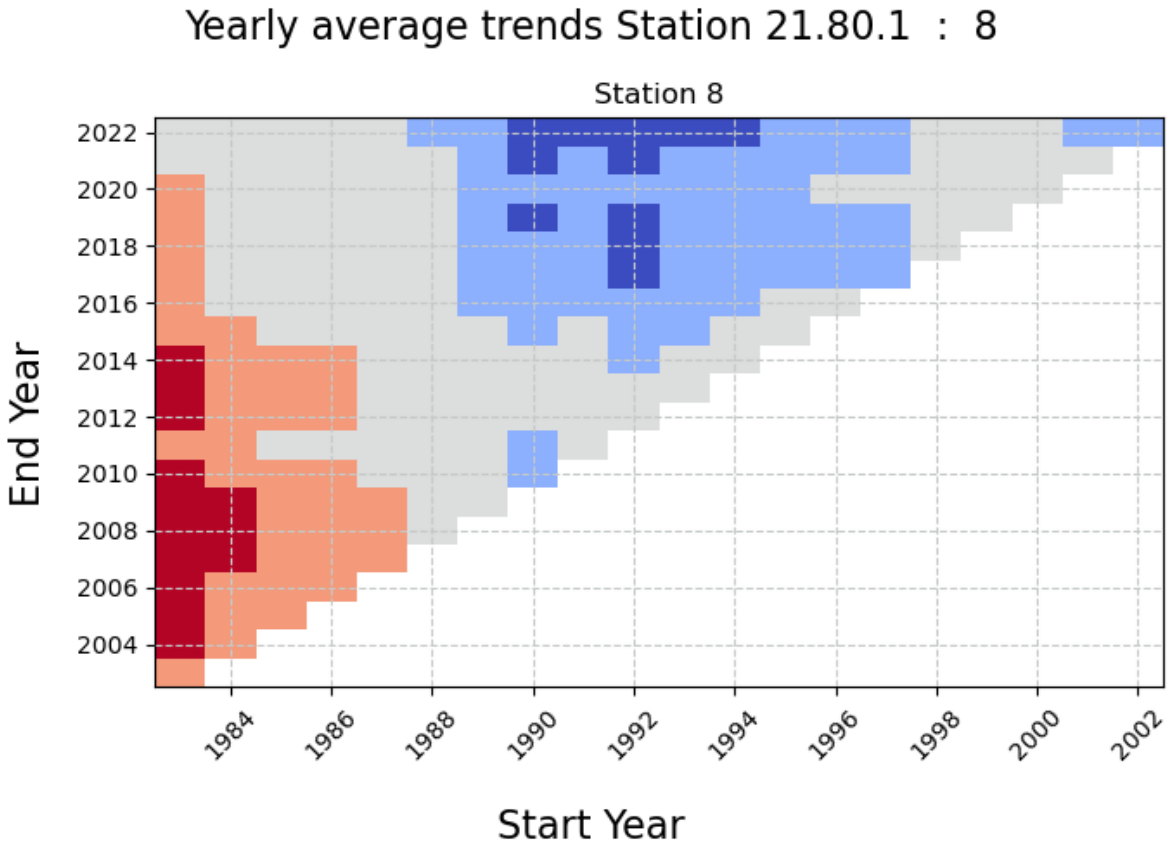

Multi temporal trends for annual GWL at Evje station (8).

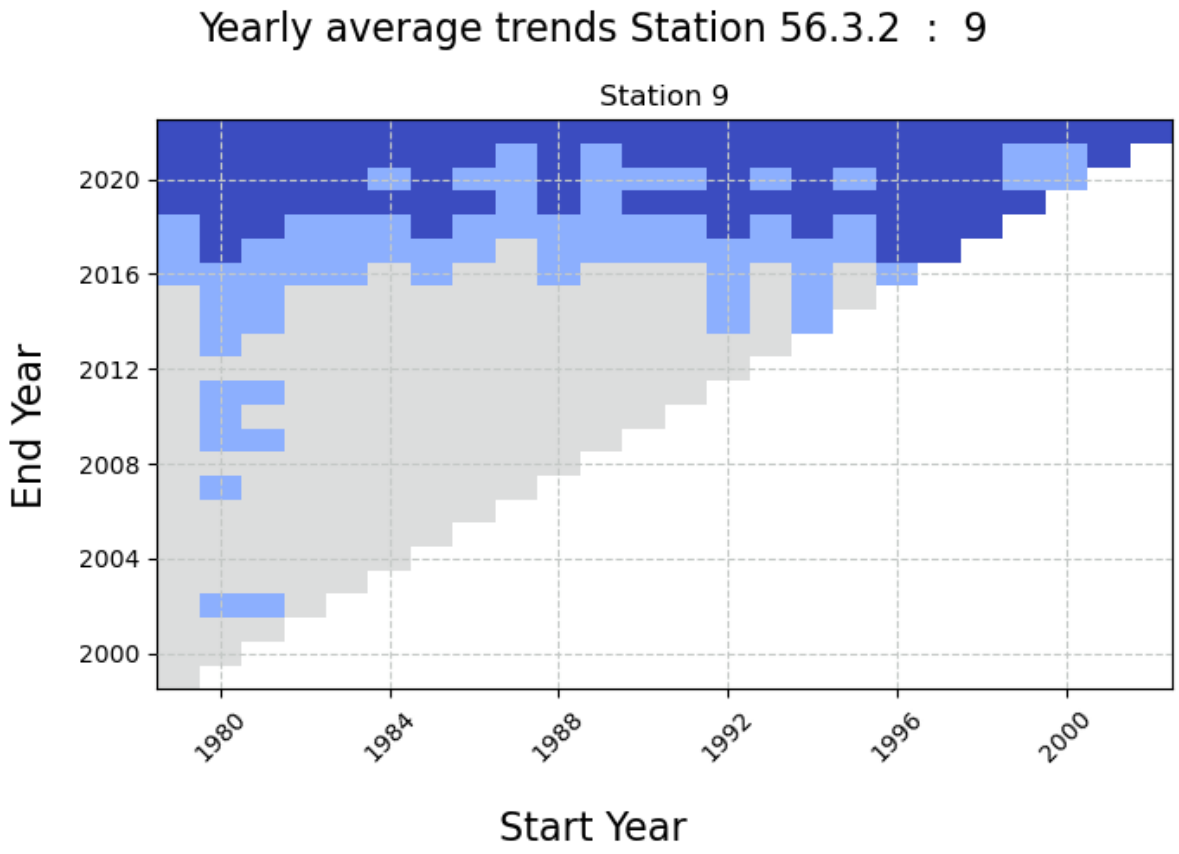

Multi temporal trends for annual GWL at Fana station (9).

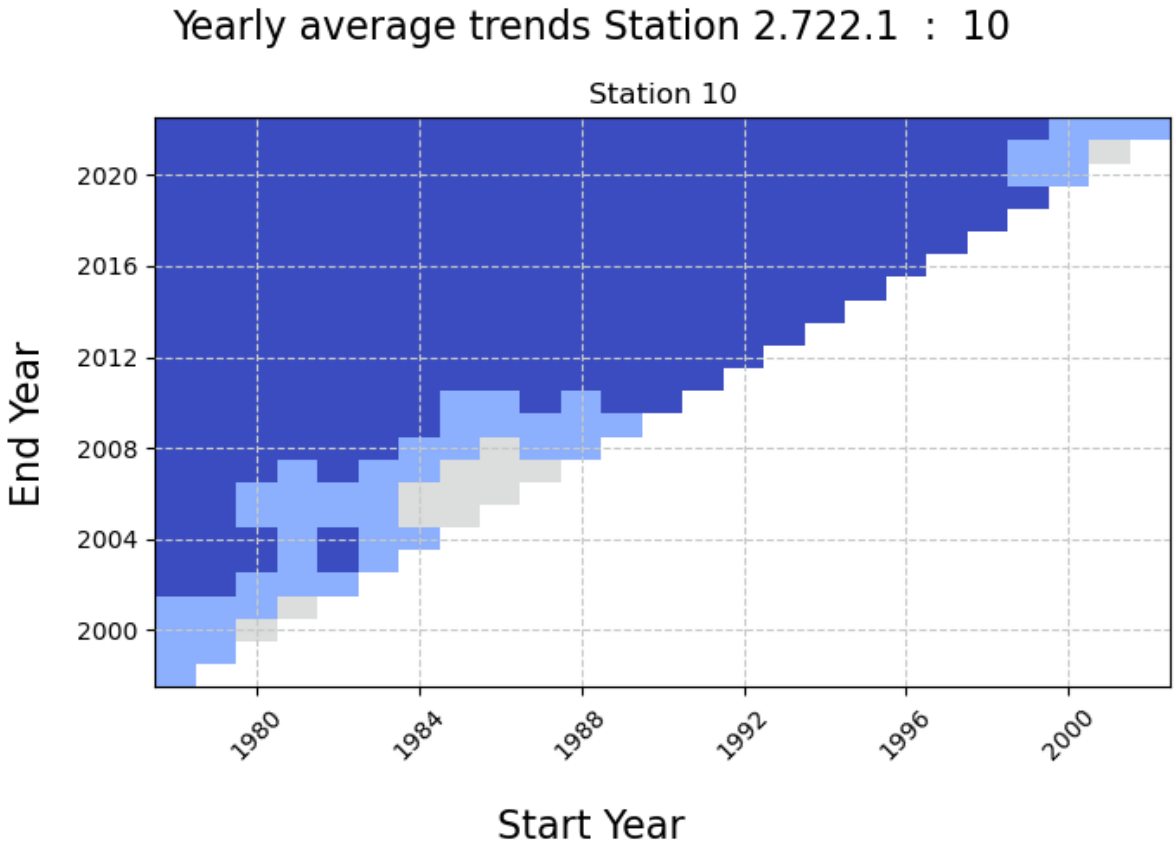

Multi temporal trends for annual GWL at Finnbølseter station (10).

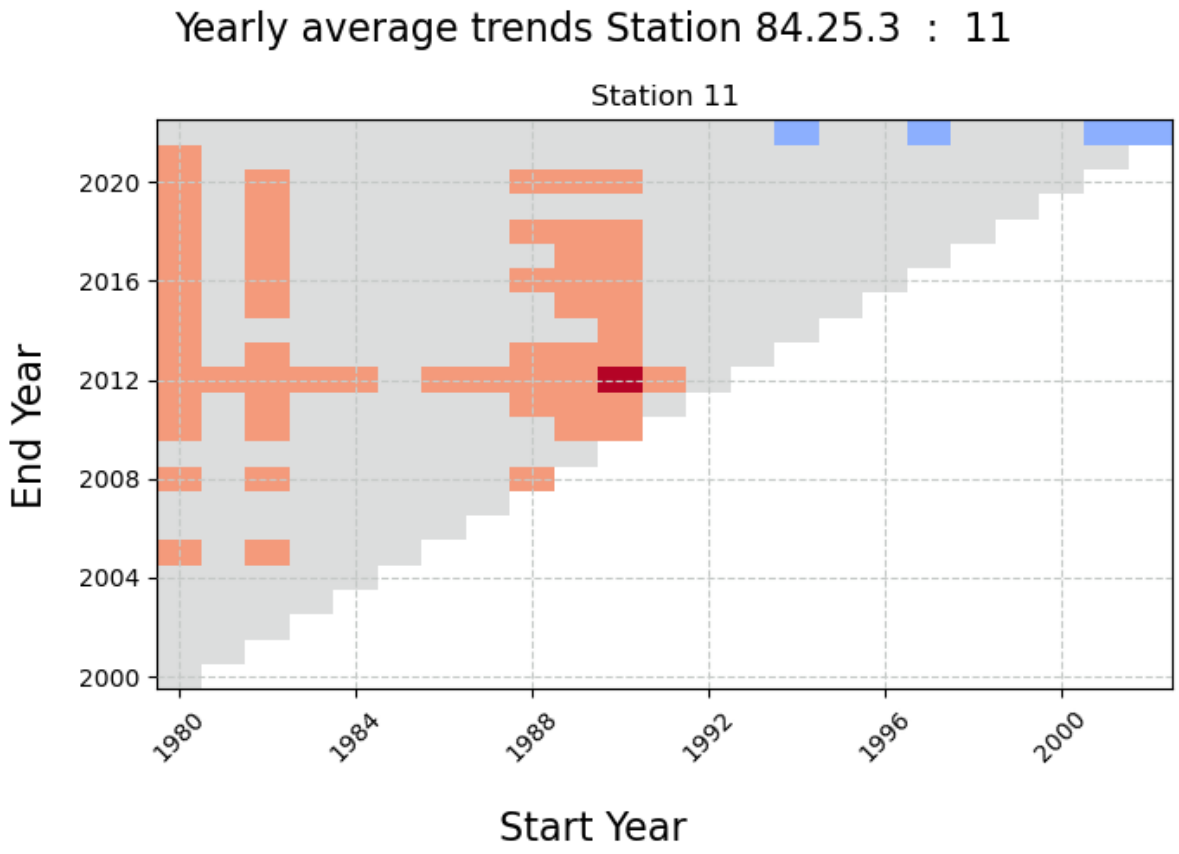

Multi temporal trends for annual GWL at Førde/Moskog station (11).

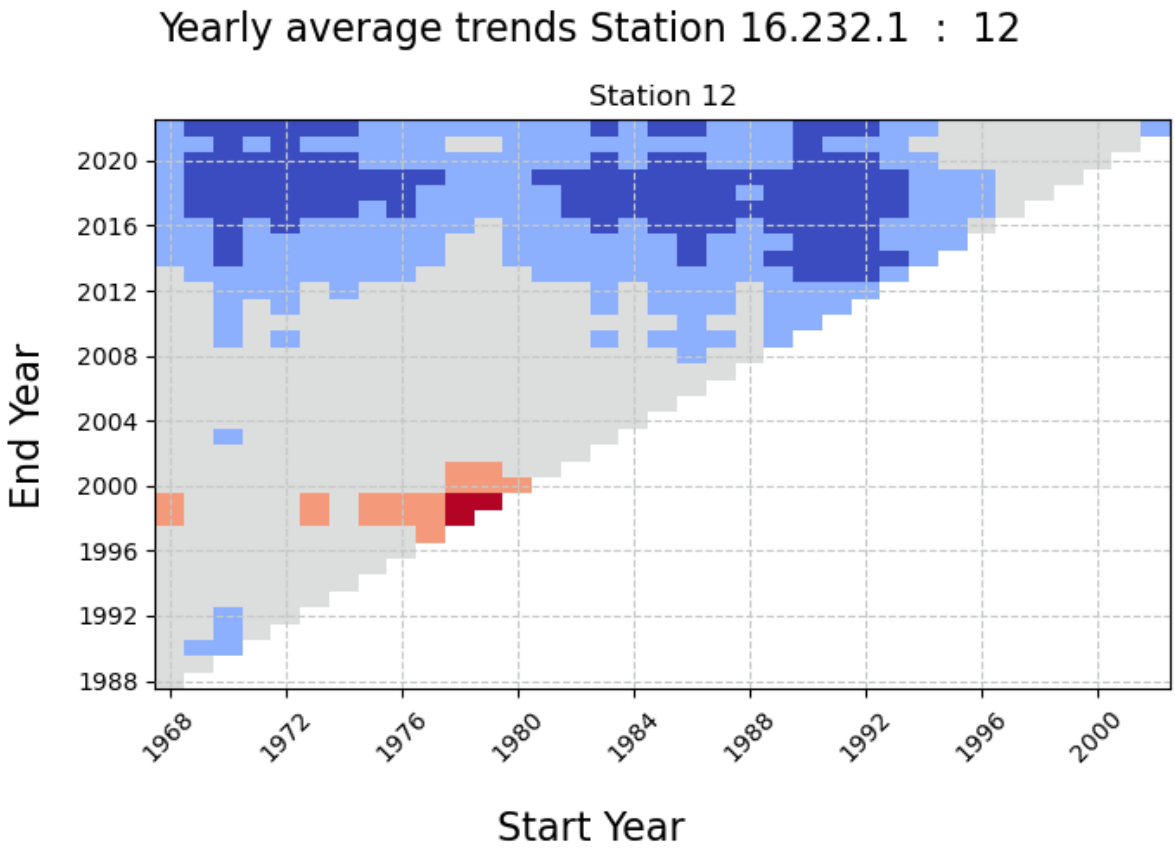

Multi temporal trends for annual GWL at Groset station (12).

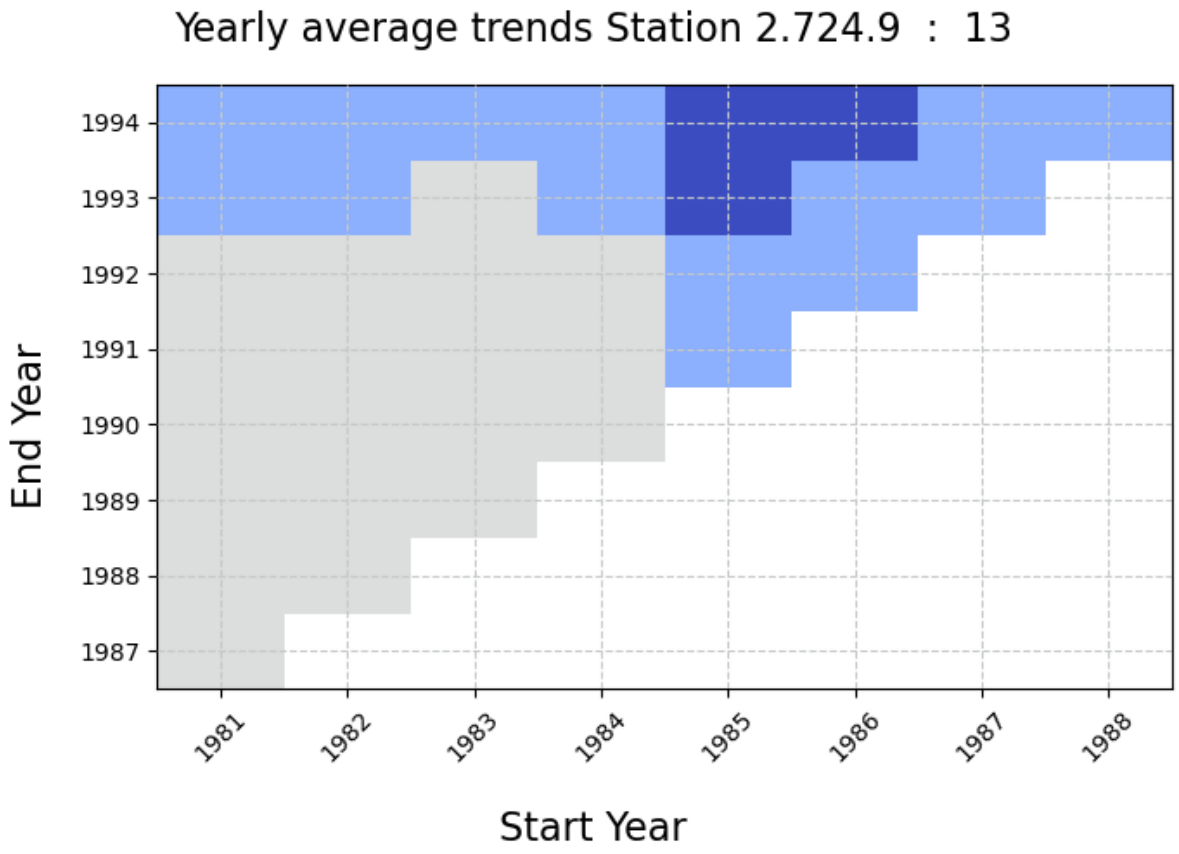

Multi temporal trends for annual GWL at Haslemoen station (13).

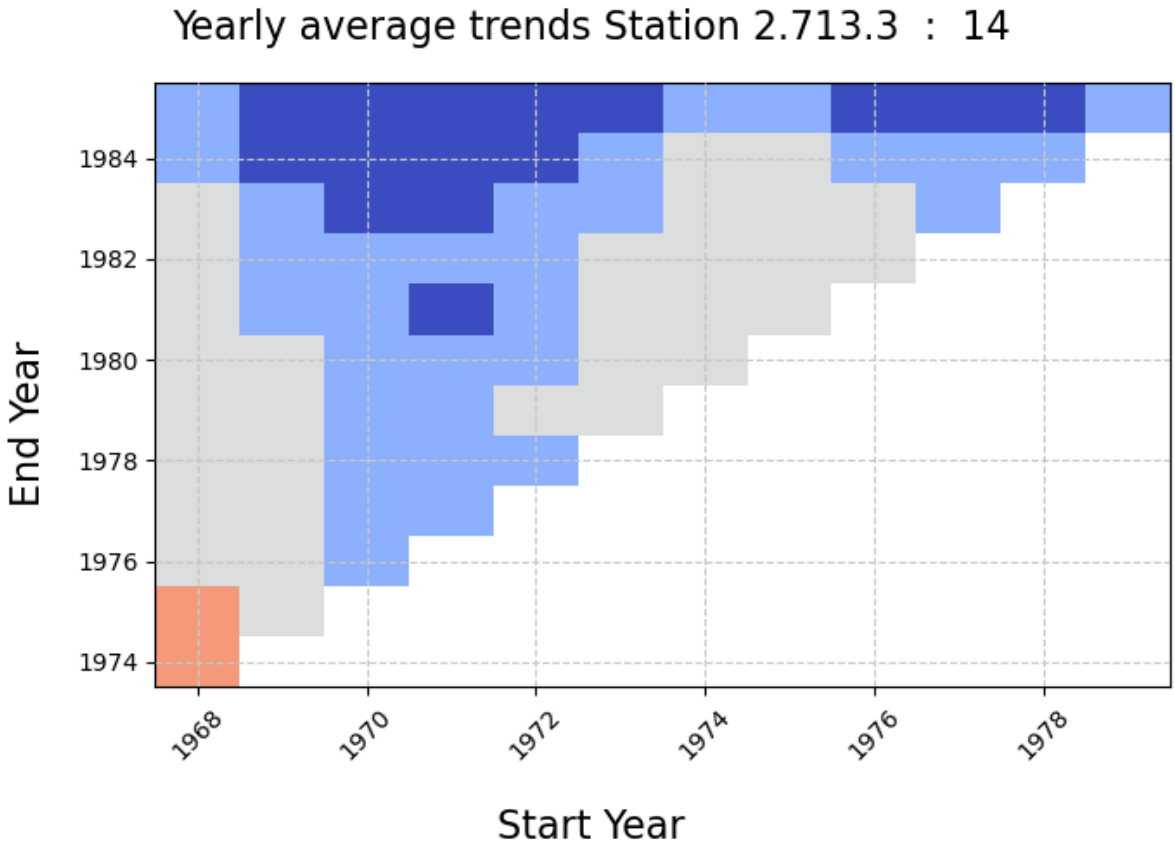

Multi temporal trends for annual GWL at Hauerseter station (14).

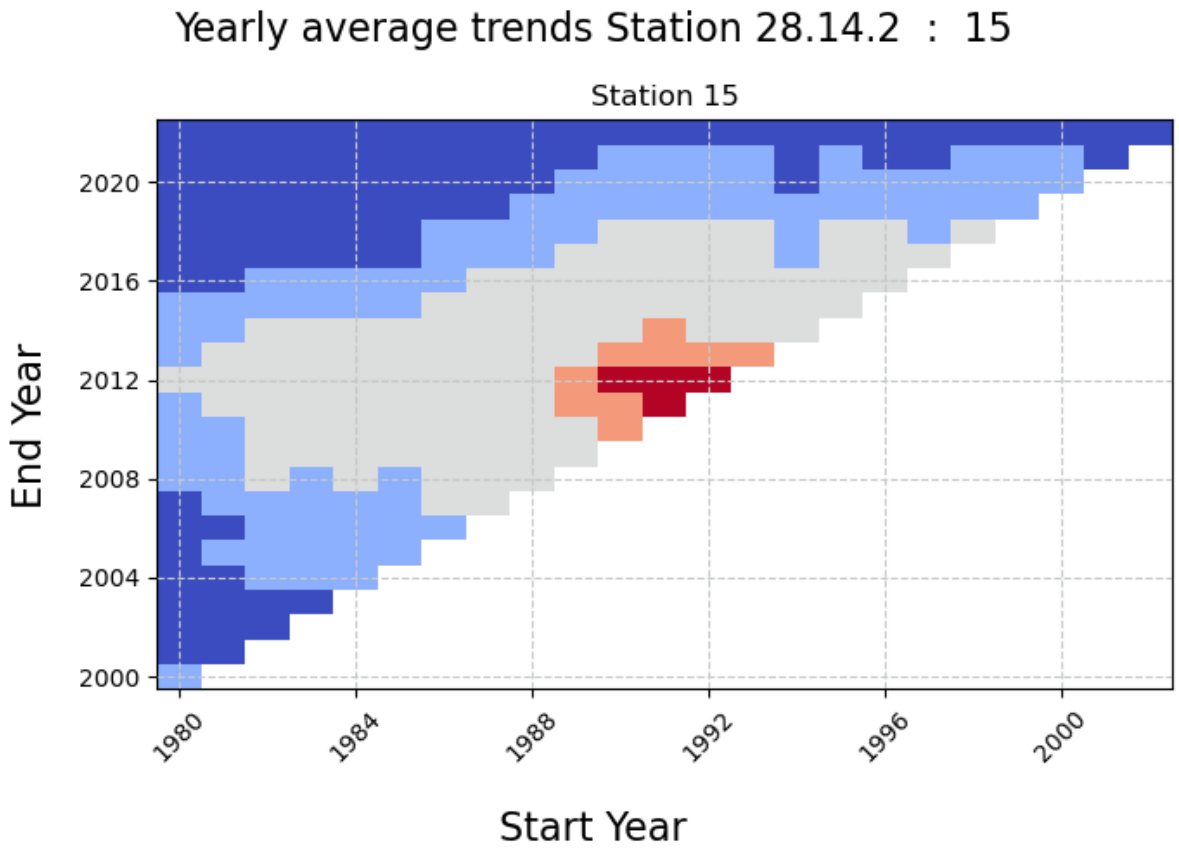

Multi temporal trends for annual GWL at Jæren station (15).

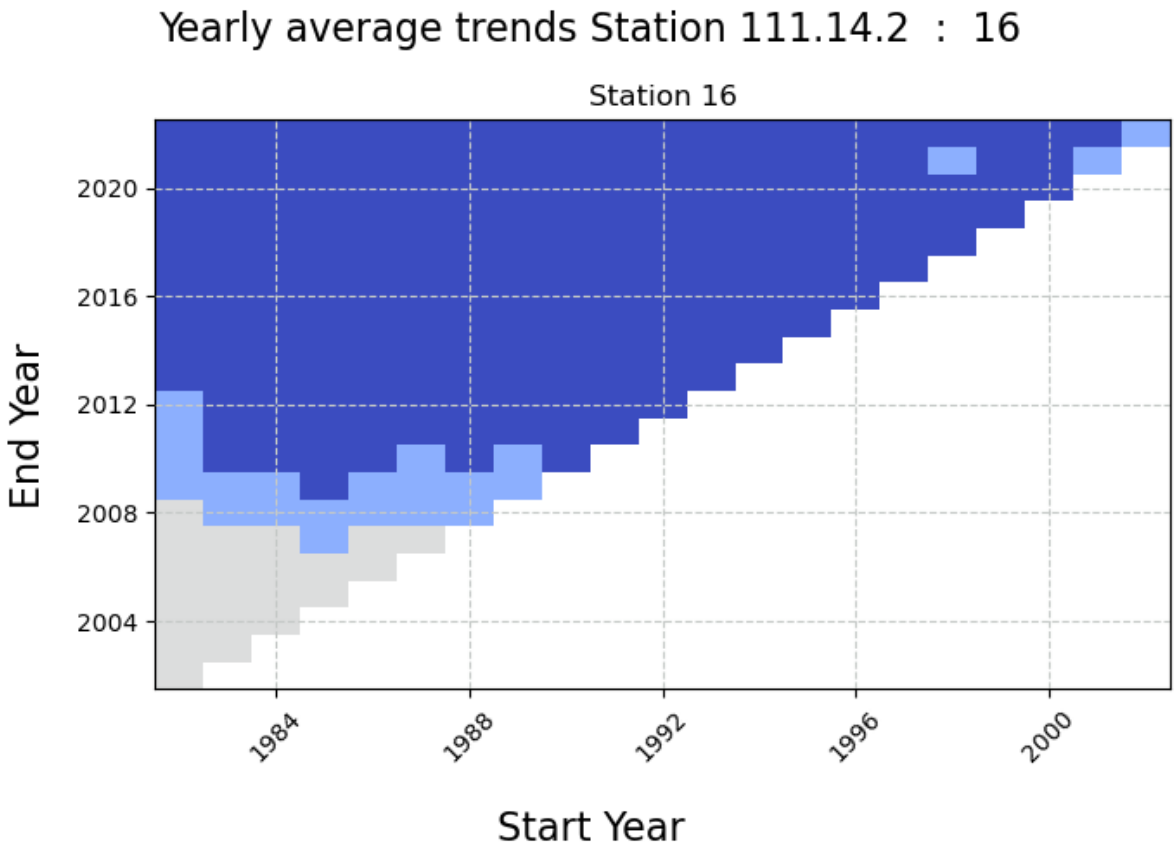

Multi temporal trends for annual GWL at Kårvatn station (16).

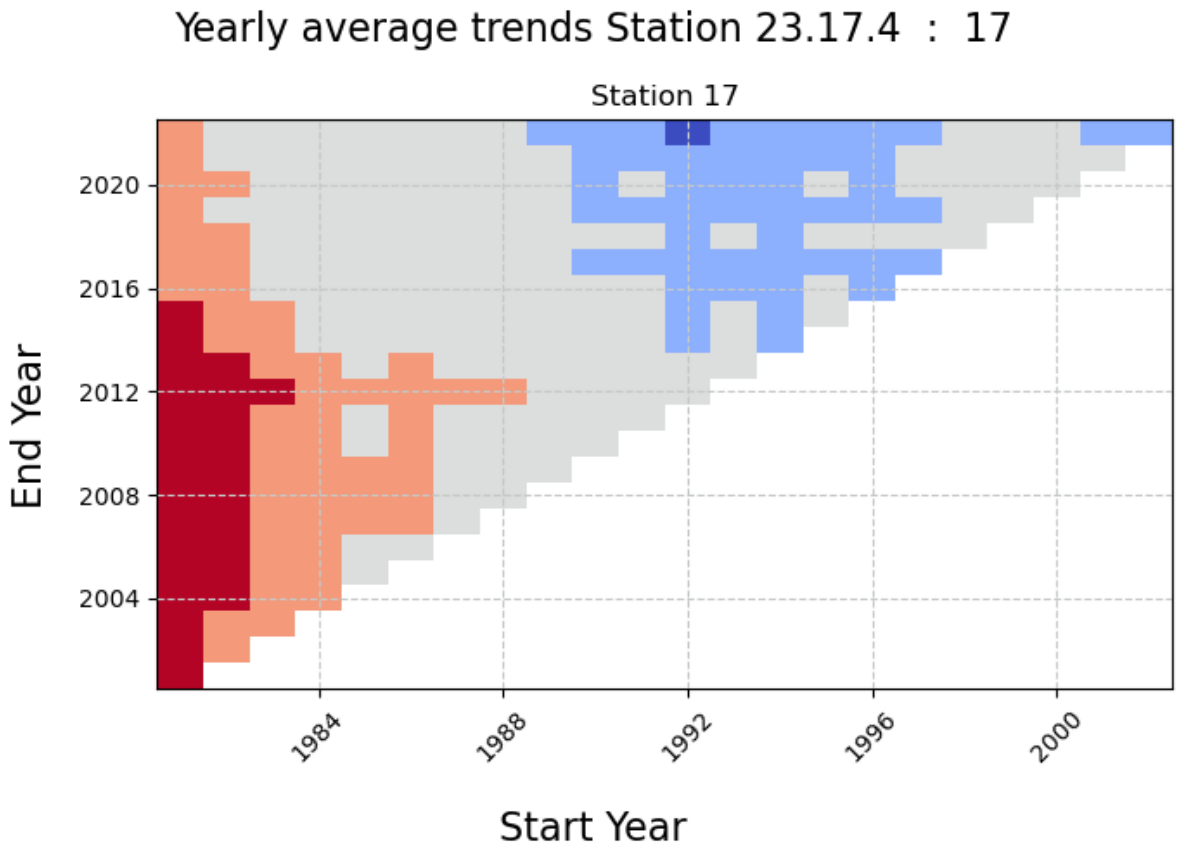

Multi temporal trends for annual GWL at Lindesnes station (17).

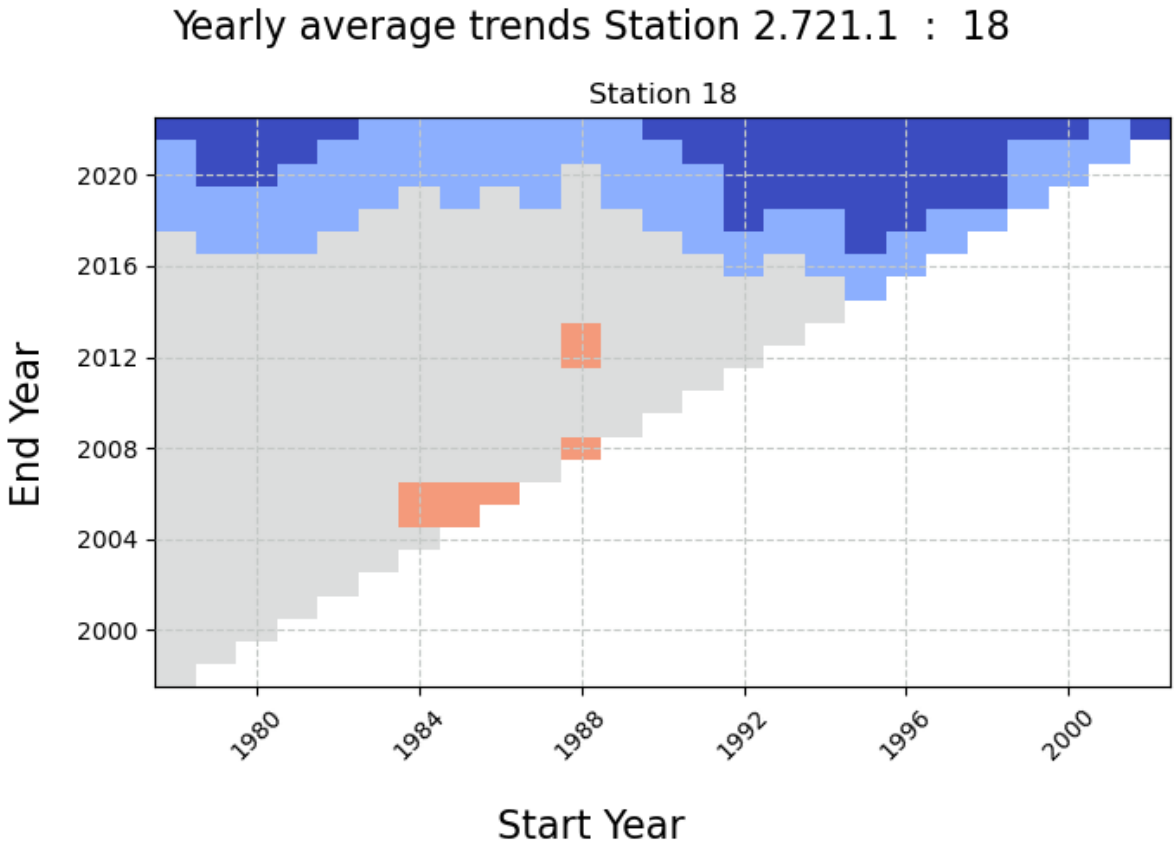

Multi temporal trends for annual GWL at Lykjestøylane station (18).

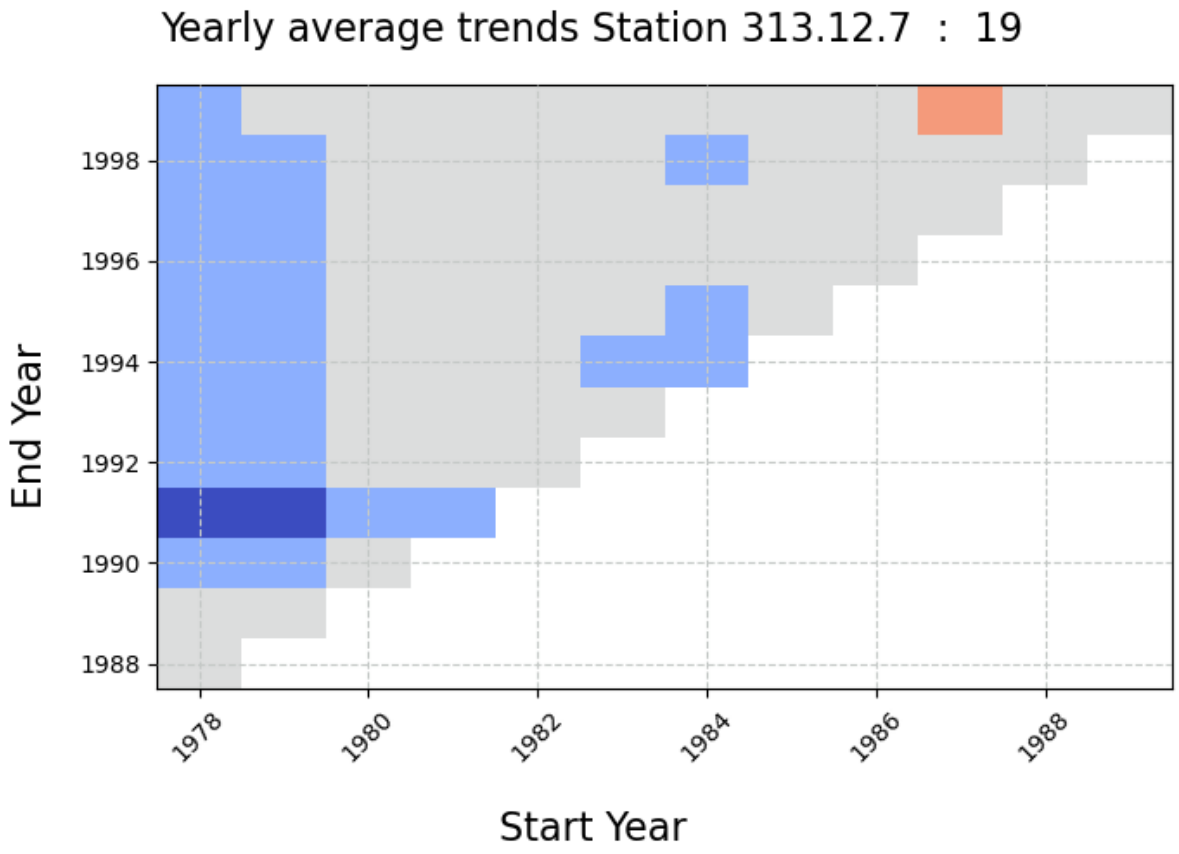

Multi temporal trends for annual GWL at Magnor station (19).

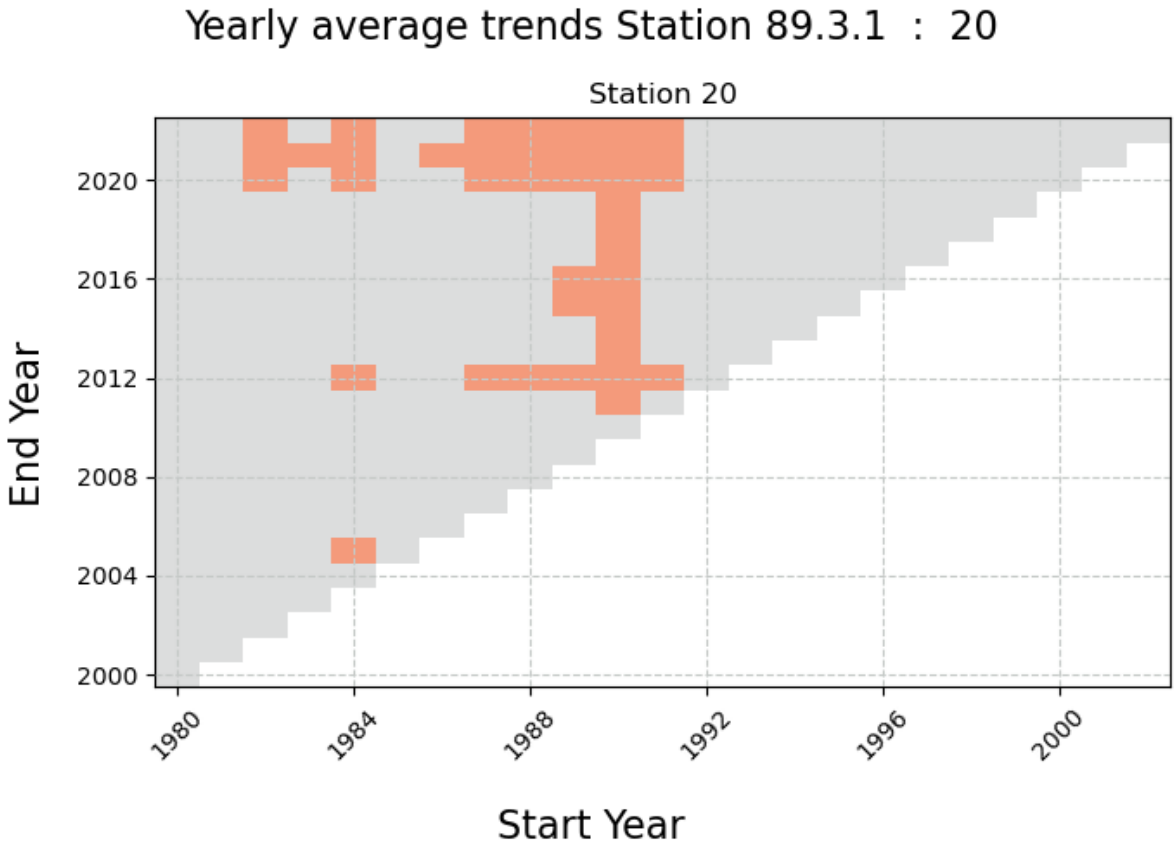

Multi temporal trends for annual GWL at Nordfjordeid station (20).

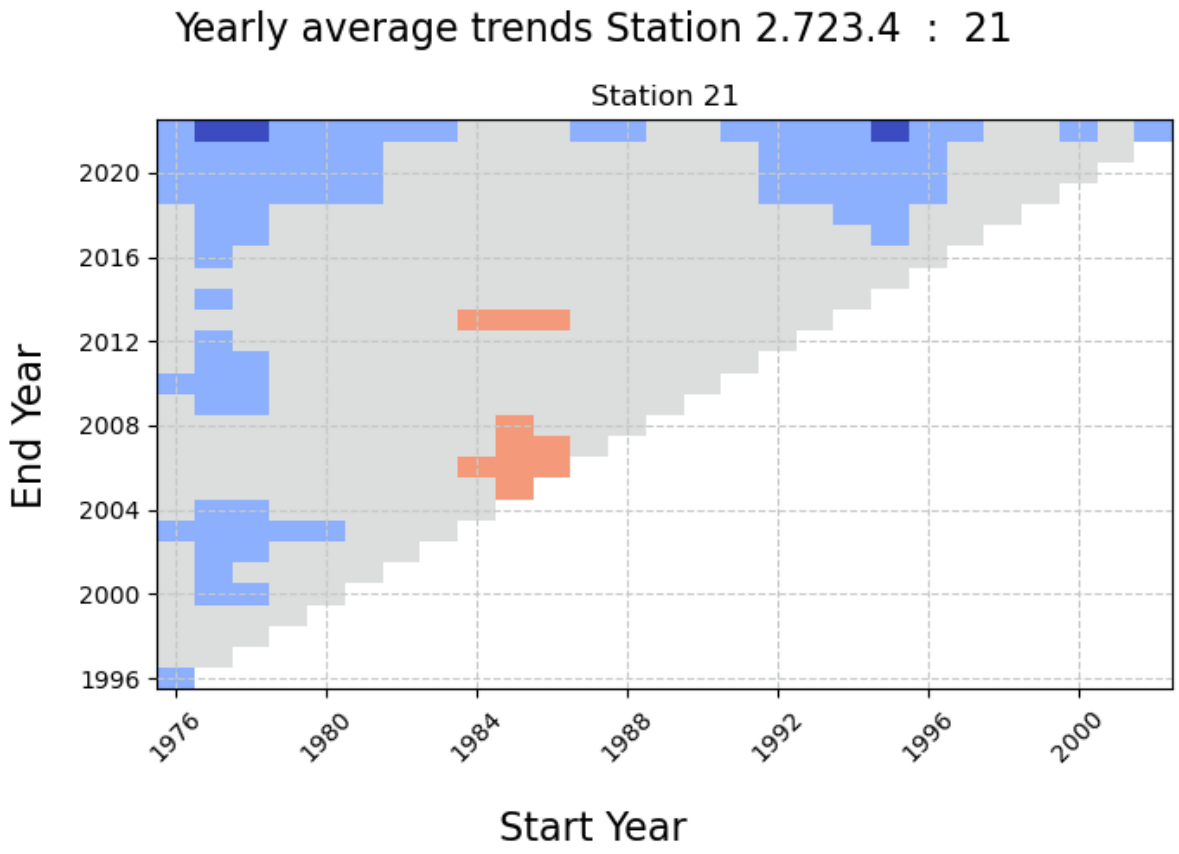

Multi temporal trends for annual GWL at Settalbekken station (21).

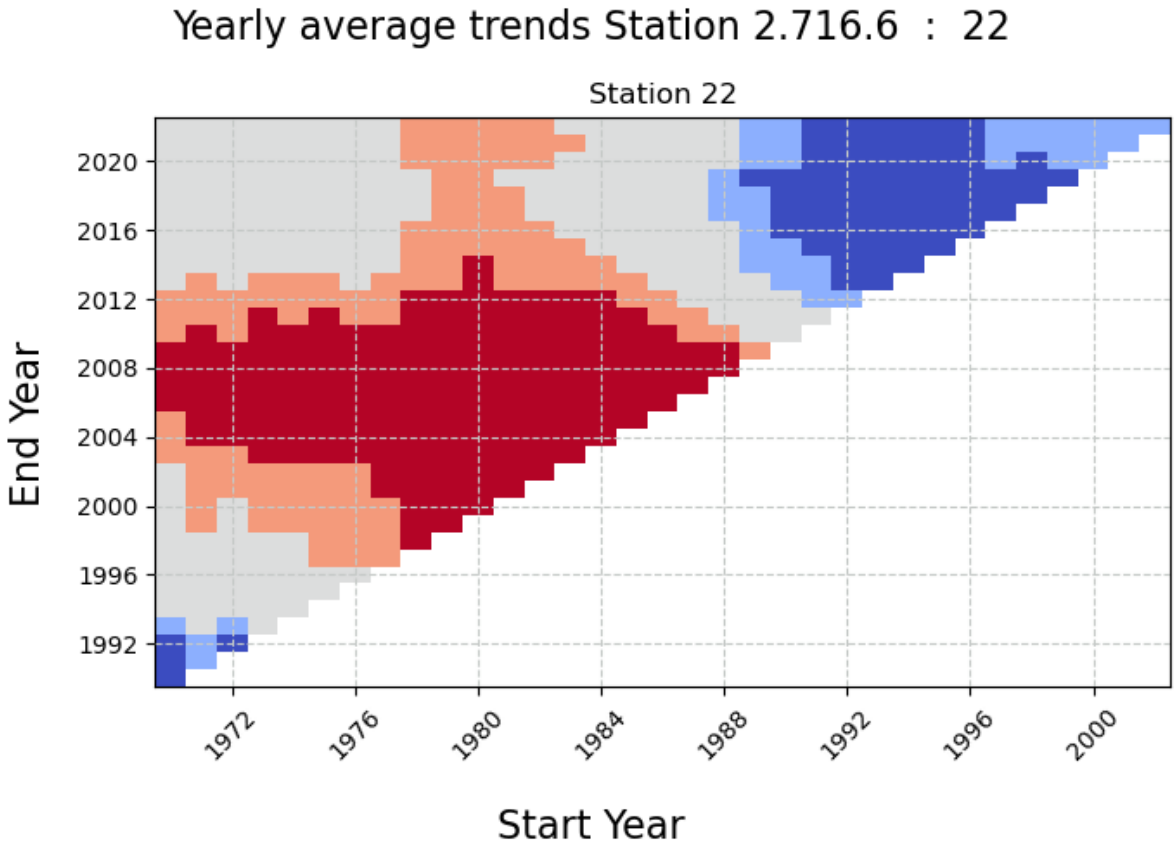

Multi temporal trends for annual GWL at stenerseter station (22).

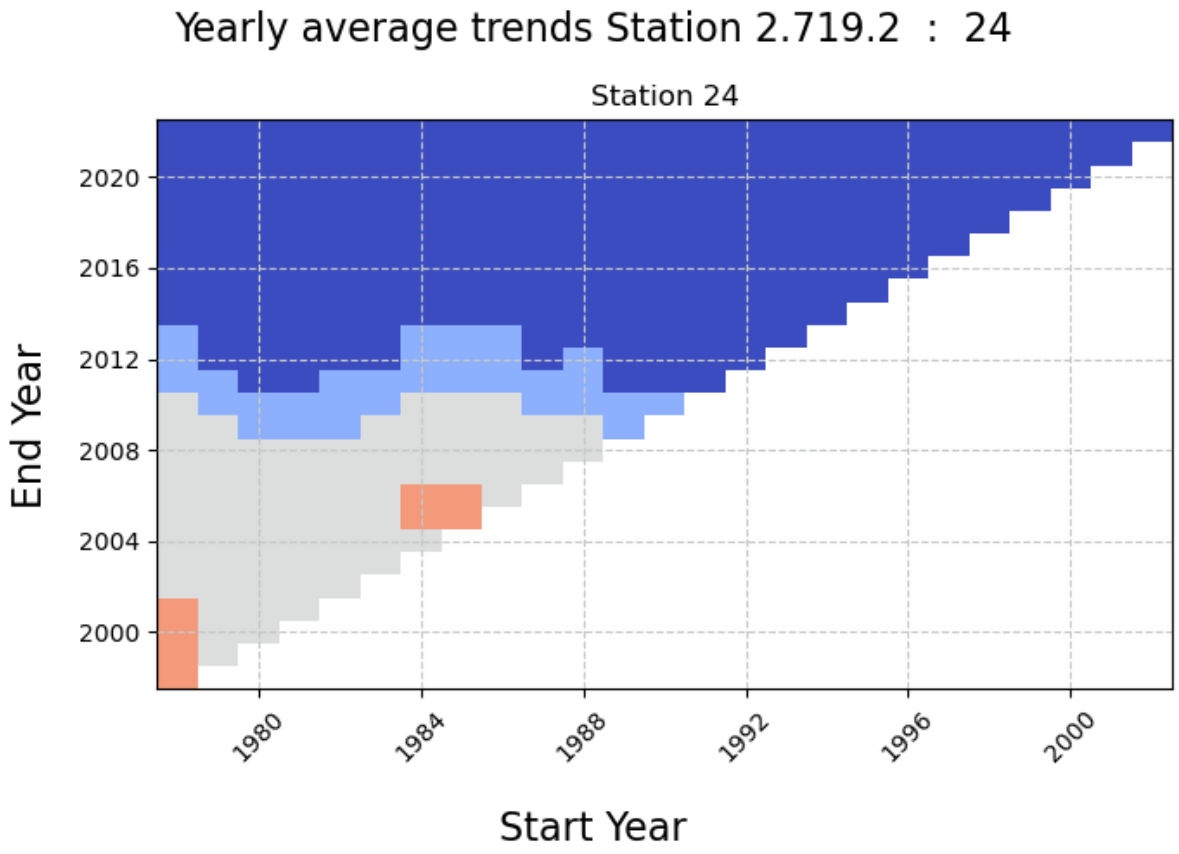

Multi temporal trends for annual GWL at Øyangen station (24).

Appendix E

Summer high and low multi temporal trend plots

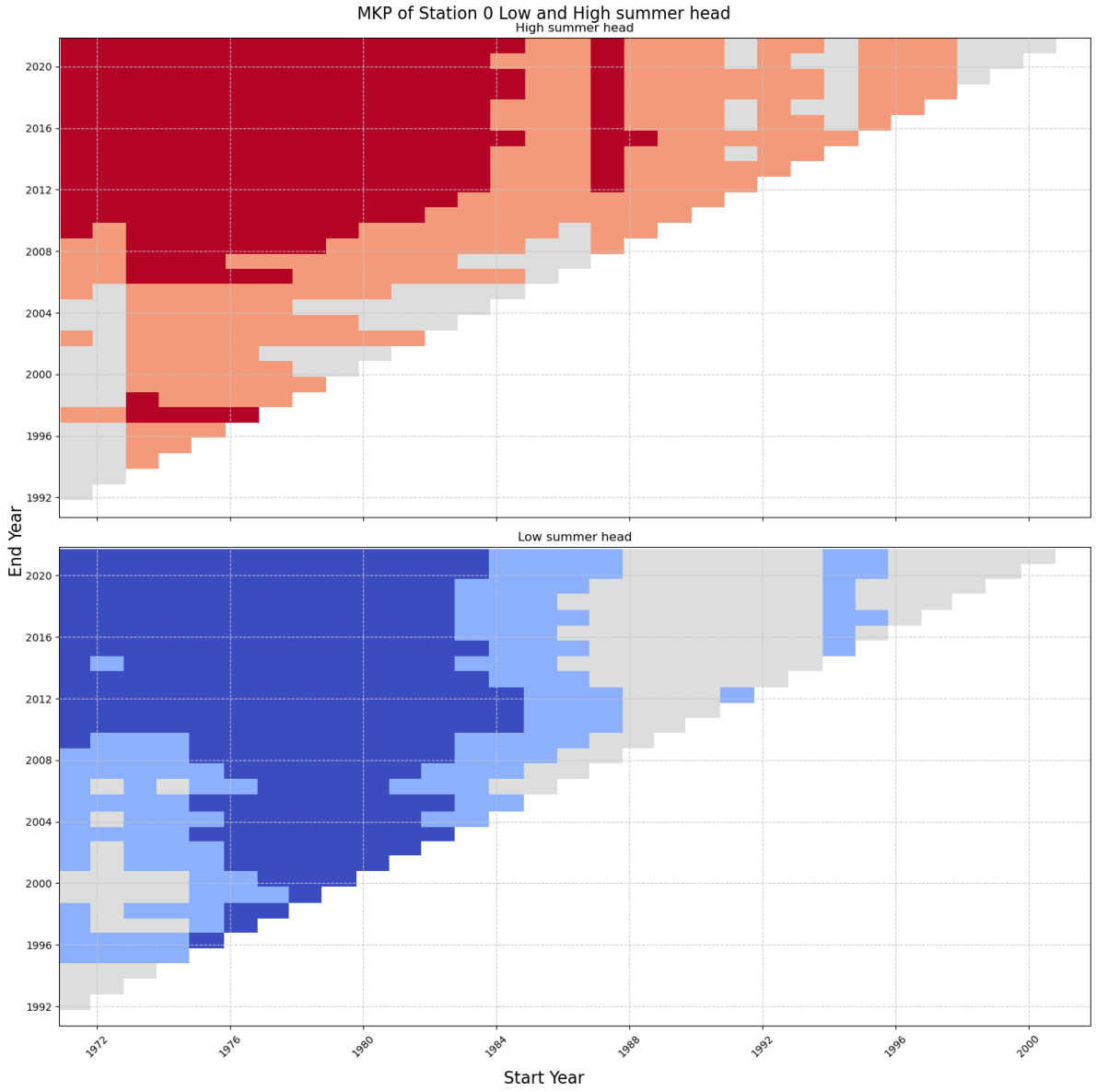

Same as figure 4.23, but for Abrahamsvoll station (0).

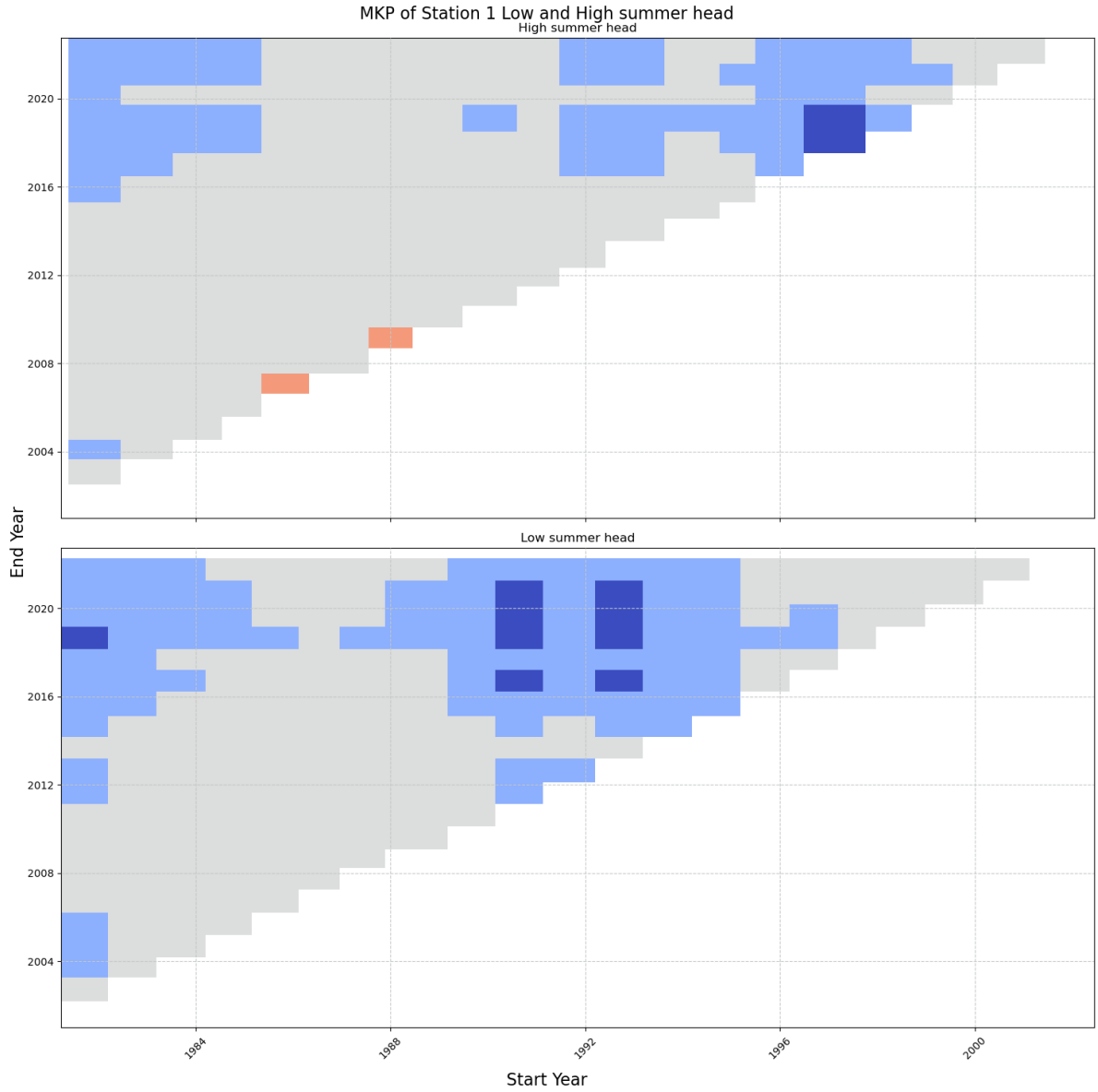

Same as figure 4.23, but for Birkenes station (1).

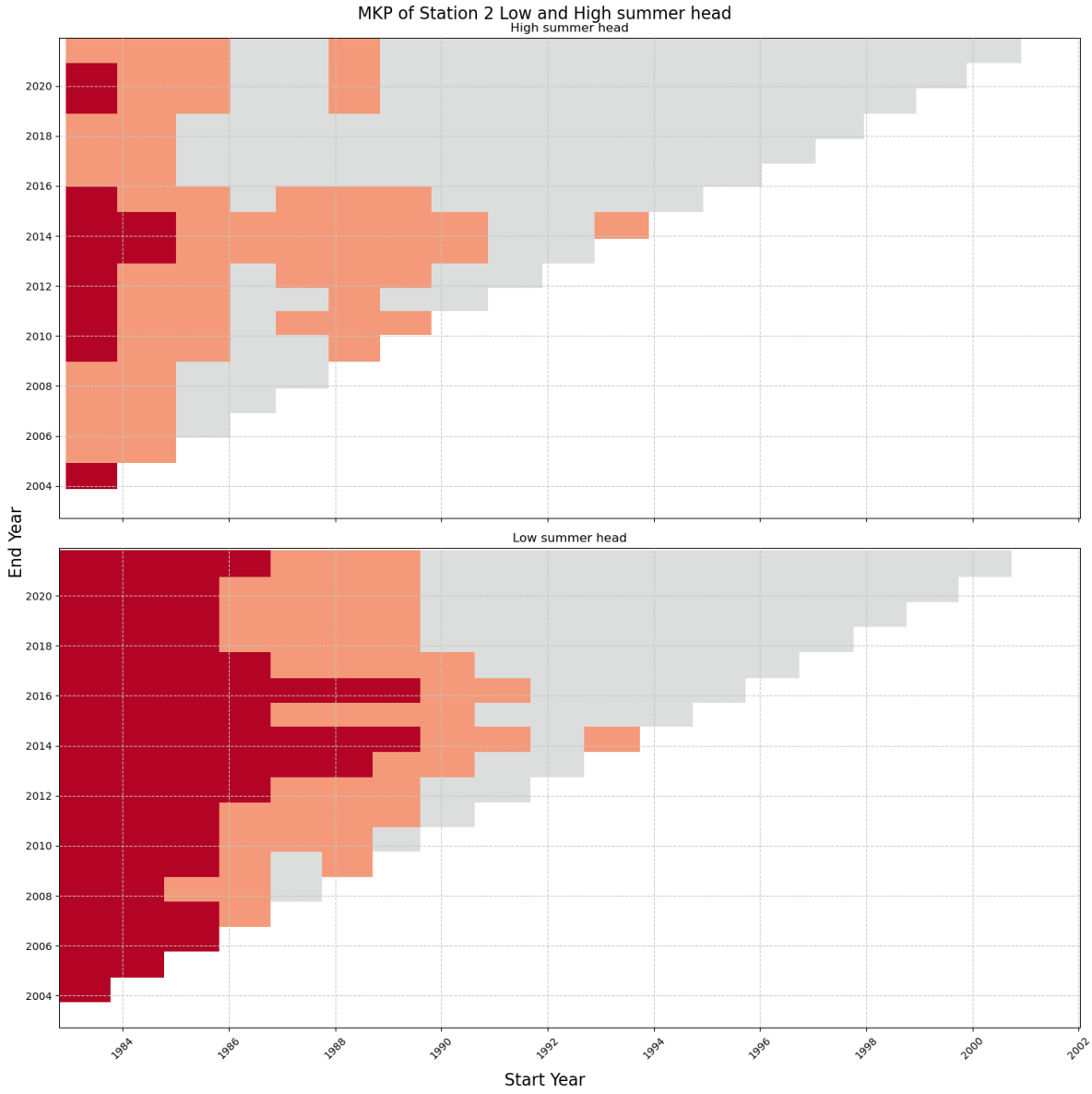

Same as figure 4.23, but for Dombås station (2).

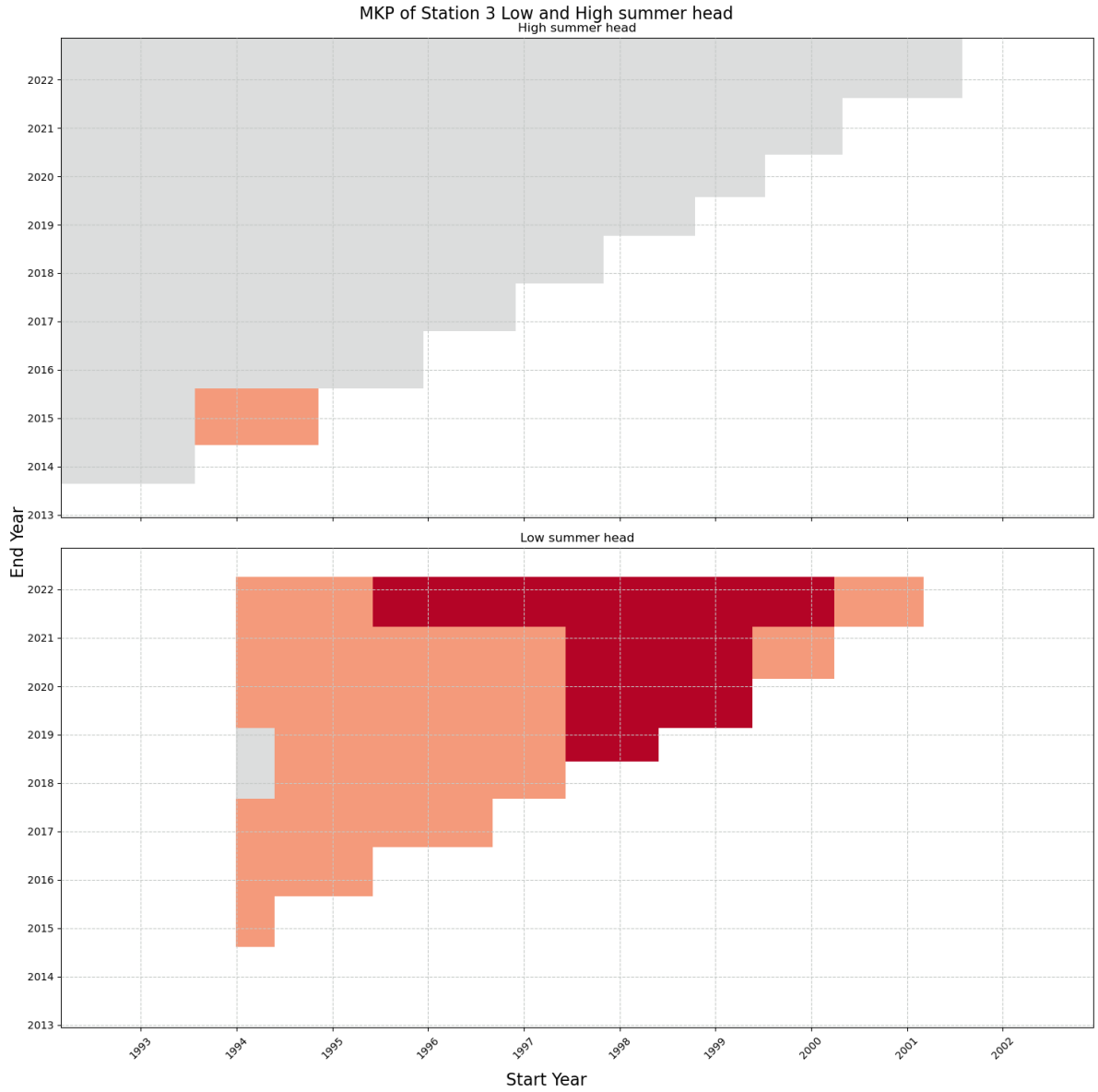

Same as figure 4.23, but for Kise station (3).

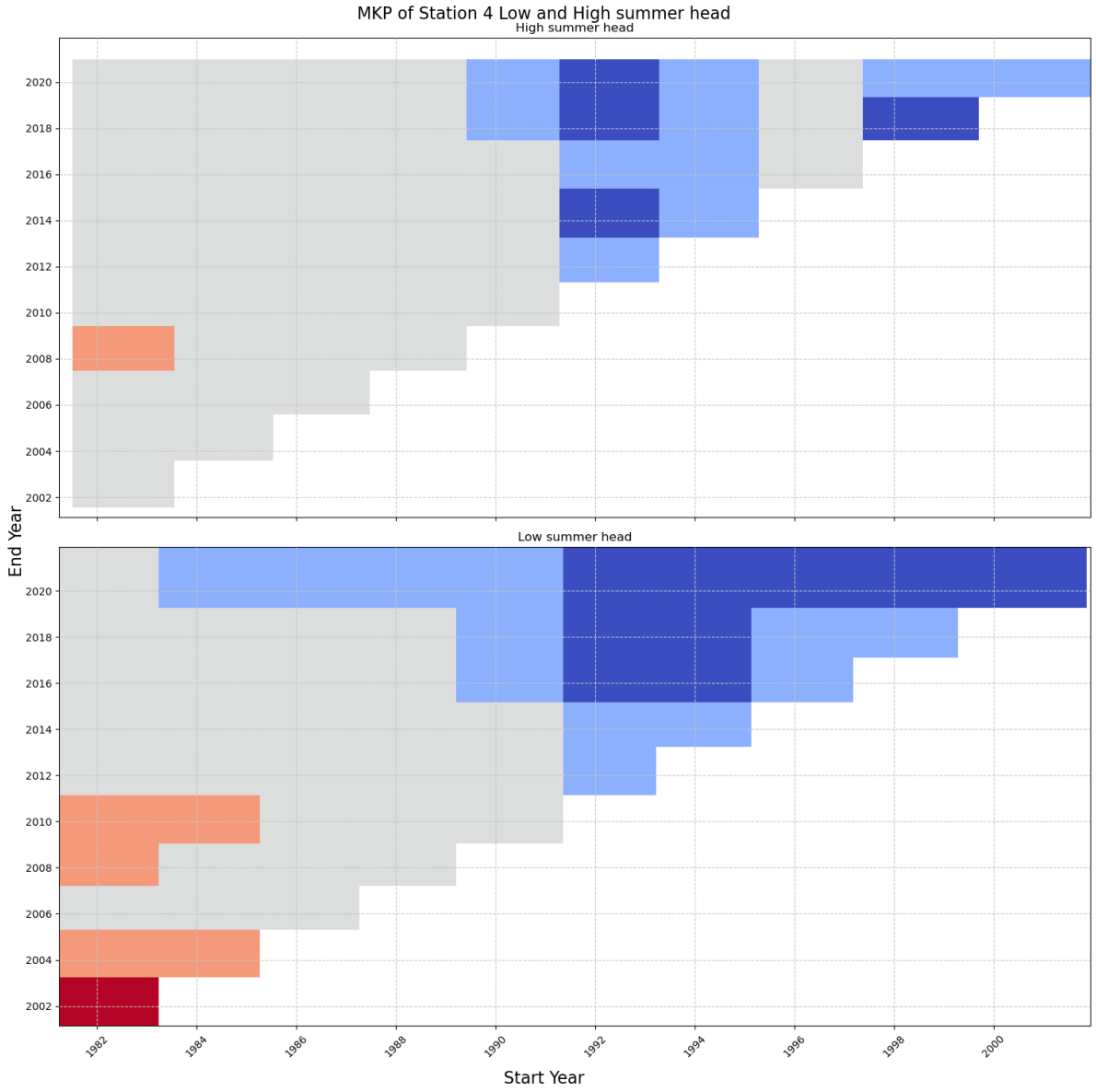

Same as figure 4.23, but for Modum station (4).

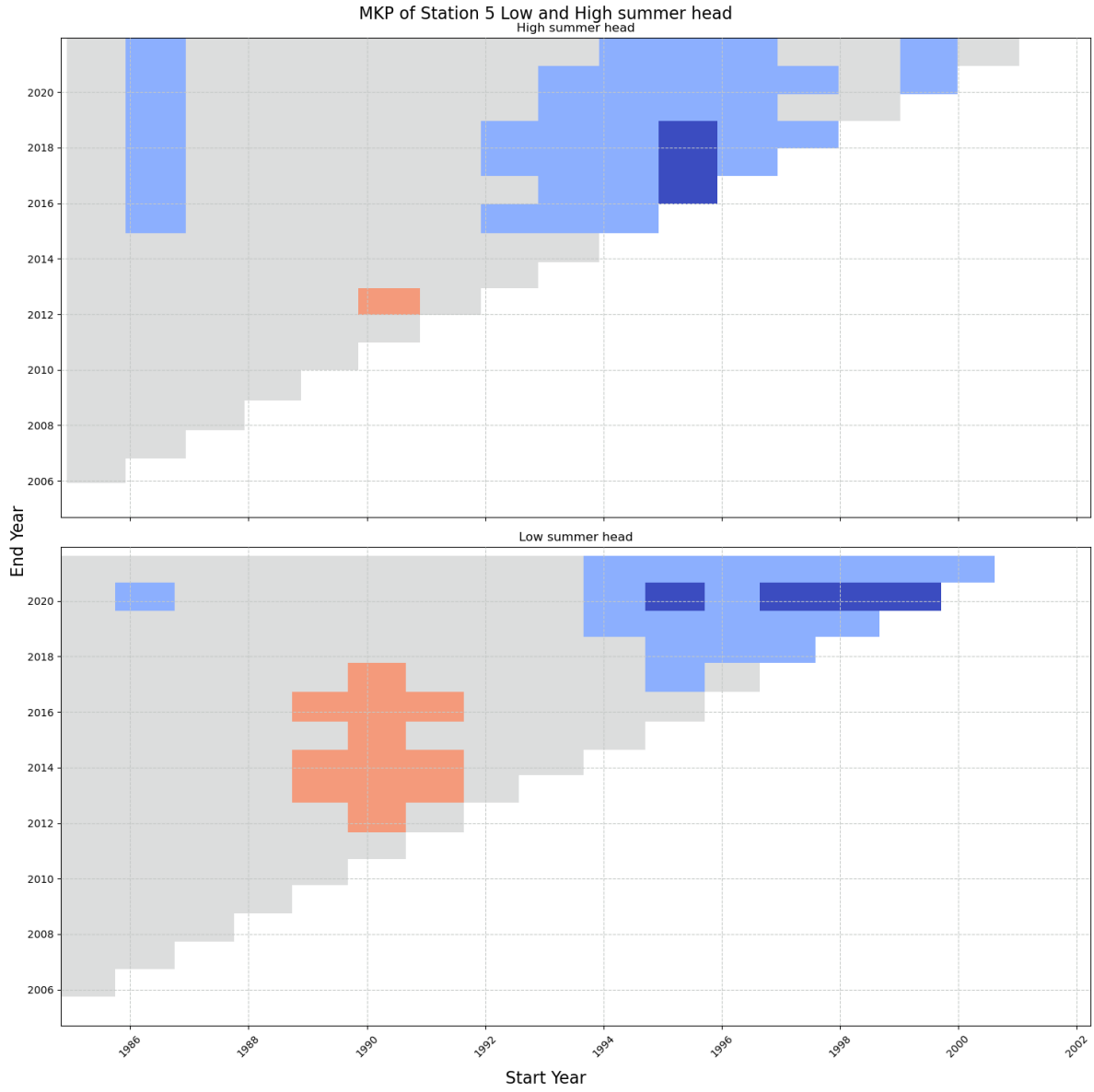

Same as figure 4.23, but for Skjomen station (5).

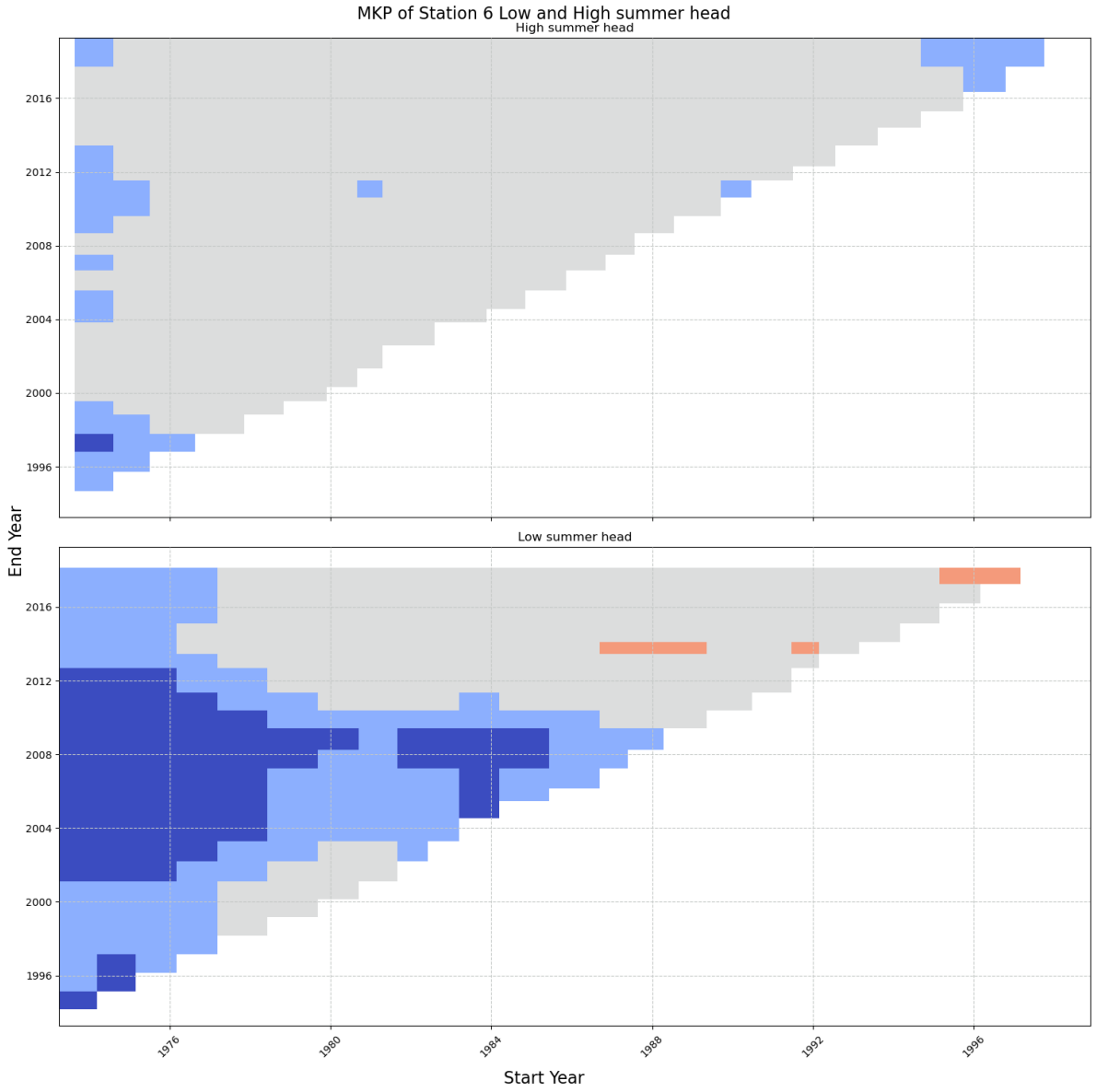

Same as figure 4.23, but for Stigvassåi station (6).

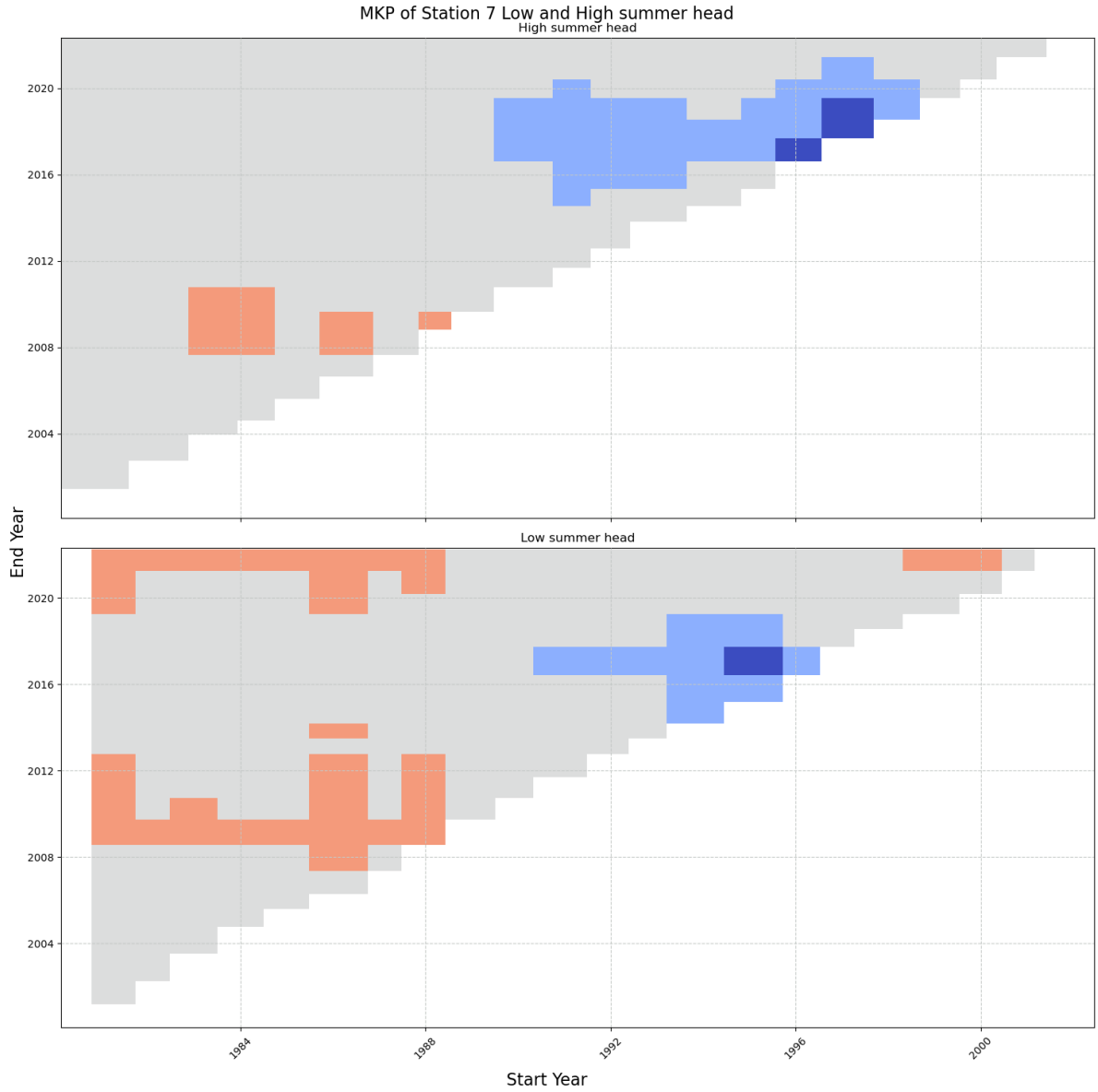

Same as figure 4.23, but for Eikamoen station (7).

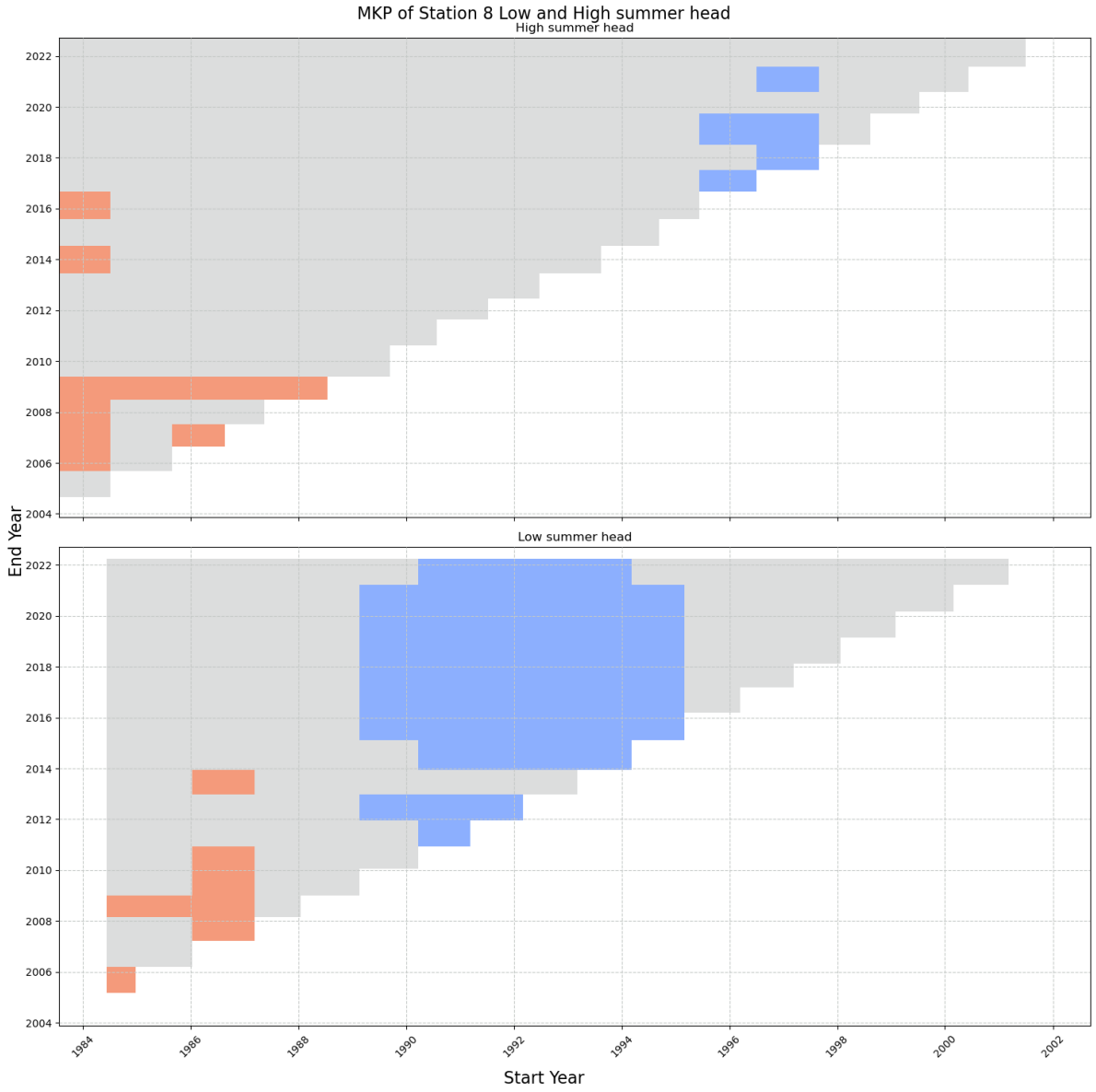

Same as figure 4.23, but for Evje station (8).

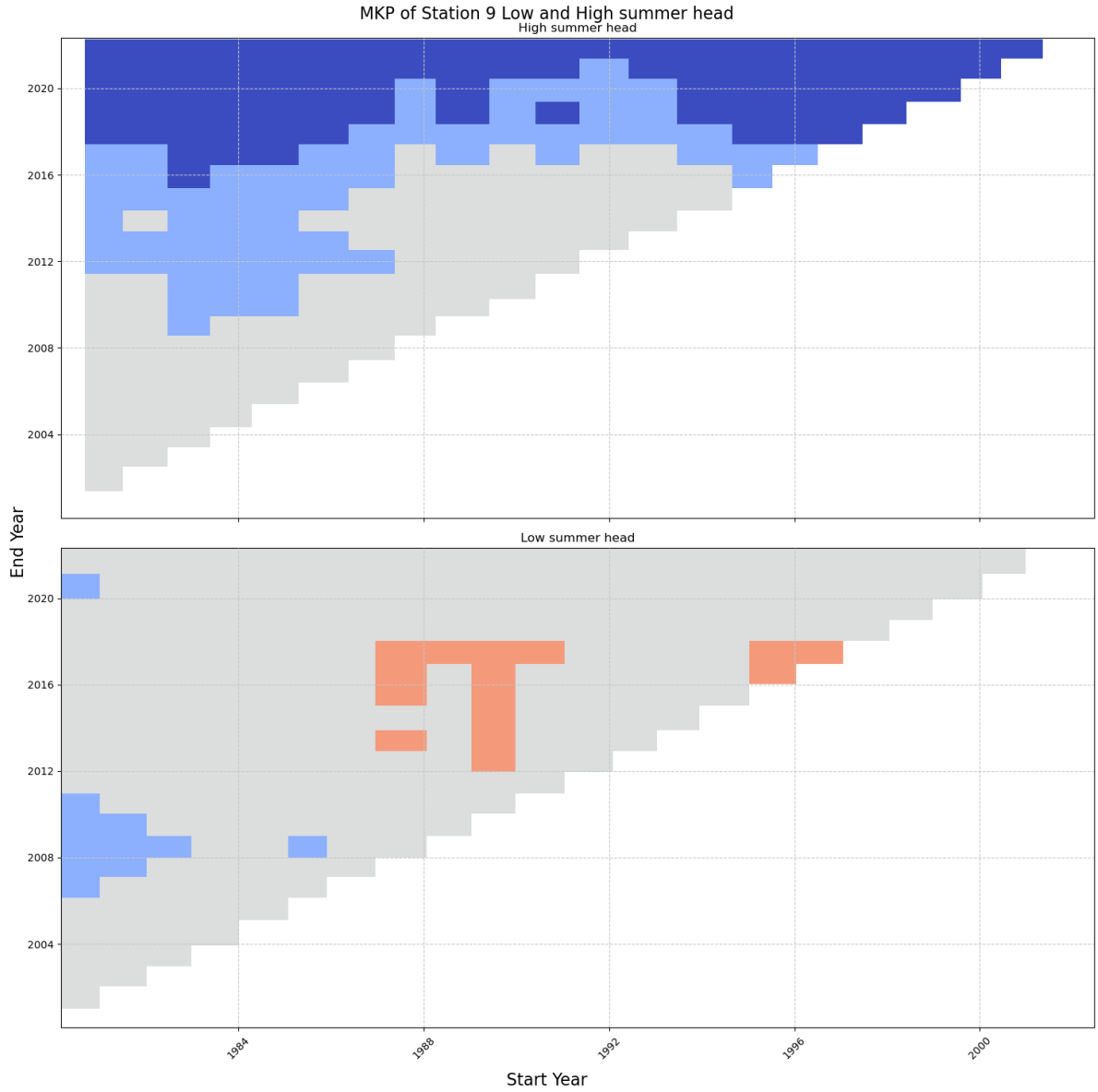

Same as figure 4.23, but for Fana station (9).

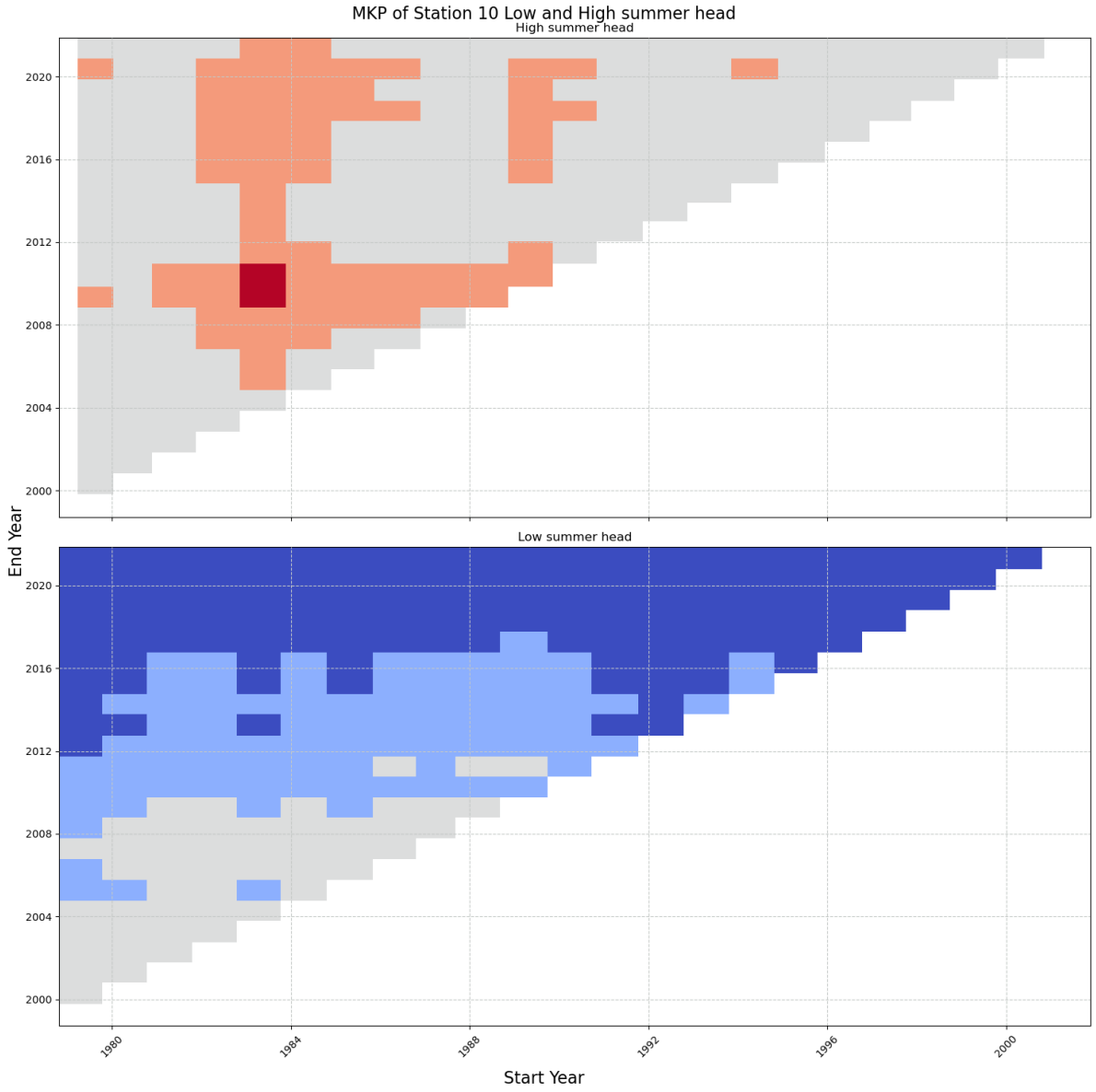

Same as figure 4.23, but for Finnbølseter station (10).

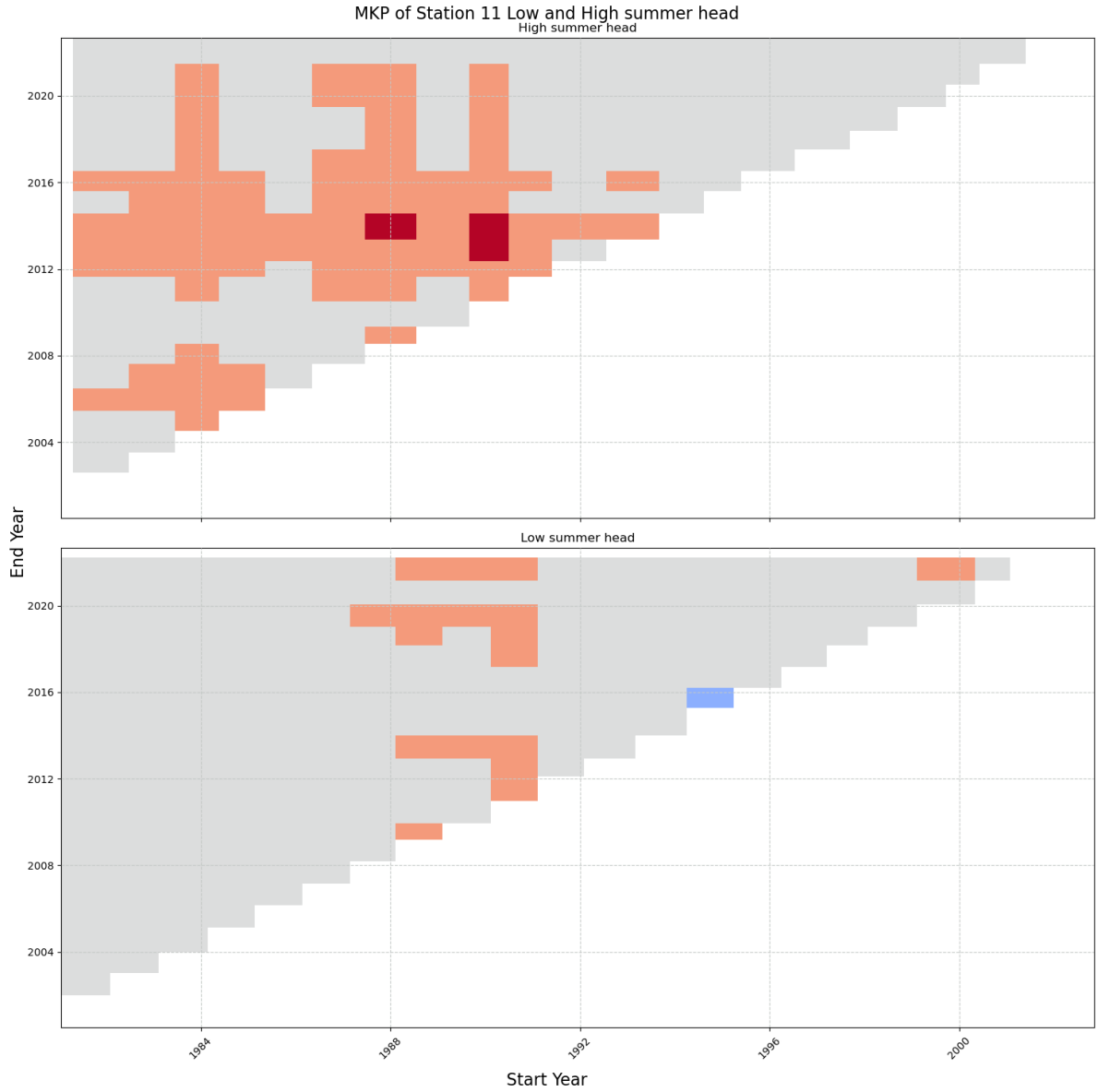

Same as figure 4.23, but for Førde/Moskog station (11).

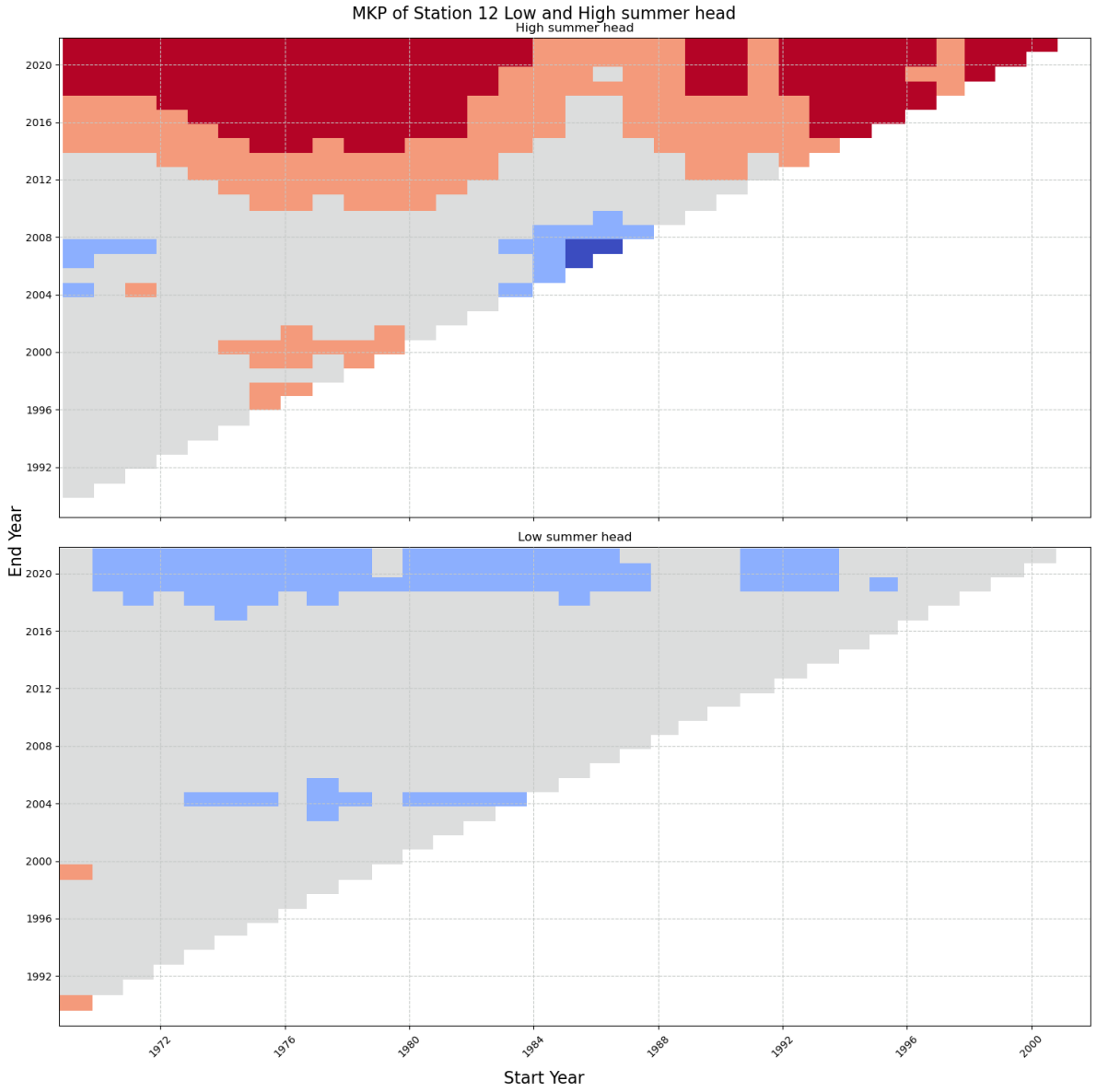

Same as figure 4.23, but for Groset station (12).

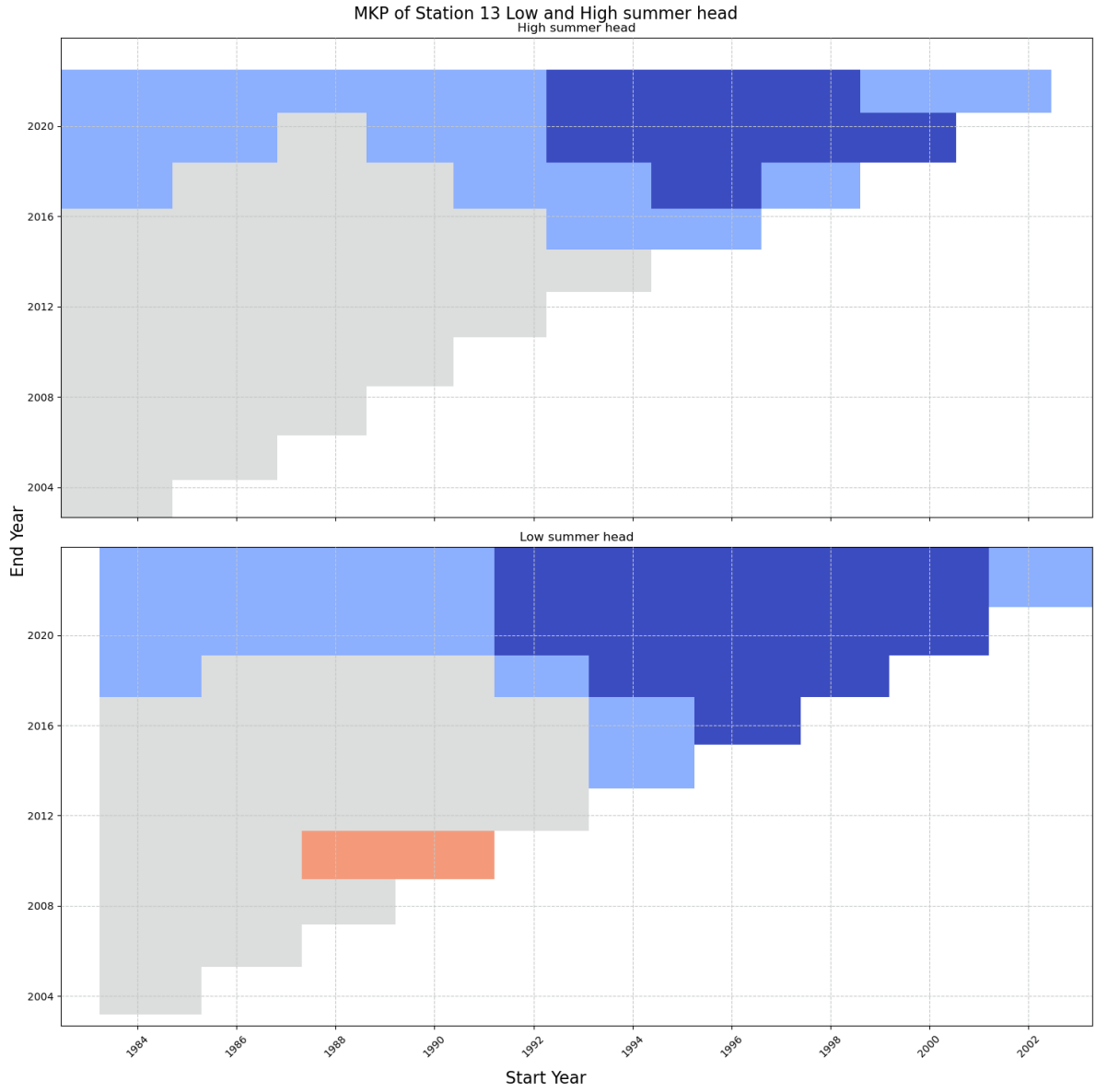

Same as figure 4.23, but for Haslemoen station (13).

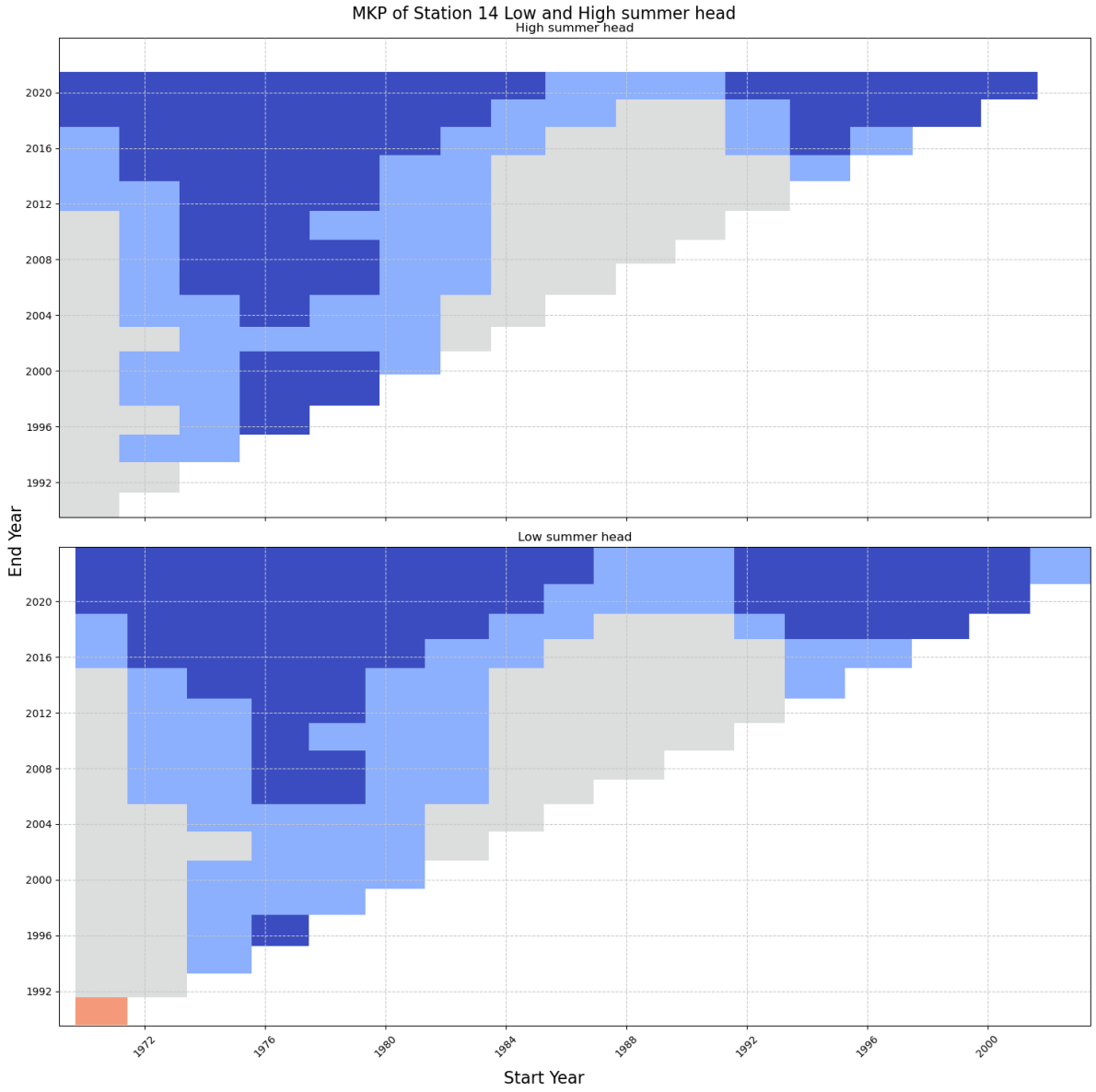

Same as figure 4.23, but for Hauerseter station (14).

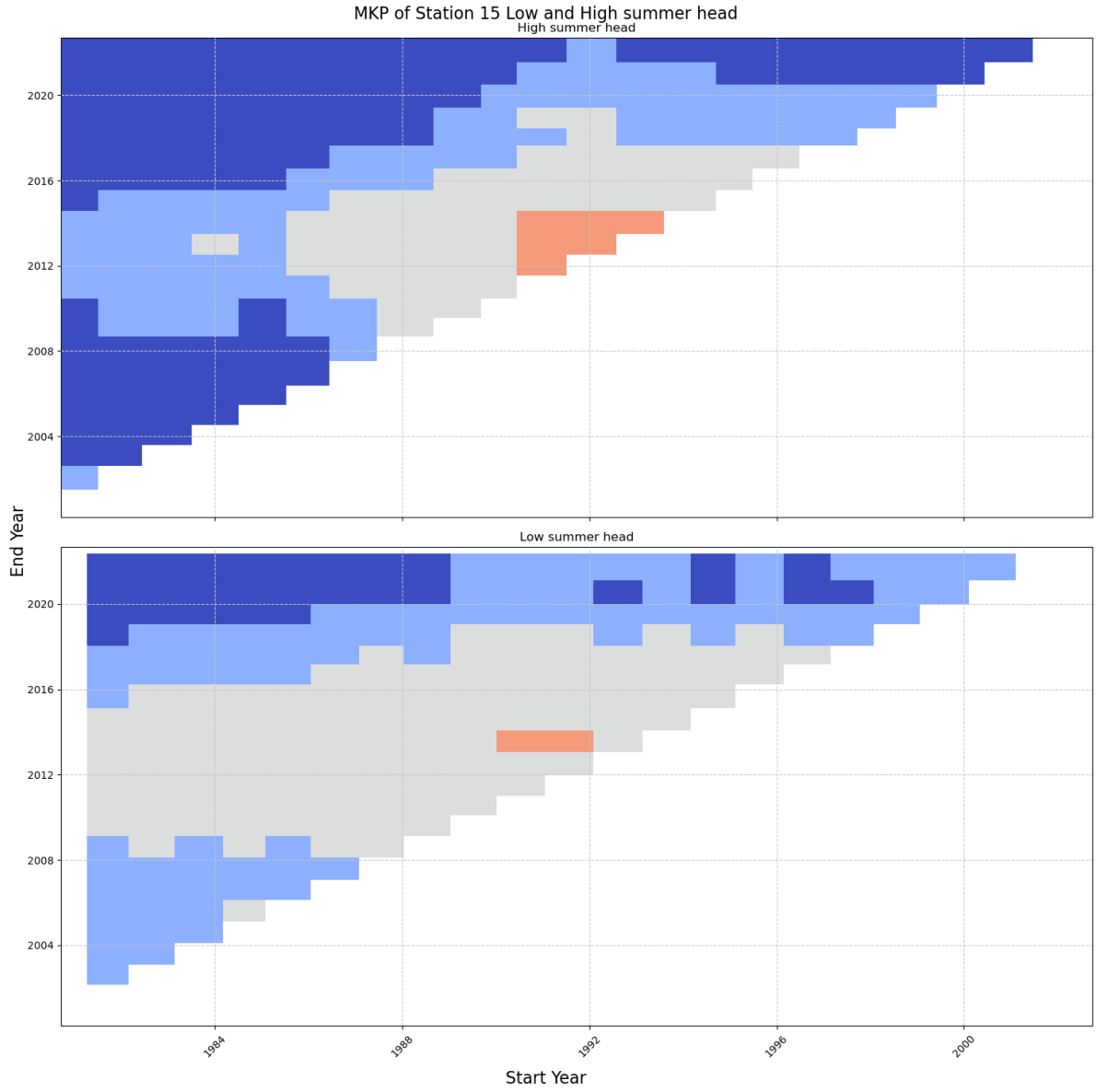

Same as figure 4.23, but for Jæren station (15).

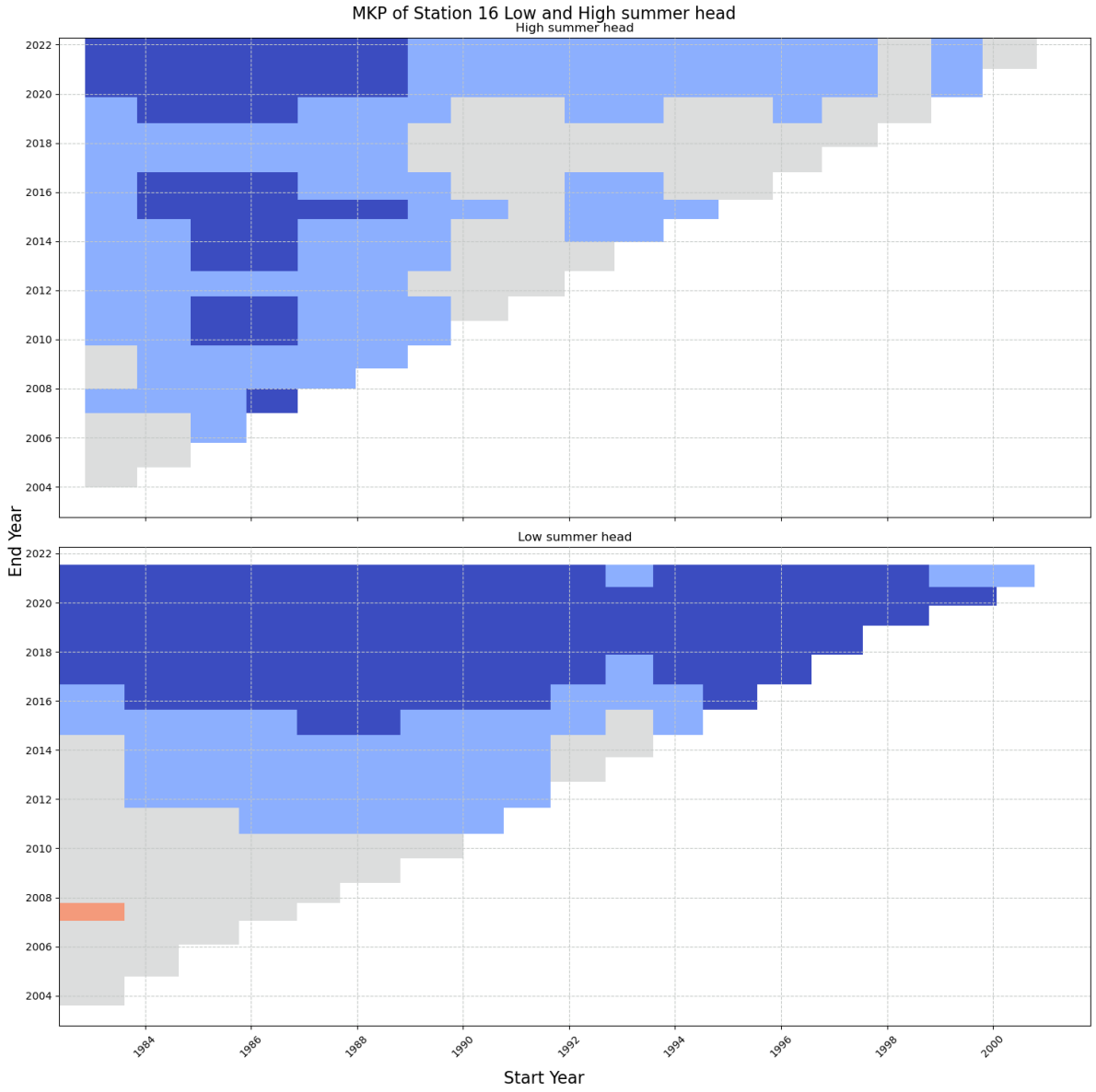

Same as figure 4.23, but for Kårvatn station (16).

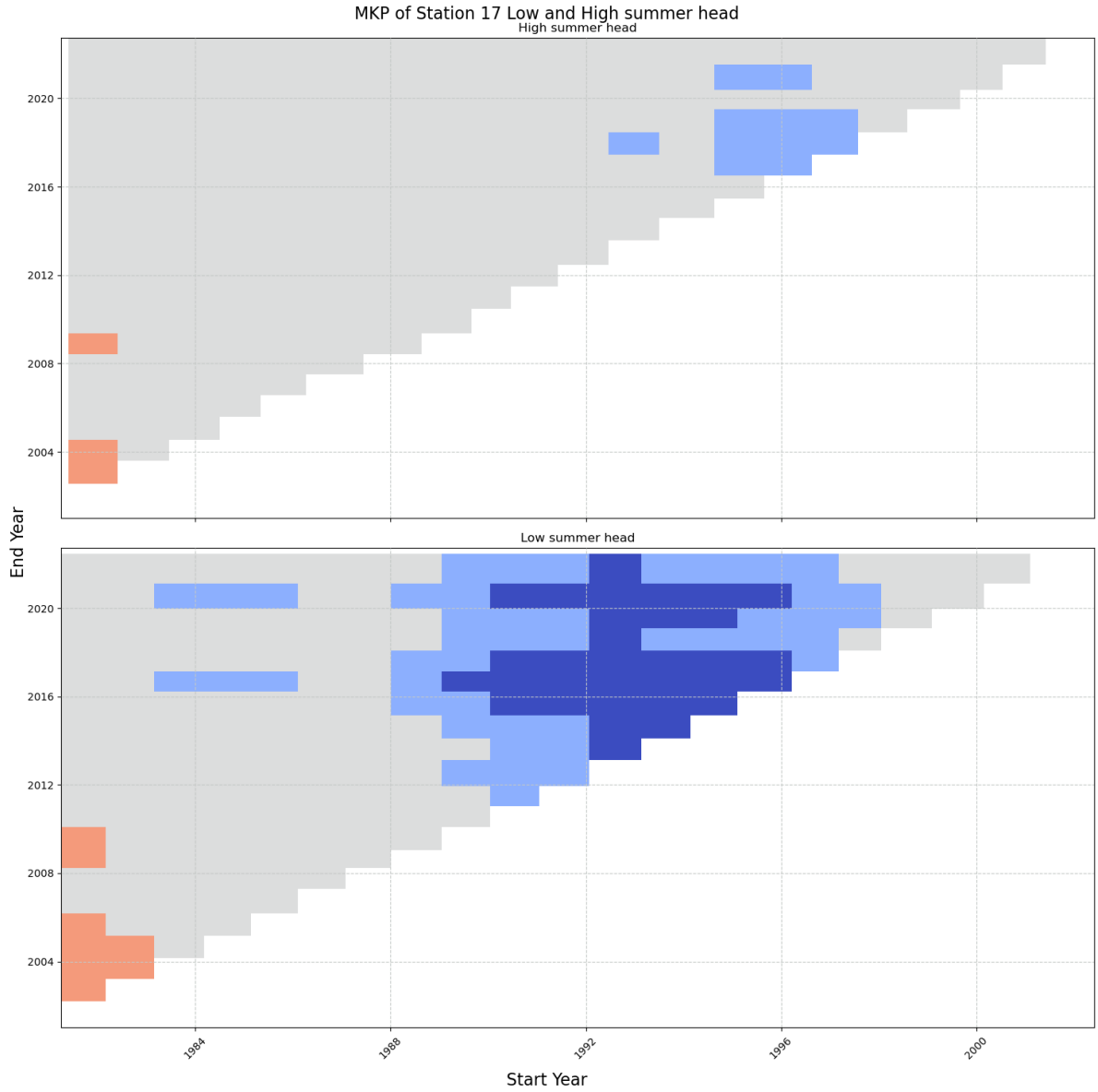

Same as figure 4.23, but for Lindesnes station (17).

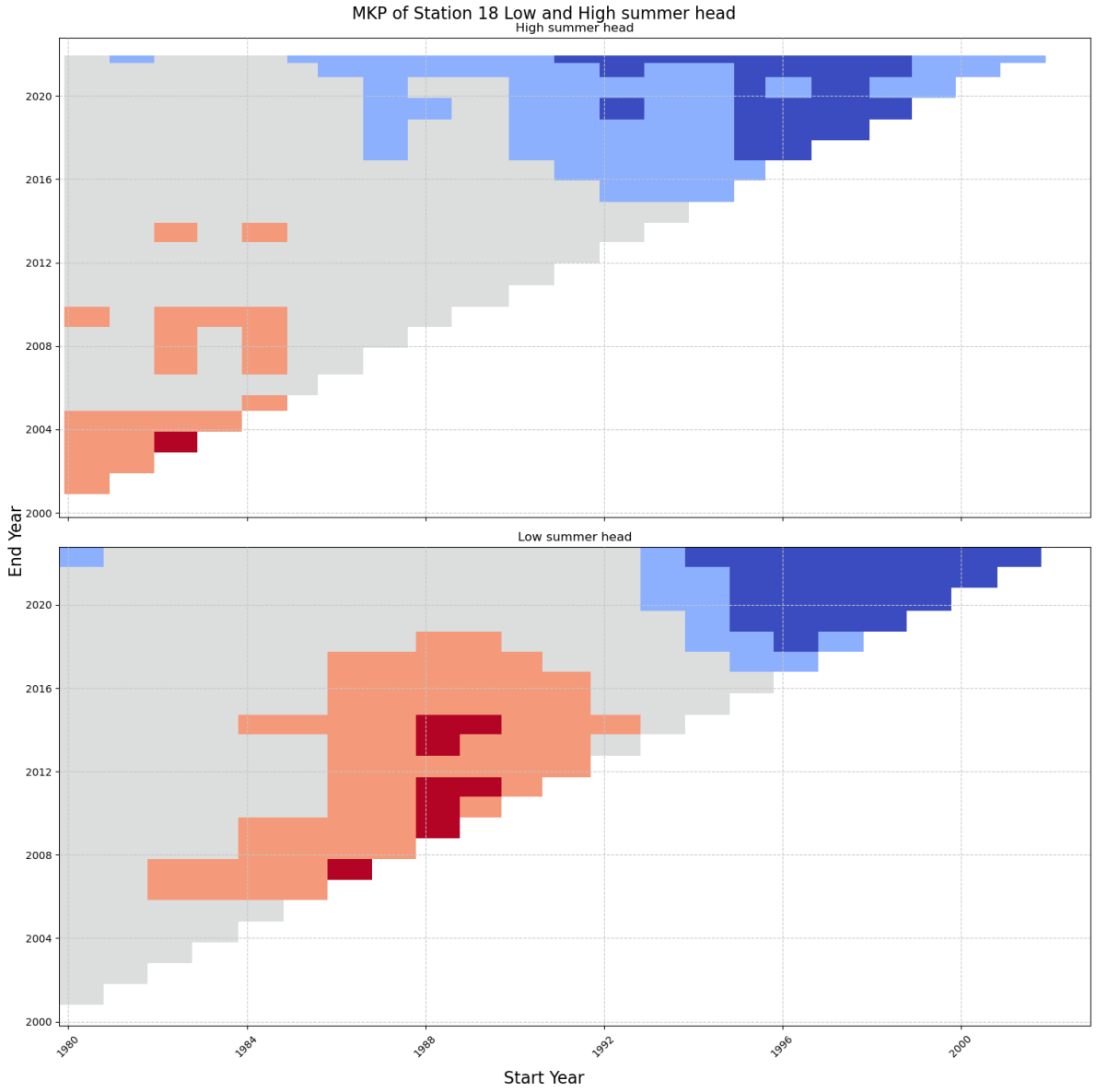

Same as figure 4.23, but for Lykjestøylane station (18).

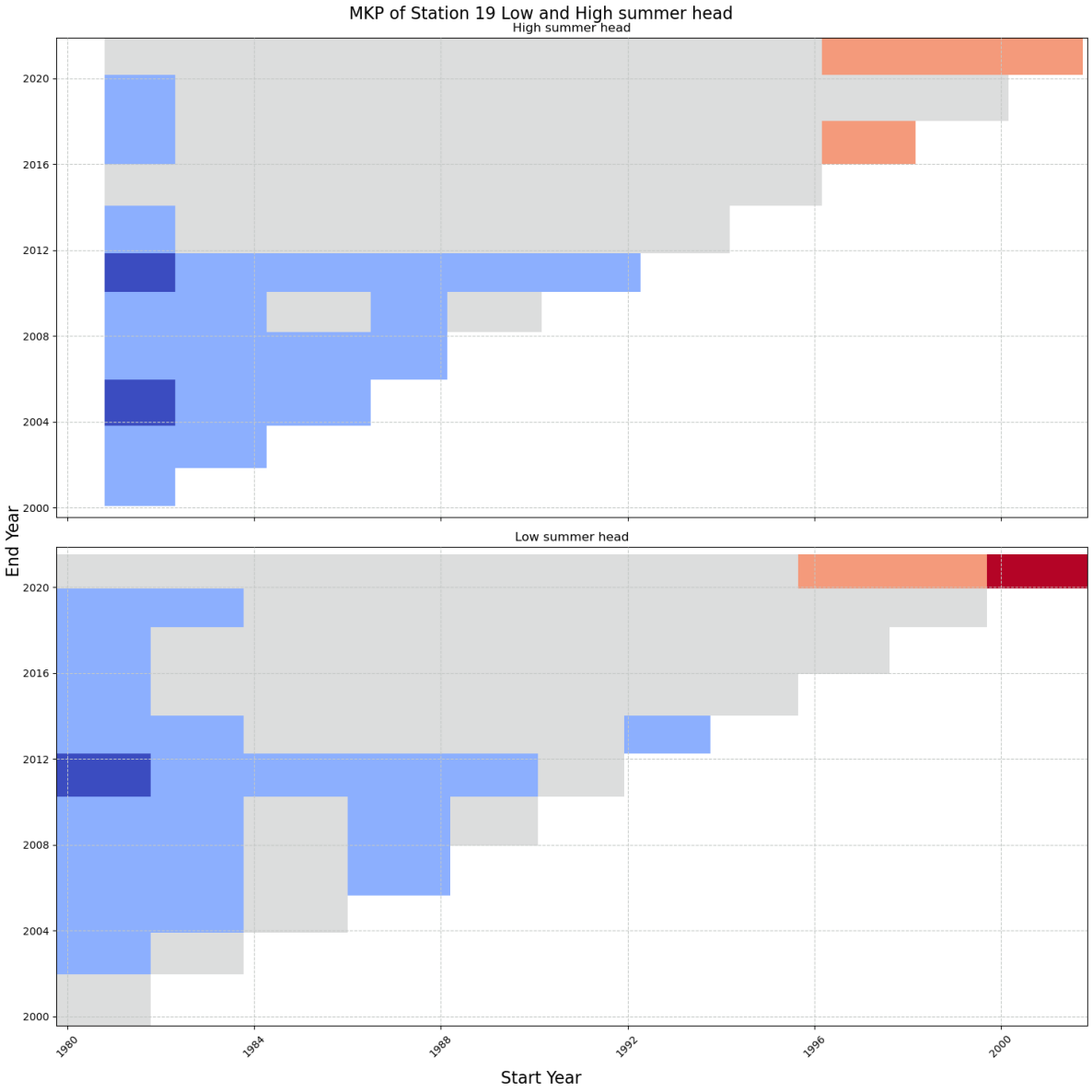

Same as figure 4.23, but for Magnor station (19).

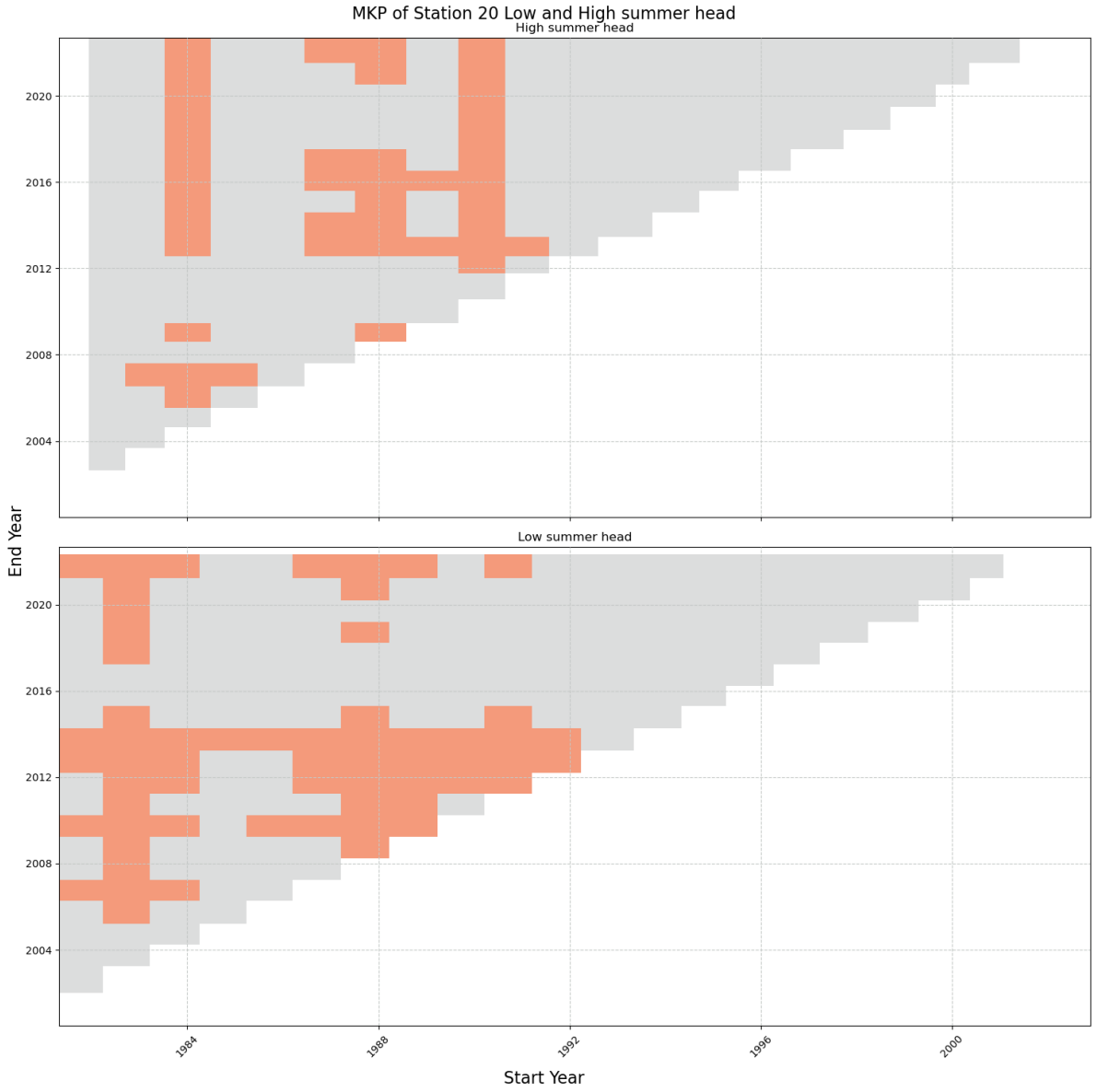

Same as figure 4.23, but for Nordfjordeid station (20).

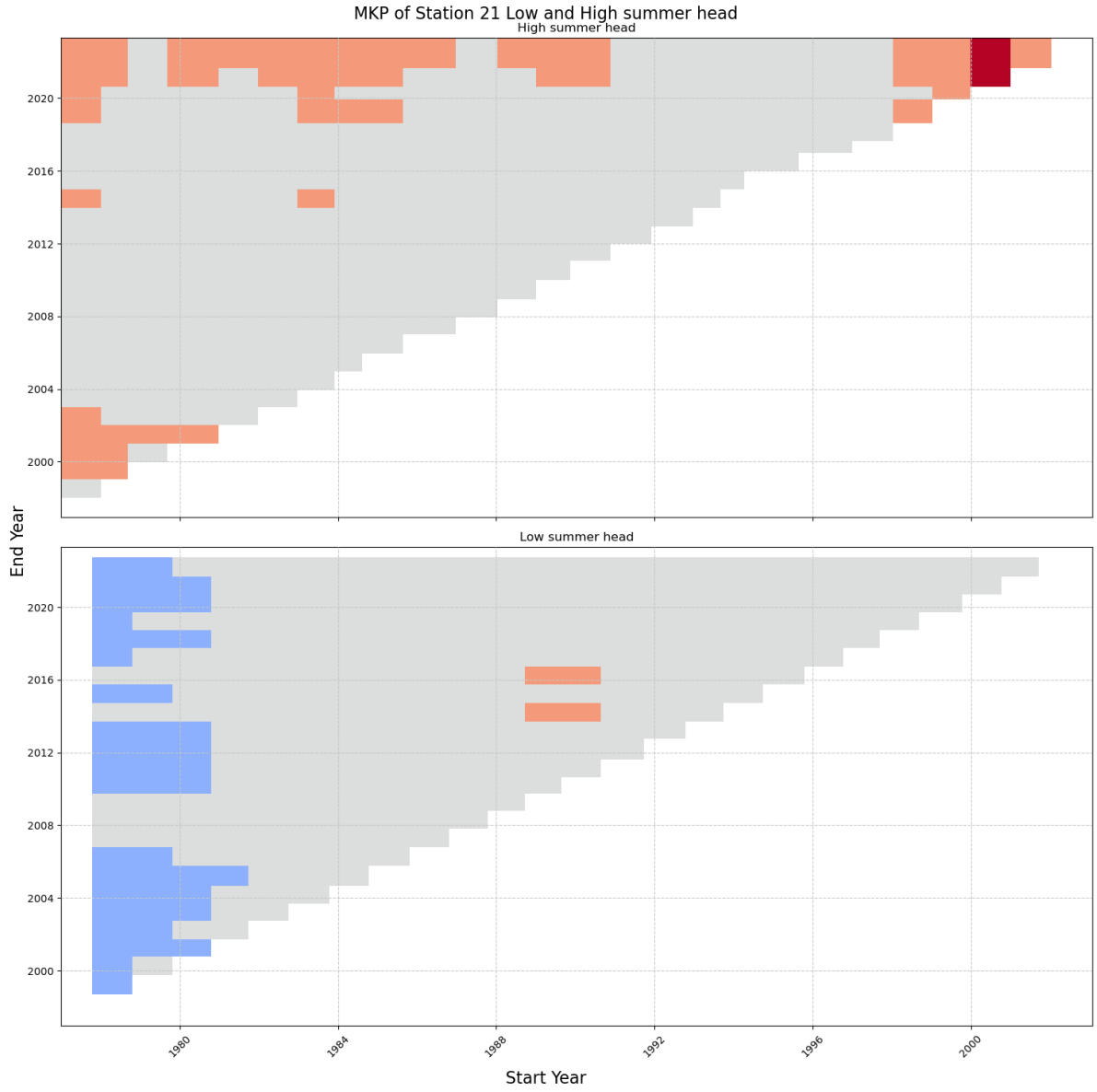

Same as figure 4.23, but for Settalbekken station (21).

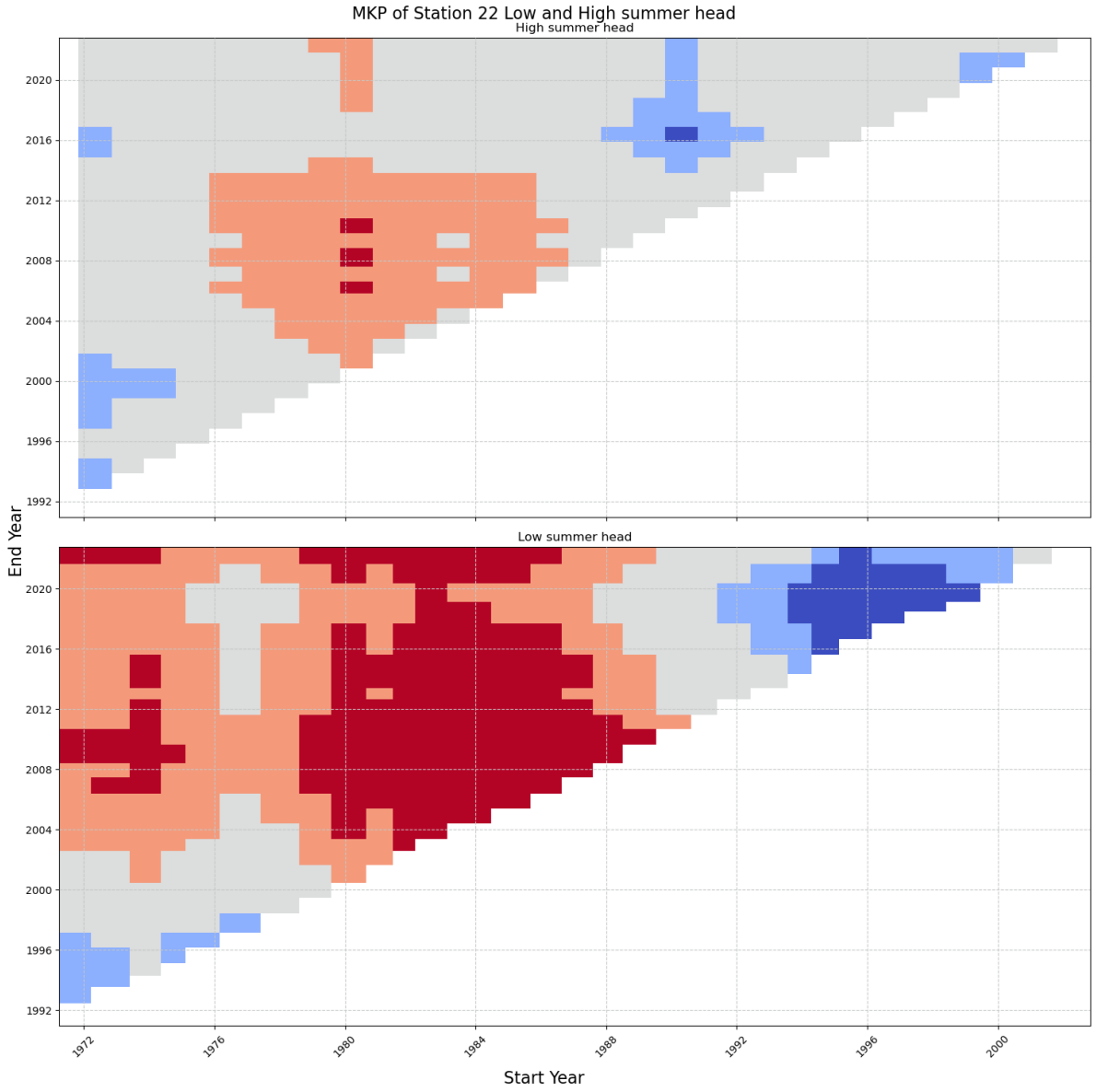

Same as figure 4.23, but for Stenerseter station (22).

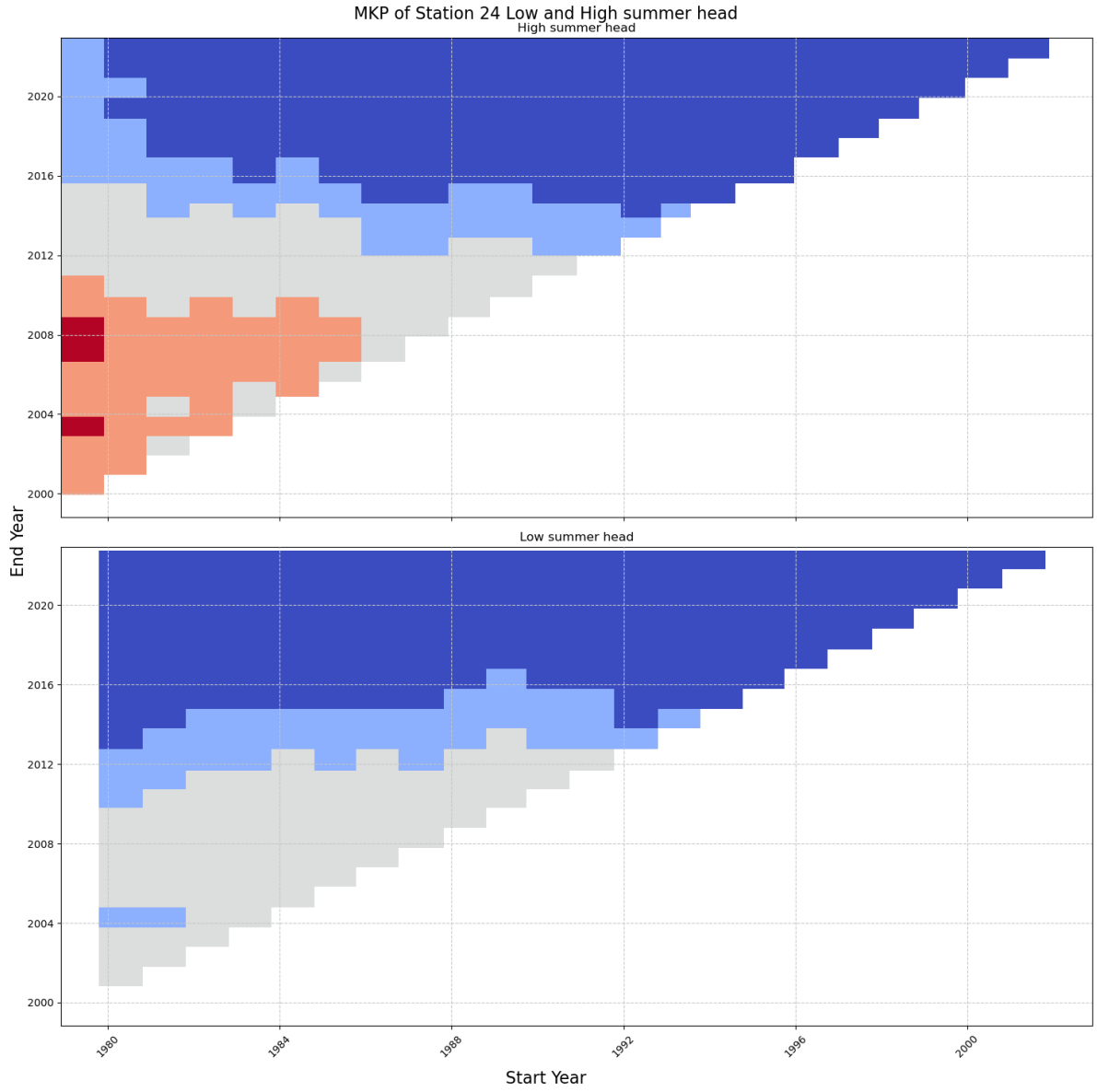

Same as figure 4.23, but for Øyangen station (24).